1968

Differential Cross-Sections for the Charged Particles Produced by 60-Mev Protons on Carbon, Iron, and Bismuth.

Fred Edmond Bertrand Jr
Louisiana State University and Agricultural & Mechanical College

DIFFERENTIAL CROSS SECTIONS FOR THE CHARGED PARTICLES PRODUCED BY 60-MeV PROTONS ON CARBON, IRON, AND BISMUTH

A Thesis

Submitted to the Graduate Faculty of the
Louisiana State University and
Agricultural and Mechanical College
in partial fulfillment of the
requirements for the degree of
Doctor of Philosophy

in

The Department of Physics and Astronomy

by
Fred Edmond Bertrand, Jr.
B.S., Southwestern at Memphis College, 1960
M.S., Louisiana State University, 1962
May, 1968

ACKNOWLEDGMENT

This experiment was performed while the author was a Graduate Fellow supported by the Oak Ridge Associated Universities. Professor D. C. Ralph, Louisiana State University, initially suggested application for the fellowship, and without this suggestion I would not have performed the work.

I would like to thank R. W. Peelle of the Neutron Physics Division, Oak Ridge National Laboratory, who suggested the problem and under whose guidance the research was performed. The experiment was designed and performed by R. W. Peelle, T. A. Love, and myself. The unique, and certainly state-of-the-art, fast and slow transistor amplifiers used were developed by N. W. Hill. Many of the computer programs used in this experiment, both for the PDP-8 and the IBM 360/75, were conceived by W. R. Burrus, who also guided the writing of these programs by B. W. Rust, P. M. Aebersold, and D. I. Putzulu. The optical model calculations presented were done with the help of J. K. Dickens. The mechanical design and construction of most of the detector system mounts were directed by R. H. Ward and the changes required in an existing scattering chamber were made under the supervision of R. J. DeBakker. H. R. Brashear was responsible for the construction of the soft collimator from Ne-102 scintillator. C. O. McNew and H. A. Todd, among others, were instrumental in electronic construction and checkout, and contributed to the data-taking phase of the work. A large amount of help in data compilation and reduction was provided by E. Beckham. I would also like to thank the staff of the Oak Ridge Isochronous Cyclotron for the assistance rendered during the experiment.

It seems almost too meager for the author to simply say that all the help, guidance, and instruction rendered by the above people and many others was deeply appreciated.

I would above all like to thank my wife for her constant encouragement during the experiment, encouragement which made the work possible for me.

This research was performed at Oak Ridge National Laboratory, operated by Union Carbide Corporation for the U. S. Atomic Energy Commission.

TABLE OF CONTENTS

LIST OF TABLES

LIST OF FIGURES

ABSTRACT

The differential cross sections for the production of proton, deuteron, triton, helium-3, and alpha particles by 60-MeV proton bombardment of ^{12}C, ^{54}Fe, and ^{209}Bi were measured over a secondary energy range from 1 to 60 MeV. The particles were detected in an all-solid state, 3-detector, total absorption counter telescope. The system resolution was ~150 keV (FWHM). Secondary charged particles were identified by both ΔE versus E and flight time versus E methods. Protons, deuterons, tritons, helium-3's, and alphas were unambiguously identified over an energy range from 1 to 60 MeV. Data were obtained at 15 to 20 angles between 12 degrees and 160 degrees. The high-energy region of each charged particle spectrum is dominated by elastic scattering and excitation of discrete nuclear levels, and differential cross sections are presented for 37 of the levels observed. The secondary proton spectra from ^{12}C, ^{54}Fe, and ^{209}Bi, below the region of discrete peaks, exhibit a structureless and nearly flat continuum region which at low energies merges into a peaked, nearly isotropic distribution except in the case of bismuth. The spectra of other secondaries have roughly the same continuum shape as the protons except that only the secondary alpha particles show a strong evaporation peak. The magnitude of the energy-integrated differential cross sections for each particle type is strongly forward peaked and decreases rapidly with increasing angle until a constant magnitude is reached for angles greater than ~120 degrees. The ratio of protons to deuterons is ~10 to 20:1 and the ratio of protons to tritons is ~100 to 300:1.

The elastic differential cross sections are found to agree with optical model calculations. The proton continuum spectra are compared with estimates from a Monte Carlo intranuclear-cascade plus evaporation calculation. The observed proton cross sections are larger than the estimates for angles larger than ~70 degrees and for angles smaller than ~20 degrees; however, between 20 and 70 degrees the agreement is within ±30%. More high energy cross section is measured at back angles than is predicted. Especially for the heavier targets, evaporation calculations do not provide enough high energy cross section for deuterons, tritons, helium-3's, or alphas, even at the largest angles of observation. The continuum proton spectra from the neighboring nuclides ^{54}Fe and ^{56}Fe are found to have equal shapes and cross sections in the energy region above 20 MeV, but ^{56}Fe exhibits a peaked low energy distribution which is only ~70% as intense as the ^{54}Fe distribution.

CHAPTER I.

INTRODUCTION

As a beam of intermediate energy protons passes through a target some of the projectiles interact with the nuclei, resulting in elastic and nonelastic collisions. These collisions result in the formation of charged and uncharged reaction particles which have unique energy and angular distributions. The work discussed in this paper is a study of the charged secondary particles emitted in such collisions initiated by 60-MeV protons.

There have been several experiments performed with incident 50- to 600-Mev protons to investigate one or more of the energy regions of the charged secondary particle spectra. Most of these experiments have been concerned with the outgoing proton spectrum only and nearly all have concentrated on a small part of the secondary energy spectrum. It is instructive to consider a few of these experiments.

Many studies have been made of the elastic and near-elastic regions of the reaction spectrum, although most of these have suffered from an energy resolution too poor to clearly resolve the inelastic levels and in some cases too poor to resolve the elastic scattering from nearby inelastic levels. Studies have been made recently with energy resolutions in the order of 1 to 2% at 155 MeV,[1] 62 MeV,[2] 55 MeV,[3] and 50 MeV[4] and some data (obtained with the detector system described

---

[1]P. G. Roos and W. Wall, Phys. Rev. 140, 1237 (1965).

[2]C. B. Fulmer et al., Phys. Letters 24B, 505 (1967).

[3]H. Kametsobo et al., J. Phys. Soc. Japan 27, 19 (1967).

[4]E. S. Burge et al., "Studies of Elastic and Inelastic Proton Scattering", Progress Report of Rutherford Laboratory (1966).

in this work) is reported with 0.2% energy resolution at 62 MeV.[5]

The secondary proton spectrum below the region of inelastic scattering peaks has been studied in several experiments. Data taken with incident protons of energy 1 BeV,[6] 650 MeV,[7] and 340 MeV[8] consistently show (at least to ~ 45 degrees, which is the largest angle of observation) the presence of a broad peak in the secondary proton data formed by the single scattering of incident nucleons from target nucleons. This distribution, called the quasi-elastic peak, has a maximum at an energy nearly the same as that expected from free nucleon-nucleon kinematics.

The presence of the quasi-elastic peak in the proton data from lower energy proton bombardment is not as consistent. Wall,[9] at 160 MeV, observed a broad quasi-elastic peak in the spectra from all targets and at all angles of detection smaller than 90 degrees, while recent data by Peelle,[10] at 160 MeV, show the presence of a peak in the secondary proton data only for angles as small as 30 degrees. The lower energy limit of detection in both of these experiments was above 20 MeV. Strauch and Titus[11] have examined with 96-MeV incident

---

[5]F. E. Bertrand et al., Phys. Letters 24B, 653 (1967).

[6]D. M. Corley, "Quasi-Free Scattering of 1 GeV Protons from C^{12} and Ca^{40}", Ph.D. Thesis, University of Maryland (1968).

[7]L. S. Azhgirey et al., Nucl. Phys. 13, 258-280 (1958).

[8]J. B. Cladis et al., Phys. Rev. 87, 425 (1952).

[9]N. S. Wall and P. R. Roos, Phys. Rev. 150, 811 (1966).

[10]R. W. Peelle et al., Phys. Rev. 167, 4, 981 (1968); R. W. Peelle et al., "Differential Cross Sections for the Production of Protons in the Reactions of 150-MeV Protons in Complex Nuclei", ORNL-3887, 1966.

[11]K. Strauch and F. Titus, Phys. Rev. 104, 1, 191 (1956).

protons the spectra of secondary protons above 30 MeV from a range of targets. These results show no quasi-elastic peak, but instead a continuum region which increases smoothly in magnitude toward lower reaction energies. Recently, Nonaka et al.[12] have investigated the secondary proton spectrum at energies above 15 MeV from several targets bombarded by 57-MeV protons. No quasi-elastic peak was observed at this energy.

Using 160-MeV protons, Fox and Ramsey[13] have examined the energy spectrum of secondary protons in the energy range of ~5 to 23 MeV and Bailey[14] has examined the outgoing protons over an energy range of ~ 5 to 80 MeV using incident 190-MeV protons. These data show a proton spectrum which is peaked just below the Coulomb barrier and is isotropic. Such a spectrum has been attributed to a nuclear evaporation process.

It is possible from the experiments described to make some general observations about the secondary proton spectra.

1. The elastic and inelastic scattering cross sections are forward peaked, being quite strongly peaked forward in the case of the elastic.

2. Although the secondary spectra are dominated by quasi-free scattering at high incident energies, the data at energies below 140 MeV show no quasi-free peak but show a smooth continuum.

3. The low energy region of the secondary proton spectrum exhibits an isotropic distribution.

---

[12] I. Nonaka et al., J. Phys. Soc. Japan 17, 12, 1817 (1962).

[13] R. Fox and N. F. Ramsey, Phys. Rev. 125, 5, 1609 (1962).

[14] L. E. Bailey, UCRL-3334 (1956).

Only a few experiments to examine the total energy spectra of charged secondaries other than protons have been reported. Hess and Moyer[15] at 340 MeV have studied the deuteron spectrum above ~ 50 MeV from several targets and Genin et al.,[16] have examined the proton, deuteron, and triton spectra produced by 155-MeV protons with a reaction energy cut off of ~ 25 MeV. These experiments, in general, find a distinct similarity in the shape of the outgoing proton, deuteron and triton spectra.

The spectra of secondary helium-3 and alpha particles have been studied with 157-MeV protons by Dubost et al.,[17] and by Muto et al.,[18] at 56 MeV.

Recently, Brun et al.,[19] and Dubost et al.[20] have studied the secondary proton, deuteron, triton, helium-3 and alpha spectra produced by 156-MeV and 90-MeV proton bombardment of medium and heavy nuclei. The data from these experiments extends down to a secondary energy of a few MeV; however, the quality of the high energy data was reduced since the thickness of the detectors was sufficient to stop only protons with energies less than ~ 30 MeV.

Perhaps the most important reason that only a few experiments have been performed to study the total spectrum of charged particles is that such experiments require significantly more development than

---

[15] W. N. Hess and B. J. Moyer, Phys. Rev. 101, 1, 337 (1956)

[16] J. Genin et al., J. Phys. Radium 22, 615 (1961).

[17] H. Dubost et al., Phys. Rev. 136, 6B, 1618 (1964).

[18] J. Muto et al., Nucl. Phys. 47, 19 (1963).

[19] C. Brun et al., Nucl. Physics A95, 337 (1967).

[20] H. Dubost et al., Journal de Physique 28, 257 (1967).

experiments which cover only a small portion of the spectrum. The largest problem is the selection of a detection system which will provide unambiguous particle-type identification over an energy range which may be greater than 200 to 1. These detection difficulties become more severe as the incident proton energy is increased since it not only becomes more difficult to find a high energy resolution total absorption detector but the selection of suitable detectors for particle identification also becomes harder. The electronics associated with a detector system satisfactory for such experiments is necessarily quite complicated. Among the other difficulties encountered in this type of experiment are the need for increased length of data acquisition time caused both by the small production cross sections for some types of charged particles and by the need to use thin targets to avoid low-energy spectrum distortion and cut off, and the necessity to prevent background "contamination" of the spectra over the entire secondary energy range.

The experiment described here was designed to detect and provide positive identification of all charged reaction particles simultaneously over their entire energy range. The experimental system was designed to meet this requirement for targets of any mass and to provide an overall energy resolution better than that previously obtained by detectors used for 60-MeV protons.

It was hoped that several types of studies could be performed simultaneously with the experimental system. The high energy resoution total absorption detector would separate, at energies up to 60-MeV, peaks in the spectra which were previously unresolved.

Thus, the data could provide "clean" elastic scattering cross sections and significant cross sections for reactions such as (p,p′) and (p,d). The narrow energy resolution might also show the presence of any existing structure in the lower energy portions of the charged particle spectra. The detection and identification of all charged particles over their entire energy range would hopefully lead to information on the reaction mechanisms involved in the production of the various types of charged particles from targets bombarded by protons and other projectiles with energies up to 60 MeV.

The choice of target materials to be used in the experiment was determined by at least three considerations. First, since the experiment would provide such diverse information from each target, it seemed desirable to cover a large range of nuclear masses. Second, since this experiment was sponsored by the NASA space shielding effort, elements were selected for targets which might have practical space application. Third, within each mass group an isotope was selected for use as a target which might provide the most useful spectroscopic information from the discrete level scattering.

CHAPTER II.

EXPERIMENTAL METHOD

A. General Technique

A schematic diagram of the technique used to perform the experiment is shown in Fig. 1.

Protons of energy ~60 MeV from the Oak Ridge Isochronous Cyclotron were used to bombard targets of thicknesses from 1 to 8 mg/cm^2. The reaction particles from the target were detected in a 3-counter telescope (B, C,and D) the collimator for which was another counter (A) that acted as a veto detector. Both linear and fast timing signals were simultaneously derived from the three detectors (B, C, and D) for each event. The fast signals served to indicate the nature of the event through coincidence and logic decisions and were used in a pile-up rejection system and in time-of-flight measurements. Slow pulses were used for all pulse-height analysis.

Forty-six bits of information containing flags from the fast system which indicated the nature of the event and the slow pulse heights for the event were merged in an interface and read into an on-line PDP-8 computer. The computer presented on-line displays, had low precision storage, and wrote events on IBM-compatible magnetic tape.

Between runs the data were analyzed on the ORNL IBM-360, Model 75 computer. The analysis program identified particle type, adjusted for dead layers, removed the effects of reaction tails, approximated physical quantities such as cross sections and Q values, and returned partly analyzed data as required for final analysis.

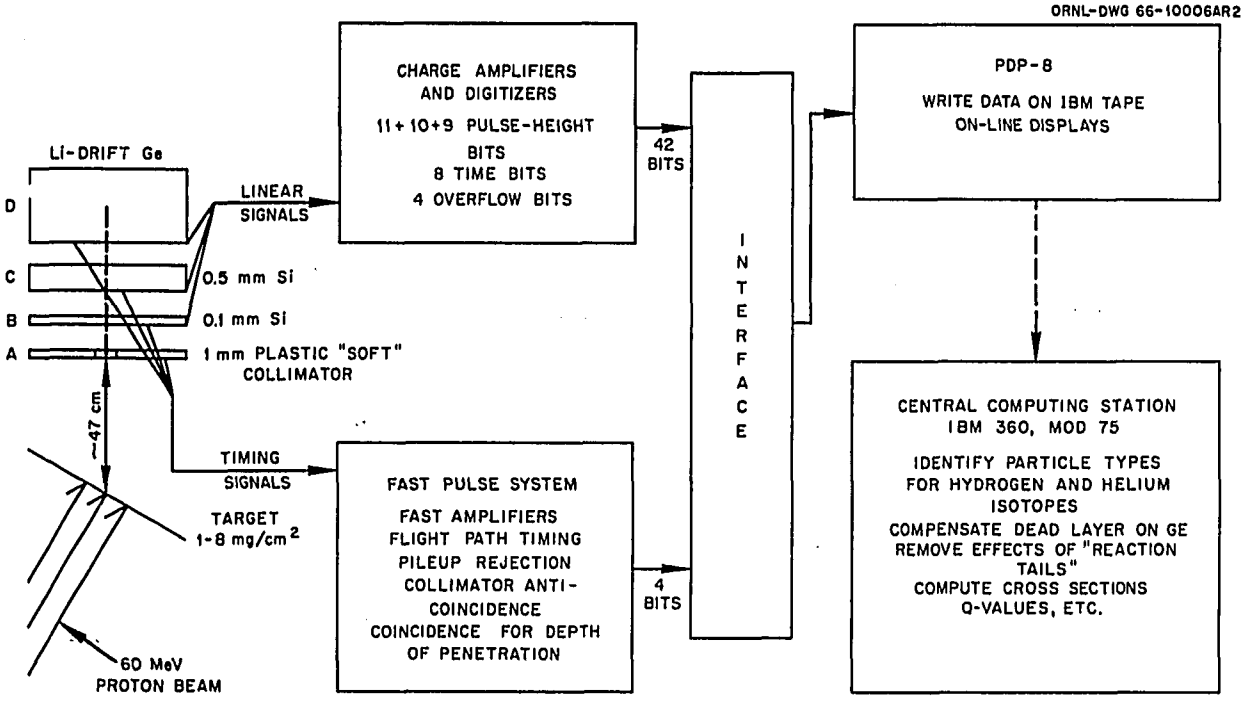

Fig. 1. Schematic of Experimental System.

B. Detector System

1. Methods for Particle Identification

The two most commonly used methods for charged particle-type identification are the $\Delta E \times E$ method and the time-of-flight method. In order to satisfy the needs of this experiment, a combination of both of these methods has been employed.

The basis of the $\Delta E \times E$ method is the Bethe-Block equation for the mean energy loss of a particle traversing a medium. This equation is well approximated by

$$-\frac{dE_p}{dx} = \frac{2\pi\ e^4\ zN}{m_e\ E_p} (Z_p^2\ M_p)\ f(V) \qquad (2.1)$$

where

eZ_p = charge of incident particle

N = atms/cm^3 in the medium

z = atomic number of medium

m_e = electron mass

E_p = incident particle energy

M_p = incident particle mass

$f(V)$ = slowly varying function of velocity

It is seen in the above approximation that the amount of energy loss from a particle with energy E_p increases with both the charge and mass of the particle through the term $(Z_p^2\ M_p)$. Therefore the energy loss will be different for particles with the same incident energy but different charge and/or mass, with the largest difference lying between particles of different charge. It is possible, therefore, to identify the type of particle by measurement of its incident energy and energy loss.

In practice, the absorbing medium is a detector from which an energy loss is measured. The incident energy is obtained as the sum of the energy lost in the "ΔE" detector and a second detector which is capable of stopping the particle.

In order to identify particle type by the time-of-flight method, the energy of the particle and the flight time of the particle over a known distance must be measured. In this experiment the particle flight time was measured with respect to the cyclotron rf. Although the timing signal provided by the rf was of high stability, an ambiguity was introduced into the time-of-flight measurement by the finite width (~ 1 to 2 nsec) of the beam burst. The effect of the burst width is to prevent accurate knowledge of the time when the incident proton strikes the target.

If a particle with kinetic energy E travels a distance D in time T, the mass of the particle is given by

$$M = \frac{2ET^2}{D^2} \qquad (2.2)$$

It is seen that for various types of particles, all of energy E, the particle mass is a function of the flight time. It is not possible by this method to distinguish between particles of different charge but like mass, e.g. tritons and helium-3's.

Although identification by time of flight may appear to be the simpler of the two methods described, it is not possible to use it as the sole discrimination system in this experiment, since the separation of flight time between different particle types with energies as high as 60 MeV is less than one nanosecond (10^{-9} sec) when the

flight path is only 50 cm. This small difference in flight time made it impossible to adequately separate particle types at high energies, due to the spread in the beam burst.

It is also apparent that the ΔE x E method can be used only when the energy of the particle is high enough to penetrate the first detector. This, of course, limits the low energy region of the reaction spectrum which can be studied.

In order to circumvent the problems encountered separately with each identification method, a combination of the two methods was employed. The particle type was identified by time of flight for energies that were stopped in the first detector, while the particles which passed through the ΔE detector were identified by a ΔE x E system.

2. ΔE Detectors

Equation 2.1, which is the basis of the ΔE x E method, calculates a mean energy loss while in practice particles of the same type with the same incident energy do not lose the same amount of energy as they traverse an absorber. Indeed there is a distribution of energy losses around the mean predicted by Eq. 2.1. Among the effects which may contribute to this distribution are nonuniformity of detector thickness, anomalous energy loss along the crystal axis of the detector, and Landau spread.[21] The thickness of the detectors was uniform to ~± 2%, a uniformity judged sufficient to prevent noticeable spread.

If charged particles traverse a thin detector along the detector's crystal axis, some of the particles may undergo fewer than normal

---

[21] K. R. Symon, Ph.D. Thesis (Harvard University, 1949).

collisions in the detector with the result that the energy loss from this particle is lower than expected. This effect, called channeling,[22] can contribute to the spread of energy loss distribution around the mean energy loss. In order to eliminate the spread, detectors used in this experiment were cut so that the protons did not traverse any of the crystal axes.

The effect of the Landau distribution as applied to particle identification is to smear together energy loss distributions from particles of the same incident energy, but of different types, so that identification may become ambiguous. The separation between energy loss distributions from various particle types with the same incident energy will increase as the thickness of the ΔE counter is increased. However, as the thickness of the ΔE counter is increased the maximum energy of particles stopped in the counter is also increased, and better time resolution is then required for unambiguous identification.

In order to select the thickness of the ΔE counters to be used in this experiment, computer calculations of the Landau distributions were performed[23] for protons, deuterons, tritons, helium-3's, and alphas of many energies, incident upon various thicknesses of silicon. Calculated energy loss distributions for 60-MeV protons, deuterons, and tritons, incident upon a 100-μ silicon detector, are shown in Fig. 2(a). Although the maximum particle energies which are stopped in 100 μ of silicon are low enough for time-of-flight identification,

---

[22] C. Erginson et al., Phys. Rev. Letters 13, 1 (1964).

[23] J. W. Wachter, ORNL-4134, Neutron Phsysics Division Annual Progress Report for Period Ending May 31, 1967, p. 136.

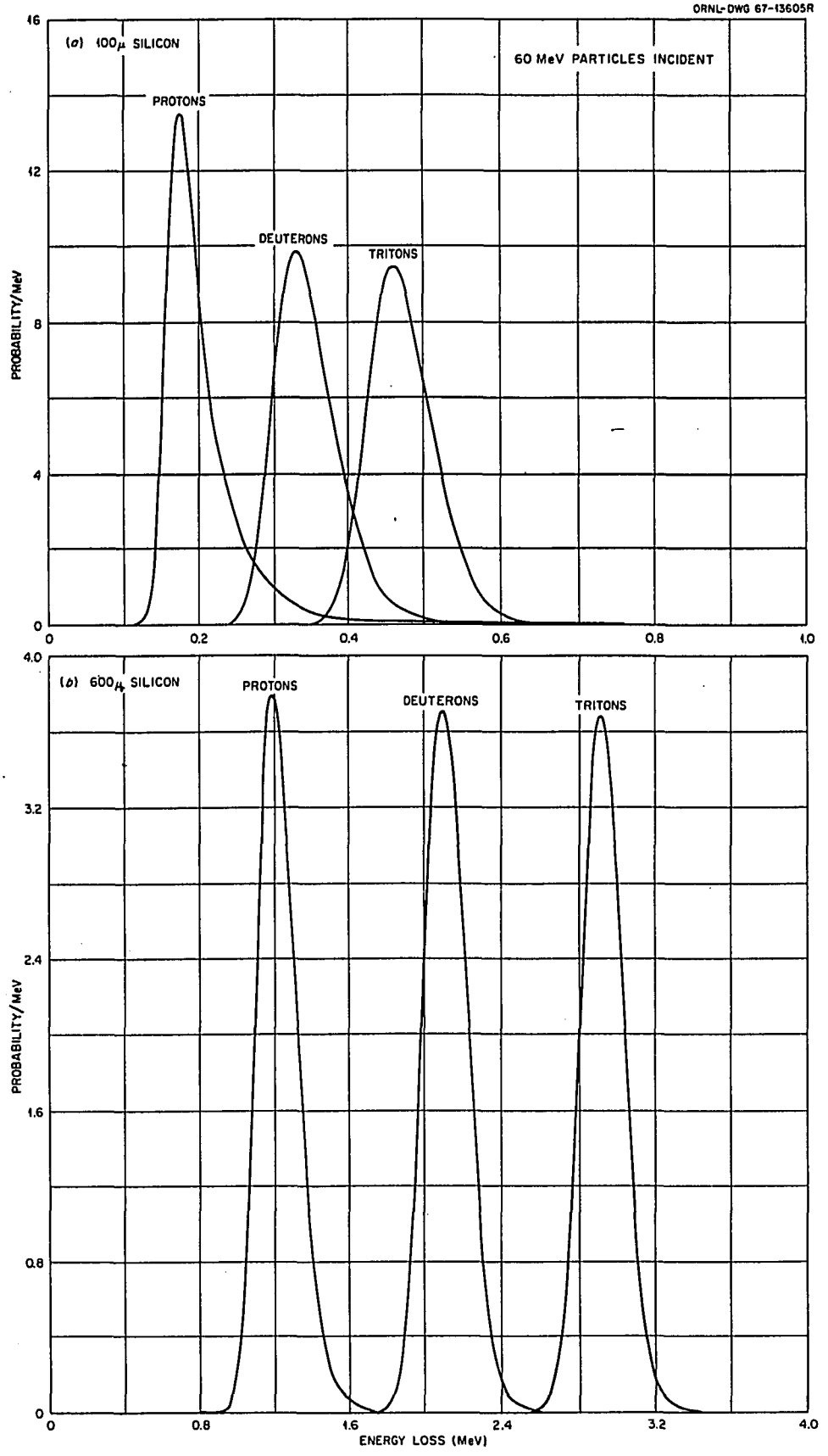

Fig. 2. Calculated Energy Loss Distributions in Silicon.

it is apparent that the overlap between energy loss distributions from the high energy particles is significant and no definite identification can be made of particles in the overlap region. On the other hand, Fig. 2(b) shows the energy loss distributions for 60-MeV protons, deuterons, and tritons traversing 600 μ of silicon, in which case separation is observed.

Figure 3 shows a comparison between the predicted and observed energy loss distribution from 61-MeV protons incident upon a 506-μ silicon detector. The calculation is seen to fit the experimental curve very well except in the high energy loss tail. The calculated curve was shifted by 30 keV to fit the data at the most probable energy loss.

The solid curves on Fig. 4 show the mean energy loss in a 600-μ silicon detector for protons, deuterons, and tritons over an energy range for each particle from 60 MeV to the energy which just penetrates the detector. The dashed curves show the maximum and minimum values (which include 99%) of the energy losses as predicted by the Landau calculations. It is seen that the effect of the Landau spread is to form an envelope of possible energy-loss values for a given particle energy E. If these envelopes are separated, as in the case shown, then particle identification by the $\Delta E \times E$ method should be unambiguous.

In order to avoid the overlap problem as shown in Fig. 2(a) and still keep the energy of particles absorbed in the ΔE counter low, two ΔE counters were used simultaneously. The choice of thicknesses for the ΔE detectors was found to be limited by several factors, which are listed below:

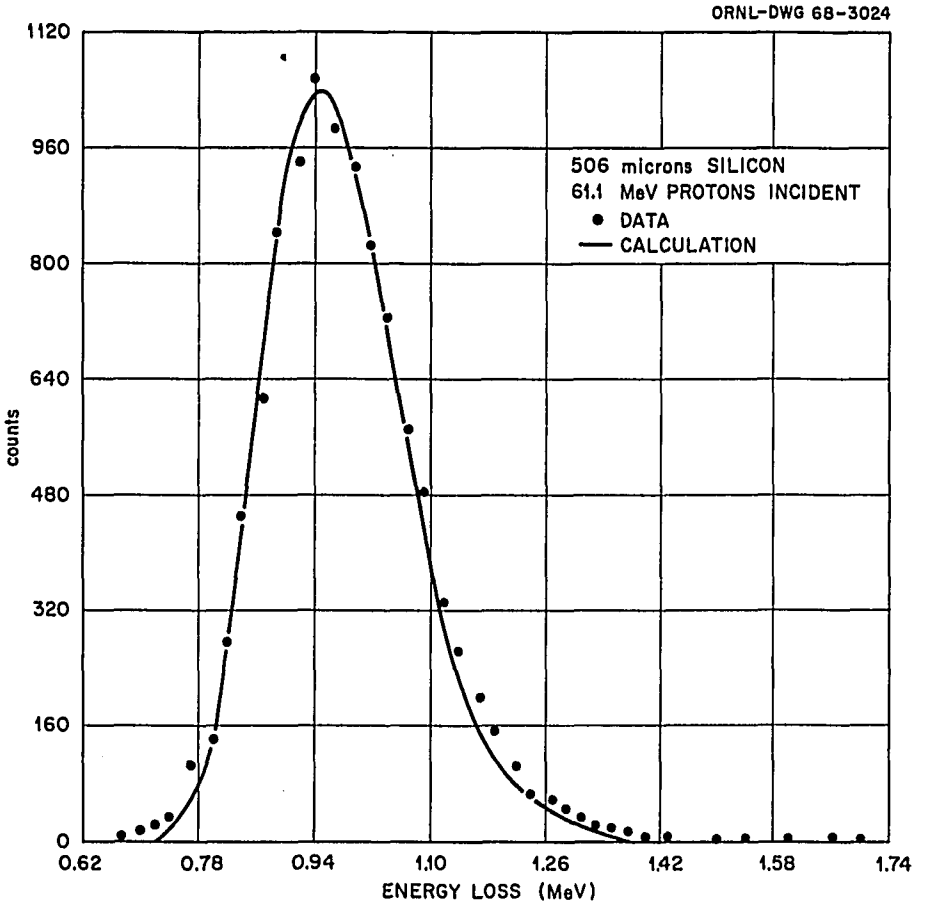

Fig. 3. Calculated and Observed Energy Loss Distributions.

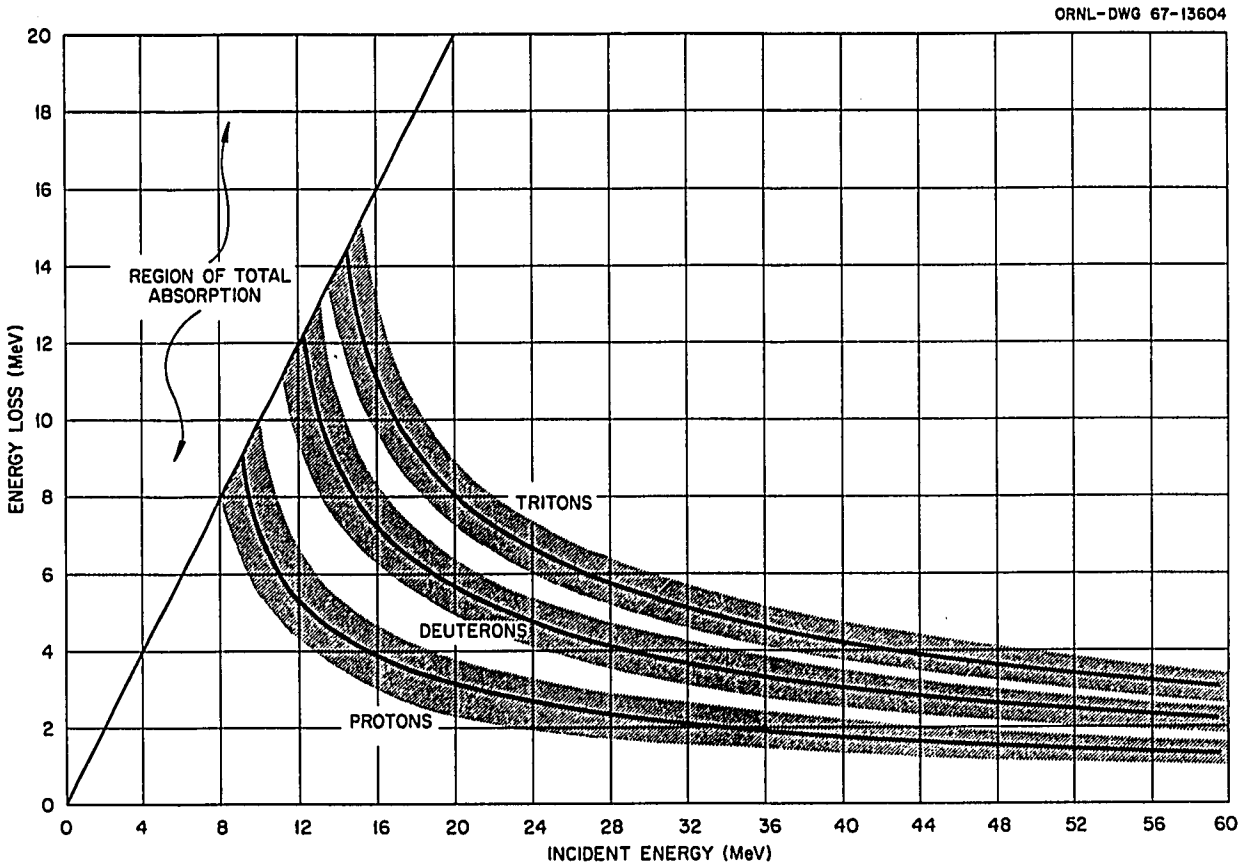

Fig. 4. Calculated Energy Loss vs Total Energy of 621-Micron Silicon Detector.

a. The maximum thickness of the first ΔE counter should be no greater than 100 μ, so that the particle types that must be identified by time of flight have maximum energies of ~3.5 MeV for protons and 14 MeV for alphas.

b. The minimum total thickness of the ΔE detector is ~600μ, so that the energy loss distributions from highest energy particles (~ 60 MeV) will be separated as is shown in Fig. 2(b).

c. The maximum thickness for the second counter and the minimum thickness for the first counter are related, since the first detector must produce the ΔE pulse for events which are stopped in the second detector. If the thickness of the second detector is increased, the energy of particles stopped in it is increased and the separation between ΔE pulses from the first detector becomes poor. On the other hand, decreasing the thickness of the first ΔE detector also causes poorer separation in the energy loss distributions.

The system used was selected by calculation of the energy loss distribution for several sets of ΔE detectors of various thicknesses. The system selected consisted of a 100-μ silicon surface detector followed by a 500-μ silicon surface barrier detector behind which was the total absorption detector. If particles stopped in the 100-μ detector (B), their energy was low enough to permit good time-of-flight identification. Particles which penetrated B and stopped in the 500-μ detector (C) were identified by the ΔE x E method, where the ΔE pulse was taken from B and E was the sum of the pulses in B and C. The highest energy protons which were stopped in the total of 600 μ of silicon were 9 MeV. This implies that for unambiguous identification

the energy loss distributions from the 100-μ detector for 9-MeV protons deuterons and tritons must be completely separated. The calculation did predict separation of these distributions. If, on the other hand, particles penetrated into the total absorption detector (D), the ΔE x E method was used where ΔE was taken from B + C and E was the sum B + C + D.

The experimental separation between particle types achieved by this system is shown in Fig. 5. This figure was made from a computer plot of total energy versus energy loss for reaction particles scattered from CH at 80°. Figure 5(b) shows a "map" of all particles which penetrated both ΔE counters. Complete separation of protons, deuterons, and tritons is observed down to the energies at which particles are absorbed. In this case total energy is the sum of B + C + D and energy loss is the sum of B + C. Clearly visible in the proton data are the elastic peak and the 4.4 MeV level, while several deuteron and triton groups are also seen. The symbols are an indication of the number of particles in each energy x energy loss "bin".

Figure 5(a) shows a ΔE versus E map of all particles which penetrated B and stopped in C. Once again complete separation between particles is observed for all energies down to the point where particles are absorbed in B. One should note that no helium-3 or alpha particles are seen in Fig. 5(b), since these particles are stopped in the 500-μ detector at 80°.

In both Figs. 5(a) and 5(b) distributions of counts are seen which indicate some flaws in the detection system. A distribution of counts with energy loss values of a few hundred keV and total energies of less

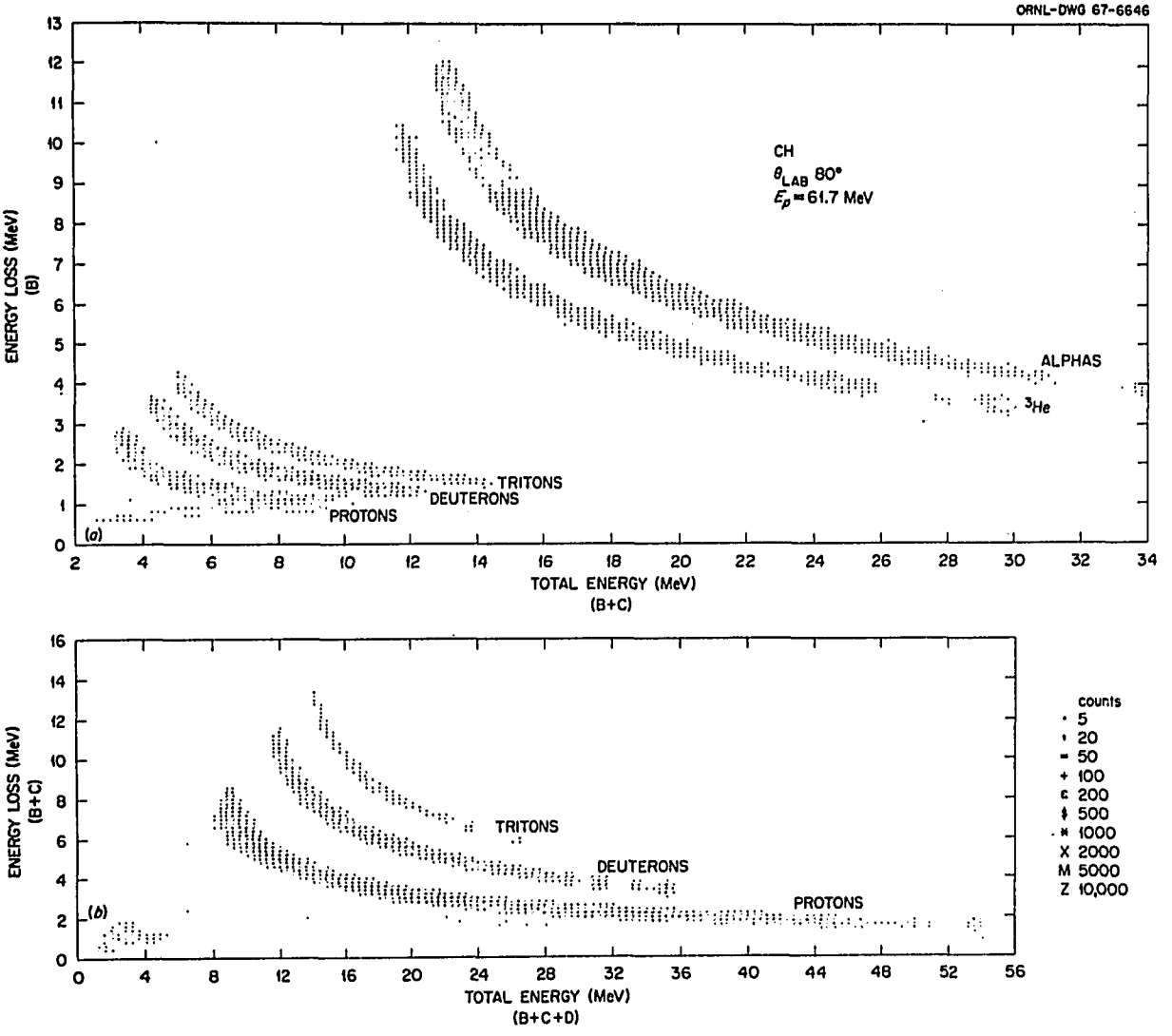

Fig. 5. Raw Data Map of ΔE X° E Identification Systems.

than 4 MeV is observed in Fig. 5(b). These counts are clearly not along the normal charged particle distributions and the group is therefore not identified as "real" data. These counts are, for the most part (some are caused by reaction tail from the total absorption detector), from gamma ray events which are detected by the system with low probability. Most of the gammas are emitted by the carbon "stopper" in the Faraday cup.

In Fig. 5(a) there is a distribution of counts located below the proton distribution, which intercepts the proton distribution at ~7 MeV on the total energy axis. This distribution is formed by events which leave the back of the second energy loss detector C at such an angle that they are not detected in the total absorption detector and will therefore not produce a CD coincidence. The magnitude of this effect, which is caused by multiple coulomb scattering in the ΔE detectors, should increase as the energy with which the particle leaves the C detector becomes smaller. It is seen that the number of counts in this distribution decreases with decreasing total energy and, since the CD coincidence was not set (although it should have been), the total energy of these events as seen in Fig. 5(a) should be the energy loss of these events if they had been detected in the total absorption detector. It is seen then that the counts in this distribution correspond to protons in Fig. 5(b) with energies between total absorption and ~24 MeV. The data presented in this work have not been corrected for this effect, but the magnitude of the effect is discussed later.

In order to identify particle type for those particles which did not penetrate the first energy loss detector (B), the time of flight

of each event was measured over the ~50-cm distance between the target and the 100-μ detector. The approximate maximum particle energies for which time-of-flight identification was solely relied upon were proton ~3.5 MeV, deuteron ~4.5 MeV, triton ~5.5 MeV, helium-3 ~11 MeV, and alpha ~13 MeV. The minimum time difference which must be resolved was between 11 MeV helium-3's and alphas and was ~3 nsec.

Figure 6 is a data map which shows estimated particle mass versus energy in the B detector for all particles which do not penetrate B. The data shown is for ^{12}C at 30°. In this case one sees clearly separated distributions of protons, deuterons, mass three ($^{3}_{2}He$, $^{3}_{1}H$) and alphas, although in earlier runs (4000, 5000, 6000 series) the separation was not as good between particles. The vertical distribution of counts seen at approximately 4.8 MeV was caused by a ^{234}U alpha calibration source placed near the face of the 100-μ (B) detector. The proton distribution below ~1 MeV is seen to be obscured by a second distribution at low energies. This "fold over" distribution is caused by particles which have flight times longer than the period between rf bursts and will "fold over" into a second rf period and be incorrectly identified. Also observed are mass 6 and 7 particles and mass 10 and 11 recoils.

3. Total Absorption Detector

It was desired in this experiment to achieve an overall detector system resolution considerably better than that previously reported for 60-MeV protons. This implied resolutions better than ~1%, since this value is typically quoted for the commonly used NaI detector.

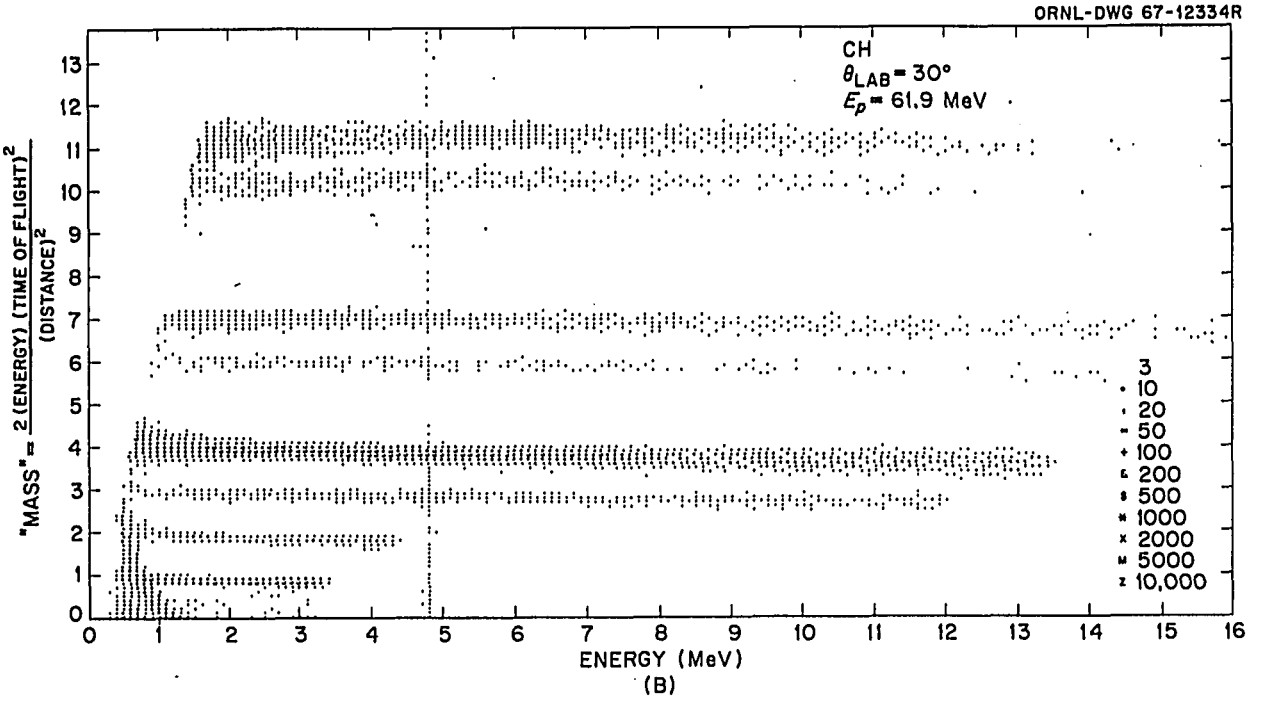

Fig. 6. Raw Data Map for Time-of-Flight Identification System.

Considerable research toward the development of a detector with improved resolution resulted in a technique which employed standard lithium-drifted germanium detectors. The details of this investigation are reported elsewhere;[24] however, the characteristics of the device and its capabilities are described below.

The detector, shown schematically in Fig. 7, was a planar lithium-drifted germanium detector which was oriented so that the protons entered the device in a direction parallel to the planes which bound the compensated region, thus affording sufficient stopping distance for 60-MeV protons (~1 cm). Some of the measured characteristics of this detector are: an energy resolution (FWHM) as good as 55 keV (FWHM) for 60-MeV protons, a peak count to total count ratio of ~94%, consistent response over the volume irradiated, and a current-pulse rise time of less than 5 nsec.

The detector, which must be kept in a vacuum and at a temperature near that of liquid nitrogen, was mounted on a "coldfinger" of copper behind a 0.0002-in.-thick nickel window, 1/2 in. in diam. The thickness of the nickel window and of the dead layer on the side of the germanium was determined by measurement of the energy loss from 5.5-MeV alpha particles. The dead layer was found to be entirely attributable to the nickel window and is ~3.6 mg/cm^2.

4. Detector System Response

The ideal total absorption detector and detector system, when used to detect monoenergetic particles, would be expected to produce

---

[24] F. E. Bertrand et al., "A Total Absorption Detector for 60-MeV Protons Using Lithium-Drifted Germanium", Proceedings of Ninth Scintillation and Semiconductor Symposium, June, 1966, p. 279.

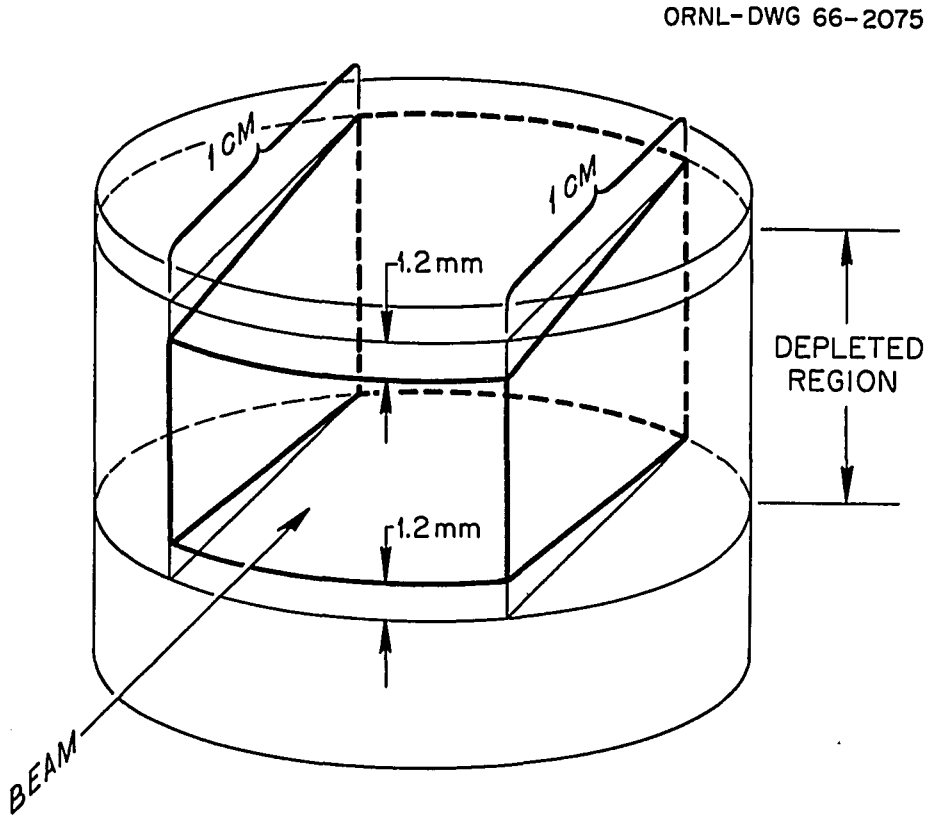

Fig. 7. Schematic of Germanium Total Absorption Detector.

an exactly monoenergetic pulse height spectrum. In practice, however, several factors conspire to prevent the realization of such a detector response even for a monoenergetic beam of particles. Among the conspiring factors are:

a. Intrinsic statistical resolution of the detector. In the case of the germanium, this was found to be less than 25 keV for 60-MeV protons.

b. Spread in the amplifier-analyzer system. In a typical run this spread was ~30 keV.

c. Scattering of the incident particles out of the detector (out of the compensated region of the germanium detector) before the total energy of the particle has been lost. It was calculated[25] that ~1.2 mm of the beam entrance window into the germanium should be masked off (see Fig. 7) in order to insure that 99% of the 60-MeV protons detected would lose at least 99.8% of their energy in the depleted retion. Such a mask was used.

d. "Pile-up" of pulses in the pulse height analysis system. An electronic system designed to reduce this effect is discussed below.

e. Particles which enter the germanium may undergo nuclear reactions with the material of the detector, and some of the incident energy may be lost through this reaction. These reactions may produce a low energy "tail" on the peak. It has

---

[25] L. Eyges, Phys. Rev. 76, 264 (1949).

been measured that ~6% of detected 60-MeV protons have such a reaction in the germanium, a figure comparable to that for 60-MeV protons detected in NaI detectors.[26] The "reaction tail" is unavoidable and the data must be corrected for this effect.

f. Particles may lose energy before they enter the detector by scattering from the edges of the detector system collimators. This scattering will also cause a low energy tail in the peak. Efforts were made to prevent this form of tail.

There is a basic difference in the manner in which the reaction tail and collimator edge tail enter the detection system used in this experiment. This difference was employed to measure the magnitude of each tail.

Since a particle scattered from the collimator edge loses energy before it enters the detector system, the energy loss pulses are based on the reduced energy (E′) and the particle is thereby identified as a scattered proton with energy E′. On the other hand, the energy lost through nuclear reactions within the total absorption detector is not lost until the particle has passed through the ΔE counters. Therefore, in the latter case the ΔE pulses are based on incident energy E, but energy is lost in the total absorption detector. This type of energy loss is observed as a distribution of events with constant ΔE, but with all values of total energy less than E.

An attempt was made to eliminate collimator tail in this experiment through the use of a thin plastic scintillator as a "soft" collimator,

---

[26] D. F. Measday, Nuclear Instruments and Methods, 34, 353 (1964).

thus reducing the collimator thickness. The "soft" collimator serves as an anti-coincidence detector which vetos any event which penetrates its body; however, a collimated event, one which does not penetrate the collimator, does not cause a veto pulse. The thickness of the "soft" collimator was 1 mm, as compared to a thickness of $\sim\frac{1}{4}$ in. of nickel and brass necessary for a "hard" collimator.

To measure the amount of tail produced by the collimator and total absorption detector, the detector system was placed in the direct beam and the response of the system measured for the incident protons at very low count rates ($\sim$200 protons/sec). The amount of spread in the incident beam was $\sim$30 keV for these tests and therefore did not affect the overall resolution.

Figure 8 shows the effectiveness of the "soft" collimator. The distributions seen in Figs. 8(a) and 8(b) were taken in the direct beam and show data maps of ΔE versus E. In Fig. 8(b) the response is shown as measured with a hard collimator of $\frac{1}{4}$-in.-thick nickel. One observes two distributions below the incident proton peak. The tail due to nuclear reactions is seen as a continuous distribution of particles along the total energy axis with constant energy loss. The second distribution is caused by collimator scattering and would be identified as real data during a "scattered" run.

Figure 8(a) shows the response obtained when only a soft collimator is used. The tail from reactions is still observed but no contribution due to collimator scattering is seen.

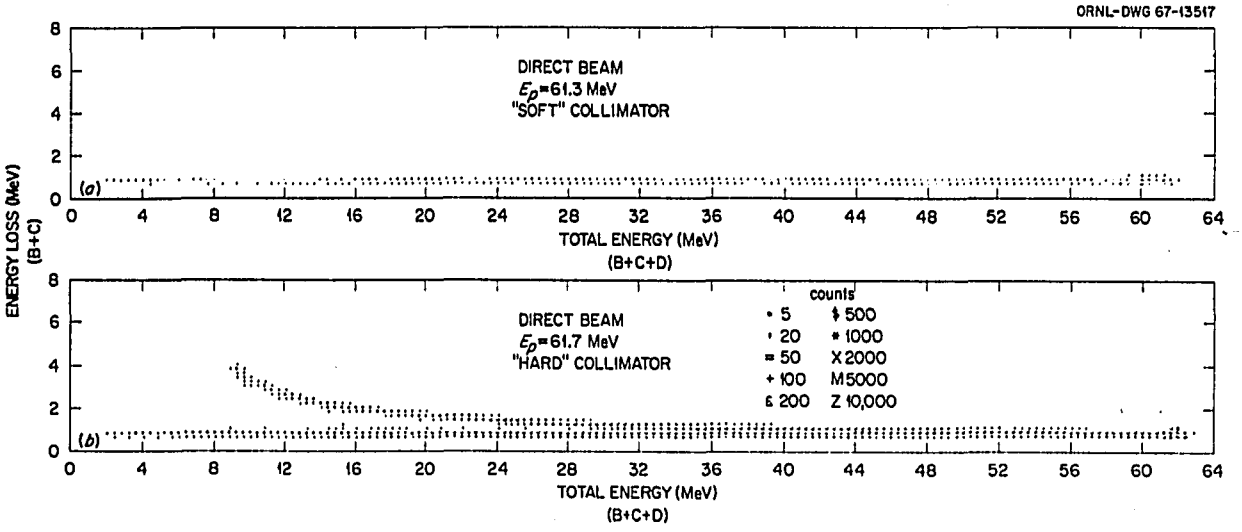

Fig. 8. Comparison of Detector System Response for "Hard" and "Soft" Collimators.

5. Detector System Mounting

Figure 9 shows the entire detector system[27] mounted in the scattering chamber.[28] Since the lithium-drifted germanium detector must be kept near a temperature of 78°K, liquid nitrogen was brought into a stainless steel dewar through one of the flexible metal vacuum lines seen in the figure and a second line was used to vent the nitrogen system. The third metal line was used to continuously pump on the vacuum jacket around the nitrogen flask. The dewar was filled remotely upon demand as indicated by the temperature of a thermocouple suspended in the liquid nitrogen. The entire assembly was mounted on a table which was rotatable to any angle within the chamber.

The silicon detectors were mounted directly behind the soft collimator and as closely as possible to each other and to the germanium detector. Contacts were made to both sides of each ΔE detector by use of nickel rings, 0.005 in. thick. In an effort to keep the length of lead between the detectors and the preamplifier and fast amplifier as short as possible,[29] a tab only $\frac{1}{2}$ in. long in the outer edge of each ring was connected directly to a BNC connector to which the preamps were connected.

The soft collimator was constructed from 1-mm-thick NE-102 plastic scintillator. The collimating hole in the plastic was rectangular,

---

[27]The design and construction of the detector mounts and the cryostat for the germanium detector were done in large part by R. W. Ward of the Physics Division of Oak Ridge National Laboratory.

[28]The design and implementation of major changes to an existing scattering chamber were done under the direction of R. J. De Bakker of the Plant and Equipment Division, Oak Ridge National Laboratory.

[29]N. W. Hill and R. W. Peelle, ORNL-3973, Neutron Physics Division Annual Report for Period Ending May 31, 1966, p. 97.

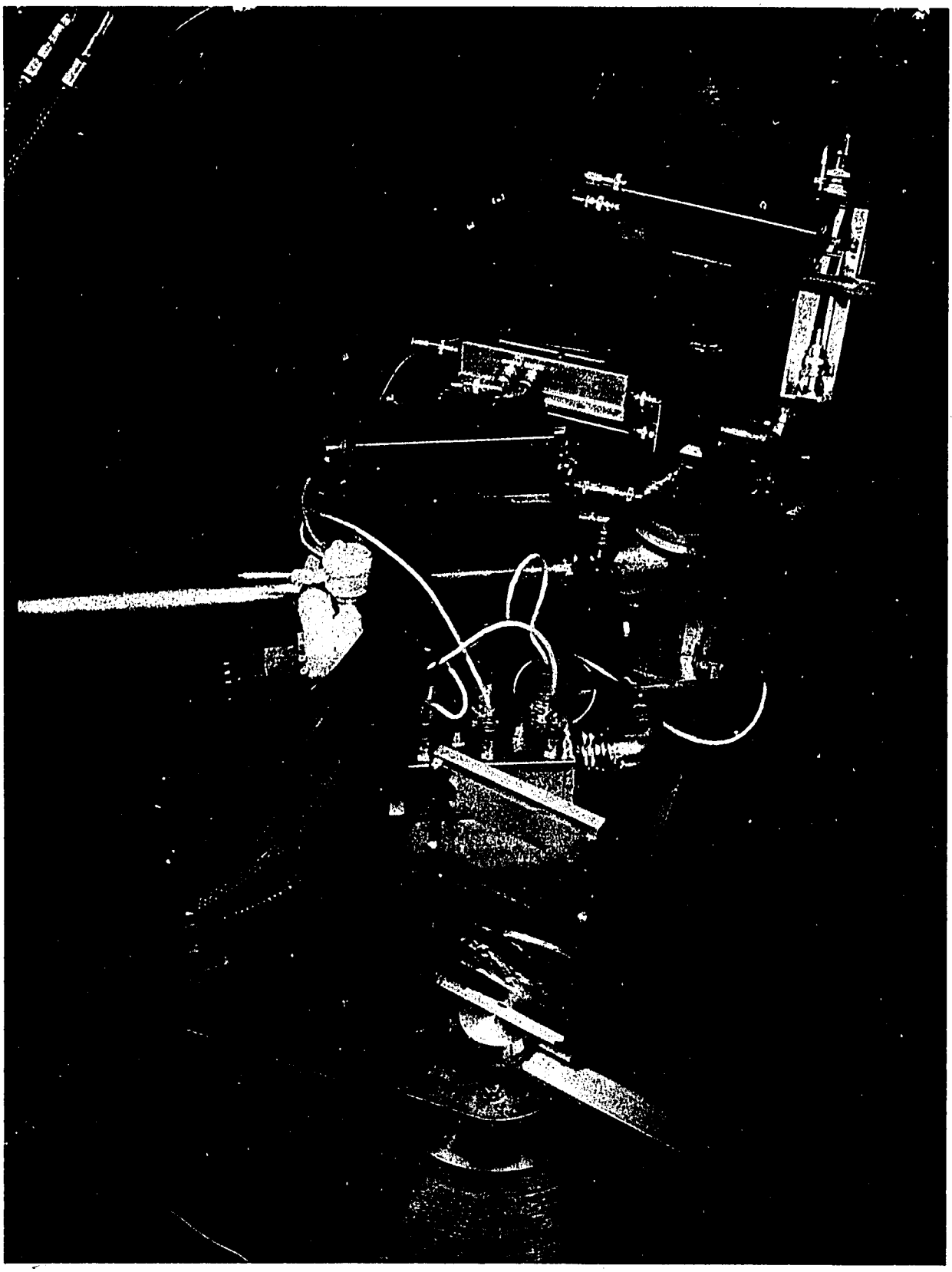

Fig. 9. Detector System Mounted in Scattering Chamber.

0.77 cm x 0.35 cm, since this was the shape of the usable entrance area of the germanium detector (see Fig. 8). The scintillator was mounted between two pieces of brass, the inner edges of which were tapered to ensure that no protons could strike any part of the brass and enter the detector system without first passing through the veto scintillator. An RCA 8575 photomultiplier tube was coupled to the top of the scintillator.

Since the usable entrance area into the germanium detector was small, the alignment between collimator and germanium was especially critical. The position of the mount which held the collimator and the ΔE detectors was therefore adjustable horizontally and vertically.

C. Electronics

The electronics used in this experiment consisted of three basic systems, the linear pulse analysis system, the fast logic system, and the interface-computer system. The fast timing system was used for all coincidence and logic decisions as well as time-of-flight analysis, while the slow system was used for linear pulse-height analysis of the data. The two systems were combined in an interface and the computer was used for on-line displays and to write data on IBM-compatible magnetic tape.

A block diagram of the electronics system is shown in Fig. 10. Shown at the top of this figure are the four detectors which comprised the counter telescope: A - the soft collimator, B - 100-μ detector, C - 500-μ detector, D - germanium, total absorption detector. A timing and linear (except A) signal were obtained simultaneously from each detector for each event. The signals were amplified in a slow

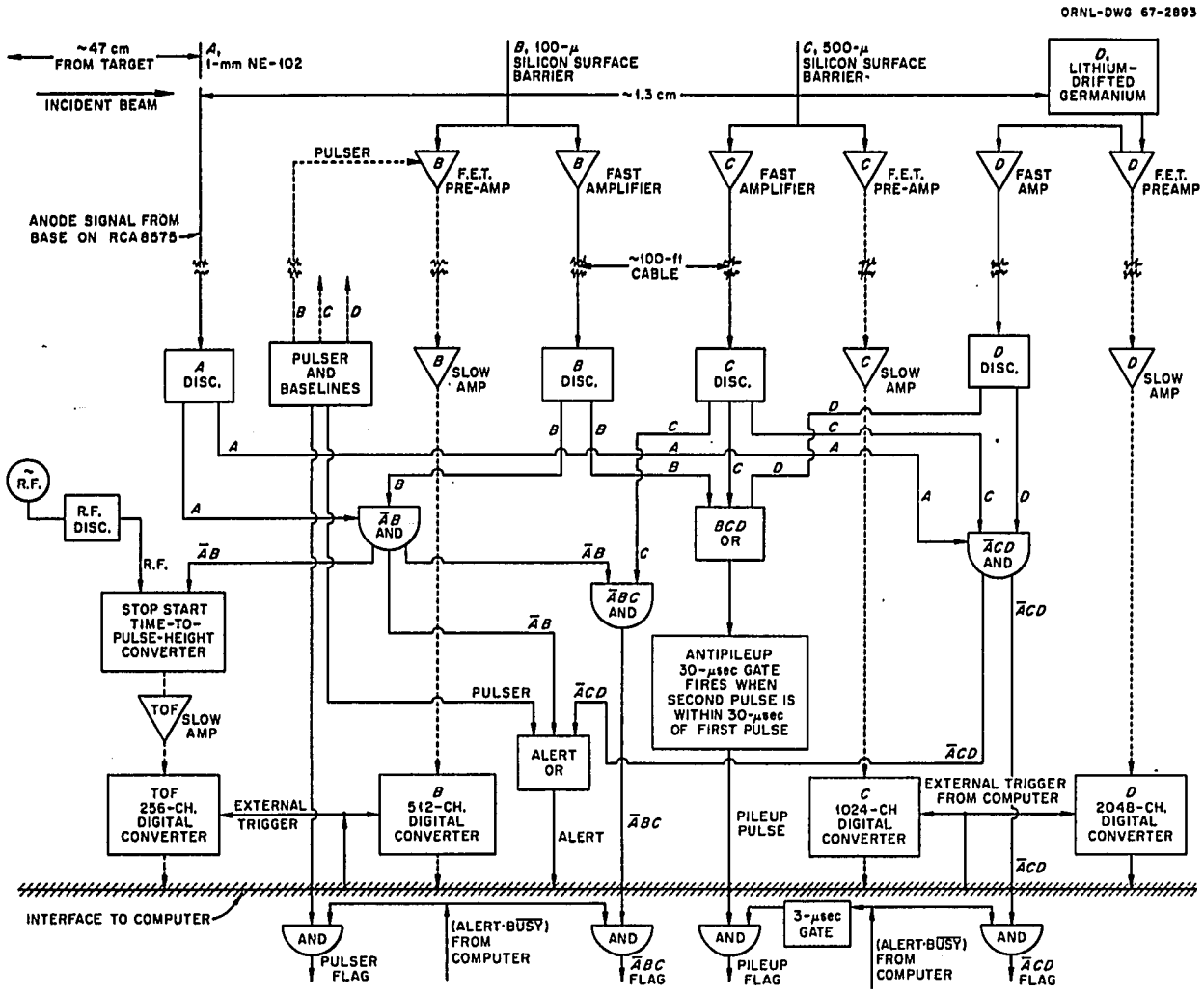

Fig. 10. Block Diagram of Electronics System.

preamplifier and a fast amplifier which were placed inside the scattering chamber in order to reduce lead length from the detectors. The preamplifiers and fast amplifiers were connected to the remainder of the electronics by ~100 ft of cable.

1. Linear Pulse System

The preamplifiers for the slow signals from each detector were all solid state with field-effect transistor inputs.[30] The preamps were designed to meet the special needs of this experiment and, in particular, to have very good stability and linearity over a large dynamic range when operating in a vacuum environment. The design and performance of the preamplifiers is discussed in the reference quoted, but it is pertinent to state that the long-term stability of the entire pulse-height analysis system was much better than 1.0% when used under experimental conditions.

The linear amplifiers used on each detector were Tennelec TC-200 amplifiers operated with 0.8-μsec integrating time constant and double differentiation time of 0.8 μsec. These time constants were judged in the case of the germanium counter to be a good compromise for values needed to reduce the effects of count rate broadening and the "Ballistic Defect".[24]

The linear pulse heights from each amplifier were analyzed at a gain of 0.05 MeV/channel in a separate analog to digital converter (ADC). A Victoreen ADC, Model No. 516 ADC-2P-B, was used for analysis of the C and D pulses where the maximum channels were 1024 and 2048,

---

[30] N. W. Hill et al., Vacuum-Hardened, Charge-Sensitive Preamplifier (To be published).

respectively. The signals from B and from the time to amplitude converter were analyzed in RIDL analyzers with maximum channels of 512 and 256, respectively. The slope intercept of each analyzer was adjusted so that zero pulse height occurred in a channel greater than zero.

2. Timing Pulse System

For each event detected in the counter system, a signal for use in the fast logic system was extracted from the three counters, B, C, and D. In the case of the silicon detectors B and C, the fast signal was taken from one side of the detector and the slow signal from the other, while for the germanium detector a fast signal was picked off from the input to the slow preamplifier since only one side of the detector was available for signals.[29] The rise times of the signals from all the detectors were a few nanoseconds, being as fast as 1 nanosecond in the case of B.

If an event hit the active collimator, a fast signal was taken from the anode of the RCA 8575 photomultiplier tube. The rise time of this signal was ~3 nsec.

The fast signals from B, C, and D were amplified in fast amplifiers designed to match the characteristics of each detector. In general, the amplifiers had a gain between 3000 and 4000, a rise time as fast as 2 nsec for $\frac{1}{4}$ nsec rise time pulse at the input, outputs terminated in 50 Ω, and were linear to ~0.5 volts at the output.[31]

3. Logic System

The purpose of the fast logic system, as shown in Fig. 10, was to characterize each event in terms of depth of penetration into the

---

[31] The fast amplifiers used were designed by N. W. Hill, Instrumentation and Controls Division, Oak Ridge National Laboratory, and are unpublished.

detector system and to inform the computer of the occurrence of an event. It has been stated previously that there are three classes of valid events: those which penetrated both silicon detectors (B and C) and stopped in the germanium detector, those which penetrated the 100-μ detector and stopped in the 500-μ detector, and those which stopped in the 100-μ detector.

All events which penetrated C and stopped in D should have produced fast signals above the C and D discriminator thresholds and would therefore have produced a coincidence unless the event also penetrated the collimator in which case a veto pulse was produced which prevented analysis of the event. This coincidence, labeled $\bar{A}CD$, was fed into an OR circuit (Alert OR), the output of which was used to inform the computer of the occurrence of an event. A second output from the $\bar{A}CD$ coincidence was used to "flag" the event (Flag 2).

If an event occurred which penetrated B and stopped in C, a coincidence between B and C was made, which set the flag labeled Flag 1, provided there was no A signal. The B discriminator fired on all events which stopped in C. It should be pointed out that the B discriminator may not have fired on the highest energy events which penetrated B and C due to the small energy loss in the 100-μ detector. In the case of a $\bar{A}BC$ coincidence and no $\bar{A}CD$ coincidence (indicating the event stopped in C), the computer system was alerted from the pulse in B. The thresholds for fast signals as determined by the discriminator level were no higher than 500 keV for B and C and 300 keV for D.

It will be recalled that in order to identify particle type for those events which stop in B, it was necessary to measure the time of

flight of the event. The flight time for each detected event was measured between the target and the 100-μ detector using an EG & G TC-100 A, time-to-amplitude converter (TAC). The start pulse for the TAC was obtained from the $\overline{A}B$ fast signal and the stop pulse from the cyclotron RF, which has a period of ~44 nsec. In the case of events which stop in B, the computer system received an alert from the $\overline{A}B$ pulse. The output of the TAC was fed into a slow amplifier, then into a 256-channel analyzer. It should be noted that no flag was used to signal a time-of-flight event; however, the lack of a $\overline{A}BC$ and a $\overline{A}CD$ flag indicates the event stopped in the 100-μ detector.

The entire system was also alerted from artificially produced pulser events. The pulser system consisted of two precision slow pulsers (one for D pulses with positive output, the other for B and C with negative output), both driven by a single driver such that the pulses fired out of phase with one another. A fast signal was extracted from each pulser as it fired and was used to alert the system through the Alert OR and set the Pulser Flag which identified the event as artificially produced. Since the two pulses did not fire at the same time, the same system was also used to check the baseline stability for the B, C, and D analyzers. This was possible since, for example, when a D pulser pulse was produced, zero pulse height was present in the B and C analyzers and the contents of all analyzers were read for each event.

4. Computer and Interface

The pulses from the fast-logic system and the pulse heights from the four analog-to-digital converters were connected to an on-line

PDP-8 computer through an interface.[32,33] The Alert pulse was the initial link between the logic system and computer system for each event. If the analysis system was busy, an (Alert·$\overline{\text{Busy}}$) coincidence was not produced and the event was not processed. If, on the other hand, the system was not busy, then a pulse called the Encode was sent from the (Alert·$\overline{\text{Busy}}$) coincidence to the experiment interface. The Encode pulse produced a trigger for each analog to digital converter which required each ADC to analyze the pulse at its inputs. It should be noted that the analyzers could only be triggered by an event which produced an Alert. The computer waited until all four ADC's had finished analysis before the ADC contents were transferred to the computer through the "data break". Upon completion of transfer of all information for the event a Transfer Accepted pulse was sent from the computer, which reset the ADC's and all flags, enabling the system to accept another event.

The content of each ADC was transmitted as one 12-bit PDP-8 word.[34] Since the contents of the ADC's did not require the full 12 bits (maximum required is 11, by D), the remaining bits were used to transmit the "status flags" for the event under analysis. For each event, the following flags were transmitted: $\overline{\text{A}}$BC, $\overline{\text{A}}$CD, Pulser, Pile-up, and an overflow flag from each ADC.

---

[32] W. R. Burrus et al., "A PDP-8 Interface for a Charged-Particle Nuclear Physics Experiment", ORNL-TM-2013, 1967.

[33] E. Madden, "Multi-Analyzer Stored Program Data Acquisition System Interface", ORNL-TM-2153, 1968.

[34] The PDP-8 computer programs used in this experiment are found in the following publications by B. W. Rust and W. R. Burrus: "Flexi-Kludge-A Multi-Parameter Nuclear Spectrum Summing System for the PDP-8", ORNL-TM-1879, 1967; and "Super-Flickers-An On-Line Data Acquisition System for the PDP-8", ORNL-TM-1878, 1967.

The data from each event, which was contained in four computer words, was examined at the program's convenience and stored in a 512-word-long (128 events) region in the computer memory. When this "buffer" region was full, the 128 events were written as one record on IBM compatible, 7-track, magnetic tape.

5. Pile-Up Rejection System

In addition to the functions described above, the fast pulses were also used in a pile-up detection system. Pile-up in the case described here was caused by the overlap of pulses from two events in the slow pulse height analysis system. Although the detectors used in the counter system recovered very rapidly from an event (all the charge is collected from the germanium detector in 100 to 150 nsec) the pulses out of the slow amplifiers may not return to within 0.1% of the base-line for ~10 μsec. If a second pulse occurs during this interval, the pulses will overlap and proper analysis of either individual pulse may be prevented.

The regions in time before and after a pulse in which pile-up may occur were determined not only by the amplifier time constants but in this case also by the operation of the Victoreen analyzers used on C and D. The gates on the inputs of these ADC's were normally closed and when triggered from predetermined external conditions, opened to accept the pulse present at their inputs and remained open for ~3 μsec, after which time they closed again. The gate could not reopen until another trigger was produced which could not occur until the present analysis was finished. Although a background event only rarely produced a trigger pulse for the system, the linear signal from the

background appeared at the analyzer input. This pulse may affect the analysis of a second pulse, which caused an alert and occurred after the arrival of the background pulse by less than 20 μsec.

The two basic conditions which could cause pile-up in the slow analysis system are:

a. An event which produced an alert followed by another event (of such a pulse height that it would increase the voltage out of the ADC) of any type within 3 μsec.

b. An event which did not produce an alert (e.g. background) followed by an event which produced an alert within 20 μsec.

Under either of the above conditions, a pile-up would occur and it was desired to "flag" these events.

Since the pulse which produced the pile-up may have originated in any of the three detectors, B, C, or D, the outputs of these fast discriminators were fed into an OR circuit labeled BCD OR in Fig. 10. This insures an output from the OR circuit for every event detected, real or background. The OR output was used as the input for an EG&G, PUG-100 anti-pile-up gate. The first pulse which arrived at the input of the pile-up gate turned the gate circuit "on" for a preset length of time (in this case 20 μsec). If a second pulse arrived at the input to the gate within this time interval, an output pulse was produced and the timer was set so it would extend an additional 20 μsec. If, on the other hand, a second pulse did not arrive within 20 μsec, the gate was reset.

Consider the first of the two conditions for pile-up in which an event occurred which produced an alert followed within 3 μsec by any

type of event. If the system was not busy, the first event produced an Encode pulse and also set the anti-pile-up gate. The arrival of the Encode pulse at the interface caused a second gate (labelled 3 μsec Gate in Fig. 10) to fire and produce a pulse lasting for 3 μsec on the input of the pile-up flag coincidence circuit. The Encode pulse triggered the analyzers and their gates were open for 3 μsec. The second pulse, whether or not it was a "true" event, caused the anti-pile-up gate to fire, and since the second pulse arrived less than 3 μsec after the first, the output of the pile-up circuit was in coincidence with the 3 μsec gate pulse and a pile-up flag was produced.

In the second condition the first pulse did not set the alert but was present at the input to the analyzer gates. This pulse turned on the pile-up gate circuit for 20 μsec. The second, "true", pulse which occurred less than 20 μsec later caused an alert and fired the pile-up and the 3 μsec pulse gate, thus producing a pile-up flag coincidence. It should be noted that, if the second pulse had been another background event, the pile-up gate would have fired (and been reset) but the lack of a 3 μsec pulse on the pile-up flag coincidence circuit input would prevent the production of a flag. This avoided setting the flags by background events.

It is seen in Fig. 10 that the pulser indicator (fast signal) and the $\overline{A}CD$ and $\overline{A}BC$ coincidence output were required to be in coincidence with the Encode pulse in order to produce a flag. This was necessary in order to prevent false setting of flags as follows. Even though the analog-to-digital converters and the computer were busy analyzing an event, the fast system generally had recovered. In this case,

an event may have occurred which would not be analyzed but may have produced, for example, a $\overline{A}CD$ coincidence. If the event currently in process in the analyzers was not a $\overline{A}CD$ type event, the flag would have been erroneously set. If, on the other hand, a coincidence must be made between the $\overline{A}CD$ coincidence out-put and the Encode pulse, the flag could only have been produced by the event in process.

6. Beam Sweeper

Since the stop pulse in the time-to-pulse-height converter used in the experiment was taken from the rf of the cyclotron, the stop pulse was normally produced every 44 nsec. If the secondary particle to be detected was a proton of energy less than 0.6 MeV, the flight time for the particle between the target and the 100-μ detector was greater than 44 nsec. (A similar statement is true for other particles with higher mass and higher energy, e.g. alphas with energy less than 2.4 MeV.) In those cases in which the particle flight time was longer than the rf period, the relationship between the start pulse and the stop pulse for the time-to-pulse-height converter was changed since one complete rf (stop pulse) period passed before the particle arrived. The effect of this was to improperly identify the particle type in the TOF system and produced an overlap in the time spectra at low energies. The "overlap" problem was of course most severe for light targets from which many low energy protons and other particles were produced.

One method used to avoid this problem is to make the time interval between incident proton bursts longer than the time of flight of the slowest particle of interest. In this experiment the time increase

must be accomplished without a change in the fundamental frequency of the rf system.

The system used in this experiment was to eliminate alternate proton bursts by deflection of these onto the entrance collimator of the beam analyzing magnet.[35] The deflector (location shown in Fig. 11) was a pair of plates 1 in. high and 3 ft long on which an rf voltage was applied with a frequency of one-fourth the fundamental rf frequency. The deflector rf was phased with respect to the cyclotron rf such that alternate beam bursts passed through the collimator on nodes of the deflector rf signal. This system would deflect every other beam burst and therefore allow one-half of the bursts to pass through the slit and into the scattering chamber. The effect of "sweeping" the beam was to increase the time between beam bursts to 88 nsec, an acceptable time interval for the experiment. When the "sweeper" was used the system used to generate the TAC stop pulse was changed to compensate for the 88-nsec time interval between beam bursts. This logic is not shown on Fig. 9.

D. Experimental Setup

Figure 11 shows the beam optics system for the Oak Ridge Isochronous Cyclotron pertinent to the experiment. The 60-MeV protons, which were extracted at a frequency of 22.45 mc, traveled from the cyclotron through switching magnet No. 1 and into a 153-degree analyzing magnet whose collimating slits fixed the beam resolution. After passing

---

[35]The "Beam Sweeper" System was designed by J. Martin and S.W. Mosko, Electronuclear Division, Oak Ridge National Laboratory.

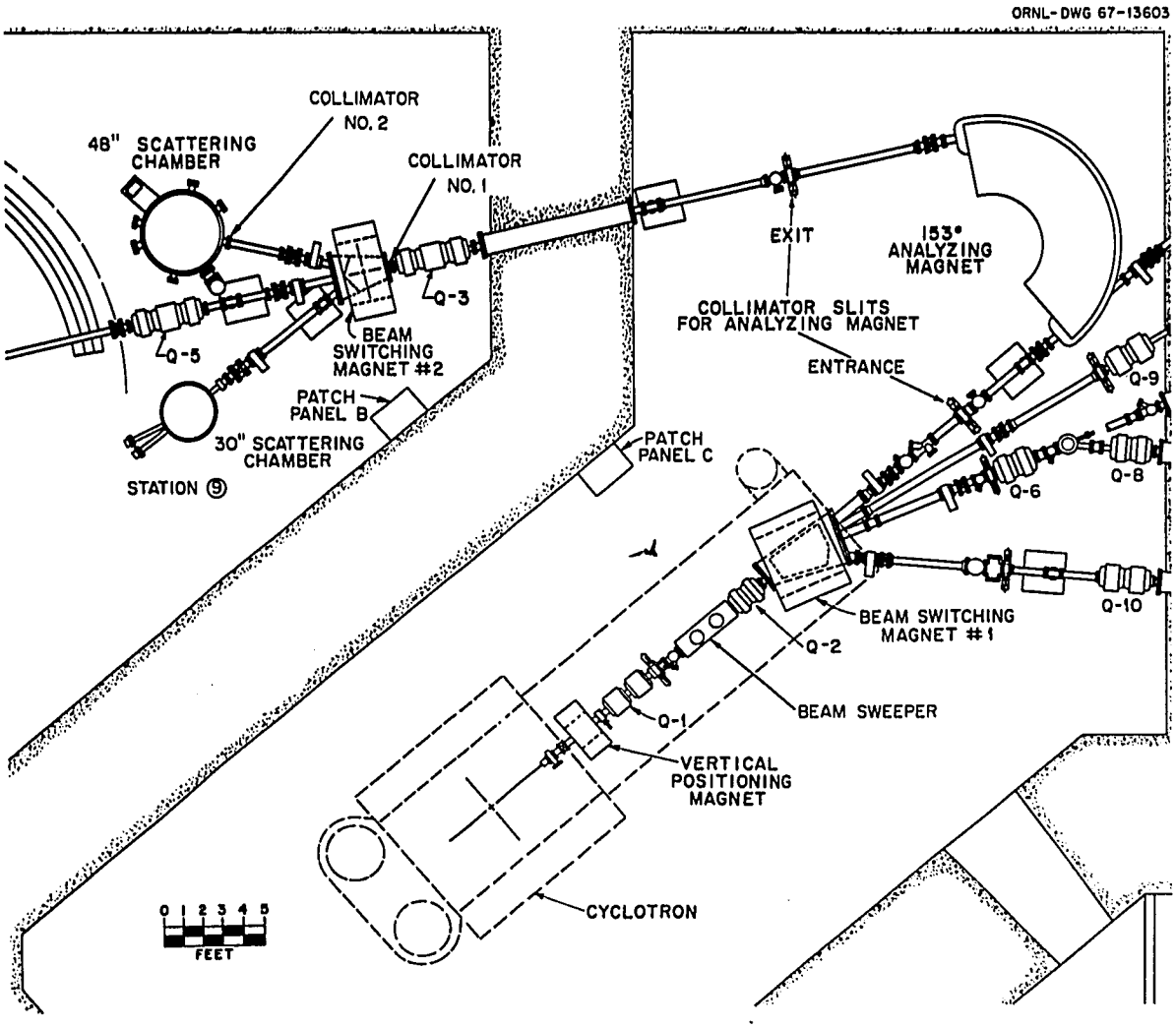

Fig. 11. Cyclotron Beam Optics System.

through the analyzing magnet exit slit, the beam passed through a focusing quadrupole then was bent 20 degrees into the scattering chamber.

The scattering chamber with the entire detector assembly mounted is shown in Fig. 12. The vacuum chamber was 48 in. in diam with two remotely rotatable detector arms and a rotatable target holder which held up to five targets. The beam entered the chamber through a lucite beam pipe seen in the upper left-hand corner of Fig. 12, passed through a 9/16-in. collimator and through an anti-scattering collimator at the end of the pipe, hit the target located at the chamber center and was stopped in the Faraday cup seen in the lower right-hand corner. Located at 20 degrees to the right (as the beam travels) of the Faraday cup is a range wheel which was used to measure the beam energy, and 20 degrees to the left of the Faraday cup is a NaI monitor counter shielded in lead. Since all slow preamplifiers and fast amplifiers were located inside the chamber, all leads (~20) were run in vacuum and were long enough (~7 ft) to move to any angle. These entered near the top of chamber above the monitor counter through vacuum-tight BNC connectors fastened in lucite plates. The metal cables entering the chamber above the detector system were used to supply and vent liquid nitrogen for the germanium detector and pump out the vacuum jacket around the liquid nitrogen supply.

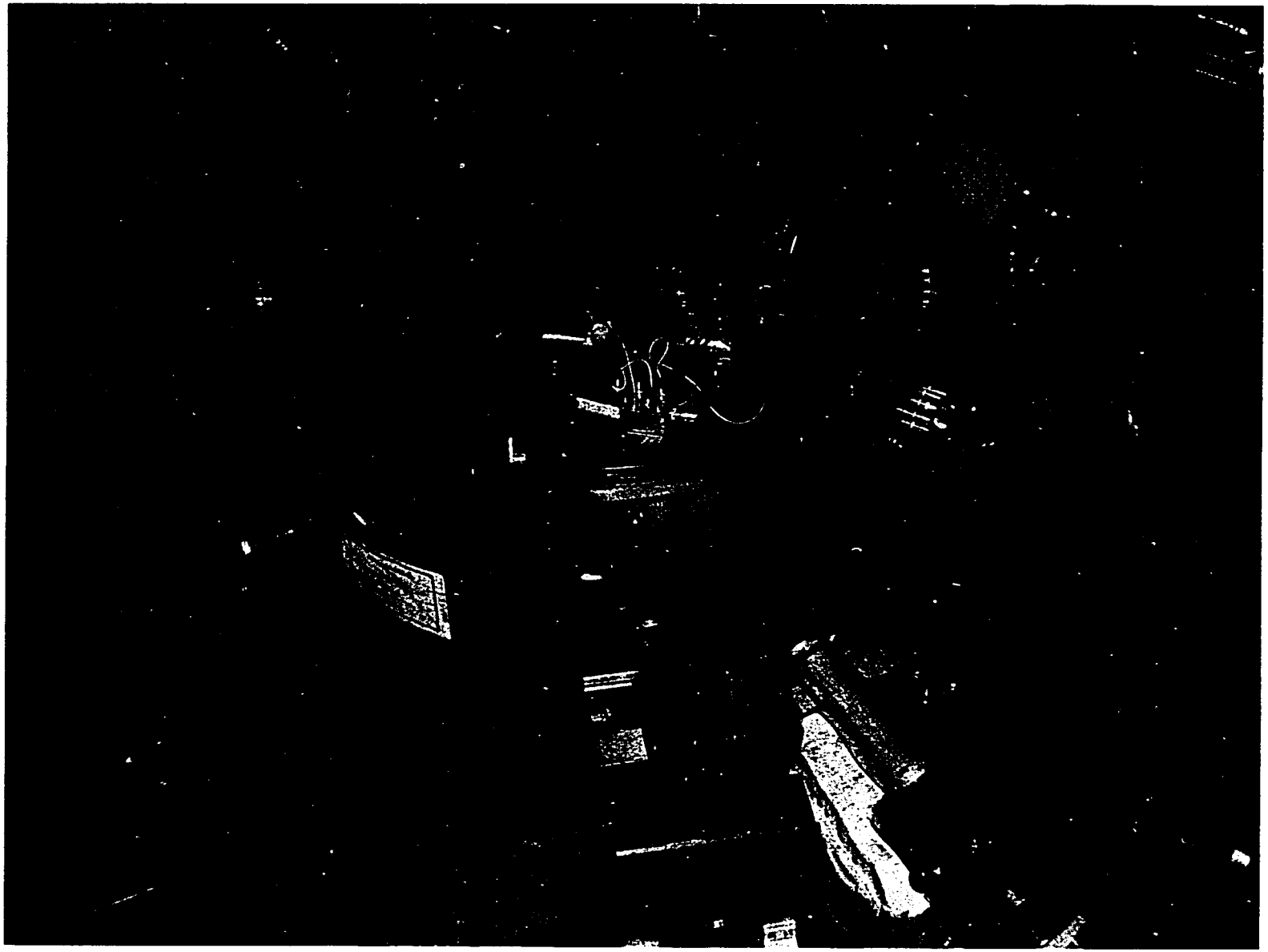

Fig. 12. Scattering Chamber.

E. Beam Monitoring

1. Incident Current Measurement

A Faraday cup[36] was used during the experiment to monitor the number of incident protons. The charge collected in the Faraday cup was measured in a transistorized current integrator of high stability[37] which was calibrated by use of a current through a 10^{10}-Ω resistor known to a precision of 0.10%. The voltage across the resistor was measured with a digital voltmeter to 0.1% accuracy. The output of the integrator was counted on a scalar, and a count rate meter in the integrator gave average beam current. Tests of the integrator calibration were made during a run with other precision current sources which had been calibrated against the standard resistor discussed above.

Since the carbon beam stop in the Faraday cup is hit by the direct beam, considerable backgrounds of gamma rays and neutrons are produced. To attenuate background neutrons a shield of lithiated paraffin was placed around the Faraday cup to moderate the neutrons. The detector system inside the scattering chamber was shielded from background gamma rays by 4 in. of lead placed on the outside of the chamber at the level of the detectors and a 1-in.-thick lead collar was placed around the germanium detector. Figure 11 shows the paraffin shield partially installed around the Faraday cup and the lead gamma ray shield.

---

[36]The basic design of the Faraday cup is given in the following reference: R. T. Santoro and R. W. Peelle, "Measurement of the Intensity of the Proton Beam at the Harvard University Synchrocyclotron for Energy-Spectral Measurements of Nuclear Secondaries", ORNL-3505, 1964.

[37]F. M. Glass et al., "A New Approach to Direct Current Integration", IEEE Transactions on Nuclear Science, Vol. NS-14, #1, Feb. 1967, p. 143.

2. Beam Energy Measurement

The energy of the incident proton beam was obtained from a measurement of the range of the protons scattered at 20 degrees by the targets used. This measurement afforded an energy calibration independent of estimates obtained from the magnetic field of the beam analyzing magnet in the cyclotron system.

The range measurement was made using a "Range-Wheel"[38] which contains up to 30 aluminum foils of known thickness, that can be remotely rotated into the beam in various combinations. The protons were detected in two silicon surface barrier detectors, a 500-μ detector placed in front of the absorber and a 300-μ detector placed after the absorber. The number of counts from a coincidence between the two detectors was plotted as a function of absorber thickness. The thickness corresponding to half height on the count axis was converted to incident beam energy through use of range-energy tables. The accuracy of the energy measurement is $\sim \pm$ 0.1 MeV.

The Range-Wheel was located at a scattering angle of 20 degrees and, since it did not interfere with use of the experimental detector system, it was used as an energy monitor at any time during a run.

3. Monitor Counter

The beam was monitored by a counter, separate from those used in the experiment, placed at a fixed angle of 20 degrees (opposite side of the beam line from the range-wheel) outside the chamber. This detector consisted of a NaI crystal which was cylindrical and tapered

---

[38] R. T. Santoro, F. E. Bertrand, et al., "Beam Energy Measurements at the Oak Ridge Isochronous Cyclotron", ORNL-TM-1382, 1966.

from 5/8 in. diam at the front to 3/4 in. diam at the back and was 3/4 in. high. The crystal was mounted on an RCA Type 7764 phototube and the entire assembly was shielded in lead. An integral pulse height discriminator was used on the signals from the phototube, so that only the protons elastically scattered from the target were counted. A stabilizer was used in the integral discriminator to insure that the threshold was always set just below the elastic peak and did not drift due to phototube gain changes.

4. Collimator System

The system used to define the incident beam size consisted of three collimators which were designed so that the beam current lost on each collimator could be monitored. The collimators are discussed below.

a. Collimator No. 1 was located, as is shown in Fig. 11, between the Focusing Quadrupole and Beam Switching Magnet No. 2, ~ 17 ft from the target. The collimator was made of $\frac{7}{8}$-in.-thick carbon with a $1\frac{1}{2}$ in. diam hole in the center and was constructed in four separate quadrants which were insulated from each other so that the current in each section could be monitored. The amount of beam lost on this collimator varied from 0 to 20%.

b. Collimator No. 2 was located 30 in. from the target on the beam line, and was made of $\frac{7}{8}$-in. carbon with a 9/16-in. hole in the center. In an experiment the beam was focused so that less than 1% of the beam current was lost on this collimator.

c. The third collimator in the system, visible in Fig. 12, was an anti-scattering baffle. The purpose was to prevent the

detector system from detecting any particles directly from the edges of Collimator No. 2. The collimator system was designed to permit data to be taken at angles as small as 7 degrees.

Although the beam was focused in a $\frac{1}{4}$-in-diam spot, it was possible with the collimator system described above for unscattered protons to be found as far as $\frac{1}{2}$ in. from the beam center line. In order to avoid the scattering of these protons from any non-target material, the targets were constructed wide enough to allow the normal to the target to be rotated as far as 55 degrees with respect to the incident beam.

F. Run Setup

The procedure necessary to set up for data taking is listed below. The order listed is not necessarily the order in which the various operations must be performed.

a. The beam was obtained in the scattering chamber and focused to a $\frac{1}{4}$-in.-diam spot at the center of the chamber.

b. The energy of the proton beam was measured.

c. The B and C detectors were calibrated using α sources which were permanently placed in back of the 100-μ detector and in front and back of the 500-μ detector. The two sources used were ^{241}Am and ^{234}U. The germanium detector was calibrated using the elastically scattered protons from the target. All three detectors were calibrated for 0.050 MeV/channel.

d. The biases on the fast discriminators were set as described below. In the case of the B detector the smallest energy loss which must be detected in the fast system in order that the

logic system operate properly was from a 10-MeV proton, which just stops in the 500-μ detector. The peak from p-p scattering at 65 degrees, from a CH target falls at ~12 MeV for 60-MeV incident protons. The bias in the B fast discriminator was set above noise but such that no counts were lost in this peak, i.e., the detector fired on every 12-MeV proton. In the case of the 500-μ detector the smallest pulse which must be detected in the fast system was produced by the protons elastically scattered at a small angle (i.e., the highest energy events). The bias on the C discriminator was therefore set so that no counts were lost from the elastic peak. This bias setting was determined from a curve of counts in the elastic peak versus discriminator setting which should exhibit a region of bias in which the number of counts in the peak was constant. The bias was chosen above noise and in the "flat" region of the curve. The bias on the D fast discriminator was set as low as possible without firing on noise from the fast amplifier or double-firing which causes malfunction of the pile-up system.

e. Since the usable entrance window on the germanium was only ~ 5mm wide, some difficulty was encountered in obtaining correct alignment between the collimator and the germanium detector. Improper alignment resulted in large low energy tails on the peaks caused by an excessive amount of scattering out of the germanium. The correct alignment was obtained by movement of the collimator until a good peak shape was obtained.

f. It was necessary to check the operation of the soft collimator. Since most of the events which hit the soft collimator pass through it, a check could be made to determine whether the collimator produced a pulse for every event hitting it. The same method was used to insure that the bias on the collimator discriminator was set below the minimum pulse height produced by an event which penetrated the collimator. The smallest energy loss in the collimator was ~ 1.5 MeV, lost by 60-MeV protons. Through the use of a CH target it was possible to see a peak in the spectrum, ~1.5 MeV below the elastic peak which was well-separated from the 4.4-MeV inelastic level. The bias on the A detector was lowered and/or the voltage on the phototube was raised until no energy loss peak was seen.

G. Data Acquisition

A "run" for the experiment is taken to mean data obtained for a given target at one angle. The procedure for each run is listed below.

a. Target to be used was placed in beam.

b. Detector angle was set remotely to angle to be studied.

c. Target angle was set so that the target normal was perpendicular to the detector system (i.e., detector angle = target angle) up to 55 degrees for the target angle. For detector angles greater than 55 degrees the target angle remained fixed at 55 degrees. (The target angles used for back-angle data were the supplement of those used at forward angles.)

f. When data was being taken:

f-1. Scalers were checked for indication of logic system malfunction.

f-2. The display options on the computer were checked. These options were: a map of B + C + D vs B + C or B + C vs B or TOF vs B in which each data point was "flickered" (momentarily intensified) as the computer received it. A time exposure photograph must be taken to determine the quality of the data being displayed. It was also possible to display a spectrum of B + C + D or B + C, both of which were stored in the computer.

g. After the run was over some magnetic tapes containing the data and the analysis program were taken to the ORNL IBM 360/75 computer for immediate analysis. The results of the analysis were used to determine the angles to be studied in the remaining runs as well as to indicate any malfunction of the detector or electronic systems.

h. After all runs were taken during a 3- or 4-day experiment, the response of the detector system was obtained by placing the detector in the direct beam. The cyclotron was adjusted so that the beam intensity was only 100 to 200 protons/second. A gold foil $\sim$ 0.002-in.-thick was inserted in the beam to insure that the beam was spread over the entire germanium detector. In this manner the response of the detector system to protons of a single energy (within the beam resolution) was measured. The information from this measurement determined

the amount of reaction and collimator tail caused by the total absorption detector and showed up any other contribution to the scattered data which may have been produced by the detector system and not by the targets under study.

CHAPTER III

DATA ANALYSIS

A. Form of Data

Each scattering event which produced an acceptable Alert as described in Chapter II, Section C 3, was characterized by four pulse heights which have been termed B, C, D, and T (time of flight). The contents of the four analyzers were read into the computer after each event and each pulse height was transmitted as one computer word which in the case of the PDP-8 was 12 bits long. The four words also contained the flag information received from the fast logic system. Figure 13 shows a diagram of the location of the 46 data and flag bits in the various words.

The contents of the four words were stored in a 512-word data buffer in the computer memory and when the buffer was full data was transferred to a second 512-word buffer, then written on IBM compatible magnetic tape. Seven-track tape was used which implied the need to split each 12-bit word into two halves so that each word was written on the tape as six bits with a parity bit, followed by the other six bits and a parity bit. In this manner each time the data buffer in the PDP-8 was written on tape, a record of 128 events was produced. An analysis[39] program on the IBM 360/75 read the data tapes and analyzed each event separately.

B. Determination of Particle Type

In order to properly fix the type and energy of the particles, the analysis program examined the flags for each event and stripped the pulse heights from the PDP-8 words. It was necessary to examine

---

[39]The analysis program was written initially by P. Aebersold and revised by D. Putzulu.

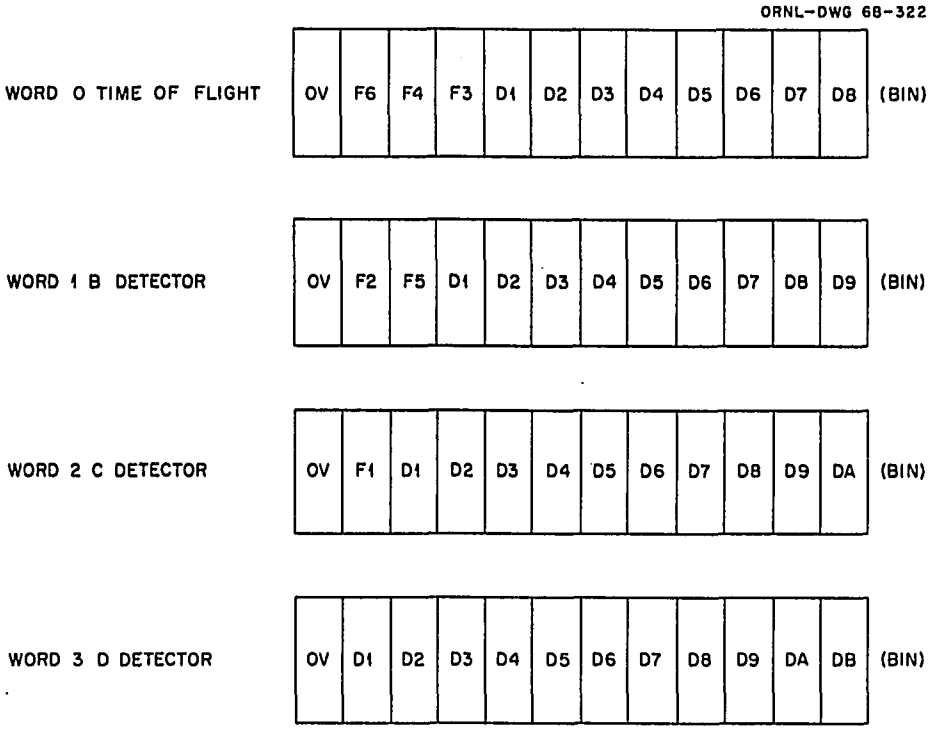

F1 = $\bar{A}$ B C COINCIDENCE FLAG
F2 = $\bar{A}$ C D COINCIDENCE FLAG
F3 = FLAG FOR INCOMPLETE BUFFER OUTPUT
F4 = PILE-UP FLAG
F6 = PULSER FLAG
OV = OVERFLOW
DN = DATA BIT N

Fig. 13. Location of Data and Flag Bits in PDP-8 Words.

the flag conditions for each event in order to determine the nature of that event. Two 12-bit PDP-8 words were combined to form one 32-bit word, with two "padded" zeros placed on the beginning of each byte (6 bits). Flags were checked by masking off the selected bit and storing the value (zero or one) in an array. After all flags had been stripped from the data words, only the pulse heights remained and these were kept in the program as four variables IB, IC, ID, and IS.

If the pulser flag had been set indicating the "event" was artificially created, the pulse heights IB, IC, and ID were stored in an array which identified pulser and baseline spectra for each detector. No further analysis was performed on this event.

If a pile-up flag or any overflow flag was present, the event was not analyzed. However, it was necessary to count the number of events not analyzed, in order to correct for dead time as discussed later.

1. $\Delta E \times E$ Identification

The flags which indicated coincidence conditions for an event were crucial to the analysis since they determined the system by which identification of particle type was to be performed.

The logic of these flags is summarized in Table I. It should be noted that, from each of the pulse heights IB, IC, and ID, the channel in which zero pulse height was stored in the respective analyzers has been subtracted.

TABLE I

Coincidence Flag Logic as Applied to Choice of Particle Type Identification

Flag 1 Status	Flag 2 Status	Type of Identification	ΔE	E
Yes	Yes	ΔE x E	IB+IC	IB+IC+ID
No	Yes	ΔE x E	IB+IC	IB+IC+ID
Yes	No	ΔE x E	IB	IB+IC
No	No	TOF	--	IB

The data, which at this point were an energy loss and a total energy, were stored in an array at reduced precision for output of the form shown earlier in Fig. 5.

The type of particle involved in the event was deduced by fitting the energy loss and total energy for each event between predicted energy loss versus total energy distributions which would arise from protons, deuterons, tritons, helium-3's and alphas entering the counter telescope. The particle type was now denoted by a number from 1 to 5 corresponding to proton, deuteron, triton, helium-3 or alpha and the event was stored at full energy precision (0.05 MeV/ch) in an array which contained the number of particles of type N which had the same ΔE and E values. If it happened that the particle could not be identified within any of the distributions, the event was stored in a separate array for later inspection.

It was pointed out in Chapter II, Section B 2, that the theoretical pulse-height distributions for the various types and energy of reaction particles were obtained from a calculation based on the Landau

distribution of energy loss. From these distributions a maximum and minimum pulse height for a particular energy and particle type were obtained. The assumption here is that all particles of the same type with the same incident energy will lose an amount of energy in the ΔE detector between the maximum and minimum of the Landau distribution.

The use of distributions based on Landau calculations to identify particle types proved successful for the intermediate and high energy events and less than satisfactory for lower energy events.

Inherent in the use of such a method for a priori prediction of energy loss distributions is the accurate knowledge of the thickness of material traversed. A small error in thickness will make a small error in the energy loss for energetic particles, but when the energy loss is an appreciable fraction of the incident energy, for instance in the case of low energy alphas, a small error in the thickness of material greatly affects the predicted distribution.

In this experiment, in which the material traversed was a detector whose characteristics made thickness measurement by mechanical means difficult or impossible, the knowledge of the thickness was not sufficiently accurate to give a proper prediction of the low energy distribution.

To circumvent this problem the distribution for the low energy data was taken directly from the raw data maps, as seen in Figs. 5(a) and 5(b). This method has proven quite satisfactory since the separation between particles was complete. A set of lines, once drawn from data taken with one set of ΔE detectors, did not have to be redrawn until a different set (different thickness) of detectors was used.

2. Time-of-Flight Identification

In the case that an event did not penetrate the first ΔE detector, identification of particle type was made by a knowledge of the particle's energy and time of flight to the 100-μ detector. As is shown in Table I, the existence of such an event was "signaled" by the presence of neither coincidence flag accompanying a valid data event.

The analysis of the time-of-flight data was performed on the PDP-8. An IBM 360/75 program calculated the mass (in AMU) of the particle for each event which required time-of-flight analysis. The event was then stored in an array as a function of particle mass and energy and the array was written on magnetic tape when all the events had been sorted. The PDP-8 program read the array from the magnetic tape and displayed the mass versus energy spectrum, such as the one seen in Fig. 6, on the oscilloscope. An energy spectrum for each mass distribution was obtained by drawing, with a light pen, discrimination lines around each distribution. The program then summed the counts between each set of discrimination lines and printed out spectra of counts versus energy for each distribution.

C. Corrections to Spectra

Corrections have been made to all the data for energy loss in dead layers in the detector system and loss of particle energy by nuclear reactions in the germanium detector. Other corrections, also described below, have been made to some of the data.

1. Dead Layer Correction

As discussed previously the dead layer in the detector system was considered to be any nondetector material in the path of the reaction

particles as they penetrated the counter telescope. The amount of dead layer in the path of the detected particles in this experiment was ~ 3.6 mg/cm^2 of Ni and was located between the second ΔE counter (C) and the total absorption counter (D). This location implies that only those particles penetrating C (i.e., Flag 2 events) had to be corrected for dead layer losses.

The correction was made to the energy spectrum of each particle by adding an amount of energy loss, based on the energy of the event after it penetrated both ΔE detectors (as determined from the raw $\Delta E \times E$ data), to each energy channel. It was assumed in the correction that the particle traversing the dead layer always lost a mean-energy loss as predicted by Range-energy tables of Peelle[40] and the mean-energy losses for each particle for a few energies were read into the program. Dead layer corrections for energies between those read in were obtained by interpolation.

2. Reaction Tail Correction

Nuclear reactions within the germanium total absorption detector resulted in an energy loss from an event, which produced a "tail" on each peak. The effect of this tail was to reduce the number of counts in the peaks and to distribute those counts in the channels below the peaks.

Since the reaction tail associated with a given peak, as observed in a $\Delta E \times E$ map as in Fig 5(b), was distributed along a constant ΔE value over all energies below the peak, it was possible for the tail

---

[40]R. W. Peelle, "Rapid Computation of Specific Energy Losses for Energetic Charged Particles", ORNL-TM-977, 1965.

from, for example, a peak in the deuteron spectrum to cross the distribution of protons. This effect is shown schematically in Fig. 14. A deuteron peak is shown at a total energy E_D, and the tail from the peak extends below the peak with a constant ΔE value. This tail crosses, and therefore adds counts to, the regions shown cross-hatched in the proton distribution as well as part of the deuteron spectrum. Since the identification of particle type is performed directly from the energy loss - total energy data, the counts added to the protons by the deuteron tail will be incorrectly identified as protons from the target.

To correct for the effects of the reaction tail, it was necessary to: 1) add counts to each energy channel to compensate for counts lost through reactions, 2) subtract counts from the region below the peak in each particle distribution affected.

Measurements were made of the amount of tail produced by various energy particles with the detector system in the direct beam as described in Chapter II, Section B 4. The results of these measurements are shown in Table II in the column labeled "Measured"..

TABLE II

Peak to Total Ratio for Germanium

Particle	Energy (MeV)	% Tail Measured	% Tail Calculated ($1/E^2$)
Proton	60	~6.0	6.0
Proton	38.6	2.25	2.48
Alpha	58.8	0.3	0.0

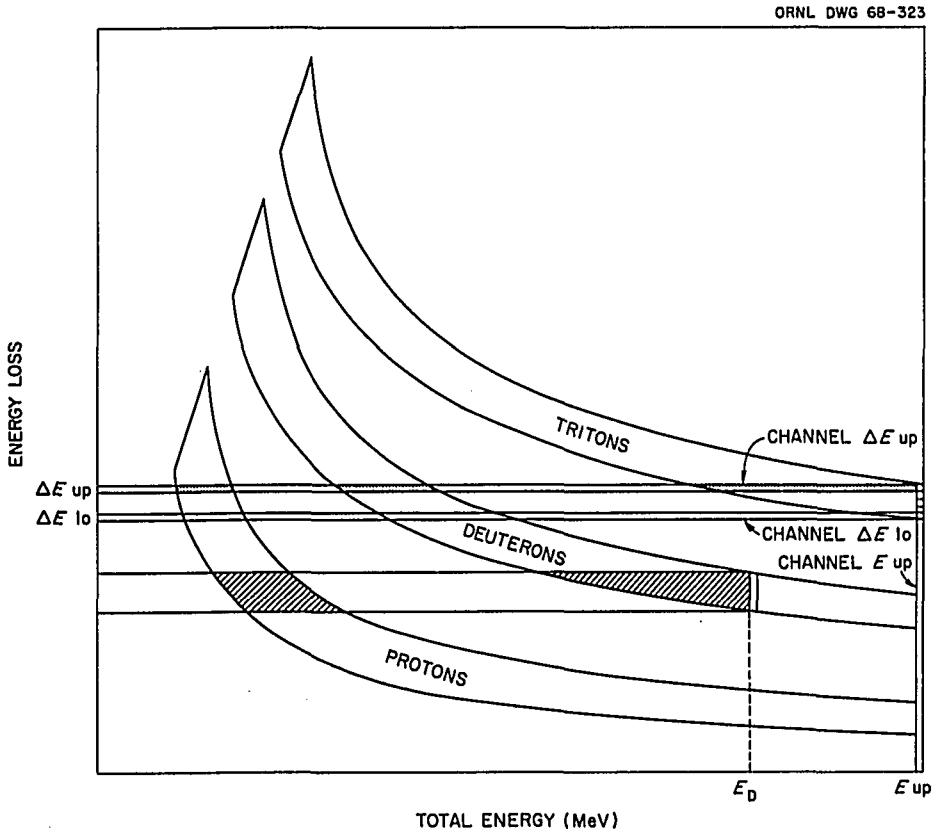

Fig. 14. Schematic Representation of Reaction Tail Correction.

The following assumptions about the amount of reaction tail were made, based on the measurements in Table II and on data reported on NaI.[26,41]

a. The reaction tail was caused only by the total absorption detector.

b. The (reaction tail area/total area) for 60-MeV protons, deuterons, and tritons is 6%.

c. The percentage tail falls off as $1/E^2$.

d. No tail was produced by helium-3 and alpha particles.

e. The tail was evenly distributed over all energies below the peak.

To perform the correction the analysis program first searched for the highest total energy channel in which counts were found in the triton distribution. This channel is shown in Fig. 14 as E_{up}. There were several ΔE channels which comprised the energy loss distribution of the tritons with energy E_{up}, the highest labeled ΔE_{up} and the lowest ΔE_{Lo} and the reaction tail was assumed to be formed from the counts in each (ΔE, E_{up}) "bin". The program began with energy loss channel ΔE_{up} and multiplied the number of counts in that bin by $\left[1 + 0.06 \left(\frac{E_{up}}{60}\right)^2\right]$, to correct for counts scattered out. The program next searched along the constant energy loss value ΔE_{up} to locate the intersections of this energy loss channel with the triton, deuteron, and proton distributions. The regions between these intersections are shown shaded in Fig. 14, and it was from these regions that counts were subtracted. The number

---

[41] Philip G. Roos, "Elastic and Inelastic Scattering of High Energy Proton from Nuclei", Ph.D. Thesis (University of Maryland, 1964).

of counts subtracted from each channel in the shaded region was determined by [Number of Counts in Bin (ΔE_{up}, E_{up})]/channel E_{up}. The program then repeated the calculation for the counts in Bin (ΔE_{up-1},E_{up}) and for each energy loss channel in the distribution down to ΔE_{Lo}.

Upon completion of the correction for all energy loss channels with total energy E_{up} in the triton distribution the calculation was repeated for the next lower energy channel, E_{up-1}, in the triton distribution, and for all channels in the triton distribution. The correction was then applied in the same manner to all channels in the deuteron spectrum, then all channels in the proton spectrum. For the data taken, the deuteron levels from the reactions $^{12}C(p,d)^{11}C$ at a small angle produced the most tail which had to be removed from the proton data. For the worst case observed the deuteron peaks in the carbon data at 15 degrees produced at most 1% of the counts in the proton energy region between ~ 17 and 22 MeV.

3. Correction for Hard Collimator Tail

In two series of runs, it was necessary to use a hard collimator made of $\frac{1}{4}$-in.-thick Ni with a 0.73 mm x 0.36 mm hole in it. The use of a hard collimator introduced a second type of tail to the data as described in Chapter II, Section B 2. Since this tail was produced along the normal distribution of reaction particles, the correction was made to the individual separated spectra.

The percentage of counts found in this "tail" was determined from a run with the detector system in the direct beam. It was found that ~ 4.5% of the counts in the direct beam peak were scattered by the collimator into a region from ~ 1.6 MeV below the peak to an energy

of ~ 2 MeV, with a maximum ~12 MeV below the peak.

To correct the scattered data, it was assumed that the tail was produced mostly by the elastic or inelastic peaks, which dominate the energy spectra between ~ 40 and 60 MeV, and 4.5% of these counts were subtracted from the spectra in a distribution as described above.

The validity of the assumption that only the high energy particles contribute to the "collimator edge tail" may be examined by considering the ways in which a scattered particle may interact with the collimator and then enter into the detector system. The reaction particles may scatter from the inside edges of the collimator, they could penetrate the material of the collimator after entering the hole and be scattered back into the system, or they may penetrate the outer face of the collimator and scatter into the system before they are stopped in the collimator material. The probability of occurrence of the first and second types of interaction is determined by the solid angle the inner edge of the collimator edge subtends at the target. It was found that the collimator edges subtended only ~1% as much solid angle as the collimator area, and therefore only a small part of the 4.5% collimator scattering observed can be explained by inner edge interactions. If, then, the collimator scattering is dominated by processes which require the particles to enter the face of the collimator and then scatter into the hole, the probability of the occurrence of such events must be a function of the range, therefore energy, of the scattered particles.

The range of protons has dropped by a factor of two from an energy of 60 MeV to 40 MeV, and the proton range drops rapidly for still lower energies. It is seen, then, that lack of correction of the data for

collimator scattering of particles with energy less than ~40 MeV does produce an error in the data. This error is at most 2% and is always a positive error since the particles are scattered into the system in all cases.

D. Systematic Errors in the Data

1. Energy Loss in Targets

The targets used in this experiment were made as thin as possible (limit was set by the large area required) in order to keep energy loss by the reaction particles in the targets to a minimum. Although high energy secondary particles lost only a small amount of energy (typically 30 KeV for 60-MeV protons) in the target, low energy particles, especially alphas, lost a more significant amount of energy. The data presented in Chapter IV have not been corrected for the effects of such an energy loss.

Since the lowest energy secondary particles lose the most energy in the target, a correction would add back more energy to these events than to ones with higher observed energies. The effect of such a correction would be to shift to higher energy the observed low energy distribution and increase the cross section in the peak of this distribution.

The energy loss in the target in this experiment was only significant for helium-3 and alpha particles and the amount of energy loss was less than 1 MeV for the data to be presented. As is pointed out in Chapter IV, the alpha particle data from carbon is cut off at 2.5 MeV since below this energy the alphas lose a large part of their energy in the target or are stopped completely in the target. The

thickness of the target did not set the low energy cutoff for any of the data from ^{54}Fe or ^{209}Bi.

The energy losses shown below are mean energy losses which assume that the reaction occurred in the center of the target.

Carbon:		
	2.5 MeV alphas	0.600 MeV
^{54}Fe		
	12 MeV alphas	0.300 MeV
	8 MeV alphas	0.500 MeV
^{209}Bi		
	26 MeV alphas	0.400 MeV
	16 MeV alphas	0.500 MeV

In the case of ^{54}Fe and ^{209}Bi no alphas were observed with energies less than 4 MeV and 13 MeV respectively.

2. Energy Accuracy

It has been pointed out in Chapter II, Section F, that the B, C, and D detector systems were each calibrated at a gain of 0.05 MeV/channel. The germanium detector (D) was calibrated using the elastic proton peak while the B and C detectors were calibrated with ^{241}Am and ^{234}U alpha sources. The data analysis program assumed that the gain was the same for the three detectors and it further assumed that the gain of the three was equal to the gain of the D detector. However, in practice the gains of the B and C detectors were at times 1.5 to 2% different from that of the germanium system.

The difference in detector gains produced little error in the energy of the high energy peaks since most of the energy for such events was deposited in the germanium detector and the error would be

at most 2% of a small energy loss in B plus C. Evidence of this small error for the peaks is provided by the small difference, ~ 1%, between the observed and published Q-values for prominent inelastic peaks.

However, when an event deposited most of its energy in B and/or C, the use of the D gain could result in a larger error in the energy. For example, the energy of a 10-MeV peak observed in the proton spectrum could be in error by 0.2 MeV.

The error of 1.5 to 2% in the calculated energy caused by unequal gains was larger than any error incurred from nonlinearity of the analyzers. The integral linearity of each analyzer was measured before and after each run and the analyzers were found to be linear to a few tenths of a percent except for the lowest 50 channels of the B analyzer.

The shape of the experimental spectra could be affected by a differential nonlinearity of the pulse height analyzers. For example, such a nonlinearity could produce artificial peaks and valleys in the experimental data. The differential linearity of each analyzer was measured several times during the course of the experiment and it was found that the C and D analyzers were linear (differential) within 2% over the upper 99% of the channels used, while the B analyzer produced this result over all but the lowest 40 channels. The nonlinearity in the low B analyzer channels could have affected the shape and resolution of the high energy peaks, since the energy loss in B from high energy events would fall in the lower channels of that analyzer.

3. Multiple Scattering Error

In Chapter II, Section B 2, it was pointed out that, due to multiple scattering, some particles left the C detector at such an angle that

they were not detected in the germanium although they should have been. These counts appear in the data as a "bogus" distribution on the B + C versus B data maps such as Fig. 5(a).

Although the data presented here has not been corrected for the multiple scattering effect, it is possible to estimate the magnitude of the error produced in the spectra. As can be seen in Fig. 5(a), the "bogus" distribution merges with the "real" proton distribution for energies on the total energy axis greater than ~6 MeV. It was also pointed out in the previous discussion that the total energy of these events as observed in Fig. 5(a) would be the energy loss of the events if they had been properly detected and placed on the B + C + D data map. Therefore, it is possible to determine the number of particles scattered out of the proton spectrum between energies of 12 MeV and 24 MeV, but it is not possible to determine the magnitude of the effect for proton energies less than 12 MeV.

For all runs except one set (2000 series) it was found that between the energies of 12 and 24 MeV of the secondary proton spectra ~6 to 10% of the total protons observed were scattered out with a distribution that increased in magnitude from ~1% at 24 MeV to ~15% at 12 MeV. The magnitude of the effect was approximately 60% larger for the 2000 series of runs.

4. Angular Resolution

The angular resolution in this experiment was determined by the collimator width and the diameter of the beam spot on the target. The angular resolution in the worst case (target and detector angle set at 55 degrees) was ±1.2% degrees.

The angular resolution of 1.2 degrees could have been considerably worse for low energy reaction particles emitted from the target. The low energy particles could have undergone considerable multiple scattering in the target and could leave the target at a different angle from which they were emitted in the initial reaction. It is to be seen in Chapter IV, however, that the angular distribution of the low energy particles is very nearly isotropic and therefore not sensitive to poor angular resolution.

E. Calculation of Physical Quantities

Once the energy spectra which give counts in each energy region or channel were obtained for all particles, it was possible to compute the cross sections for scattering into each energy region of the spectra. The expression used to compute the differential cross sections was

$$\frac{d\sigma(\theta)}{d\Omega} = \frac{I(\theta)\ A}{I_o\ N_o\ t\ \Delta\Omega} \qquad (3.1)$$

where:

I_o = number of incident particles

$I(\theta)$ = number of particles scattered through an angle θ into the detector

$\Delta\Omega$ = solid angle into which the particles are scattered

N_o = Avogadro's number

A = atomic weight of target

t = target thickness in g/cm^2.

The absolute monitor of the number of incident protons was a Faraday cup used with the current integrating system described in Chapter II, Section E.1. The output pulses from the integrator were counted and

the number of incident protons were computed from the integrator calibration.

The area of the rectangular collimator was obtained by measuring the length and width of the opening with a traveling microscope, and the distance from target to collimator center was measured in the same manner. The error in measurement of the beam-to-collimator distance was ~1%. The solid angle is calculated from these quantities as A/D^2. The use of the center of the collimator as the point for distance measurement resulted in an over-estimate of the solid angle by 1.5% The data reported in this work have not been corrected for this error. The target average thickness and uniformities are given in the next chapter.

In order to facilitate cross section calculations for the major, well separated peaks in the spectra, a peak search was included in the analysis program. Peaks were found by testing the number of counts in a four-channel region for significance above the sum of counts in the two channels below and above this region. The four-channel region was moved across the spectrum until a peak was found. When a peak was located, the maximum width and peak channel were determined, and the program computed the number of counts in the peak, subtracted the background which was the average of the counts in the channels $\frac{1}{2}$ peak width above and below the peak region, calculated the total cross section in millibarns per steridian for the peak and calculated errors in the cross section based on counting statistics.

To calculate the Q value of the reaction leading to the detected peaks, the analysis program used classical kinematic formula

$$Q = E_3 \left(1 + \frac{M_3}{M_4}\right) - E_1 \left(1 - \frac{M_1}{M_4}\right) - \frac{2\sqrt{M_1 M_3 E_1 E_3}}{M_4} \cos\theta \qquad (3.2)$$

where

M_1, M_3, and M_4 = mass of the incident particle, mass of the light reaction product, and mass of the recoil, respectively

E_1, E_3 = energy of incident particle and light reaction product, respectively

θ = laboratory scattering angle of the light product.

To calculate the Q value accurately it was necessary to know the energies of the peaks as accurately as possible. The gain (MeV/ch) was obtained by calculating the energy of the elastic peak and dividing this by the elastic channel as obtained in the peak search.

The masses of the scattered particle and the recoils were obtained from mass tables by Mattauch.[42]

Although the peak search worked adequately for peaks that were well above background and were well separated, it missed many peaks in the spectrum. The cross sections for these peaks were obtained by hand calculations or by a "peak-stripping" program written for the PDP-8.

---

[42] J. H. E. Mattauch et al, Nuclear Physics 67, 1-31 (1965).

CHAPTER IV

RESULTS

A. General

The experimental system as described in Chapter II adequately fulfilled the capabilities required in the first chapter. The raw data maps of energy loss versus total energy and TOF versus energy, as shown in Figs. 5 and 6, are typical of the separation between secondary particles for all targets. The lower limit of observed secondary energy was in most cases determined by the target nucleus and not by the apparatus.

The best resolution obtained with the germanium detector was approximately 0.1% over an incident proton energy range of 20- to 60-MeV. However, the germanium resolution typically obtained during the experiment, when using two ΔE detectors preceding the germanium as described in Chapter II and using analyzing magnet slit openings wide enough to permit reasonable beam currents, was ~180 keV. The 180-keV resolution was typical for data taken with 60-, 39-, and 28-MeV incident protons. The resolution of the silicon surface barrier detectors used as ΔE detectors for this experiment was less than 50 keV for a 5-MeV alpha particle.

The detector system and associated electronics as described were assembled in the final form over a series of runs during the period of approximately 12 months. It is for this reason that not all of the data taken show the secondary spectra down to the lowest energies. A brief description of the character of the data from each run is listed in Table III along with the date of the run.

TABLE III. CHARACTERISTICS OF RUNS

Series	Date	Incident Particle	Incident Energy (MeV)	Collimator Type	Description of Data	System Malfunctions
1000	8/66	Proton	60.5	Soft	Only 1 ΔE detector FL(2) used and no time-of-flight. Energy cut off for protons ~9 MeV. Energy cut off for alpha particles ~36 MeV.	Some flag 2's set falsely.
3000	10/66	Proton	61.5	Soft	Two ΔE detectors used as in final system - no time-of-flight.	Some flag 1's and flag 2's set falsely.
4000	12/66	Proton	61.3	Soft	Two ΔE detectors used - few time-of-flight runs.	Anti-pile up circuit failure prevented use of pile up flag. Poor peak shape.
5000	2/67	Proton	61.7	Hard	Two ΔE detectors used - time-of-flight without beam sweeper.	Time-of-flight resolution poor (2 nsec)
6000	4/67	Proton	38.6	Soft	Final system.	
6100	4/67	Alpha	58.8	Soft	Final system. Sweeper not used.	
7000	6/67	Proton	60.9	Hard	Final system.	
2000	10/67	Proton	61.9	Hard	Final system.	Some data lost due to apparent failure of Victoreen overflow system. D detector eliminated from pile up.
0000	12/67	Proton	28.5	Hard	Final system.	
0100	12/67	Proton	61.5	Hard	Final system.	Some elastic and inelastic data lost due to poor germanium resolution at very low detector voltage. Some FL(2) not set.

As was pointed out in Chapter I, it was desired to cover a wide mass range of target nuclei during this experiment. This necessitated a compromise between the amount of data taken for each run (i.e., each angle for each target) and the number of angles and targets to be used. The presentation of a good angular distribution of differential cross sections for scattering to discrete levels requires many angles, while the small cross section for (p, ^{3}He) reactions, for example, necessitates a counting time much longer than would be needed to present the total spectrum or the (p,p′) and (p,d) levels. The compromise attempted was to count for a long time at a few of the angles in order to ascertain the Q-values and a rough indication of the differential cross sections of all the reactions to discrete levels, while the other data were taken for only enough time to obtain (p,p′), (p,d), and total spectra with sufficient statistics. For this reason, the statistics in even the ground state transitions for (p,t), (p,^{3}He), and (p,α) data are too poor in many cases to yield a cross section for many runs.

It was mentioned previously that the germanium detector was encapsulated behind a 0.0002-in. Ni window. Since the window was in the path of the detected particles, it constituted a dead layer to the particles. Although the energy lost in such a thin dead layer is small for a 60-MeV proton, for each particle there is an energy for which the particles end their range in the window.

If a particle, for example a proton, loses nearly all of its energy in the first two detectors (B and C), it may stop in the nickel window. This event would look like a "BC" event and not a "CD" event since the

particle never reached D. The total energy would, of course, be incorrectly summed since some of the energy is lost in the nickel.

For protons, the effect of the dead layer should first be noticed at ~9.3 MeV since this is the maximum proton energy that is stopped in 621 μ of silicon. The dead layer increases the effective thickness of the silicon detector so that ~9.45-MeV protons are stopped in the combinations. Since the fast discriminator bias on the germanium (D) detector was set at ~300 keV, the effective range of the ΔE detectors plus dead layer plus effect of the germanium bias. However, those protons between the energies of 9.3 and 9.75 MeV should have been detected in the germanium, but were suppressed by the effective dead layer and appear in the B + C spectrum with an incorrect energy. The same argument is true for alpha particles in the energy range of ~37.2 MeV to 37.75 MeV.

Since the 3.6 mg/cm^2 dead layer of nickel can absorb a maximum of 600 keV proton energy, or 2.4 MeV alpha energy, the region below 9.3 MeV for protons and 37.2 MeV for alphas contain events which rightfully belong in the B + C + D spectrum but were stopped by the dead layer.

B. Targets

Data was obtained from the following targets: ^{12}C, ^{16}O, ^{27}Al, ^{54}Fe, ^{56}Fe, ^{89}Y, ^{120}Sn, ^{197}Au, and ^{209}Bi. This paper will be concerned only with the ^{12}C, ^{54}Fe, and ^{209}Bi data.

The targets, with the exception of carbon, oxygen, aluminum, and gold, were prepared by the Isotope Division of the Oak Ridge National Laboratory. The targets used for carbon were made of polystyrene (4000, 5000, 7000, and 2000 runs) and polyethylene (1000, 3000, and some 2000) plastic foil. The aluminum target used was commercial high purity foil.

Table IV shows the characteristics of each target used. The thickness of each target except the bismuth target was obtained from the weight of the $\frac{1}{4}$-in-diam piece of the target that the beam struck. The accuracy of the weight and the uniformity of the $\frac{1}{4}$-in. diameter provided a measurement good to less than 1%. The thickness of the bismuth target was obtained from the energy loss of ~5 MeV alpha particles in the target. This measurement was good to ~±2%.

The uniformity of each target was measured by scanning the target, in 2-mm sections, with an alpha source. The incident alpha energy and the energy remaining after foil penetration were converted to range (mg/cm^2) by the use of tables by Janni[43] which were normalized to experimental specific energy loss data.[44] The uniformity was obtained from the change in energy loss from the alpha particles with the location of the 2-mm spot on the target. The maximum and minimum thickness were taken as those thicknesses within a 1-cm^2 area around the target center, which encompassed 75% of the thickness values

---

[43] J. F. Janni, "Calculations of Energy Loss, Range, Pathlength, Straggling, Multiple Scattering, and the Probability of Inelastic Nuclear Collisions for 0.1- to 1000-MeV Protons", Tech. Report No. AFWL-TR-65-150, Air Force Weapons Lab., Research and Technology Div., Air Force System Command, Kirkland Air Force Base, New Mexico.

[44] S. Gorodetzky et al., Nuclear Phys., A6702, 133 (1967).

TABLE IV. TARGET CHARACTERISTICS

Material	Isotopic Purity (%)	Thickness (mg/cm^2)	Fabrication
CH_2	natural carbon	0.94 ± 0.009	plastic foil
CH	natural carbon	2.40 ± 0.024	plastic foil
Mylar	natural oxygen	0.927 ± .009	plastic foil
^{27}Al	100	4.78 ± 0.048	rolled
^{27}Al	100	1.24 ± 0.012	rolled
^{54}Fe	97.2	3.26 ± 0.033	rolled
^{56}Fe	99.7	4.00 ± 0.040	rolled
^{89}Y	100	3.66 ± 0.037	rolled
^{120}Sn	98.4	4.85 ± 0.049	rolled
^{197}Au	100	7.02 ± 0.070	rolled
^{209}Bi	100	9.25 ± 0.093	evaporated

measured. The uniformity of the three targets reported in this work was ~±3%.

The isotopic purity of those target elements for which there are more than one stable isotope was obtained from the Isotopes Division of the Oak Ridge National Laboratory and is the result of a spectroscopic analysis. Some carbon and oxygen contamination of the foils was observed in the data: however, the contamination was very small and, in cases where the contaminant peak fell inside an inelastic level from the target, the inelastic data was not analyzed.

C. Backgrounds

It was pointed out in Chapter II that the data acquisition system could be "triggered" only by the occurrence of:

1) An event which produced a "B" fast pulse above the discriminator setting.
2) An $\overline{A}CD$ event.

Since the B detector thickness was only 0.1 mm, the probability was small that anything but a charged particle could produce a B "alert". The requirement of a CD coincidence for an alert also made the probability of analysis of noncharged particle events small even though the germanium detector was sensitive to gamma rays. However, a large number of target-associated events with energies less than ~400 keV were detected in the 100μ detector. These events, probably electrons, were discriminated against by a 400-keV "software" bias in the PDP-8 data accumulation program.

Since it was possible for charged particles from other sources than the target to trigger the detection system, data was taken to evaluate the background contribution to the data. Data was obtained

using a blank target holder with the detector system at 15 degrees and target at 15 degrees and with the detector at 90 degrees and target at 55 degrees. These angles represent what should have been the worst case for background.

Essentially no background was observed at 90 degrees and the background observed at 15 degrees would contribute at most 1% of the data obtained at 15 degrees with a light mass target. No correction has been made to the data for this small contribution from background since the contribution is smaller than the errors in the cross-section measurement, as will be seen below.

D. Background from Bismuth Target Holder

The bismuth target used in this experiment was to be extremely fragile due to its zize, thickness, and character. It was necessary to mount the target in a rigid frame made of 0.020-in.-thick aluminum so that the target would not break. An identical "blank" target holder was used to measure the contribution to the observed spectra from the aluminum frame in the same manner as the background contributions were measured.

The "blank" spectra were taken at detector angles of 15 degrees and 60 degrees, with the target angles at 15 degrees and 55 degrees, respectively. It was found that at 15 degrees the bismuth frame could have contributed as much as 50% of the experimental counts for secondary energies less than 10 MeV. For angles greater than 30 degrees, however the contribution to the data from the bismuth holder was negligible.

It was judged that the particles scattered into the detector system, which were nearly all of energy less than 10 MeV, were low energy protons elastically scattered from the aluminum target holder. Since "blank" data had been obtained at 15 degrees, the 15-degree data from the bismuth target was corrected directly from the background run after the background counts were normalized to the number of incident protons used in the target run. Corrections were made to the 20-, 25-, and 30-degree data by reducing the counts obtained from the 15-degree blank run by the ratio of the Rutherford cross section for aluminum at 15 degrees to the Rutherford cross section for the angle in question, then subtracting the "reduced" background from the target data. The Rutherford cross section has been found to give a good prediction of the elastic scattering from aluminum at energies between 9 and 17 MeV, [45,46] for angles this small.

E. Faraday Cup Calibrations

It was pointed out in Chapter II that a Faraday cup was used for the absolute measurement of the number of incident protons for each run. It is generally assumed that the charge collection efficiency is unity; however, the accuracy of a Faraday cup is dependent on the number of charged particles which scatter into or out of the cup.

There are several factors which may contribute to an imperfect current measurement with a Faraday cup. Among these factors are: backscattering of electrons created by collisions of protons with

---

[45] A. E. Glassgold et al., Phys. Rev., 106, 6, 1207 (1967).

[46] A. E. Glassgold and P. J. Kellog, Phys. Rev., 107, 5, 1372 (1957).

atomic electrons of the cup; Compton electron production in the cup; electrons from the target entering the cup; ion formation in the cup; and connector leakage. Although the Faraday cup used in the present work was designed[36] to prevent or reduce the effect of the above factors, it was believed necessary to experimentally measure the charge collection efficiency of the cup. Very few such efficiency measurements have been made, and perhaps the most accurate measurement[36] was to ~±5%. It was hoped that with the use of "fast" counting equipment a significant improvement could be made in the accuracy of this measurement.

The efficiency was measured by placing two NE-102 plastic scintillators (in coincidence) in the direct beam, in line with and ~3 in. from the Faraday cup entrance. The total thickness of the counters was 1.5 mm and it was calculated that less than 0.1% of the incident protons would be scattered out of the Faraday cup by this thickness of material. Although it was possible for electrons to be produced in the scintillators, a magnet placed at the Faraday cup entrance was calculated to provide sufficient field strength to prevent these electrons from entering the cup. (The same magnet also reduced the number of electrons which were scattered out of the cup.)

The measurements were made with count rates between 0.5×10^6 and 1×10^6 protons/sec. In order to obtain such a low beam intensity, the cyclotron was operated with the arc off, the gas flow turned off, the filament off, and at times the Dee voltage was mistuned. The charge deposited in the cup was measured with a vibrating-reed electrometer capable of the measurement of currents as small as 10^{-13} amps. This

electrometer and associated Roysan integrator were calibrated against the current integrator used in the data collection and described earlier.

The electronics used in this measurement were capable of counting at rates of 100 megacycles, so that dead time corrections were negligible. The number of times protons occurred in successive beam bursts was measured and from this measurement the number of beam bursts which contained two protons can be calculated. This correction is necessary since the counting apparatus cannot distinguish two protons in one burst although the Faraday cup measures the appropriate charge for two protons in a burst. The magnitude of "two in burst" corrections was typically 1 to 3%.

The average difference between the number of protons measured with the counters and that as measured by the cup was less than 1% over a series of seven runs with varying incident count rates.

Although this measurement showed the error in Faraday cup efficiency to be negligible, it did not measure the effect which multiple Coulomb scattering of the incident protons by the target could have on the measurement of the number of incident protons. A calculation was performed based on the multiple scattering theory of Moliere, as described by Bichsel,[47] in order to determine the magnitude of such effects in this experiment. The results of these calculations show that less than 0.5% of the incident protons were scattered in the target through an angle so great that they would miss the Faraday cup.

---

[47]H. Bichsel, Passage of Charged Particles Through Matter, American Institute of Physics Handbook, 2nd ed., McGraw-Hill, 1963.

F. Dead Time Correction

In general, the experimental dead time was considered to be the period of time that was taken up on the analysis of an event and during which other events occurred and were not analyzed. There were several factors which contributed to the dead time in the present experiment. A few of these are charge collection time of the detectors (no larger than 200 nsec), resolving time of the fast logic system (the limit was determined by the ~1.6 μsec dead time of the D fast discriminator), conversion time for Analog-to-Digital converter (~100 μsec), and time taken to write data on magnetic tape. It is seen that the limiting factors were the conversion and tape writing times.

In this experiment, the total dead time correction factor was determined by the ratio of the total number of events acceptable for analysis to the total number of events actually analyzed and put on tape. It will be recalled that the total number of acceptable events detected could be obtained by a count of the numbers of "Alert" pulses, and the number of hardware-analyzed events could be determined from a count of the "Trigger" (Encode) pulses, since the system analyzed an event for each Trigger pulse. It is seen, then, that the relative dead time or percentage of time that the analysis system is busy is given by [(Alerts/Triggers)-1] x 100. (If the system analyzed each event detected, it is seen that this ratio would be one which would imply zero dead time.) The data is compensated for this dead time by increasing the factor by which counts are multiplied to obtain cross section, by the quantity "Alerts/Triggers".

The ratio of Alerts to Triggers is a measure of the system dead time only if the Alerts and Triggers are produced by a "real" events. It was found that at times the B fast amplifier produced an rf oscillation of very fast frequency, with a pulse height above the discriminator threshold, and this noise produced a great number of artificial Alerts for which there were no Triggers. In such cases, the ratio of Alerts to Triggers is not a true measure of the dead time. The dead time for runs in which a large number of Alerts were produced artificially was calculated from the ratio of all Flag 2 (CD) events detected to the number of Flag 2 events analyzed. This ratio, in general, is sensitive to the same analysis system dead times that the ratio of Alerts to Triggers is; however, since the CD flag can only be fired from a coincidence, this count is less susceptible to noise in the detectors or amplifiers. A comparison of the dead time correction, as measured by these two systems, shows a typical variation between the measurements of less than ±2%.

A second, effective dead time was caused by nonanalysis of an event or whole tape record by either an analysis program logic decision or by the failure of the analysis program to read a record from the tape. It war rare for the program to encounter more than one record-reading error out of ~2000 records.

The "software" dead time was determined from the ratio of the number of events eliminated in the analysis program to the total number of "real" events analyzed. The eliminated events were of the following types: each tape record not read eliminated 128 events; any event which produced an overflow; any event which produced a pileup

flag; and any event which produced a sum of the type B+C or B+C+D which was greater than the 1264 channels. It should be noted that each event could only be eliminated once, even if the event produced more than one condition for elimination. The number of real events was taken to be (128 x number of records) - (number of pulser events) - (number of padded events). A padded event is one that is written on tape as the uncompleted part of the PDP-8 data buffer at the time of a run termination. These events were flagged. The "software" dead time is compensated for by multiplying the factor (number by which counts must be multiplied to give cross section) by the ratio; total number of events/(total number of events-number of eliminated events).

The criterion which determines whether a particular type of eliminated event affects the dead time should be whether the eliminated spectrum, i.e., are the eliminated counts random in energy? It seems clear that the events not analyzed due to tape reading failure or the events not analyzed due to pileup are random in energy and their elimination could affect the entire spectrum. However, the elimination of an event because the event produced, for example, a B overflow does not imply that these eliminated events affected all regions of the energy spectrum. In the case of bismuth, for example, many high energy fission fragments were detected (and stopped) in the B detectors. These events produced a number of overflows; however, it is clear that these overflows (therefore eliminated events) could not affect cross sections of other regions of the bismuth spectra. The inclusion of such eliminated events in the "software" dead time produced

an error of less than 0.5% for all cases and is therefore considered to be negligible.

G. Errors in Cross-Section Calculations

The error incurred in the cross-section measurement is a combination of the errors in the measurement of the quantities which comprise the cross-section calculation. It is assumed that the combined error for each measurement is the square root of the sum of the squares of each individual relative (%) error.

1. The error in the measurement of the total number of incident protons was measured to be less than 1%.
2. The nonuniformity of the targets reported in this work was ~±3% and this variation introduced a maximum error in the thickness of the target of ~±1.5%.
3. The maximum typical discrepancy in the dead time measurement is ±2%. This value is used for all runs except as noted by larger errors.
4. The measurement of the target thickness is known to less than ±1%, except for the bismuth target in which case the uncertainty is ~±2%.

The combination of the above errors leads to a total nonstatistical error of ±3%, except in the case of bismuth where the error is ±4%.

H. Data Compilation and Presentation

The cross sections for excitation of discrete levels of the nucleus through reactions of the type (p,p′), (p,d), etc., were calculated by hand extraction of the number of counts in the peak or by extraction of the peak counts through the use of a light pen on the PDP-8 computer.

(Figure 26 shows a typical spectrum from which the peak counts were extracted.) It was assumed (in both the hand calculations and the PDP-8 calculations) that the peaks rose from a smooth continuum which ended a few MeV before the elastic peak energy. The continuum cross section was not included in the cross section for the peak. In cases in which the separation between peaks was not complete the counts in each peak were determined by drawing the assumed peak shape over each peak and dividing the counts in the overlap regions between the two levels. No error was assigned to the data due to ambiguity in the peak "stripping" method for imperfectly separated peaks. The cross sections, in millibarns per steradian, for the excitation of discrete levels are given in tables to follow for both the center of mass and laboratory systems. The error, in millibarns per steradian, and the lab and center of mass scattering angles are also given in the tables.

The cross section in the region below the elastic peak, including the discrete levels, were averaged over 1-MeV bins. That part of the binned data which was obtained by the ΔEXE system is listed in Appendix A. The data at each angle is represented by the energy of the bin center in MeV, the average cross section in the 1-MeV bin in millibarns per steradian per MeV, and the error due only to counting statistics given in millibarns per steradian per MeV. The systematic errors discussed in Chapter III, Section G, and in this Chapter, Section G, must be considered with the error listed. The data which were obtained by the time-Of-flight system are also listed in 1-MeV bins. These data are listed in Appendix B and are labeled with the same energy and

cross-section headings as described above.

Data is also presented in a form which is integrated over energy or angle. The integral over energy at a given angle was performed by summing all the counts in a given spectrum down to the low energy cut-off. In the case of the proton spectra the counts in the elastic peak were excluded; however, all inelastic levels were included in the sums. The resolution was sufficient to unambiguously separate the elastic peak from any inelastic levels except in the case of ^{209}Bi where the 0.95-MeV level is unseparated from the tail of the elastic peak at most angles. This level is, however, very weakly excited and introduces negligible error into the sum. The cross sections integrated over energy in millibarns/steradian are listed in the body of the dissertation under the respective target headings.

An integral over angle (from 0° to 180°) was performed for each energy bin of 1-MeV width. The cross section over all angles for each energy bin E_j is obtained from the sum

$$2\pi \sum_{i=1}^{n} \sigma(E_j,\theta_i) \tfrac{1}{2}[\cos(\theta_{i-1}) - \cos(\theta_{i+1})] \qquad (4.1)$$

where i=1 and i=n represent, respectively, the smallest and largest angles at which data was obtained, $\theta_o = -\theta_1$, $\theta_{n+1} = -\theta_n$ degrees. The term $\sigma(E_j,\theta_i)$ represents the cross section of the energy bin E_j for the angle θ_i. The cross sections at each angle between zero degrees and θ_1 and between θ_n and 180 degrees are assumed to be constant and equal to the value of the cross section at θ_1 and θ_n, respectively. The integrals over angle, in millibarns/MeV, for each energy bin are listed in this Chapter.

The total integrated cross section in millibarns for each charged particle from the target is obtained by summation of the angle integrated cross sections for each energy bin over all bins. This cross section in the case of secondary protons excludes all elastic events.

Table V gives a list, for each target, of the angles at which data was taken, the run number, and the factors by which the number of counts must be multiplied to obtain cross sections in millibarns/steradian. The factors allow an estimation of statistical error to be made, based on the cross sections listed in the data tables.

I. ^{12}C Results

The spectra of secondary protons, deuterons, tritons, helium-3, and alphas from ^{12}C at 35 degrees are shown in Fig. 15. The low energy cut-offs observed on these spectra were not set by the lowest energy of emission by the target nucleus (physical cut-off) but were caused by the target thickness. In all of the data reported the thickness of the CH_2 target used ($\sim$0.9 mg/cm^2) caused considerable distortion of the energy spectra below $\sim$2.5 MeV for alphas and $\sim$600 keV for protons. The cut-off in the proton spectrum which was placed at 1 MeV was caused by "fold-over" in the time-of-flight spectrum from events whose time of flight was longer than 88 nsec. It is clear from the raw data time-of-flight maps of ^{12}C, such as the one seen in Fig. 5, that many low energy particles of heavy mass (6 and 7) were observed. For this reason it would be difficult with only 88 nsec between beam bursts to extend the low energy proton data below 1 MeV even with a thinner target. In the case of the helium-3 and triton spectra, the low energy limit was set by still another experimental

TABLE V

List of Angles, Runs, and Factors for Each Target

^{12}C			^{54}Fe			^{209}Bi		
Lab Angle Degrees	Run Number	Factor	Lab Angle Degrees	Run Number	Factor	Lab Angle Degrees	Run Number	Factor
15	7110	1.74×10^{-3}	12	0123	1.40×10^{-2}	15	5030	2.95×10^{-3}
20.8	2007	3.68×10^{-3}	15	5016	3.11×10^{-3}	20	5027	1.32×10^{-3}
25	2052	3.17×10^{-3}	20	4020	1.18×10^{-3}	25	5026	1.68×10^{-3}
30	2000	1.24×10^{-3}	27	5020	3.12×10^{-4}	30	5021	6.01×10^{-4}
35	2001	5.85×10^{-4}	30	5007	3.36×10^{-4}	35	5025	5.43×10^{-4}
40	2033	1.79×10^{-3}	35	4021	1.53×10^{-3}	40	5031	5.23×10^{-4}
45	7102	1.87×10^{-4}	40	5002	9.05×10^{-4}	45	5024	4.12×10^{-4}
55	0103	8.52×10^{-4}	45	4031	3.42×10^{-4}	50	5032	3.45×10^{-4}
60	7115	1.37×10^{-4}	47	5042	5.47×10^{-4}	55	5022	2.20×10^{-4}
65	0105	8.30×10^{-4}	50	5010	5.07×10^{-4}	60	5033	2.54×10^{-4}
70	2032	1.32×10^{-3}	55	4024	3.62×10^{-4}	70	5037	3.14×10^{-4}
75	2017	2.69×10^{-4}	60	5043	5.14×10^{-4}	75	7006	5.62×10^{-4}
82	4001	2.17×10^{-5}	65	5011	1.65×10^{-4}	80	5035	3.31×10^{-4}
90	2023	3.94×10^{-4}	70	5044	6.86×10^{-4}	90	5023	1.71×10^{-4}
110	7113	1.34×10^{-4}	80	5012	1.29×10^{-4}	110	5036	1.66×10^{-4}
160	2060	3.94×10^{-4}	90	4010	1.12×10^{-4}	120	7007	4.24×10^{-4}
			100	2070	1.05×10^{-3}	135	2064	2.46×10^{-4}
			110	5015	1.13×10^{-4}			
			120	7002	3.68×10^{-4}			
			135	4011	7.70×10^{-5}			
			160	2067	1.11×10^{-3}			

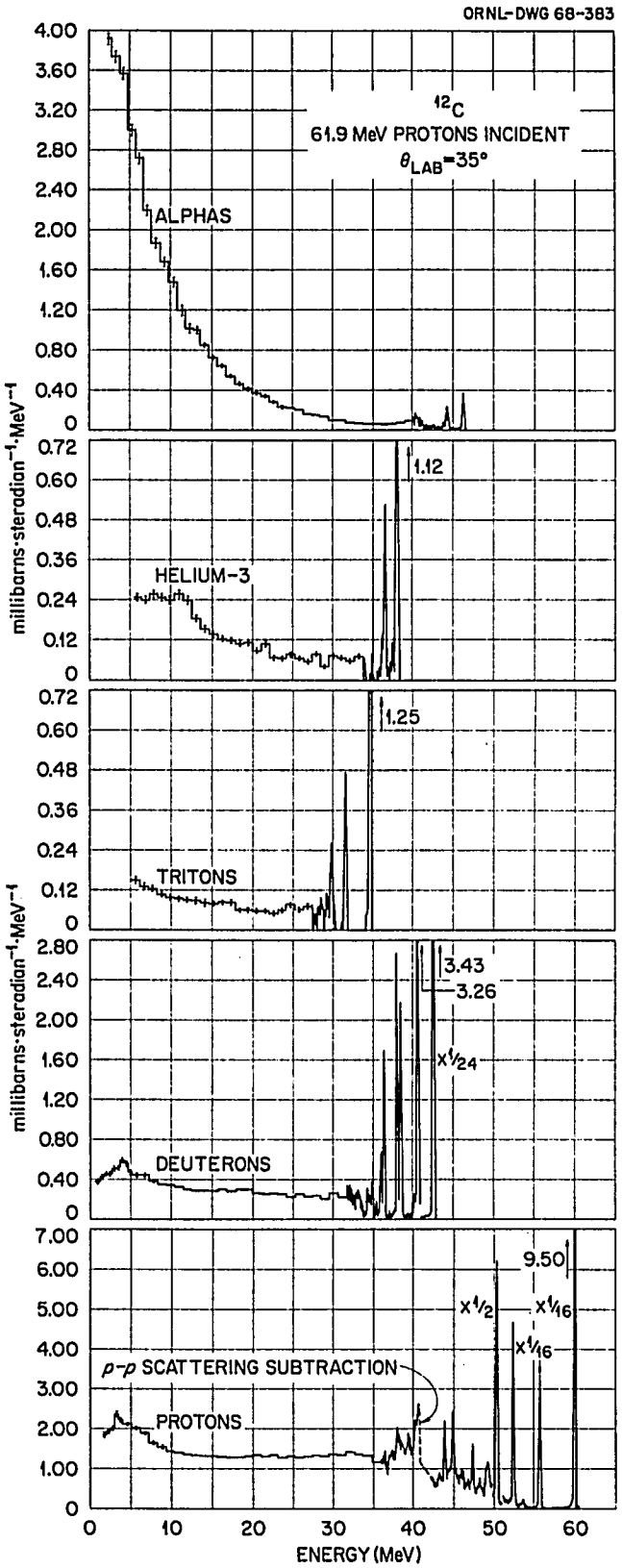

Fig. 15. Proton, Deuteron, Triton, Helium-3, and Alpha Spectra ^{12}C at 35 Degrees.

parameter. The 100-μ detector stopped both triton and helium-3 particles which had energies below ~5.5 MeV and, since both particles have the same mass, it was not possible to distinguish between them in the time-of-flight data. It can also be observed in the triton and helium-3 data shown in Fig. 15 that the cross sections for the production of these particles are not equal nor is the ratio of the cross sections constant, a fact which makes extraction of individual spectra from the combined time spectra ambiguous. It was therefore decided to present the mass-3 data only down to ~5.5 MeV. However, the combined mass-3 cross sections between the energies of 2 and 5 MeV are listed in Appendix B. Although the data was obtained for production of secondary mass 6 and 7 particles, this data was not analyzed for presentation in this work.

The following summarizes the low energy cut-offs for the carbon data:

Protons:	1.2 MeV
Deuterons:	1.2 MeV
Tritons:	5.5 MeV
Helium-3's:	6.0 MeV
Alphas:	2.5 MeV
Combined Mass 3:	2.0 to 5.0 MeV

The use of hydrogenous plastic targets for carbon (CH and CH_2) necessitated the subtraction from the proton data of the peak from proton-proton scattering for angles less than 90 degrees. For forward angles the p-p peak covered part or all of some inelastic proton level from ^{12}C and therefore some angle "gaps" are seen in the inelastic differential cross sections. At most angles, however, the peak from

the hydrogen was quite easy to subtract and left little ambiguity in the shape of the spectrum or magnitude of the cross section. The region from which the peak was subtracted is shown as a dashed line and labeled on Fig. 15.

Figure 16 shows the proton spectra from ^{12}C at 30 degrees and 35 degrees for the first 22 MeV of excitation. It is seen that the good resolution obtained has allowed separation of many inelastic peaks. The levels observed are in good agreement with known levels in the ^{12}C nucleus and with experiments performed at lower energies.[48] The most prominent peaks observed are from excitation of the well-known 4.43, 7.66, 9.76 MeV states. The peak observed at ~10.3 MeV of excitation is too wide to have been formed by scattering by a single level; however, the peaks with Q values -11.85, -12.8, -15.25, -16.25 do appear to be formed by scattering from a single level. These levels are not excited strongly enough to permit extraction of cross sections for angles larger than ~45 degrees. The differential cross sections for elastically scattered protons and for protons scattered by the 4.4, 7.6, 9.6, 12.8, 15.2, and 16.25 MeV levels are listed in Tables VI to X. The differential cross sections for the elastic scattering and for scattering from the 4.4, 7.6, and 9.6 MeV are shown plotted in Figs. 17 and 18. Figure 17 shows the differential cross sections in the center of the mass system for elastic scattering of protons from ^{12}C, ^{54}Fe, and ^{209}Bi. The experimental data are shown as points and the solid curve is a fit to the data based on the optical model and

---

[48] J. K. Dickens et al., Phys. Rev. 129, 2, 743 (1963).

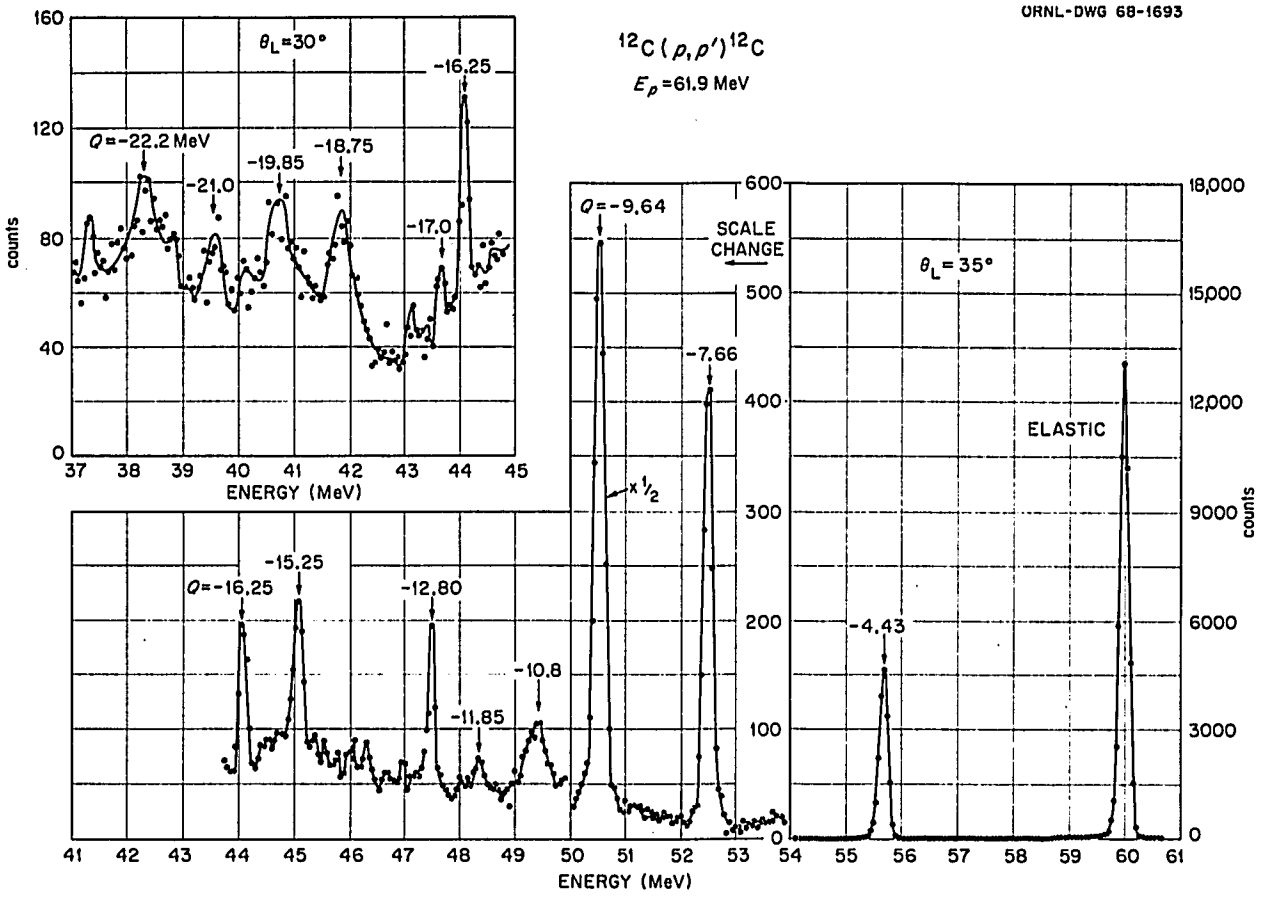

Fig. 16. Spectrum of Inelastic Proton Peaks from ^{12}C.

TABLE VI. TABULATED DIFFERENTIAL CROSS SECTIONS

$^{12}C(p,p)^{12}C$

Elastic Scattering

Lab. Angle (deg)	C.M. Angle (deg)	Cross Section (lab.) (mb/sr)	Cross Section (C.M.) (mb/sr)	Error (± %)
12	13.07	708	598	3
15	16.3	673	570	3
20.8	22.8	359	306	3
25	27.2	156	133	3
30	32.6	81.4	70.2	3
35	38	30.3	26.3	3
40	43.3	8.04	7.05	3
45	48.6	6.26	5.55	3
55	59.2	3.68	3.34	3
60	64.4	2.28	2.10	3
65	69.5	1.17	1.09	3
70	74.8	0.4573	0.4492	6
75	79.9	0.3498	0.3355	6
82	87.1	0.2772	0.2716	5
90	95.1	0.180	0.181	7
110	114.8	0.041	0.0438	7
135	138.6	0.011	0.013	6
160	161.7	0.004	0.0048	33

TABLE VII. TABULATED DIFFERENTIAL CROSS SECTIONS

$^{12}C(p,p')^{12}C$

Q = -4.43 MeV

Lab. Angle (deg)	C.M. Angle (deg)	Cross Section (lab.) (mb/sr)	Cross Section (C.M.) (mb/sr)	Error (± %)
12	13.1	7.62	6.40	3
15	16.4	9.94	8.37	3
20.8	22.9	10.55	8.93	3
25	27.3	10.60	9.02	3
30	32.7	11.3	9.69	3
35	38.1	10.40	8.99	3
40	43.4	5.72	4.99	3
45	48.8	3.89	3.43	3
55	59.4	1.64	1.49	3
60	64.6	1.10	1.01	3
65	69.8	0.823	0.77	5
70	75.0	0.418	0.39	7
75	80.1	0.317	0.30	6
82	87.3	0.16	0.16	5
90	95.3	0.058	0.055	9
110	115	0.029	0.031	9
135	138.7	0.030	0.034	5
160	161.8	0.020	0.024	14

TABLE VIII. TABULATED DIFFERENTIAL CROSS SECTIONS

$^{12}C(p,p')^{12}C$

Q = -7.66 MeV

Lab. Angle (deg)	C.M. Angle (deg)	Cross Section (lab.) (mb/sr)	Cross Section (C.M.) (mb/sr)	Error (± %)
12	13.1	0.677	0.566	10
15	16.4	0.277	0.232	5
25	27.3	0.82	0.696	10
30	32.8	0.83	0.708	6
35	38.2	0.91	0.785	5
40	43.5	0.54	0.475	6
45	46.8	0.38	0.335	5
55	59.5	0.19	0.168	9
60	64.8	0.12	0.106	6
65	70.0	0.68	0.0738	12
70	75.1	0.038	0.0343	19
75	80.3	0.02	0.0190	13
82	87.4	0.015	0.0147	7
90	95.5	0.0073	0.0071	50
110	115.1	0.0085	0.00909	13
135	138.8	0.0045	0.0052	7

TABLE IX. TABULATED DIFFERENTIAL CROSS SECTIONS

$^{12}C(p,p')^{12}C$

Q = -9.64 MeV

Lab. Angle (deg)	C.M. Angle (deg)	Cross Section (lab.) (mb/sr)	Cross Section (C.M.) (mb/sr)	Error (± %)
12	13.2	0.75	0.63	10
15	16.5	0.90	0.75	8
20.8	23.0	1.084	0.91	12
30	32.8	2.40	2.04	4
35	38.2	2.91	2.50	4
40	43.6	2.18	1.89	5
45	48.9	1.99	1.75	4
55	59.6	1.04	0.94	5
60	64.8	0.74	0.68	4
65	70.1	0.59	0.55	6
70	75.2	0.35	0.33	8
75	80.4	0.29	0.28	6
82	87.5	0.17	0.166	5
90	95.6	0.077	0.077	9
110	115.2	0.014	0.015	12
135	138.9	0.0086	0.010	6
160	161.9	0.0104	0.013	20

TABLE X. TABULATED DIFFERENTIAL CROSS SECTIONS

$^{12}C(p,p')^{12}C$

Q = -12.7 MeV

Lab. Angle (deg)	C.M. Angle (deg)	Cross Section (lab.) (mb/sr)	Cross Section (C.M.) (mb/sr)	Error (± %)
12	13.2	0.35	0.29	14
15	16.5	0.36	0.30	12
25	27.5	0.33	0.28	18
30	32.9	0.33	0.28	10
35	38.3	0.21	0.18	10
40	43.7	0.23	0.20	13
45	49.1	0.16	0.14	7
55	59.7	0.13	0.12	11
		Q = -15.2 MeV		
12	13.2	1.16	0.96	8
15	16.5	0.98	0.81	7
20.8	23.1	0.68	0.57	15
25	27.5	0.69	0.58	11
30	33.0	0.56	0.47	10
35	38.4	0.33	0.28	8
40	43.8	0.29	0.25	11
45	49.2	0.09	0.08	10
		Q = -16.2 MeV		
15	16.6	0.40	0.33	12
25	27.5	0.23	0.19	25
30	33.0	0.29	0.24	12
35	38.5	0.29	0.25	7
40	43.9	0.18	0.16	17
45	49.2	0.10	0.09	10

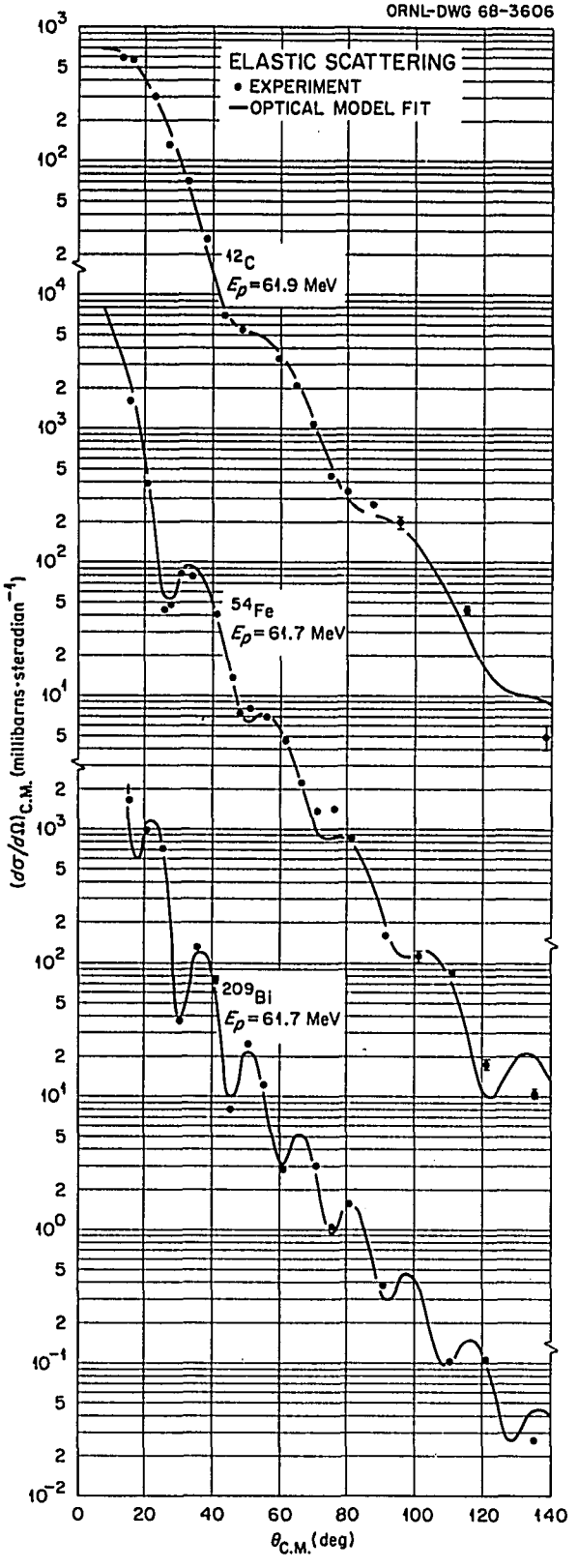

Fig. 17. Elastic Scattering of 62-MeV Protons from ^{12}C, ^{54}Fe and ^{209}Bi Compared to Optical Model Calculations.

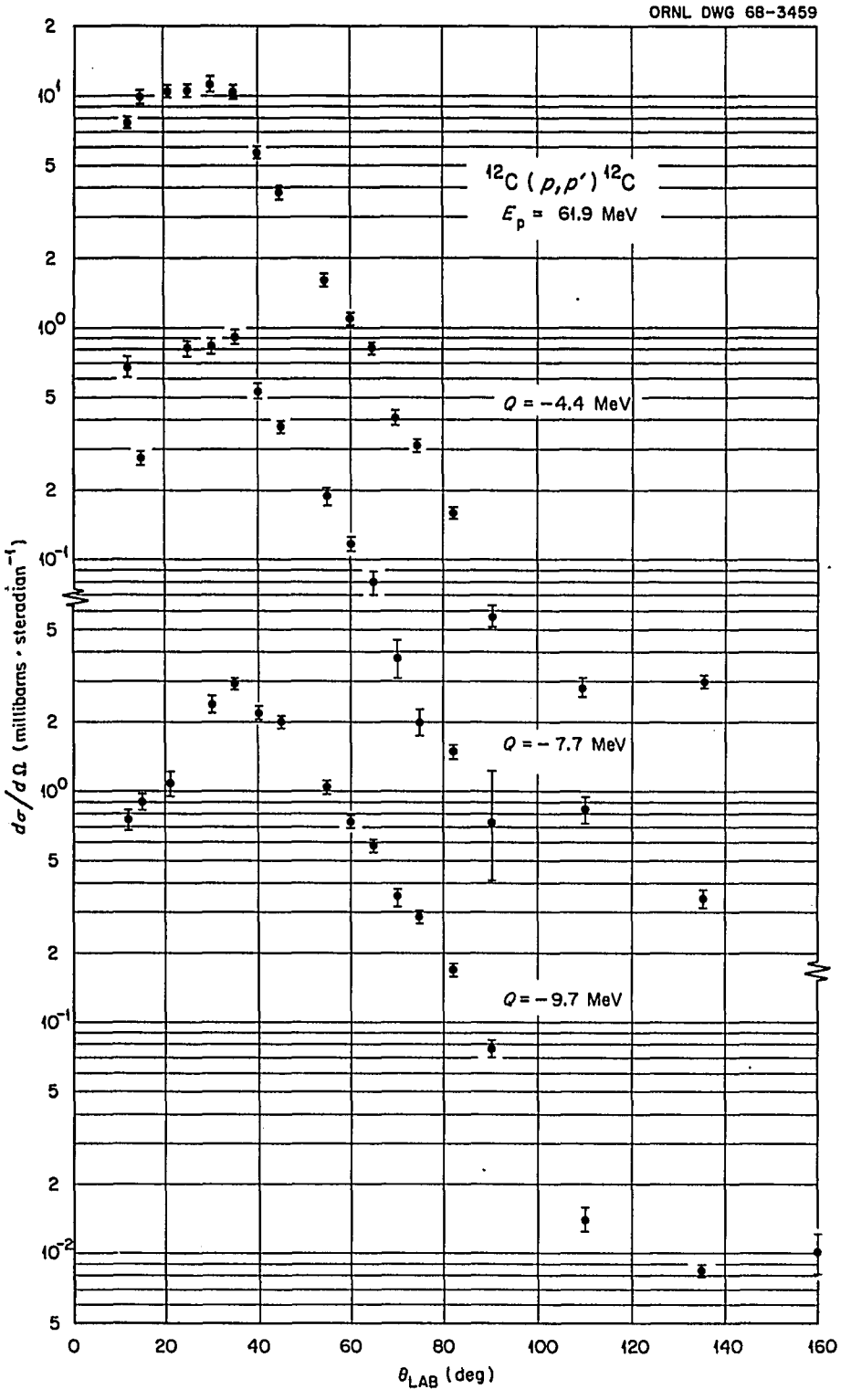

Fig. 18. Differential Cross Sections for the 4.4-, 7.6-, and 9.6-MeV Levels in ^{12}C.

will be discussed in Chapter V. If no error bars are shown for a point on the differential cross-section curves, the error is less than the size of the point shown.

The shape of the differential cross-sections for the elastic and inelastic protons scattered from carbon agree well with data obtained at 40,[48] 50,[4] and 55[50] MeV. It should be pointed out that the minimum in the differential cross-section curve for the -7.7-MeV level is real and supported by the references listed above; however, the errors shown for this point on Fig. 18 are too small (see Table VIII).

The levels observed with Q values of ~20 MeV lie within the dipole resonance region of ^{12}C. Proton excitation of the dipole resonance in carbon has been observed previously;[12] however, the poorer energy resolution of these experiments showed the region to be a broad peak of a few MeV width. The data taken in this experiment show that the region is composed of several levels excited by the incident protons. Levels which are consistently observed have Q values of -18.7, -19.8, -21.0, and -22.2 MeV. The shape and the width of the peaks, however, seem to imply that each peak may be formed by scattering from more than one level in the ^{12}C nucleus.

Figure 19 shows the upper ~11 MeV of excitation for the deuteron spectrum obtained at 35 degrees. Six prominent peaks are observed with Q values of -16.7, -18.7, -21.1, -21.6, -23.3, -23.7, and, although the statistics are poor, three other levels with Q values of 24.3, 24.9, and 25.2 (not labeled on Fig. 17) appear consistently in the

---

[49]M. P. Fricke and G. R. Satchler, Phys. Rev. 139, B567 (1965).

[50]H. Taketani et al., "Numerical Differential Cross Sections of Some Reactions on ^{12}C Induced by 54.9 MeV Protons", Inst. for Nuclear Study, University of Tokyo, Report No. INS J-88 (1965).

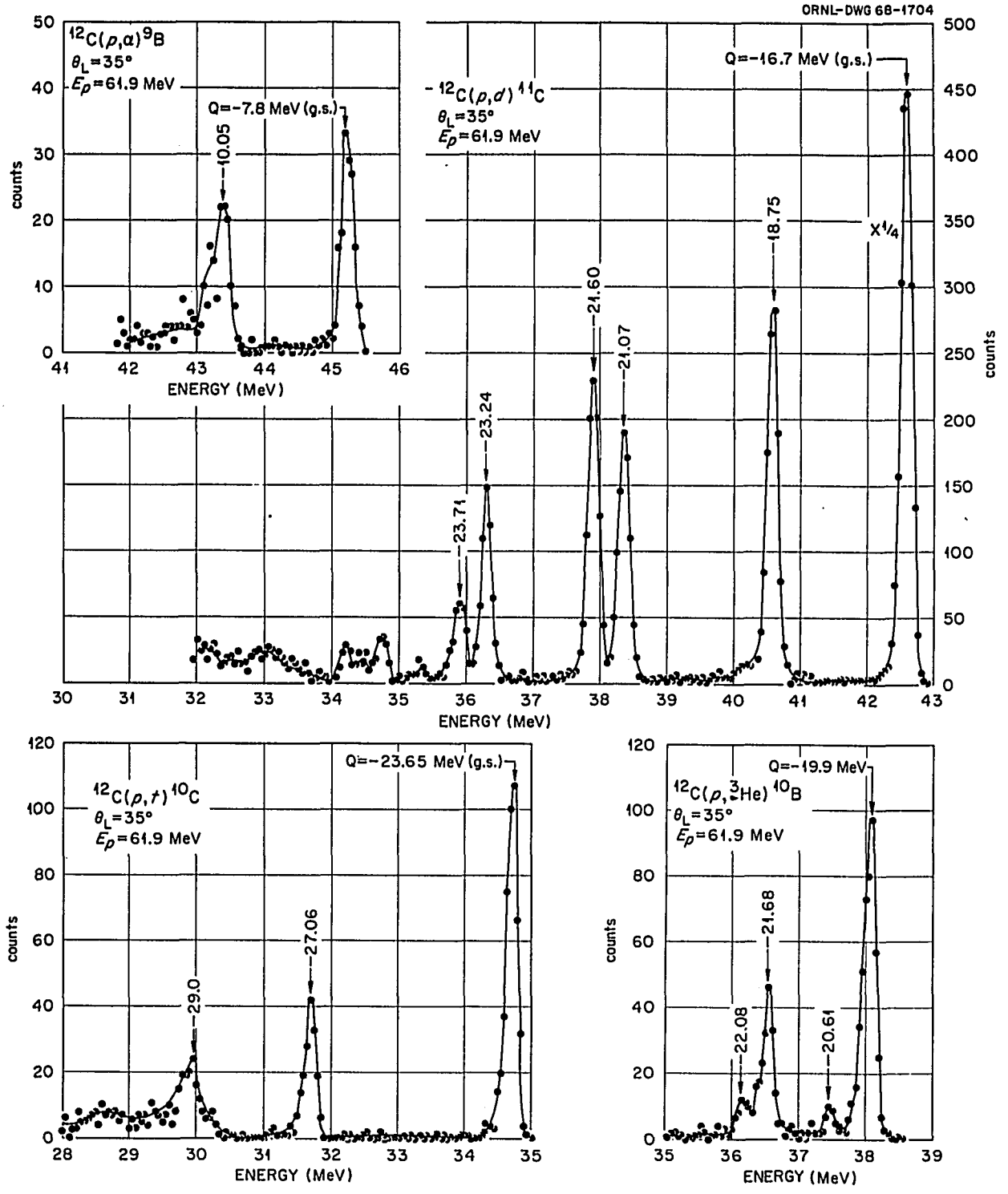

Fig. 19. High Energy Deuteron, Triton, Helium-3 and Alpha Spectra from ^{12}C at 35 Degrees.

data. The peaks observed correspond to ^{11}C states with approximate excitation of 0.0, 2.0, 4.4, 4.9, 6.6, 7.0, 7.6, 7.9, 8.5 MeV. The differential cross section for the ground state transition and the first three excited states in ^{11}C are given in Tables XI and XII and plots of the differential cross sections are shown in Fig. 20. The statistics for the 6.6 and 7.0 MeV levels for angles larger than 45 degrees were too poor to permit cross-section extraction and the statistics in the higher excitation levels would only permit cross-section computation for a few angles, and therefore these cross sections are not listed in this work.

The levels observed in the deuteron spectra agree well with those observed at 55 MeV;[50] however, the 6.6- and 7.0-MeV states are resolved in the data shown on Fig. 19, while the above reference did not resolve the peaks. Data taken with poorer resolution at 100 MeV[51] shows apparently no excitation of the 6.6- and 4.9-MeV levels; however, this may be hard to determine with the resolution attained in the experiment. The character of the angular distribution for the levels obtained at 55 and 100 MeV agree well with those shown in Fig. 20.

The levels observed in the $^{12}C(p,t)^{10}C$ reaction are shown in Fig. 19 at 35 degrees. One observes three prominent peaks with Q values of -23.7, -27.1, and -29.0 MeV which correspond to known levels in ^{10}C of 0.0, 3.4, and 5.3 MeV. The 5.3-MeV level is seen in Fig. 19 to have a low energy shoulder which indicates that the peak is composed of scattering from more than one unresolved level. This shoulder is

---

[51] J. K. P. Lee et al., Nuclear Phys. A106, 357 (1967).

TABLE XI. TABULATED DIFFERENTIAL CROSS SECTIONS

$^{12}C(p,d)^{11}C$

Q = -16.7 MeV

(Ground State)

Lab. Angle (deg)	C.M. Angle (deg)	Cross Section (lab.) (mb/sr)	Cross Section (C.M.) (mb/sr)	Error (± %)
12	13.8	16.86	12.76	4.5
15	17.3	16.17	12.28	4
20.8	24.2	8.75	6.71	4.5
25	28.7	5.21	4.03	6
30	34.4	4.73	3.70	4
35	40.0	4.54	3.60	4
40	45.6	2.75	2.21	5
45	51.2	2.06	1.69	4
55	62.2	1.24	1.06	5
60	67.6	0.92	0.80	4
65	73.0	0.74	0.66	5
70	78.2	0.42	0.38	7
75	83.5	0.26	0.24	6
82	90.7	0.14	0.14	5
90	98.8	0.118	0.13	8
110	118.2	0.055	0.062	8
135	141.2	0.011	0.014	7
160	163	0.016	0.022	17
		Q = -18.7 MeV		
		(2-MeV State)		
12	13.9	3.14	2.36	6
15	17.3	3.01	2.27	5.5
20.8	24.2	1.47	1.12	8
25	28.8	1.01	0.78	8
30	34.5	0.85	0.66	6
35	40.2	0.64	0.50	6
40	45.8	0.28	0.22	8.5
45	51.4	0.25	0.20	6
55	62.4	0.19	0.16	8.5
60	67.8	0.16	0.14	6
65	73.2	0.082	0.073	11
70	78.5	0.032	0.029	18
75	83.7	0.018	0.017	15
82	90.9	0.020	0.019	7
90	99.0	0.014	0.014	20
110	118.4	0.0094	0.011	13
135	141.3	0.002	0.0025	10

TABLE XII. TABULATED DIFFERENTIAL CROSS SECTIONS

$^{12}C(p,d)^{11}C$

Q = -21.1 MeV

(4.4 MeV State)

Lab. Angle (deg)	C.M. Angle (deg)	Cross Section (lab.) (mb/sr)	Cross Section (C.M.) (mb/sr)	Error (± %)
12	13.9	0.24	0.18	13
15	17.4	0.33	0.25	8
25	28.9	0.41	0.31	11
30	34.6	0.45	0.35	7
35	40.3	0.48	0.38	6.5
40	46.0	0.28	0.22	11
45	51.6	0.29	0.23	6
55	62.6	0.14	0.12	10
65	73.4	0.088	0.078	11
75	84.0	0.034	0.032	11
82	91.2	0.033	0.032	6
110	118.7	0.019	0.022	11
135	141.5	0.0079	0.0103	6
		Q = -21.6 MeV		
		(4.9-MeV State)		
12	13.9	1.81	1.35	7
15	17.4	1.79	1.34	6
25	29.0	0.73	0.56	8.5
30	34.7	0.65	0.50	6.5
35	40.4	0.57	0.45	6
40	46.0	0.25	0.20	11
45	51.6	0.19	0.15	6
55	62.7	0.10	0.084	11
65	73.5	0.086	0.076	11
75	84.0	0.029	0.027	12
82	91.2	0.020	0.019	6.5
110	118.7	0.01	0.11	10
135	141.6	0.0052	0.0067	6

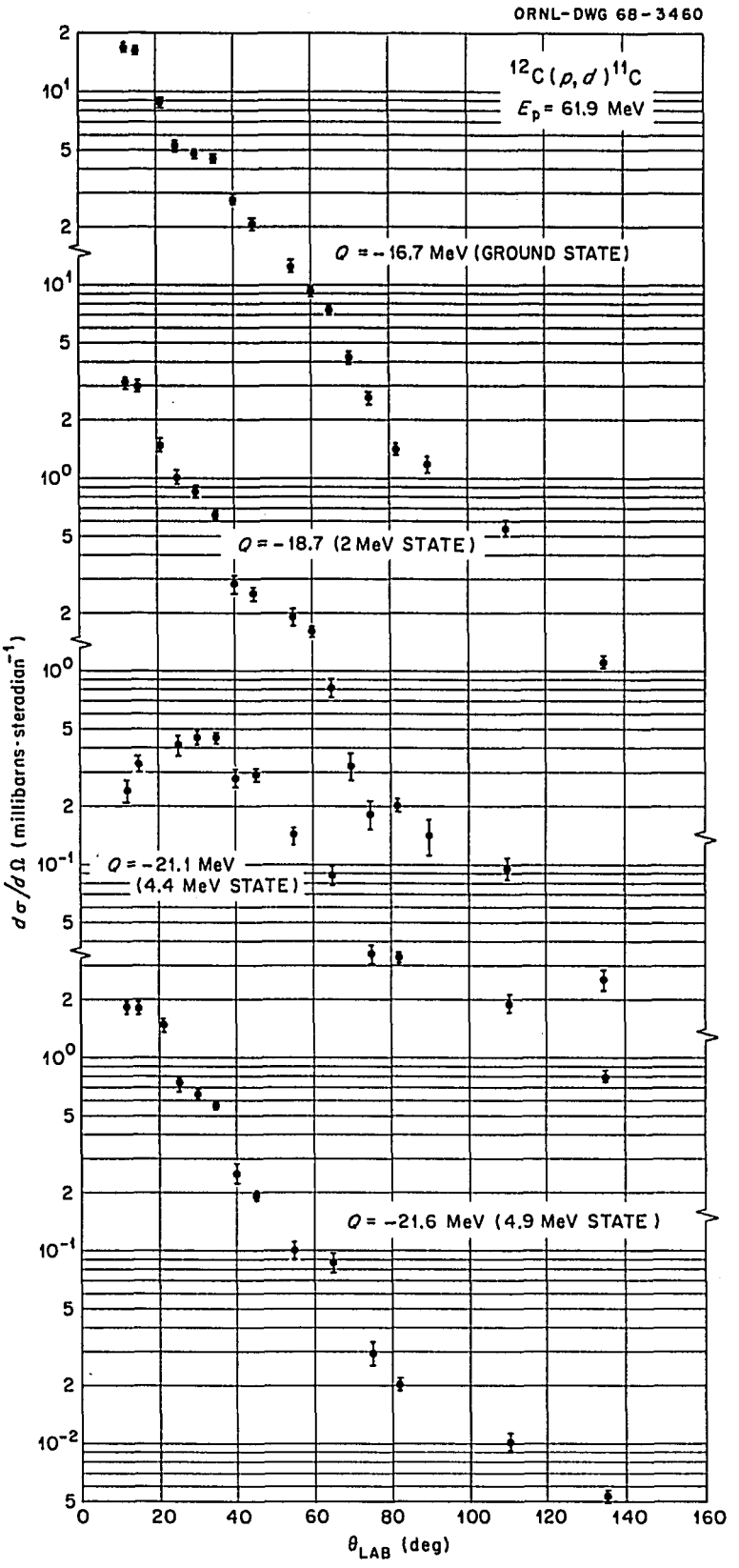

Fig. 20. Differential Cross Sections for the Levels Observed in the $^{12}C(p,d)^{11}C$ Reaction.

observed at other angles and gives the peak a decidedly different shape than those formed by scattering to the single levels at 0.0 and 3.4 MeV.

Data obtained on the $^{12}C(p,t)^{10}C$ reactions with ~43-MeV incident protons[52] has shown the presence of a 10.7-MeV state in ^{10}C, with a magnitude comparable to that of the 5.3-MeV state at some angles. Within the statistics of the experiment reported here, this level was not seen to be excited. The shape of the angular distribution obtained at 43 MeV for the ground state and the 3.4-MeV level agree well with those obtained at 60 MeV.

The differential cross-section data for the ground state and 3.4-MeV transitions are listed in Table XIII and are plotted in Fig. 21. No differential cross section is presented for the 5.3-MeV level.

Four levels are clearly observed in the $^{12}C(p,^3He)^{10}B$ reaction, an example of which is seen in Fig. 19 for the scattering angle of 35 degrees. The Q values of these levels are -19.9, -20.6, -21.7, -22.1 MeV, which correspond to excitations in the ^{10}B nucleus of 0.0, 0.7, 1.8, and 2.2 MeV, respectively.

Only the differential cross sections for the ground state reaction are shown in this work. The thickness of the CH target used for the 15-, 45-, 60-, and 82-degree runs caused considerable broadening of the helium-3 peaks, which prevented separation of the close-lying states, so these angles have been omitted from the lists of differential cross sections which are shown in Table XIV.

---

[52]D. J. Baugh et al., Nuclear Phys. A99, 203 (1967).

TABLE XIII. TABULATED DIFFERENTIAL CROSS SECTIONS

$^{12}C(p,t)^{10}C$

Q = -23.7 MeV

(Ground State)

Lab. Angle (deg)	C.M. Angle (deg)	Cross Section (lab.) (mb/sr)	Cross Section (C.M.) (mb/sr)	Error (± %)
12	14.6	1.07	0.73	7
15	18.2	0.48	0.33	7
20.8	25.4	0.28	0.20	12
25	30.2	0.43	0.30	10
30	36.2	0.41	0.29	7
35	42.1	0.26	0.19	7
40	47.9	0.052	0.039	18
45	53.7	0.028	0.021	11
55	65.1	0.066	0.053	13
60	70.1	0.052	0.043	7
65	76.2	0.039	0.033	16
70	81.6	0.016	0.014	30
75	86.9	0.0054	0.0049	25
82	94.2	0.0029	0.0028	11
90	102.3	0.004	0.0041	30
110	121.5	0.0017	0.0020	30
135	143.6	0.0006	0.0084	12
		Q = -27.1 MeV		
		(3.5-MeV State)		
12	14.7	0.36	0.25	11
15	18.4	0.48	0.33	7
20.8	25.7	0.37	0.26	11
25	30.5	0.17	0.12	15
30	36.5	0.12	0.086	11
35	42.4	0.10	0.073	9
40	48.3	0.118	0.088	14
45	54.2	0.12	0.091	7
55	65.6	0.048	0.039	15
60	71.3	0.025	0.021	7.5
65	76.8	0.012	0.010	29
70	82.2	0.016	0.014	30
75	87.6	0.011	0.010	25
82	94.9	0.0008	0.0066	7
90	103.0	0.0059	0.0060	27
110	122.2	0.0023	0.0027	27
135	144.1	0.001	0.0014	10

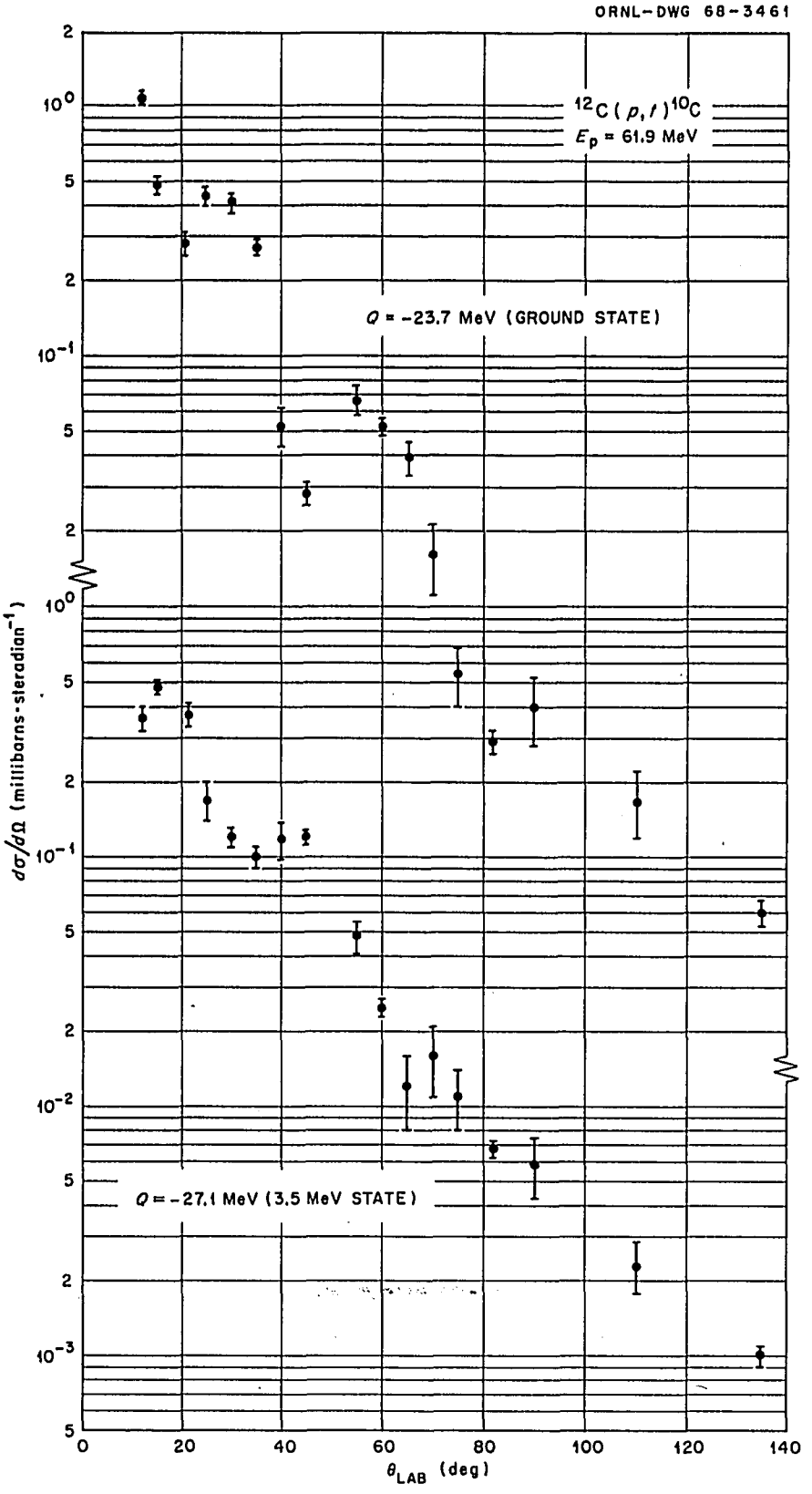

Fig. 21. Differential Cross Sections for the Levels Observed in the $^{11}C(p,t)^{10}C$ Reaction.

The resolution of peaks observed in the alpha particle spectrum is broadened by the target thickness also. Two levels are observed in the alpha spectra with Q values of -7.8 MeV (Ground state) and ~ -10 MeV (3.2-MeV state). It is seen in Fig. 19 that the cross sections for the reaction leading to these peaks are small and for this reason statistics allowed the extraction of only the ground state cross section at a few angles. These are shown in Table XIV.

The cross sections, averaged over 1-MeV-wide energy bins, for the proton (nonelastic), deuteron, triton, helium-3, and alpha spectra are listed in Appendix A in Tables AI to AV. The errors listed are based on the counting statistics within each 1-MeV bin and should be used with the systematic errors discussed earlier. The cross sections for the protons, deuterons, helium-3's, and alphas analyzed in the time-of-flight system are listed in Appendix B, Table AI. This data is averaged in 1-MeV-wide bins.

The proton and deuteron spectra exhibit at all angles a small low energy peak located near the Coulomb barrier which is ~2 MeV for the protons. The alpha spectra consistently show a very rapidly increasing magnitude at low energies. It was expected that the alpha distribution would peak at low energies and the alpha spectrum seen in Fig. 15 does show this tendency; however, the target thickness required the energy spectra to be cut off before a peak could be observed.

The magnitude of the low energy cross section for the alpha spectra was found to be much larger than the cross section for even the highest energy region of the spectrum.

TABLE XIV. TABULATED DIFFERENTIAL CROSS SECTIONS

$^{12}C(p,^{3}He)^{10}B$

Q = -20.0 MeV

(Ground State)

Lab. Angle (deg)	C.M. Angle (deg)	Cross Section (lab.) (mb/sr)	Cross Section (C.M.) (mb/sr)	Error (± %)
12	14.4	1.05	0.730	7
25	29.9	0.33	0.240	11
30	35.8	0.42	0.31	7
35	41.7	0.26	0.19	7
55	64.6	0.069	0.056	13
70	81.0	0.060	0.053	21
75	86.3	0.03	0.028	11
90	101.7	0.01	0.010	21
		$^{12}C(p,\alpha)^{9}B$		
		Q = -7.8 MeV		
		(Ground State)		
12	14.6	0.57	0.39	10
15	18.2	0.37	0.25	9
25	30.2	0.16	0.11	15
30	36.1	0.18	0.13	10
35	42.1	0.094	0.068	9
45	53.7	0.019	0.015	10
60	70.7	0.026	0.022	8

The region of each spectrum below the discrete peaks has been tested for structure by statistical tests. Within the resolution of this experiment no structure was observed in any energy region of the spectra below inelastic levels.

Figure 15 shows a strong similarity between the shapes of the various spectra in the energy regions below the inelastic levels. The similarity between the spectra is consistent over all angles of observation and for other targets.

The proton spectra obtained from ^{12}C at several angles are shown in Fig. 22. The discrete peaks at the high energy end of the spectra have been removed by drawing a smooth continuum beneath the levels. The remainder of the smooth curves were drawn through the center points of the histogram plots, as seen in Fig. 15. The histogram, plotted with the experimental curves, is a calculation of the spectrum and will be discussed in the next Chapter.

The proton spectra at all angles larger than 30 degrees are smooth and structureless and rather flat between the angles of 30 and 60 degrees. It is evident from the data in Fig. 22 that no quasi-elastic peak is observed in the data. The proton spectra for angles smaller than 30 degrees do show a peak at high energies, however the location of the peak does not correspond to the expected location of a quasi-elastic peak. The absence of a quasi-elastic peak in the data is consistent with results reported with 100- and 55-MeV incident protons as discussed in Chapter I.

There are several trends in the data which are observed in Fig. 22. The low energy spectra are seen to be peaked at ~3.5 MeV in each

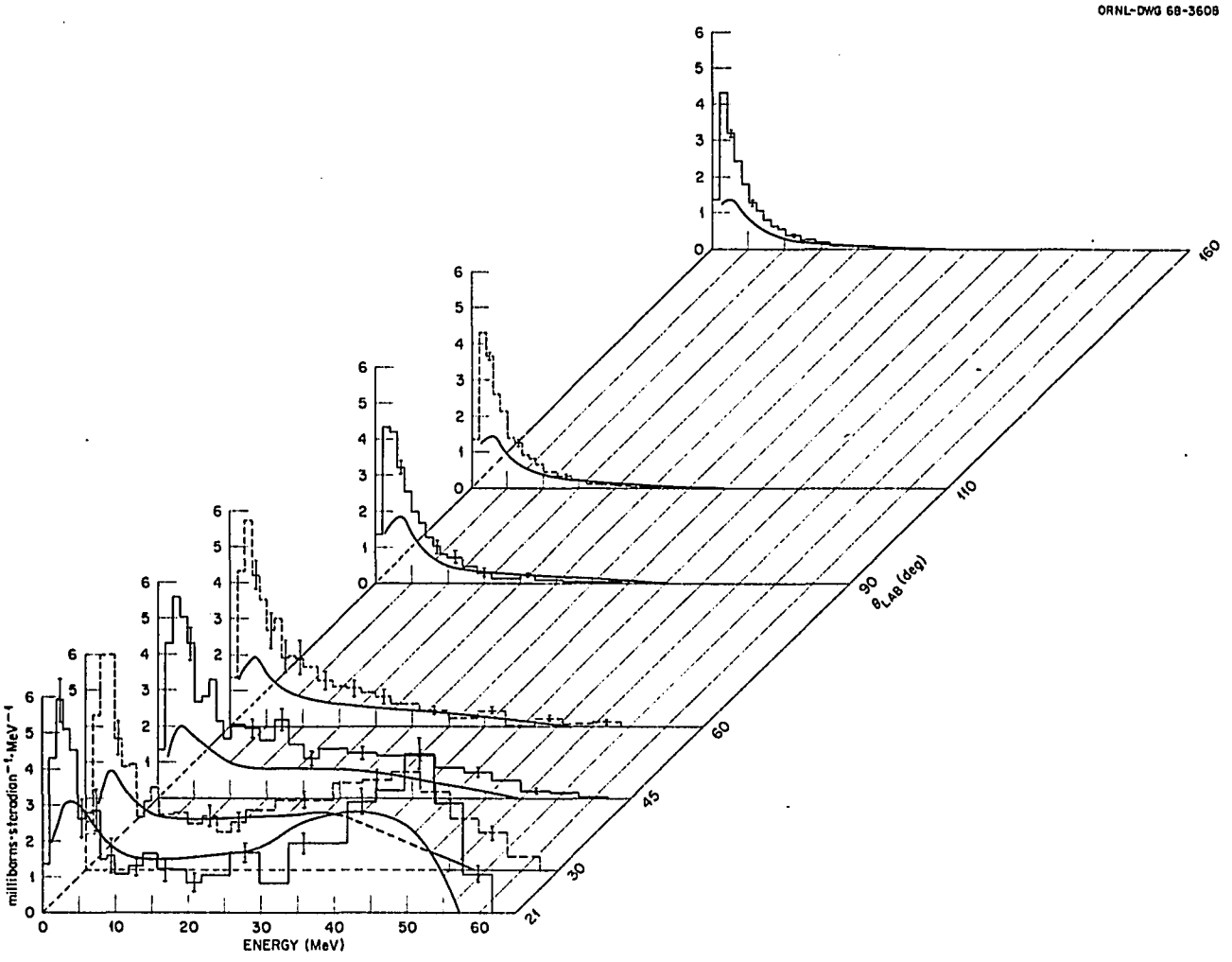

Fig. 22. Proton Continuum Spectra from ^{12}C Compared with Intranuclear Cascade Calculations.

spectrum and the magnitude of the peak is seen to decrease by approximately a factor of 2 to 3 from 20 to 160 degrees.

The cross section for the higher energy regions of the proton spectra are seen to fall off much more rapidly with increasing angle and for the highest energies the cross section goes to zero for angles greater than ~100 degrees.

Nonaka et al.[12] have observed the secondary proton spectrum from ^{12}C produced by 55-MeV incident protons. The data in reference 12 are ~40% higher than the present data at 15 degrees; however, at other angles (30, 60, 90, 120 degrees) the 55-MeV data are only 15 to 20% higher. No errors are quoted in the earlier work and the data points were read from small published graphs. The authors of the 55-MeV paper acknowledge that their experimental errors were largest at the smallest angle (15 degrees); however no magnitude is quoted.

Figure 23 shows the behavior of the cross section with increasing angle for three energy regions of the proton spectra from carbon. The region between 28 to 30 MeV was picked to be just below the region of discrete levels for all angles of observation. It is seen that the cross section in each energy region is peaked in the forward direction and approaches a constant value for angles larger than ~100 degrees. The decrease in cross sections is seen to be largest for the highest energy "slice" (~20 to 1) and smallest for the low energy distribution (~3 to 1). For angles larger than 120 degrees the cross section in the low energy region comprises most of the total cross section. The trend of various energy regions of the other charged particle spectra is similar to that for protons.

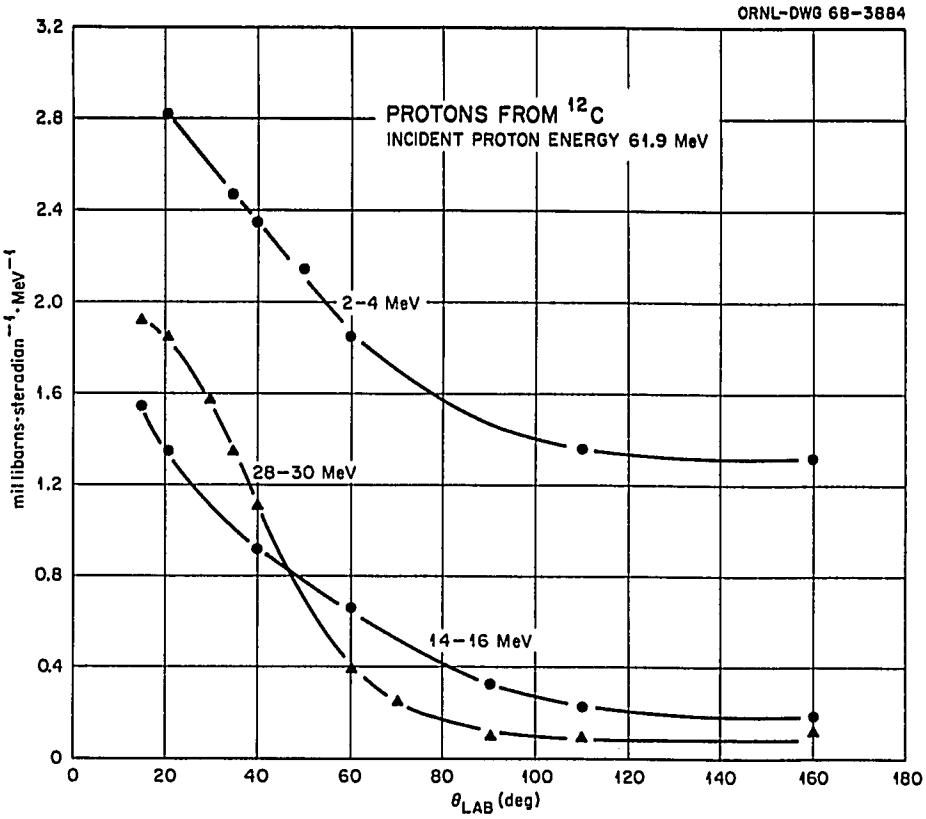

Fig. 23. Differential Cross Sections for Three Regions of the Secondary Proton Spectrum from ^{12}C.

The energy integrated differential cross sections for production of protons, deuterons, tritons, helium-3's, and alphas from ^{12}C are listed in Table XV and Fig. 24 shows a plot of these cross sections versus laboratory angle. It is seen that the shapes of the differential cross-section curve for each particle type are very similar. The curves are strongly forward peaked in all cases and the cross section approaches a constant value for angles greater than ~110 degrees. It should be noted that the observed drop in cross section at 15 degrees is a "real" decrease.

The angle integrated cross sections for the charged particles from ^{12}C are listed in Table XVI, and the total production cross section in millibarns (integral over angle and energy) for each particle is listed in Table XVII. It is observed that the cross section for alpha-particle production is twice as large as that for deuterons and only one-half as large as the proton production. The large cross section is produced mostly by the large and nearly isotropic low energy distribution, while a large part of the proton and deuteron cross section is provided by high energy secondary particles.

J. ^{54}Fe Data

Most of the data taken from ^{54}Fe was obtained in the 4000 and 5000 series of runs and, for this reason, time-of-flight data was obtained for only a few angles. The need for time-of-flight information for the iron data was smaller than the need for the carbon since the physical energy cut-off of particle emission from iron is higher than that from carbon. Only for the case of secondary alpha particles from iron is the majority of cross section detected in the time-of-flight system.

TABLE XV

Energy Integrated Total Differential Cross Sections

^{12}C

Lab Angle Degrees	Total Cross Sections (mb/sr)				
	Proton $E_p > 1.2$ MeV (nonelastic)	Deuteron $E_D > 1.2$ MeV	Triton $E_T > 5.5$ MeV	Helium-3 $E_{^3He} > 6$ MeV	Alpha $E_\alpha > 2.5$ MeV
15	111.9	34.5	4.3		
20.8	147.9	24.8	4.0	7.1	43.8
30	95.3	19.2	3.2	4.9	35.2
35	82.9	17.7	2.8	4.3	33.0
40	62.5	12.5	2.2	3.4	29.5
45	47.7	10.1	1.6		
50	41.7	7.7	1.3	2.3	22.9
60	30.5	6.2	0.83		
70	23.8	4.7	0.55	1.4	13.4
90	17.0	2.9	0.29	0.83	8.0
110	11.4	1.7	0.15		
135			0.14	0.48	4.5
160	10.5	1.3	0.10	0.31	4.2

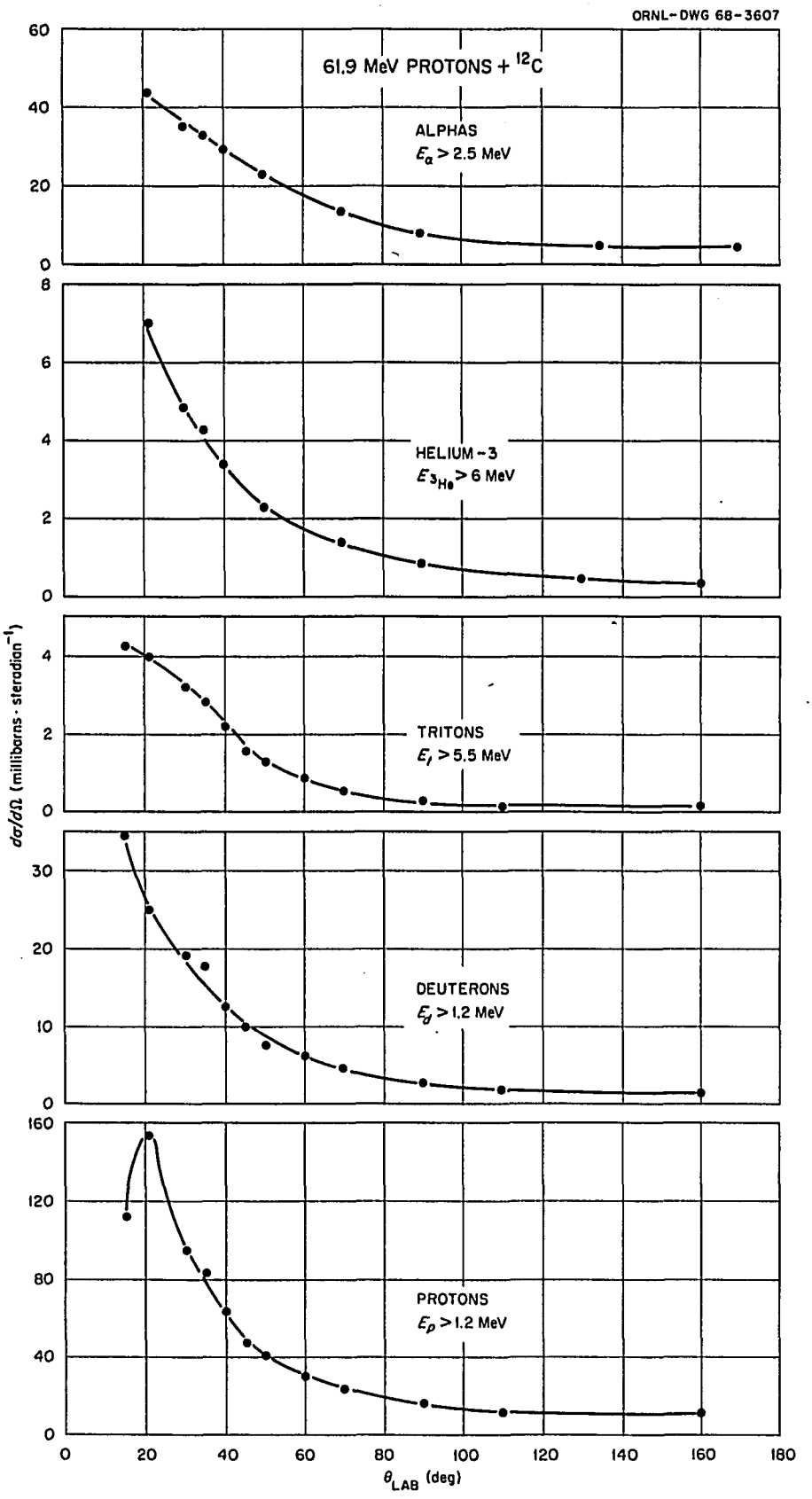

Fig. 24. Energy Integrated Differential Cross Sections for the Protons, Deuterons, Tritons, Helium-3's, and Alphas from ^{12}C.

TABLE XVI

Angle Integrated Cross Section

^{12}C

Energy (MeV)	Cross Section (mb/MeV)				
	Proton	Deuteron	Triton	Helium-3	Alpha
1.5	18.25	3.54	0	0	0
2.5	19.58	3.62	0	0	26.21
3.6	22.54	3.43	0	0	24.04
4.6	17.01	3.74	0	0	20.22
5.7	14.87	2.77	0.67	0	16.82
6.7	13.19	2.41	0.62	0	14.66
7.8	11.70	2.20	0.53	1.73	11.84
8.8	10.69	1.90	0.46	1.60	10.19
9.9	7.20	1.78	0.41	1.44	8.32
10.9	6.85	1.76	0.35	1.23	6.87
12.0	6.74	1.56	0.32	1.13	5.91
13.1	6.38	1.33	0.31	0.74	4.81
14.1	6.18	1.19	0.27	0.62	3.38
15.2	6.25	1.13	0.22	0.57	2.79
16.2	5.90	1.08	0.20	0.54	2.44
17.3	5.87	1.02	0.18	0.41	2.06
18.3	5.68	1.07	0.17	0.38	1.76
19.4	5.44	0.95	0.16	0.32	1.42
20.4	5.58	0.91	0.16	0.34	1.25
21.5	5.30	0.95	0.15	0.27	1.07
22.5	5.18	0.90	0.13	0.24	0.88
23.6	5.05	0.87	0.15	0.22	0.75
24.7	4.95	0.81	0.15	0.18	0.65
25.7	4.76	0.88	0.14	0.22	0.54
26.8	4.64	0.72	0.13	0.22	0.47
27.8	4.72	0.75	0.10	0.15	0.41
28.9	4.63	0.78	0.14	0.14	0.31
29.9	4.42	0.72	0.14	0.17	0.26
31.0	4.47	0.69	0.11	0.24	0.22
32.0	4.36	0.65	0.10	0.20	0.16
33.1	4.27	0.77	0.25	0.11	0.16
34.1	4.42	0.72	0.10	0.15	0.17
35.2	4.35	0.34	0.02	0.11	0.16
36.2	4.42	1.03	0.08	0.09	0.05
37.3	4.60	1.60	0	0.27	0.14
38.4	4.75	1.59	0	0.20	0.15
39.4	4.27	1.07	0	0.39	0.10
40.5	4.21	1.25	0	0	0.18
41.5	3.78	1.60	0	0	0.18
42.6	3.38	1.99	0	0	0.12
43.6	3.36	6.98	0	0	0.07
44.7	3.74	0	0	0	0.06
45.7	3.81	0	0	0	0.06
46.8	3.57	0	0	0	0.01
47.8	2.76	0	0	0	0.18
48.9	3.99	0	0	0	0
50.0	3.83	0	0	0	0
51.0	4.08	0	0	0	0
52.1	3.14	0	0	0	0
53.1	1.79	0	0	0	0
54.2	3.95	0	0	0	0
55.2	7.91	0	0	0	0
56.3	9.22	0	0	0	0
57.3	1.88	0	0	0	0
58.4	1.05	0	0	0	0
59.4	0	0	0	0	0

TABLE XVII

Total Cross Sections

Target	Cross Sections[a] (millibarns)				
	Proton	Deuteron	Triton	Helium-3	Alpha
^{12}C[b]	349	65	7	14.6	173
^{54}Fe[c]	1271	70	5.6	5.5	136
^{209}Bi[d]	699	91	25	2	29

(a) These cross sections include all particles detected between the energy limits given in the notes below.

(b) ^{12}C energy limits: elastic $< E_p > 1.2$ MeV; $E_D > 1.2$ MeV; $E_T > 5.5$ MeV; $E_{^3He} > 6$ MeV; $E_\alpha > 2.5$ MeV

(c) ^{54}Fe energy limits: elastic $< E_p > 3.5$ MeV; $E_D > 4.5$ MeV; $E_T > 5.5$ MeV; $E_{^3He} > 11$ MeV; All alphas

(d) ^{209}Bi - all particles.

Figure 25 shows the spectra of secondary protons, deuterons, tritons, helium-3's, and alphas from ^{54}Fe obtained at 47 degrees. It should be noted that the vertical (cross section) scale changes by factors of ten between the five plots shown. The data shown on Fig. 25 includes information from the time-of-flight system for the proton, deuteron, and alpha spectra; however, time-of-flight data is not included on the triton or helium-3 spectra even though some mass-3 particles were observed in the time-of-flight data taken during the 2000 runs (100 and 160 degrees). The low energy limits of the data for the spectra shown on Fig. 25 are: protons - 1 MeV; deuterons - all particles; tritons - 5.5 MeV; helium-3's - 11 MeV; and alphas - all particles.

The alpha particle spectrum shows two dashed regions. The region between 35 and 36 MeV shows the effect of energy loss in the nickel dead layer discussed earlier. The dashed region between ~12 and 14 MeV indicates an absence of data in this region caused by a malfunction of the experimental system during the 5000 series of runs. All time-of-flight data taken during the 5000 run suffered from the same problem between the energy of 12 and 14 MeV and only the the alpha particle data was affected. The alpha cross sections in this region were estimated by assuming a smoothly increasing cross section between 12 and 14 MeV.

The low energy cut-off for the data presented from ^{54}Fe are given in the following:

Protons:	3.5 MeV	Helium-3's:	11 MeV
Deuterons:	4.5 MeV	Alphas:	All particles
Tritons:	5.5 MeV		

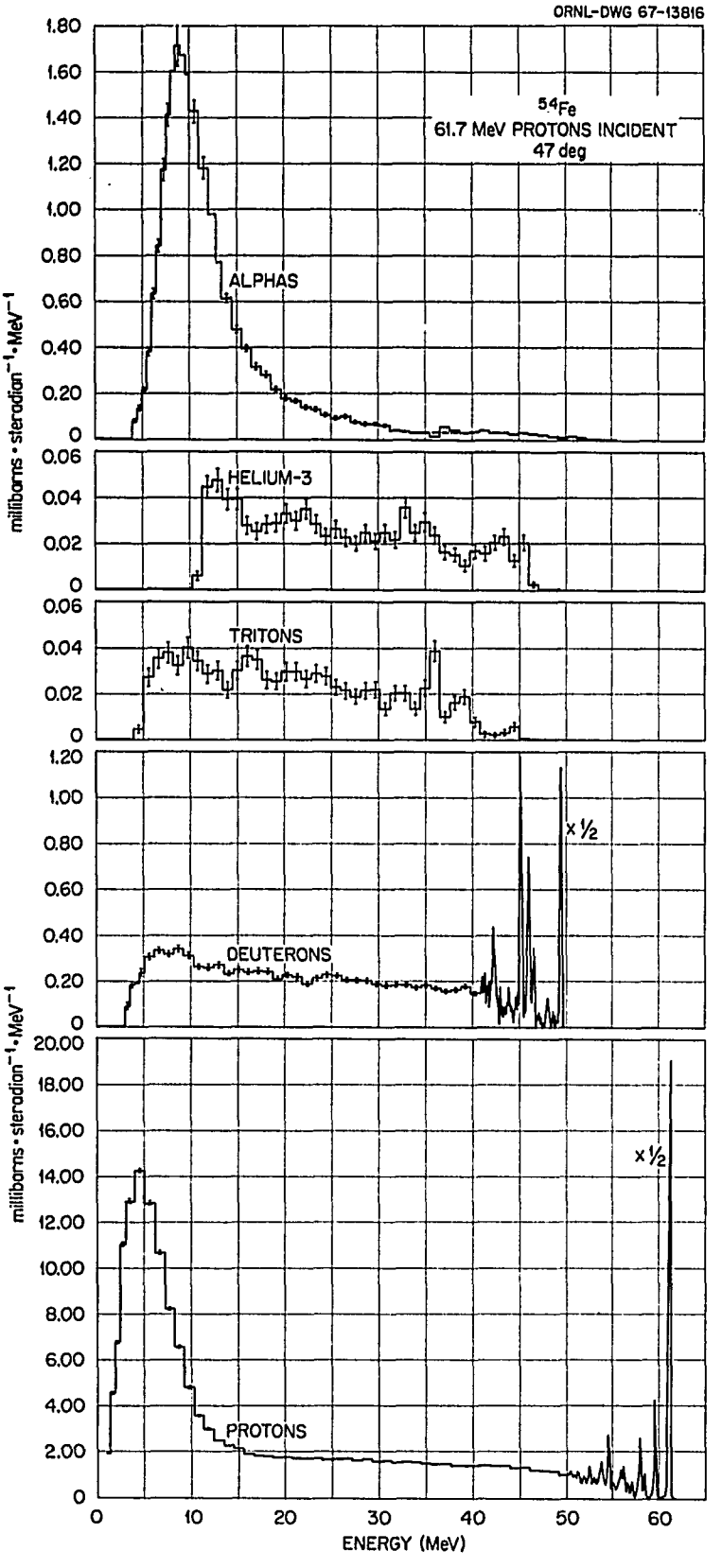

Fig. 25. Proton, Deuteron, Triton, Helium-3, and Alpha Spectra from ^{54}Fe at 45 Degrees.

It should be noted that the low energy cut-offs for the data listed in the tables are higher than the cut-offs shown on Fig. 25. The reason for the different cut-offs is that time-of-flight data was obtained for ^{54}Fe at only a few angles.

The inclusion of time-of-flight data for the protons, deuterons, tritons, and helium-3's would have affected the total cross section for these particles very little at small angles. However, at larger angles (greater than 120 degrees) the amount of cross section in the time-of-flight system may be 10% of the total for the protons and deuterons and may double the cross section for the helium-3's. The total integral over energy and angle is changed very little by the exclusion of the time-of-flight data.

Figure 25 shows that the high energy portion of the proton and deuteron spectra are dominated by excitation of discrete nuclear levels. No peaks are seen in the triton, helium-3, and alpha spectra since the counting statistics in these levels were very poor due to the small cross sections.

The spectrum of inelastic peaks observed in the proton spectrum at 30 degrees are plotted in Fig. 26. The elastic peak is plotted on a scale thirty times smaller than the scale shown on the vertical axis. The peaks labeled with Q values are those peaks which are strongly enough excited for cross-section extraction at most angles. The cross sections for the levels at -4.3, -7.2, and -8.6 MeV were not extracted for presentation in this work. The spectrum agrees with others obtained with lower energy incident protons;[52] however, the resolution attained in the present work allowed partial separation of some states,

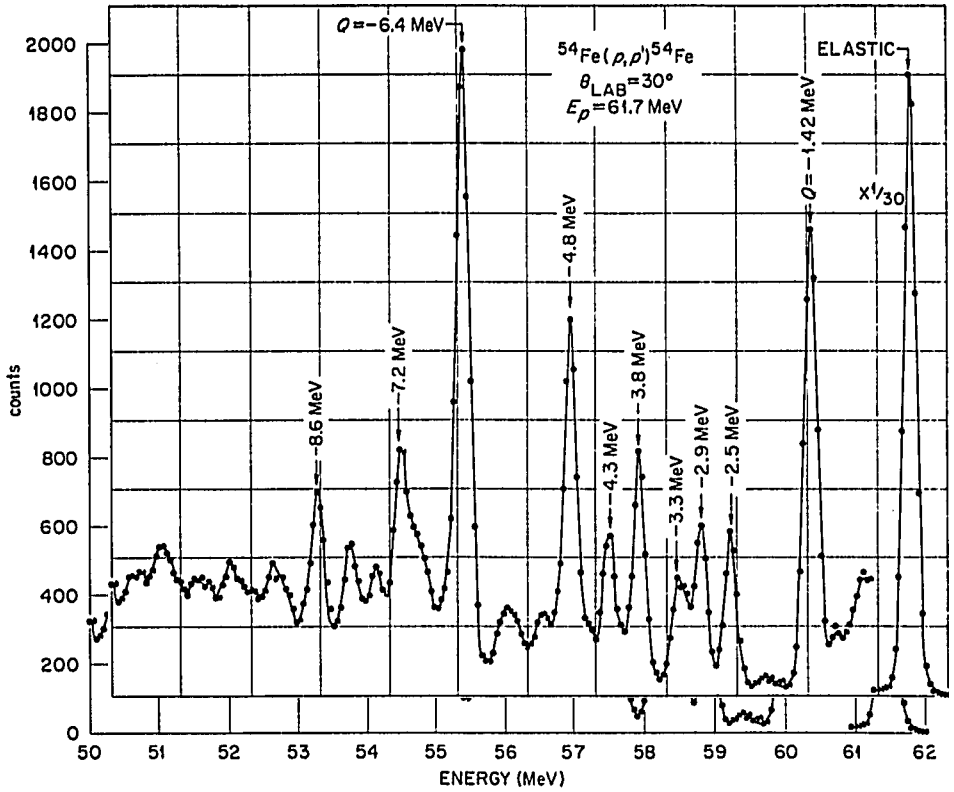

Fig. 26. Spectrum of Inelastic Proton Peaks from ^{54}Fe at 30 Degrees.

such as the 2.9- and 3.3-MeV levels, which were largely unresolved in previous work. The 2.5-MeV level is much more strongly excited at 60 MeV than in the data reported in reference 52, taken with 30-MeV incident protons. It seems apparent from its shape that the peak with Q value -7.2 MeV is comprised of more than one unresolved level; however the peak at -8.6 MeV appears to be from a single level. In general the Q values of the inelastic levels observed in the ^{54}Fe data agree very well with the levels reported for ^{54}Fe in the nuclear data sheets; however, the strong states at -7.2 and -8.6 MeV are not listed.

The differential cross sections for the elastic scattering of protons from ^{54}Fe are given in Table XVIII and the cross sections are plotted in Fig. 17 along with an optical model calculation. It is seen that the elastic differential cross-section curve shows considerably more structure than the curve for elastic scattering from ^{12}C.

The differential cross sections for the inelastic scattering of protons from the 1.42-, 2.56-, 2.92-, 3.89-, 4.85-, and 6.4-MeV levels of the ^{54}Fe nucleus are listed in Tables XIX to XXIII and these differential cross sections are plotted in Fig. 27. The shape of the angular distributions shown on Fig. 27 for the 1.42- and 2.92-MeV levels agrees quite well with the shape reported at 40 MeV. In the 40-MeV work[52] both states were identified as 2^+ levels. At 30 MeV[51] the reported differential cross section for the 1.42-MeV level is also similar in character to the present data. The 60-MeV differential cross-section curves for the 4.8- and 6.4-MeV states are similar to those of the earlier work. These states were interpreted as 3^- states in reference 43. No cross sections for the 2.56 or 3.89 levels, seen

TABLE XVIII. TABULATED DIFFERENTIAL CROSS SECTIONS

$^{54}Fe(p,p)^{54}Fe$

Elastic Scattering

Lab. Angle (deg)	C.M. Angle (deg)	Cross Section (lab.) (mb/sr)	Cross Section (C.M.) (mb/sr)	Error (± %)
12	12.2	4221	4061	3
15	15.3	2190	2108	3
20	20.4	406.7	391.9	3
25	25.5	45.34	43.75	3
27	27.5	50.67	48.92	3
30	30.6	84.40	81.56	3
35	35.7	80.56	78.0	3
40	40.7	42.20	40.95	3
45	45.8	14.20	13.81	3
47	47.8	7.65	7.45	3
50	50.9	8.20	8.00	3
55	55.9	7.18	7.00	3
60	61.0	4.74	4.65	3
65	66.0	2.27	2.23	3
70	71.1	1.41	1.39	3.5
75	76.1	1.47	1.46	3.5
80	81.1	0.87	0.86	4
90	91.1	0.16	0.16	6
100	101.1	0.11	0.11	11
110	111.1	0.084	0.085	7
120	121.0	0.017	0.017	15
135	135.8	0.010	0.010	10

TABLE XIX. TABULATED DIFFERENTIAL CROSS SECTIONS

$^{54}Fe(p,p')^{54}$

Q = -1.42 MeV

Lab. Angle (deg)	C.M. Angle (deg)	Cross Section (lab.) (mb/sr)	Cross Section (C.M.) (mb/sr)	Error (± %)
12	12.2	6.40	6.15	8
15	15.3	7.13	6.86	6
20	20.4	6.78	6.53	6
25	25.5	4.69	4.52	5
27	27.5	3.59	3.47	5
30	30.6	2.07	2.00	5
35	35.7	0.99	0.96	7
40	40.7	1.34	1.30	6
45	45.8	1.56	1.53	6
47	47.8	1.05	1.02	6
50	50.9	0.69	0.70	6
55	56.0	0.37	0.36	7
60	61.0	0.33	0.33	6
65	66.1	0.30	0.30	6
70	71.1	0.16	0.16	8.5
75	76.1	0.10	0.10	7
80	81.1	0.055	0.055	7
90	91.2	0.040	0.040	7
100	101.1	0.013	0.0126	30
110	111.1	0.0083	0.0084	11
120	121.0	0.0092	0.0094	20
135	135.8	0.0018	0 0018	21

TABLE XX. TABULATED DIFFERENTIAL CROSS SECTIONS

$^{54}Fe(p,p')^{54}Fe$

Q = -2.56 MeV

Lab. Angle (deg)	C.M. Angle (deg)	Cross Section (lab.) (mb/sr)	Cross Section (C.M.) (mb/sr)	Error (± %)
25	25.5	0.52	0.50	7
27	27.5	0.52	0.50	6
30	30.6	0.59	0.57	6
40	40.8	0.57	0.55	7
45	45.8	0.44	0.43	6
47	47.9	0.25	0.24	7
50	50.9	0.19	0.19	9
60	61.0	0.084	0.082	9
65	66.1	0.043	0.042	7
70	71.1	0.025	0.025	20
80	81.2	0.015	0.015	11
90	91.2	0.0074	0.0074	11
110	111.1	0.0020	0.0020	21

TABLE XXI. TABULATED DIFFERENTIAL CROSS SECTIONS

$^{54}Fe(p,p')^{54}Fe$

Q = -2.92 MeV

Lab. Angle (deg)	C.M. Angle (deg)	Cross Section (lab.) (mb/sr)	Cross Section (C.M.) (mb/sr)	Error (± %)
15	15.3	3.97	3.82	7
20	20.4	2.15	2.07	7
25	25.5	1.65	1.59	6
27	27.5	1.37	1.32	6
30	30.6	0.58	0.56	6
35	35.7	0.25	0.24	17
40	40.8	0.94	0.91	7
45	45.8	0.96	0.93	7
47	47.9	0.74	0.72	6
50	51.9	0.45	0.44	7
60	61.0	0.19	0.19	7
65	66.1	0.18	0.18	7
70	71.1	0.11	0.11	9
75	76.1	0.076	0.075	8
80	81.2	0.058	0.058	7
90	91.2	0.027	0.027	7
110	111.1	0.0067	0.0068	13
120	121.0	0.0081	0.0083	24

TABLE XXII. TABULATED DIFFERENTIAL CROSS SECTIONS

$^{54}Fe(p,p')^{54}Fe$

Q = -3.89 MeV

Lab. Angle (deg)	C.M. Angle (deg)	Cross Section (lab.) (mb/sr)	Cross Section (C.M.) (mb/sr)	Error (± %)
12	12.3	1.31	1.26	20
15	15.3	0.69	0.66	15
20	20.4	0.31	0.30	20
25	25.5	0.29	0.28	10
27	27.5	0.72	0.69	10
30	30.6	0.95	0.92	6
35	35.7	0.37	0.36	12
40	40.8	0.39	0.38	11
47	47.9	0.15	0.15	10
55	56.0	0.078	0.076	11
65	66.1	0.061	0.060	8
75	76.1	0.040	0.04	11
80	81.2	0.035	0.035	8
110	111.1	0.0037	0.0038	18
		Q = -4.85 MeV		
15	15.3	0.92	0.88	13
20	20.4	1.06	1.02	8
27	27.5	1.40	1.35	6
30	30.6	1.20	1.16	6
35	35.7	0.49	0.47	11
40	40.8	0.36	0.35	11
47	47.9	0.27	0.26	8
50	50.9	0.16	0.16	11
60	61.0	0.091	0.089	13
65	66.1	0.044	0.043	12
75	76.1	0.042	0.042	11
80	82.2	0.036	0.036	11

TABLE XXIII. TABULATED DIFFERENTIAL CROSS SECTIONS

$^{54}Fe(p,p')^{54}Fe$

Q = -6.4 MeV

Lab. Angle (deg)	C.M. Angle (deg)	Cross Section (lab.) (mb/sr)	Cross Section (C.M.) (mb/sr)	Error (± %)
12	12.3	2.39	2.29	14
15	15.3	2.27	2.18	7
20	20.4	2.12	2.04	7
25	25.5	2.69	2.59	6
27	27.6	3.29	3.17	5
30	30.6	2.60	2.51	6
35	35.7	1.20	1.16	7
40	40.8	0.85	0.82	7
47	47.9	0.61	0.59	10
50	50.9	0.42	0.41	7
55	56.0	0.33	0.32	7
60	61.0	0.23	0.23	7
65	66.1	0.20	0.20	7
70	71.1	0.17	0.17	10
75	76.2	0.12	0.12	8
80	81.2	0.066	0.066	7
90	91.2	0.020	0.020	11
110	111.1	0.0084	0.0085	13

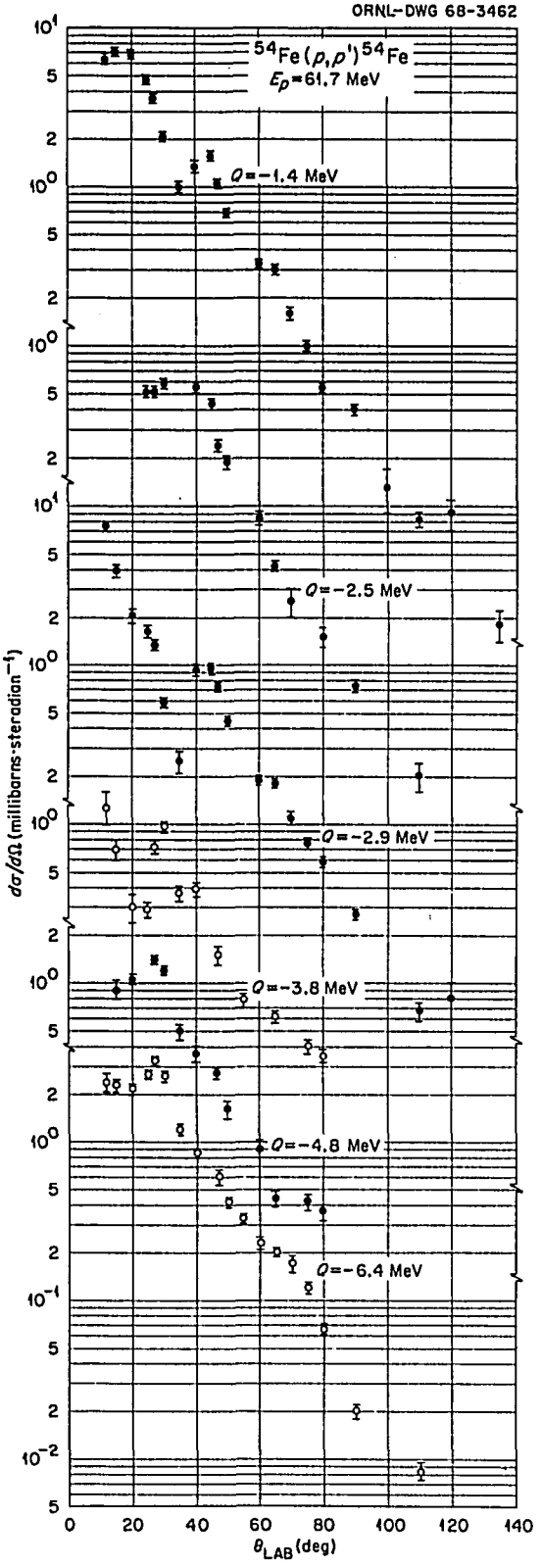

Fig. 27. Differential Cross Sections for Inelastic Proton Levels from ^{54}Fe.

strongly excited in the present work, were reported at 30 or 40 MeV.

Four peaks were found to be strongly excited in the deuteron spectrum from ^{54}Fe as is shown in Fig. 28. The Q values of these peaks from the reaction ^{54}Fe(p,d)^{53}Fe are -11.31-, -14.21-, -14.71-, and -15.64-MeV. These levels correspond to the ground state and 2.9-, 3.5-, and 4.33-MeV levels in the ^{53}Fe nucleus. The tabulated differential cross sections for these levels are given in Tables XIV and XV, and plots of the differential cross sections are shown on Fig. 29.

The shape of the secondary proton spectrum from ^{54}Fe for energies between 20 and 50 MeV is quite similar to that seen earlier for ^{12}C at 35 degrees. The proton spectrum in this region is structureless and shows no evidence of a peak from quasi-elastic scattering. The ^{54}Fe proton cross sections in this energy region are, however, higher than the ^{12}C cross section in the same region. The proton data below 20 MeV exhibits a marked difference from the ^{12}C spectrum in that a strong low-energy distribution, peaked just below the coulomb barrier (~6 MeV), is now observed. Although the low-energy proton data is cut off at ~1 MeV, there are still protons emitted at the energy well below the classical cut-off.

The spectra of deuterons and tritons, while distinctly similar to the proton spectrum in the energy region just below the discrete levels to ~15 MeV, do not show the strong low-energy peak but fall off steadily in magnitude below the coulomb barrier. It is, however, found that, although and tritons do not peak at low energies, the magnitude of the cross section in these regions falls off much more slowly with increasing angle than the magnitude for the higher energy regions of the spectra.

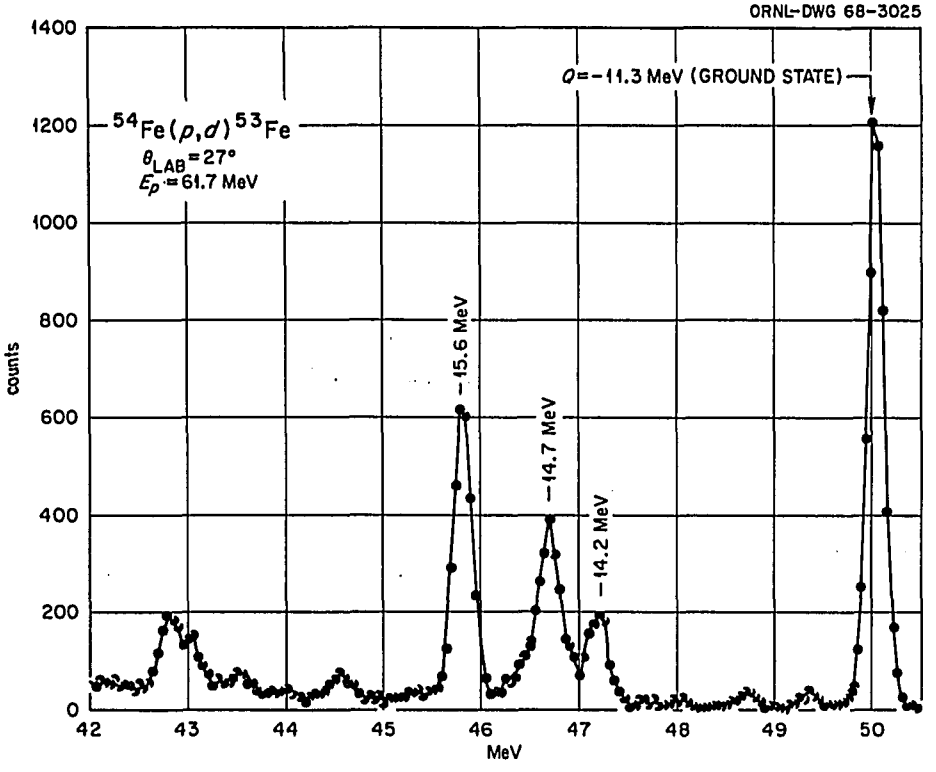

Fig. 28. Spectrum of Deuteron Peaks from ^{54}Fe at 30 Degrees.

TABLE XXIV. TABULATED DIFFERENTIAL CROSS SECTIONS

$^{54}Fe(p,d)^{53}Fe$

Q = -11.31 MeV

(Ground State)

Lab. Angle (deg)	C.M. Angle (deg)	Cross Section (lab.) (mb/sr)	Cross Section (C.M.) (mb/sr)	Error (± %)
12	12.4	4.26	4.02	8
15	15.5	3.98	3.76	6
20	20.6	2.95	2.79	6
25	25.7	2.09	1.98	5
27	27.8	1.86	1.76	5
30	30.9	1.47	1.39	5
35	36.0	1.27	1.21	6
40	41.1	1.04	.99	6
45	46.2	.69	.66	6
47	48.3	.54	.52	6
50	51.3	.51	.49	6
55	56.4	.36	.35	6
60	61.5	.33	.32	7
65	66.6	.22	.21	6
70	71.6	.16	.16	9
75	76.7	.15	.15	7
80	81.7	.093	.092	6
90	91.8	.037	.037	9
100	101.7	.027	.027	20
110	111.6	.011	.012	12
		Q = -14.21 MeV		
		(2.9-MeV Level)		
12	12.4	0.98	0.92	12
15	15.5	1.39	1.31	7
20	20.6	1.22	1.15	6
25	25.8	.54	.51	7
27	27.8	.34	.32	6
30	30.9	.21	.20	7
35	36.0	.23	.22	11
40	41.2	.29	.28	8
45	46.3	.11	.11	10
47	48.3	.081	.078	10
50	51.4	.064	.061	11
55	56.5	.063	.061	10
60	61.6	.057	.056	17
65	66.6	.043	.042	8
70	71.7	.038	.037	13
75	76.7	.021	.021	21
80	81.8	.017	.017	11

TABLE XXV. TABULATED DIFFERENTIAL CROSS SECTIONS

$^{54}Fe(p,d)^{53}Fe$

Q = -14.71 MeV

(3.4-MeV Level)

Lab. Angle (deg)	C.M. Angle (deg)	Cross Section (lab.) (mb/sr)	Cross Section (C.M.) (mb/sr)	Error (± %)
12	12.4	1.73	1.63	12
15	15.5	1.96	1.85	6
20	20.6	1.13	1.07	7
25	25.8	.70	.66	6
27	27.8	.65	.61	6
30	30.9	.48	.45	6
35	36.0	.36	.34	8
40	41.2	.25	.24	9
47	48.3	.18	.17	8
50	51.4	.18	.17	8
55	56.5	.15	.14	7
60	61.6	.108	.105	13
65	66.6	.075	.073	7
70	71.7	.068	.067	11
80	81.8	.041	.041	8
		Q = -15.64 MeV		
		(4.3-MeV Level)		
12	12.4	1.84	1.73	10
15	15.5	1.98	1.86	6
20	20.6	1.47	1.39	7
25	25.8	1.02	.96	6
27	27.8	.86	.81	5
30	30.9	.71	.67	6
35	36.0	.60	.57	7
40	41.2	.46	.44	7
45	46.3	.30	.29	8
47	48.3	.27	.26	7
50	51.4	.26	.25	7
55	56.6	.20	.19	7
60	61.6	.17	.16	8
65	66.6	.12	.12	5
70	71.7	.11	.11	10
75	76.7	.10	.10	8
80	81.8	.065	.064	7
90	91.8	.022	.022	10
110	111.7	.012	.012	11

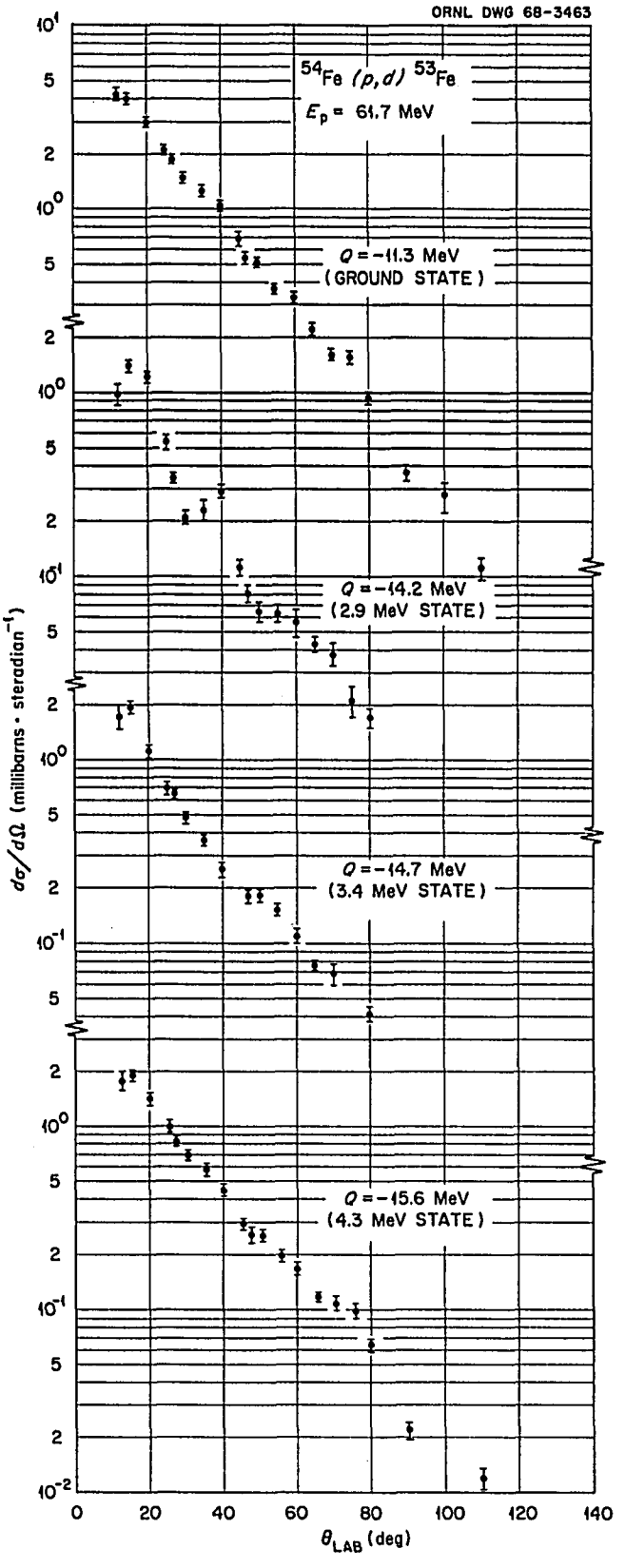

Fig. 29. Differential Cross Sections for Levels Observed in the $^{54}Fe(p,d)^{53}Fe$ Reaction.

Although the helium-3 data is cut off at ~11 MeV, it seems clear that the spectrum does not strongly peak as does the alpha spectrum. The alpha spectrum from ^{54}Fe is seen to be strongly peaked at an energy slightly below the coulomb barrier. The cross section in the peak is an order of magnitude larger than the cross section for the high-energy portions of the alpha spectrum, even for the smallest angles.

The cross sections, averaged over 1-MeV bins, for the proton (nonelastic), deuteron, triton, helium-3, and alpha data are listed in Appendix A, Tables AVI to AX. Alpha particle cross sections obtained from the time-of-flight system are listed in Appendix B, Table AII. No statistical errors are shown in the time-of-flight data; however, the largest error is ~10%. The statistical errors for the other runs may be obtained by converting the listed cross sections into counts through the use of the factors given in Table V of this Chapter. The behavior of the secondary proton spectra from ^{54}Fe as a function of angle is seen on Fig. 30 on which several secondary proton spectra are plotted. On this plot, as in the case for carbon, a smooth continuum has been drawn under the discrete peaks in the spectra and these peaks have been removed. It is seen that only a few of the spectra show data down to ~1 MeV which indicates that time-of-flight data were taken for those angles. Also plotted on Fig. 30, along with the experimental data, is a calculation of the spectrum which will be discussed in Chapter V.

It is seen that the cross section for the low-energy peak in the data is isotropic within ~30%, being forward peaked. The cross sections for the highest energy region of the spectra decrease very

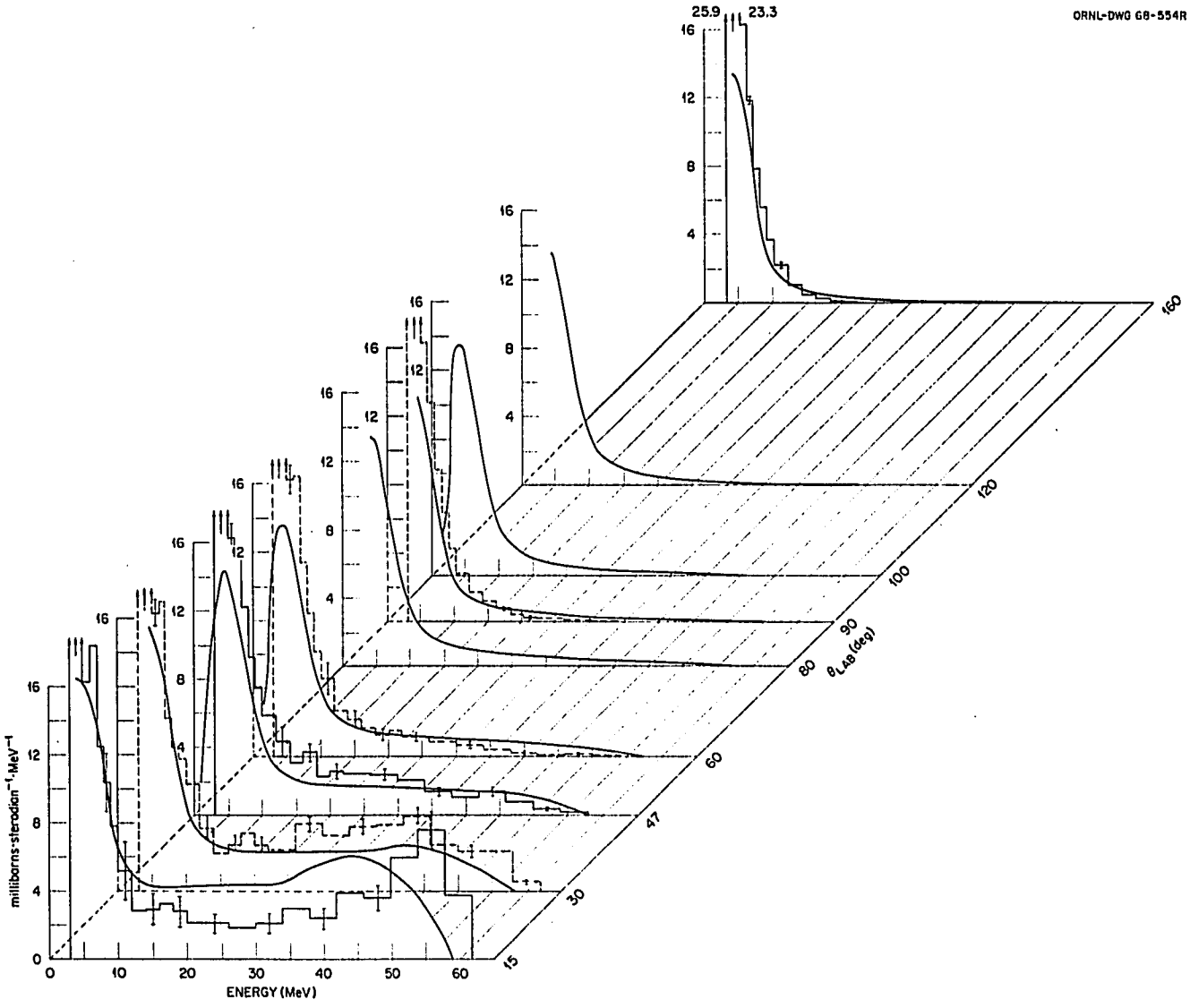

Fig. 30. Proton Continuum Spectra from ^{54}Fe Compared with Intranuclear Cascade Calculations.

rapidly with increasing angle and approach zero for angles greater than ~100 degrees. The spectra at the largest angles are comprised mostly of a low-energy, nearly isotropic, distribution. Although a peak is observed in the high energy proton spectra (~45 MeV) for angles smaller than 30 degrees, the location of the peak does not change in a manner which would identify it as a quasi-elastic peak. The proton continuum spectra at all angles were found to be structureless and are rather flat.

The spectra of alpha particles from ^{54}Fe at several angles are plotted on Fig. 31. The strong similarity between the angular variation of the alpha spectrum and the proton spectrum is evident. The magnitude of the cross sections for the high energy alpha regions decreases very rapidly with increasing angle, while the cross section in the low-energy distribution is nearly isotropic.

The behavior with angle of four different energy regions of the secondary proton spectrum from ^{54}Fe is shown on Fig. 32. Plotted on this figure are differential cross sections for the energy regions between 4 to 6 MeV (just below the coulomb barrier), 14 to 16 MeV, 24 to 26 MeV, and 44 to 46 MeV (below inelastic levels). The cross sections for each energy region are seen to be forward peaked; however, the lowest energies are peaked only ~30% and have a high magnitude, as seen in Fig. 30. The cross section for the highest energy region is seen to rapidly decrease with increasing angle until the cross section is nearly gone by 100 degrees. The intermediate energy region and the low-energy region are observed to approach a constant cross section for large angles. The behavior of the alpha spectra is the

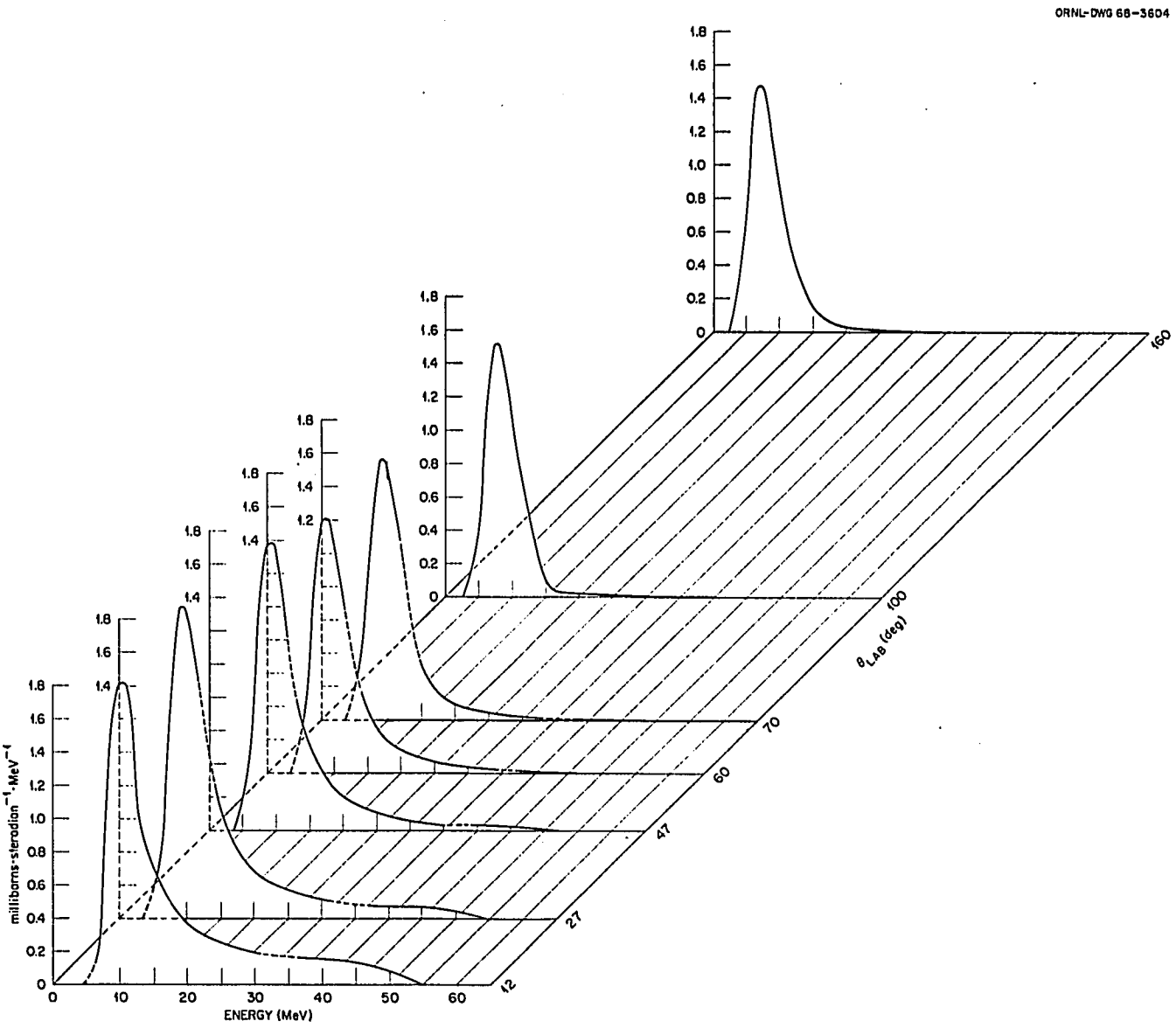

Fig. 31. Alpha Continuum Spectra from ^{54}Fe.

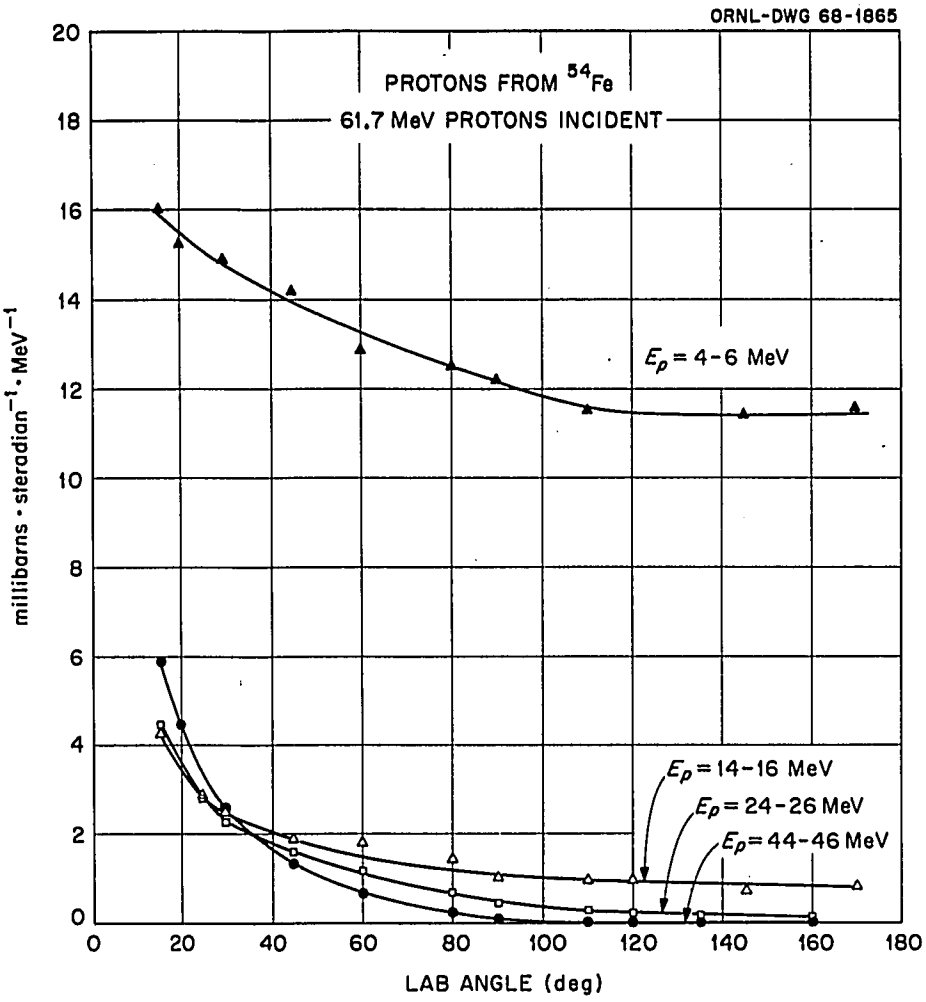

Fig. 32. Differential Cross Sections for Four Energy Regions of the Secondary Proton Spectrum from ^{54}Fe.

same as that shown in Fig. 32 for the protons and, although there is no low energy peak in their spectra, the deuterons and tritons behave in a manner similar to the protons.

The behavior with angle of the total energy integrated differential cross sections for the charged particles from ^{54}Fe is seen in Fig. 33 and the values of the cross sections are listed in Table XXVI. Although the magnitude of the various cross sections are different from the comparable cases for ^{12}C, the shape of the angular distributions are the same. Each differential cross section is seen to be strongly forward peaked and falls off rapidly to an approximately constant value for angles larger than 100 degrees. The shape of the angular distributions indicates that the mechanism for production of the various charged particles is comprised of more than one type of process and, further, the similarity of the shapes of the distributions for the various types of particles suggests that the same combination of processes are involved in the production of each type of secondary particle. The constant cross section approached by each distribution indicates that an isotropic reaction mechanism is present in the production at all angles; however, this isotropic mechanism is strongly enhanced by a different process, one which has a strong forward peaked characteristic, at angles smaller than ~90 degrees.

The angle integrated cross sections (millibarns/MeV) for protons, deuterons, tritons, helium-3's, and alphas from ^{54}Fe are listed in Table XXVII and the total cross sections (millibarns) for the production of the various particles are listed in Table XVII.

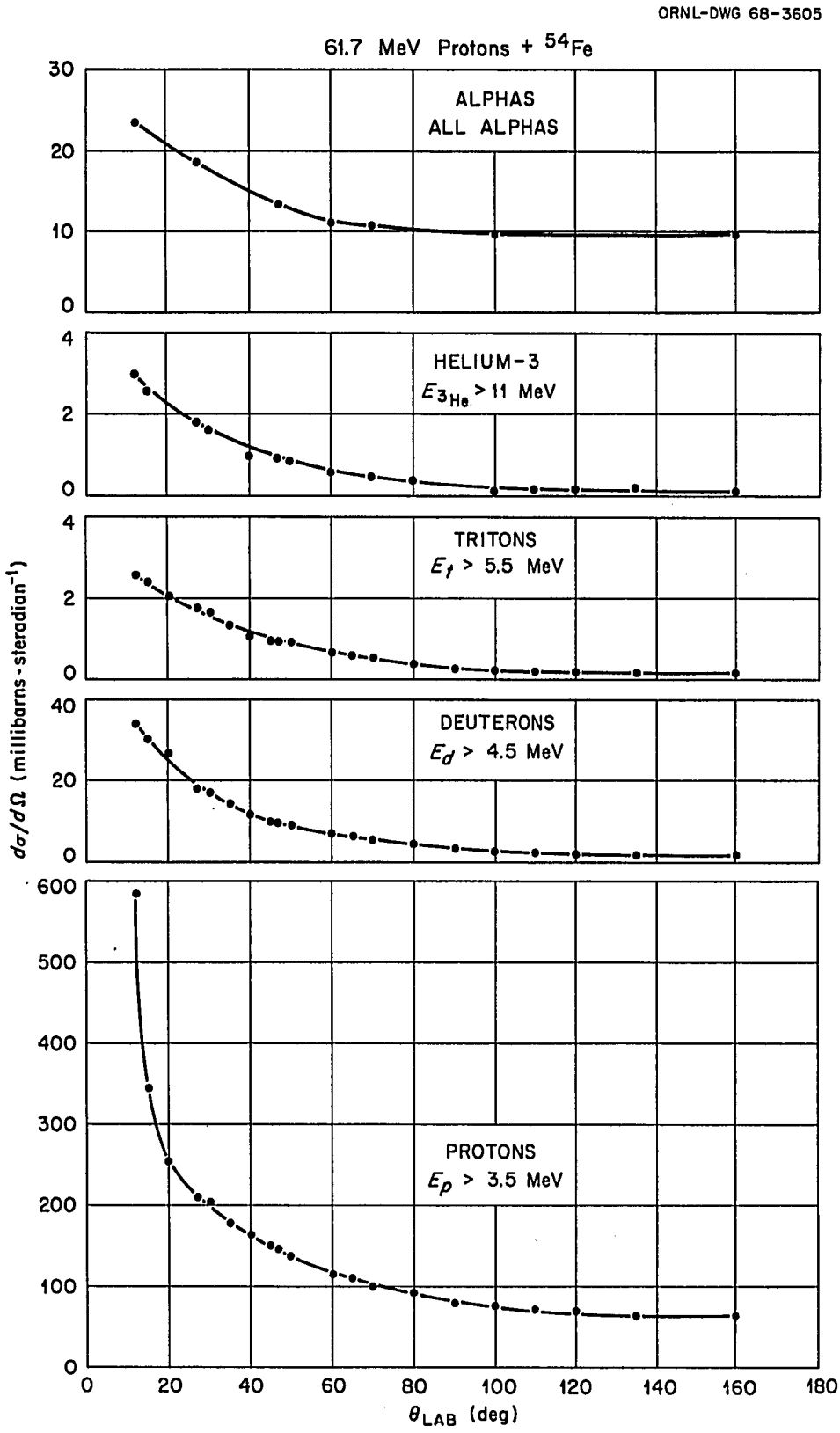

Fig. 33. Energy Integrated Differential Cross Sections for Protons, Deuterons, Tritons, Helium-3's, and Alphas from ^{54}Fe.

TABLE XXVI

Energy Integrated Total Differential Cross Sections

^{54}Fe

Lab Angle Degrees	Total Cross Sections (mb/sr)				
	Proton $E_p > 3.5$ MeV (nonelastic)	Deuteron $E_D > 4.5$ MeV	Triton $E_T > 5.5$ MeV	Helium-3 $E_{^3He} > 13$ MeV	Alpha All Particles
12	585.0	33.9	2.56	3.0	23.4
15	344.7	30.5	2.39	2.59	
20	255.0	27.3	2.03		
27	211.0	18.3	1.77	1.80	18.5
30	205.2	16.8	1.64	1.63	
35	177.7	14.6	1.30		
40	164.0	11.8	1.03	0.98	
45	149.8	10.1	0.95		
47	147.5	9.80	0.94	0.92	13.3
50	137.8	9.14	0.92	0.87	
60	117.5	6.91	0.63	0.57	12.1
65	111.9	6.40	0.57		
70	100.7	5.06	0.50	0.43	11.2
80	93.2	4.50	0.38	0.36	
90	79.0	3.15	0.26		
100	78.3	2.87	0.22	0.10	9.5
110	72.6	2.39	0.20	0.16	
120	71.9	2.04	0.18	0.14	
135	63.7	1.78	0.14	0.20	
160	67.2	1.76	0.13	0.10	9.5

TABLE XXVII

Angle Integrated Cross Section

^{54}Fe

Energy (MeV)	Cross Section (mb/MeV)				
	Proton	Deuteron	Triton	Helium-3	Alpha
1.5	0	0	0	0	0
2.5	0.08	0	0	0	0
3.6	126.80	0.04	0	0	1.70
4.6	167.40	2.72	0.05	0	4.24
5.7	145.09	3.48	0.28	0	9.41
6.7	115.41	3.37	0.29	0	14.99
7.8	89.41	3.11	0.28	0	17.81
8.8	67.63	2.84	0.30	0	17.11
9.9	39.90	2.54	0.26	0	14.77
10.9	30.51	2.23	0.25	0.06	12.00
12.0	25.07	2.08	0.21	0.35	9.16
13.0	21.36	1.74	0.19	0.37	6.75
14.1	18.87	1.57	0.20	0.32	5.15
15.1	17.22	1.58	0.17	0.25	3.51
16.2	15.77	1.45	0.17	0.22	3.00
17.2	14.63	1.43	0.16	0.19	2.21
18.3	13.71	1.42	0.15	0.20	1.89
19.3	13.45	1.35	0.15	0.21	1.42
20.4	12.74	1.34	0.14	0.20	1.19
21.4	12.47	1.29	0.14	0.16	1.06
22.5	12.06	1.27	0.14	0.15	0.96
23.5	11.76	1.27	0.14	0.16	0.82
24.6	11.62	1.23	0.13	0.14	0.73
25.6	11.13	1.21	0.14	0.13	0.61
26.6	10.91	1.15	0.12	0.14	0.59
27.7	10.76	1.15	0.12	0.13	0.45
28.7	10.87	1.16	0.12	0.14	0.43
29.8	10.38	1.08	0.13	0.13	0.38
30.8	10.08	1.11	0.11	0.14	0.33
31.9	9.78	1.09	0.11	0.12	0.28
32.9	9.60	1.05	0.11	0.19	0.20
34.0	9.48	1.08	0.11	0.14	0.19
35.0	9.53	1.09	0.14	0.12	0.15
36.1	9.28	1.09	0.13	0.12	0.09
37.1	9.16	1.11	0.12	0.11	0.34
38.2	9.12	1.18	0.09	0.11	0.22
39.2	9.07	1.16	0.09	0.10	0.21
40.3	9.46	1.20	0.06	0.09	0.20
41.3	9.80	1.35	0.04	0.11	0.17
42.4	9.56	1.31	0.01	0.12	0.18
43.4	9.48	1.45	0.02	0.16	0.14
44.5	9.19	1.74	0.04	0.12	0.19
45.5	8.84	2.53	0.03	0.05	0.18
46.6	8.62	1.66	0	0.05	0.16
47.6	8.01	1.05	0	0	0.10
48.7	7.85	1.13	0	0	0.09
49.7	7.36	1.18	0	0	0.08
50.8	7.16	0	0	0	0.10
51.8	6.87	0	0	0	0.07
52.8	7.18	0	0	0	0.03
53.9	7.46	0	0	0	0.02
54.9	8.02	0	0	0	0.01
56.0	5.28	0	0	0	0.03
57.0	6.51	0	0	0	0
58.1	8.30	0	0	0	0
59.1	4.27	0	0	0	0
60.2	0	0	0	0	0

K. ^{209}Bi Data

Data were obtained from the bismuth target entirely during the 5000 series of runs (only two angles were taken in the 7000 series). The physical low energy cut-off of the data from bismuth was high enough so that the $\Delta E \times E$ systems detected essentially all the particles. However, the time-of-flight system detected large quantities of fission fragments from the bismuth target since 60 MeV (protons) is above the fission threshold for bismuth. These heavy fragments were totally stopped in the first detector and therefore never entered the $\Delta E \times E$ identification system. The fragments did, however, obscure in the time-of-flight system some small portion of the extreme low-energy proton spectrum for the smallest angles.

The spectra of protons, deuterons, tritons, helium-3's, and alphas observed from ^{209}Bi at 45 degrees are shown on Fig. 34. The proton and deuteron spectra, as in the same spectra for ^{12}C and ^{54}Fe, exhibit several well-resolved discrete peaks at the highest energies. No levels are shown for the triton, helium-3 and alpha spectra due to poor statistics. It should be pointed out that the alpha particle ground state reaction has a positive Q value and the highest alpha particle energies for angles less than ~25 degrees were not analyzed. This unanalyzed portion represents a very small portion of the total alpha cross section.

The proton spectrum shown on Fig. 34 again exhibits a structureless, flat continuum region between ~50 and 20 MeV as the spectra from ^{12}C and ^{54}Fe have shown. The low energy portion of the spectrum from bismuth is different from the other elements in that no low energy

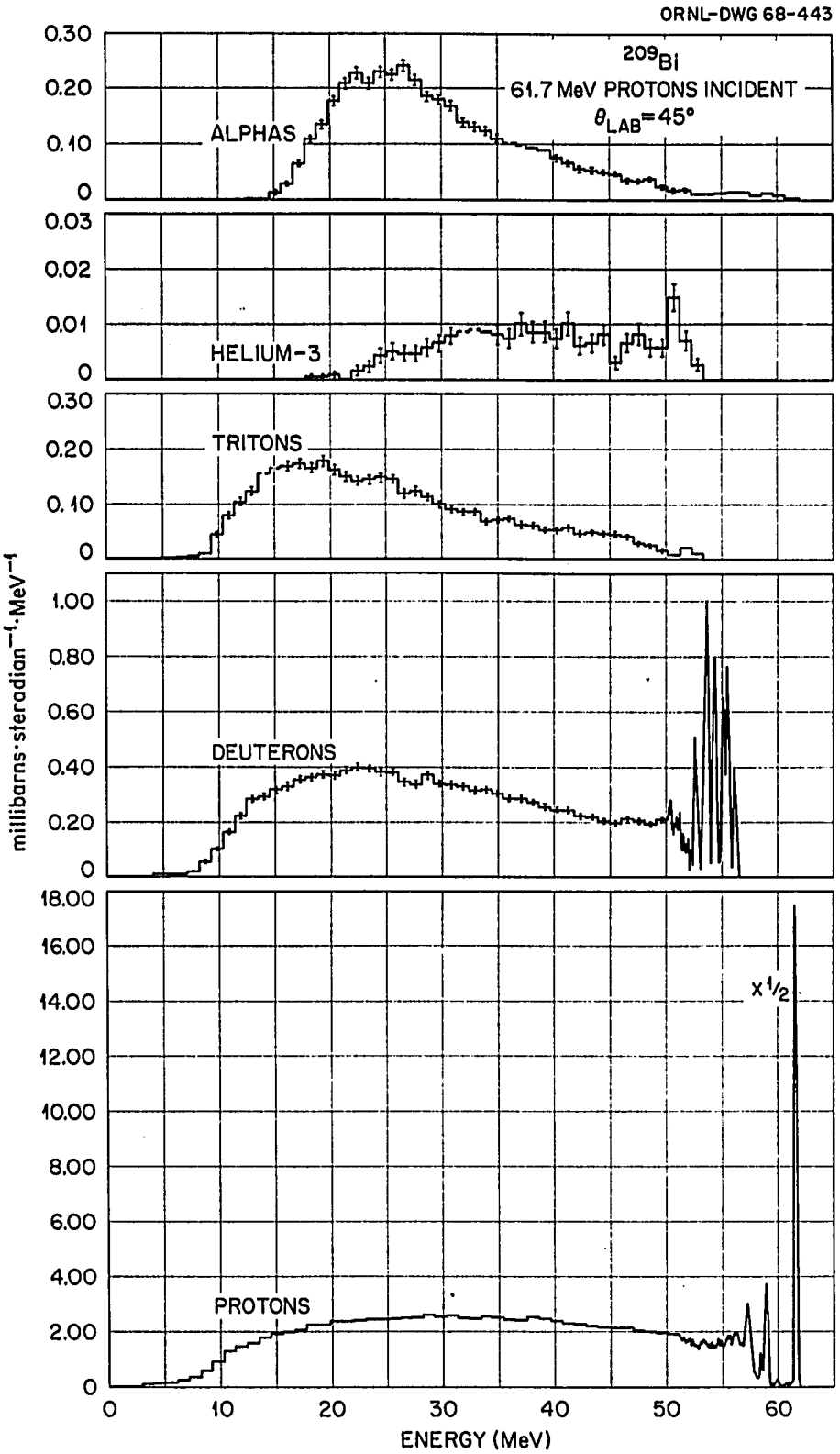

Fig. 34. Proton, Deuteron, Triton, Helium-3, and Alpha Spectra from ^{209}Bi at 45 Degrees.

peak is observed. The data is seen to fall off smoothly below the Coulomb barrier which is located at ~6 MeV. The deuteron and triton spectra, although in general similar in shape to the proton spectrum, show more of a peaking at the lowest energies, although the peak in their case is very broad. The alpha spectrum in Fig. 34 shows a distribution which is peaked at approximately the Coulomb barrier for the alphas and which drops off rapidly at the higher energies, a situation similar to the alpha spectra from carbon and iron. The helium-3 spectrum, however, is different from the others in that the cross section is not peaked near the Coulomb barrier but rather has a stronger cross section at the higher energies. It should also be noted that the magnitude of the helium-3 cross section is ten times less than that for the triton, a ratio unlike those for carbon or iron, as can be seen in Table XVI. It should be noted again that the low energy cut-offs observed in the spectra in Fig. 34 are physical and not determined by the detector or electronic systems or by the target thickness.

Figure 35 shows the spectrum of inelastic proton peaks and the spectrum of deuteron peaks observed from ^{209}Bi at 40 degrees. The proton spectrum is dominated by the elastic scattering which is much stronger than the nearby inelastic levels. The inelastic levels with Q values of -1.62, -2.69, and -3.17 MeV appear to be single levels; however, the level at 4.38 MeV seems too broad to be produced by excitation from a single state. The first excited state in ^{209}Bi has a Q value of ~0.95 MeV and is very weakly excited. Due to its nearness to the elastic peak and its weakness, this level was observed above the

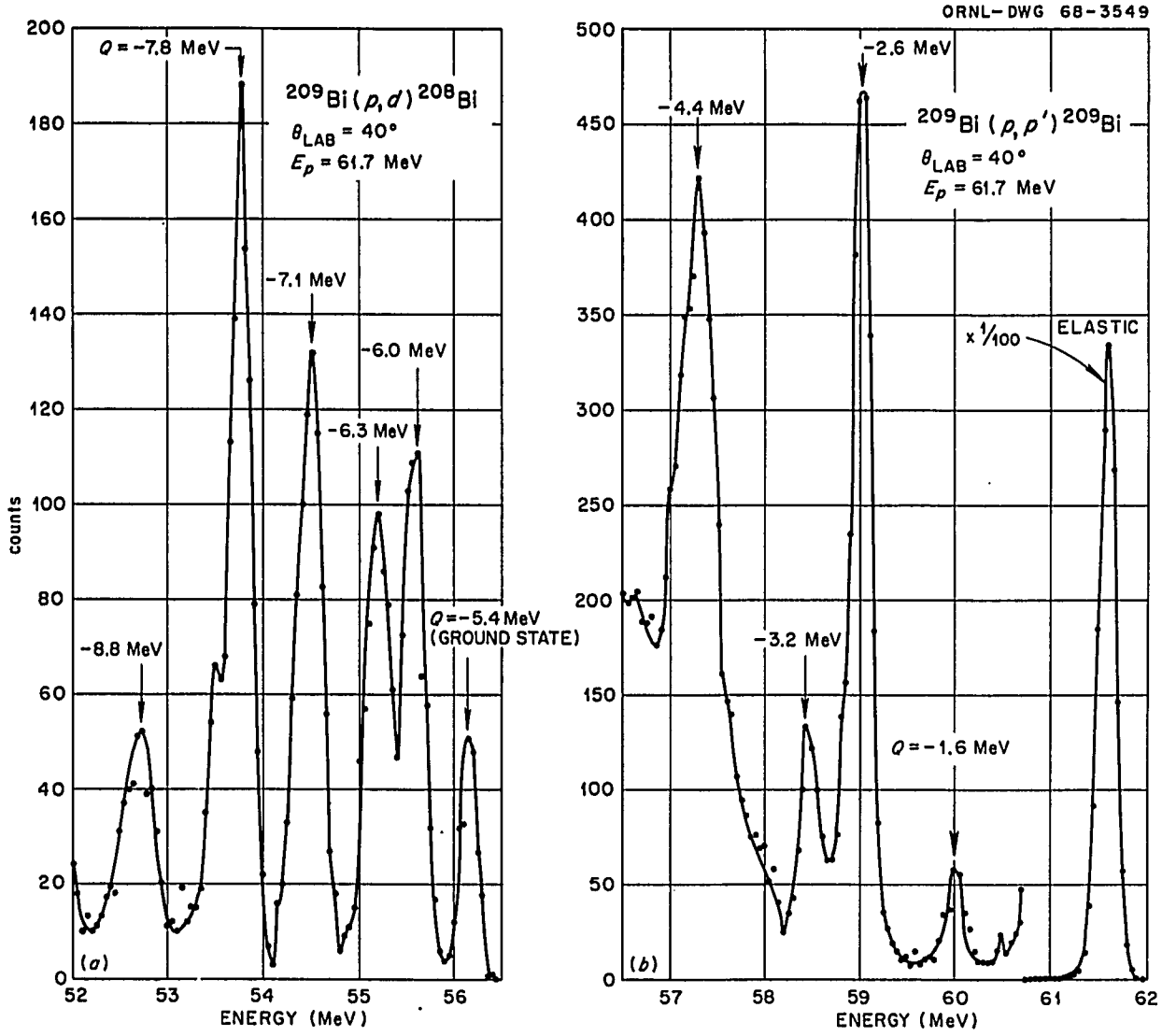

Fig. 35. Spectra of the Inelastic Proton Peaks and the Deuteron Peaks from ^{209}Bi at 40 Degrees.

tail of the elastic peak at only a very few angles and cross sections for this level could not be extracted. If this level happened to be included in the elastic cross section, the effect on the elastic data would be negligible. There is a very prominent and broad peak observed in the bismuth proton spectra with an approximate Q value of -6 MeV. This distribution must be composed of several closely spaced levels which are completely unresolved in this experiment. The differential cross section for the elastic scattering and for the 1.62-, 2.64-, 3.17-, and 4.38-MeV levels are listed in Tables XXVIII to XXX. The elastic cross sections are plotted in Fig. 17, along with an optical model fit, and the inelastic cross sections are plotted in Fig. 36.

The deuteron spectrum plotted in Fig. 35 shows the presence of six prominent peaks. The cross sections for the reactions leading to these peaks are strong enough to permit extraction of differential cross sections for all six levels at least out to 70 degrees. The Q values of these apparent levels are -5.37, -5.97, 6.32, -7.07, -7.82, and -8.82 MeV and these correspond to the ground state and excited states of 0.6, 1.0, 1.7, 2.5, and 3.5 MeV in the ^{208}Bi nucleus. The differential cross sections for these states are tabulated in Tables XXXI to XXXIII, and the cross sections are plotted on Fig. 37.

The inelastic proton spectra observed in this experiment are similar to those obtained at 55 MeV shown in reference 12; however, the energy resolution of the present work was approximately an order of magnitude better than the 55-MeV work and permitted separation of the 1.6-MeV level from the elastic peak and also allowed separation of the 2.6- and 3.2-MeV levels. The deuteron spectra were obtained by

TABLE XXVIII. TABULATED DIFFERENTIAL CROSS SECTIONS

$^{209}Bi(p,p)^{209}Bi$

Elastic Scattering

Lab. Angle (deg)	C.M. Angle (deg)	Cross Section (lab.) (mb/sr)	Cross Section (C.M.) (mb/sr)	Error (± %)
15	15.08	1658	1642	4
20	20.1	1001	991.4	4
25	25.12	723.1	716.5	4
30	30.15	37.26	36.93	4
35	35.17	131.7	130.6	4
40	40.19	75.69	75.1	4
45	45.21	8.10	8.04	4
50	50.23	25.11	24.94	4
55	55.24	12.42	12.35	4
60	60.26	2.86	2.85	4
70	70.28	3.04	3.03	4
75	75.28	1.066	1.063	4.5
80	80.29	1.56	1.56	4.5
90	90.29	0.38	0.38	4.5
110	110.28	0.099	0.0993	6.5
120	120.26	0.1066	0.1066	6
135	135.21	0.026	0.0262	12.0

TABLE XXIX. TABULATED DIFFERENTIAL CROSS SECTIONS

$^{209}Bi(p,p')^{209}Bi$

Q = -1.62 MeV

Lab. Angle (deg)	C.M. Angle (deg)	Cross Section (lab.) (mb/sr)	Cross Section (C.M.) (mb/sr)	Error (± %)
20	20.1	.58	.57	9
25	25.1	.51	.51	9
30	30.1	.13	.12	10
40	40.2	.11	.11	10
45	45.2	.064	.063	10
50	50.2	.080	.080	9
55	55.2	.034	.034	11
60	60.3	.028	.028	11
70	70.3	.019	.019	14
		Q = -2.64 MeV		
15	15.1	11.83	11.71	4
20	20.1	10.78	10.68	4
25	25.1	4.48	4.43	4
30	30.2	3.24	3.21	4
35	35.2	3.78	3.75	4
40	40.2	1.40	1.39	4
45	45.2	1.09	1.08	4
50	50.2	1.31	1.30	4
55	55.2	.49	.49	4
60	60.3	.43	.43	5
70	70.3	.22	.22	6
75	75.3	.14	.14	8
80	80.3	.20	.20	7

TABLE XXX. TABULATED DIFFERENTIAL CROSS SECTIONS

$^{209}Bi(p,p')^{209}Bi$

Q = -3.17 MeV

Lab. Angle (deg)	C.M. Angle (deg)	Cross Section (lab.) (mb/sr)	Cross Section (C.M.) (mb/sr)	Error (± %)
15	15.1	.88	.89	13
20	20.1	1.47	1.45	6
30	30.2	.88	.87	6
35	35.2	.39	.39	7
40	40.2	.31	.31	7
45	45.2	.35	.34	6
50	50.2	.10	.10	11
55	55.2	.078	.078	8
60	60.3	.089	.089	8
70	70.3	.029	.029	14
75	75.3	.025	.025	19
80	80.3	.034	.034	11
		Q = -4.38 MeV		
15	15.1	5.31	5.26	6
20	20.1	4.44	4.40	6
25	25.1	3.52	3.49	6
30	30.2	3.34	3.31	5
35	35.2	1.58	1.56	6
40	40.2	1.21	1.20	6
45	45.2	1.03	1.02	6
50	50.2	.28	.28	8
55	55.2	.44	.44	6
60	60.3	.33	.33	6
70	70.3	.15	.15	8

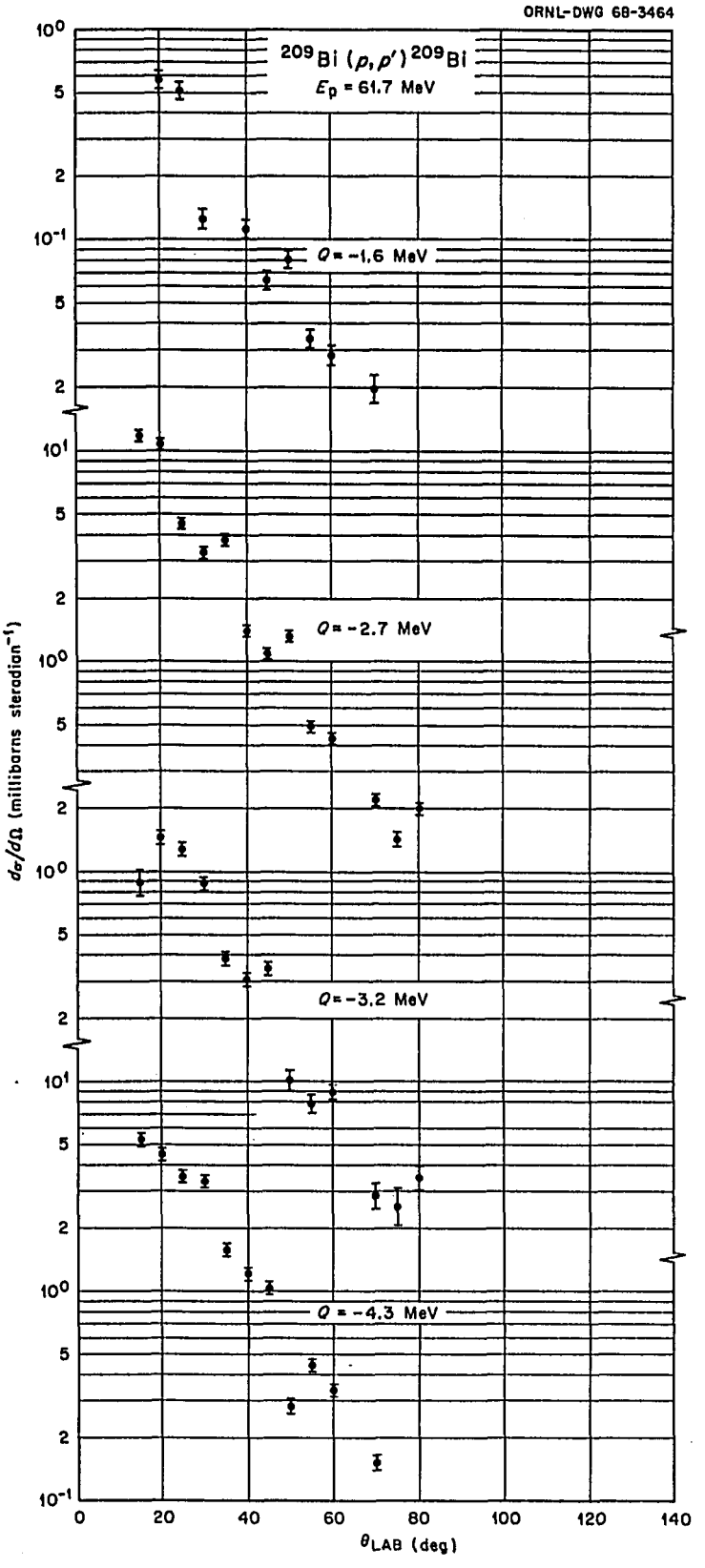

Fig. 36. Differential Cross Sections for Inelastic Proton Levels from ^{209}Bi.

TABLE XXXI. TABULATED DIFFERENTIAL CROSS SECTIONS

$^{209}Bi(p,d)^{208}Bi$

Q = -5.37 MeV

(Ground State)

Lab. Angle (deg)	C.M. Angle (deg)	Cross Section (lab.) (mb/sr)	Cross Section (C.M.) (mb/sr)	Error (± %)
15	15.1	.76	.75	8
20	20.1	.48	.47	8
25	25.2	.37	.37	9
30	30.2	.27	.27	7
35	35.2	.23	.23	7
40	40.3	.10	.10	9
45	45.3	.084	.083	9
50	50.3	.041	.041	11
55	55.3	.023	.023	12
60	60.4	.023	.023	12
70	70.4	.0066	.0066	26
90	90.5	.0053	.0053	20
		Q = -5.97 MeV		
		(0.6-MeV State)		
15	15.1	3.78	3.72	6
20	20.1	2.04	2.02	6
25	25.2	1.33	1.31	6
30	30.2	.92	.91	6
35	35.2	.50	.50	6
40	40.3	.31	.31	7
45	45.3	.18	.18	7
50	50.3	.12	.12	7
55	55.4	.060	.060	8
60	60.4	.044	.043	9
70	70.4	.024	.024	13
80	80.4	.011	.011	19

TABLE XXXII. TABULATED DIFFERENTIAL CROSS SECTIONS

$^{209}Bi(p,d)^{208}Bi$

Q = -6.32 MeV

(1-MeV State)

Lab. Angle (deg)	C.M. Angle (deg)	Cross Section (lab.) (mb/sr)	Cross Section (C.M.) (mb/sr)	Error (± %)
15	15.1	2.14	2.11	6
20	20.1	1.40	1.38	6
25	25.2	.96	.94	6
30	30.2	.71	.70	6
35	35.2	.44	.44	6
40	40.3	.30	.30	7
45	45.3	.20	.20	6
50	50.3	.11	.11	8
55	55.4	.091	.091	7
60	60.4	.039	.039	10
70	70.4	.020	.020	14
80	80.4	.011	.011	19
		Q = -7.07 MeV		
		(1.7-MeV State)		
15	15.1	2.79	2.75	6
20	20.1	2.62	2.60	6
25	25.2	1.50	1.48	6
30	30.2	.83	.82	6
35	35.2	.66	.65	6
40	40.3	.43	.43	6
45	45.3	.24	.24	7
50	50.3	.24	.23	6
55	55.4	.11	.11	7
60	60.4	.11	.11	7

TABLE XXXIII. TABULATED DIFFERENTIAL CROSS SECTIONS

$^{209}Bi(p,d)^{208}Bi$

Q = -7.82 MeV

(2.5-MeV State)

Lab. Angle (deg)	C.M. Angle (deg)	Cross Section (lab.) (mb/sr)	Cross Section (C.M.) (mb/sr)	Error (± %)
15	15.1	4.10	4.00	5
25	25.2	2.41	2.37	4
30	30.2	1.34	1.33	4
35	35.2	.85	.84	5
40	40.3	.50	.49	5
45	45.3	.31	.30	5
50	50.3	.26	.25	5
55	55.4	.12	.12	5
60	60.4	.066	.065	7
70	70.4	.030	.030	13
		Q = -8.82 MeV		
		(3.5-MeV State)		
25	25.2	.53	.53	9
30	30.2	.47	.46	6
35	35.3	.31	.30	7
40	40.3	.16	.16	10
45	45.3	.15	.15	8
50	50.3	.11	.11	8
55	55.4	.065	.064	8
60	60.4	.049	.049	10
70	70.4	.033	.033	12

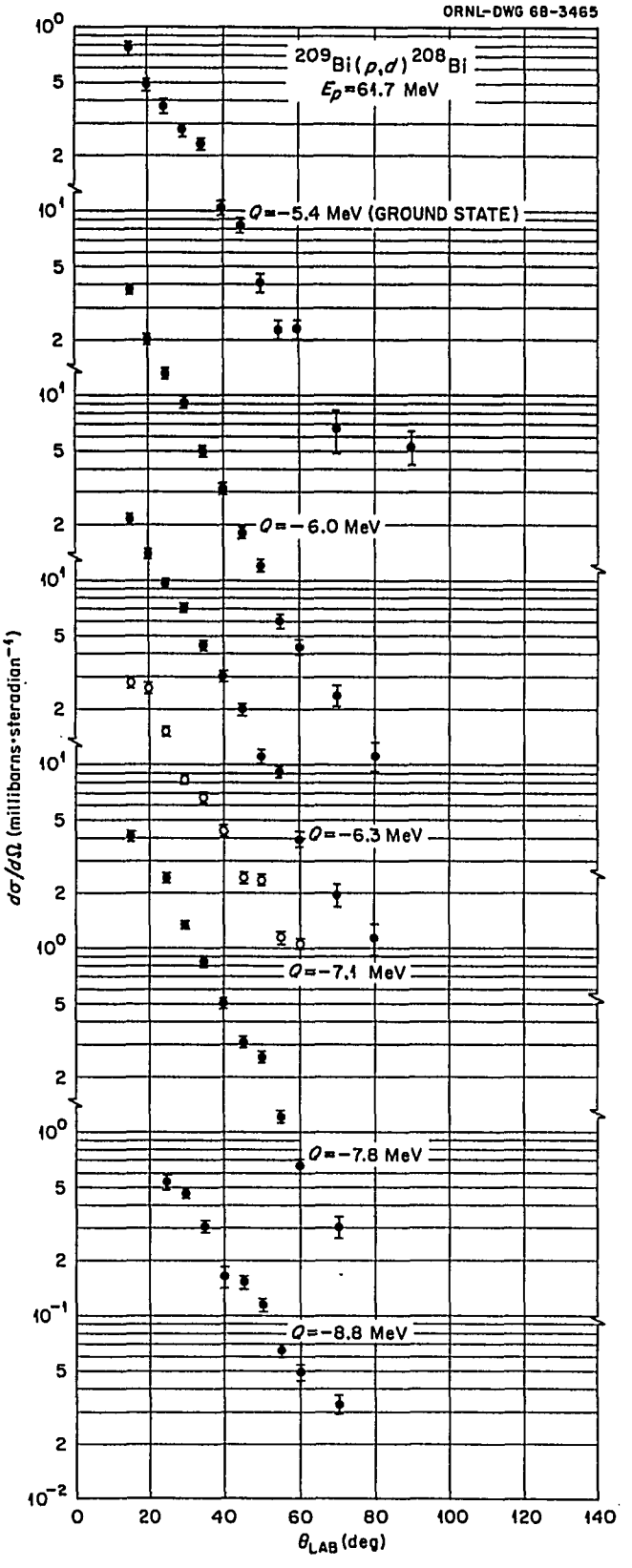

Fig. 37. Differential Cross Sections for Levels Observed in the $^{209}Bi(p,d)^{208}Bi$ Reaction.

Ishizaki et al.[53] at 57 MeV and again general agreement of level structure is noted with the present work. However, in the case of the deuteron spectrum, the levels are closely spaced and the improved resolution (~15 times better in this case) separated several levels unreported at 57 MeV.

Cross sections for the protons, deuterons, tritons, helium-3's, and alphas from ^{209}Bi are listed in Appendix A in Tables AXI to AXV. These cross sections are averaged over 1-MeV intervals and the energy shown is the center of the interval.

Secondary proton spectra from ^{209}Bi at several angles are plotted on Fig. 38, along with a calculation discussed in the next chapter. As in the previous cases for carbon and iron, the inelastic levels have been removed and a smooth continuum has been drawn under the peaks. The low energy region of the proton spectra, although no longer peaked at all angles, again becomes constant in magnitude for large angles while the highest energy protons of the spectra decrease rapidly in magnitude to a small or zero cross section for angles greater than ~110 degrees. The spectra at angles smaller than 30 degrees again exhibit a high energy peak; however, as is the case for the carbon and iron data, the location of the peak does not move as it should if the peak were produced by quasi-elastic scattering.

Differential cross sections for three energy regions of the proton spectra from bismuth are plotted on Fig. 40. The region from 14 to 16 MeV is near the coulomb barrier, while the high energy region between 49 and 51 MeV is just below the inelastic proton peaks. The

---

[53]Y. Ishizaki et al., J. Phys. Soc. Japan 20, 12, 2118 (1965).

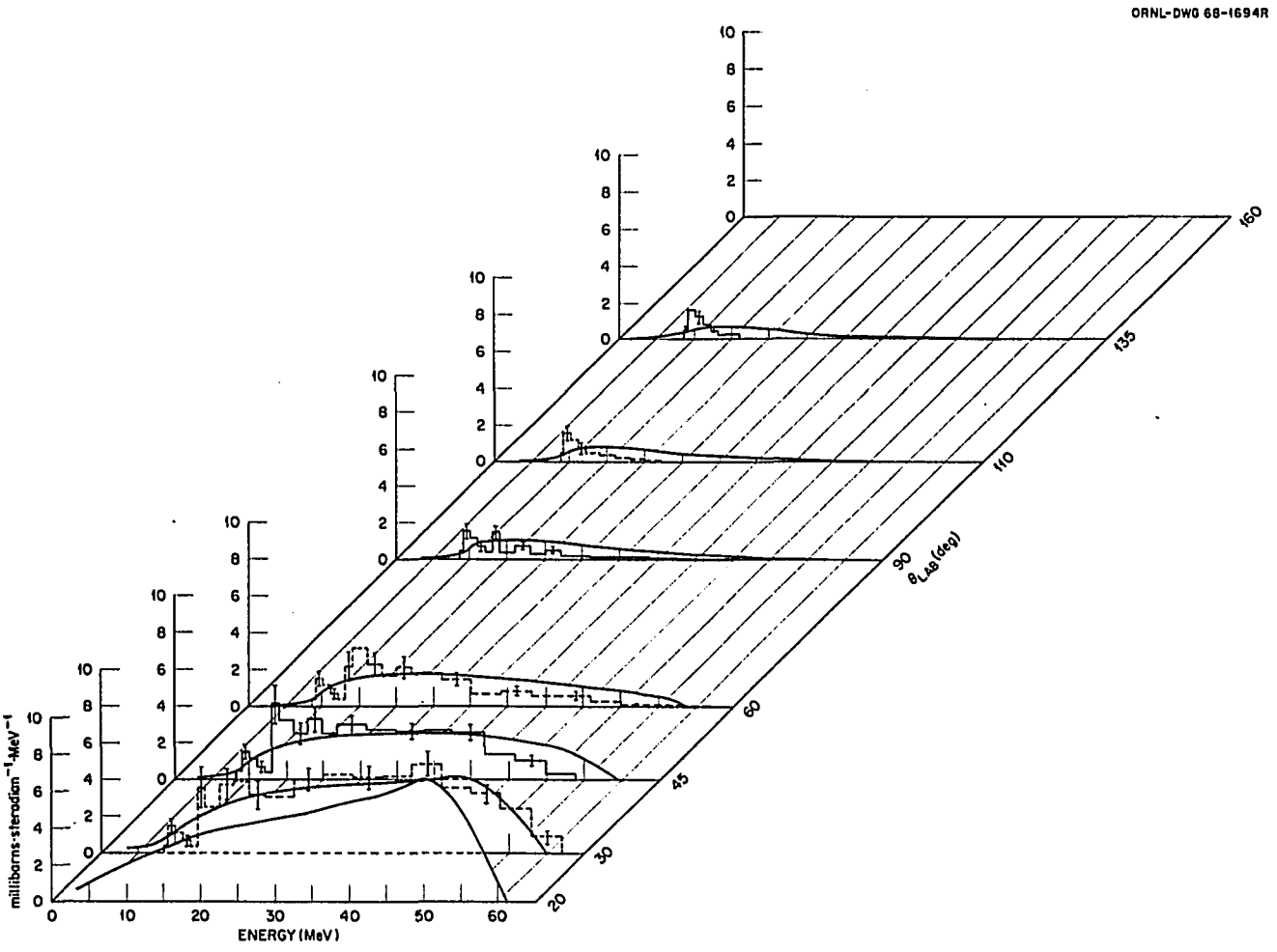

Fig. 38. Proton Continuum Spectra from ^{209}Bi Compared with Intranuclear Cascade Calculations.

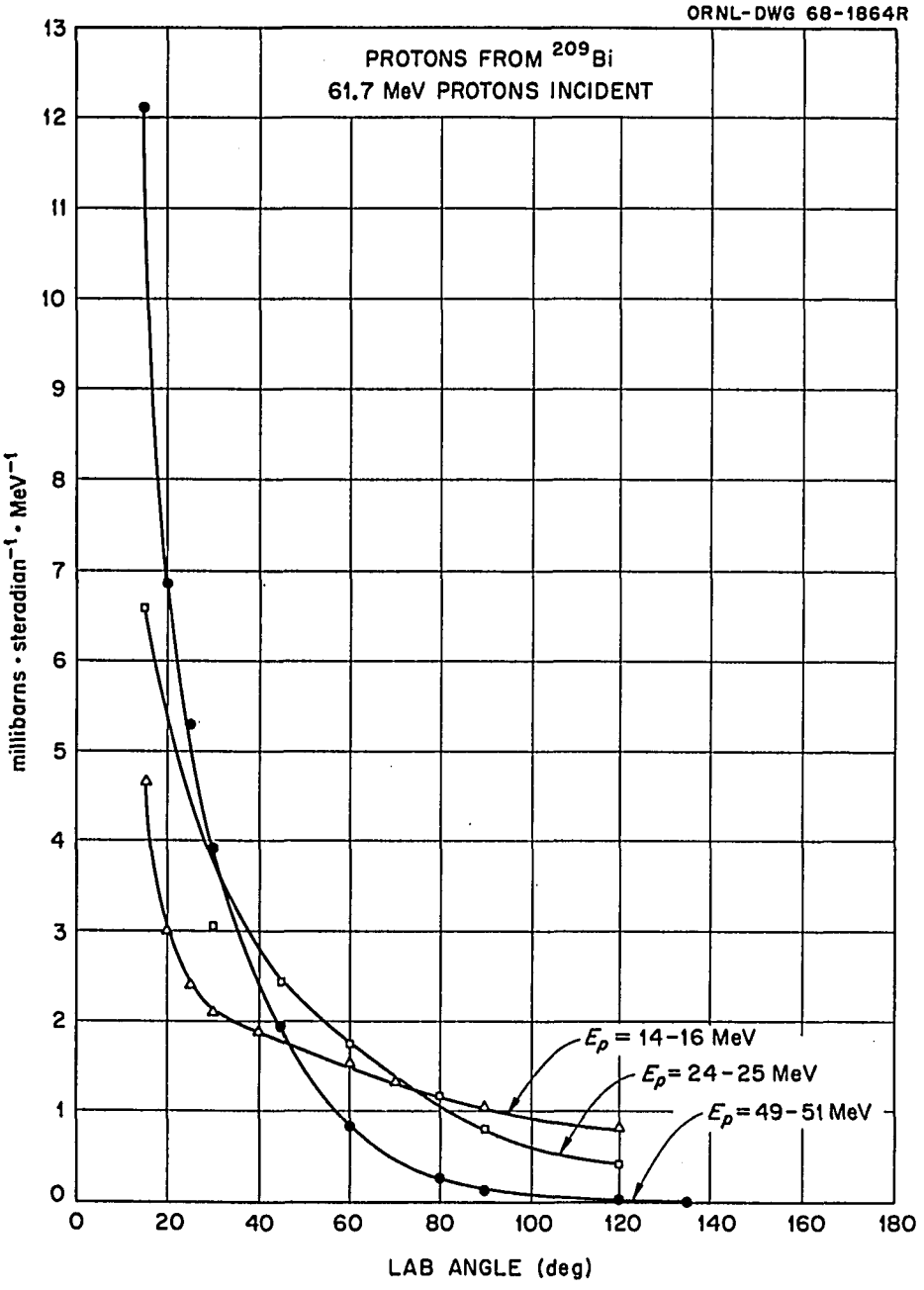

Fig. 39. Differential Cross Sections for Three Energy Regions of the Secondary Proton Spectrum from ^{209}Bi.

behavior of the cross section for the energy regions shown is similar to corresponding regions in the carbon and iron spectra. The low energy region is shown to be approaching a constant value for angles larger than 120 degrees and for the larger angles the low energy distribution provides the majority of the cross section. All three regions are forward peaked, with, as is the case for the carbon and iron proton data, the highest energy region exhibiting the strongest peaking and the most rapid decrease of cross section with angle.

The proton spectrum from bismuth produced by 55-MeV protons has been reported for energies above ~15 MeV.[12] It is found that, as in the case for carbon, the magnitude of the 55-MeV data is ~40% higher at 15 degrees than the data reported here. However, the agreement between the two sets of data for 30, 60, 90, and 120 degrees is within our errors. The spectrum of deuterons from ^{209}Bi is shown for several angles in Fig. 40. The spectra are very similar in shape to the proton spectra seen on Fig. 38 and the change in magnitude of the spectra with increasing angle is similar to that for the proton spectrum. Again, it is to be noted that the discrete levels have been removed and a smooth continuum drawn in their place.

As is seen in Fig. 41, the behavior of the alpha particle energy spectra from bismuth is very similar to that of the protons and deuterons, except that the low energy distribution dominates the magnitude of the spectra at all angles. It is again seen that the spectra are forward peaked for all energy regions and that the high energy cross sections fall off very rapidly while the magnitude of the low energy distribution becomes constant at large angles.

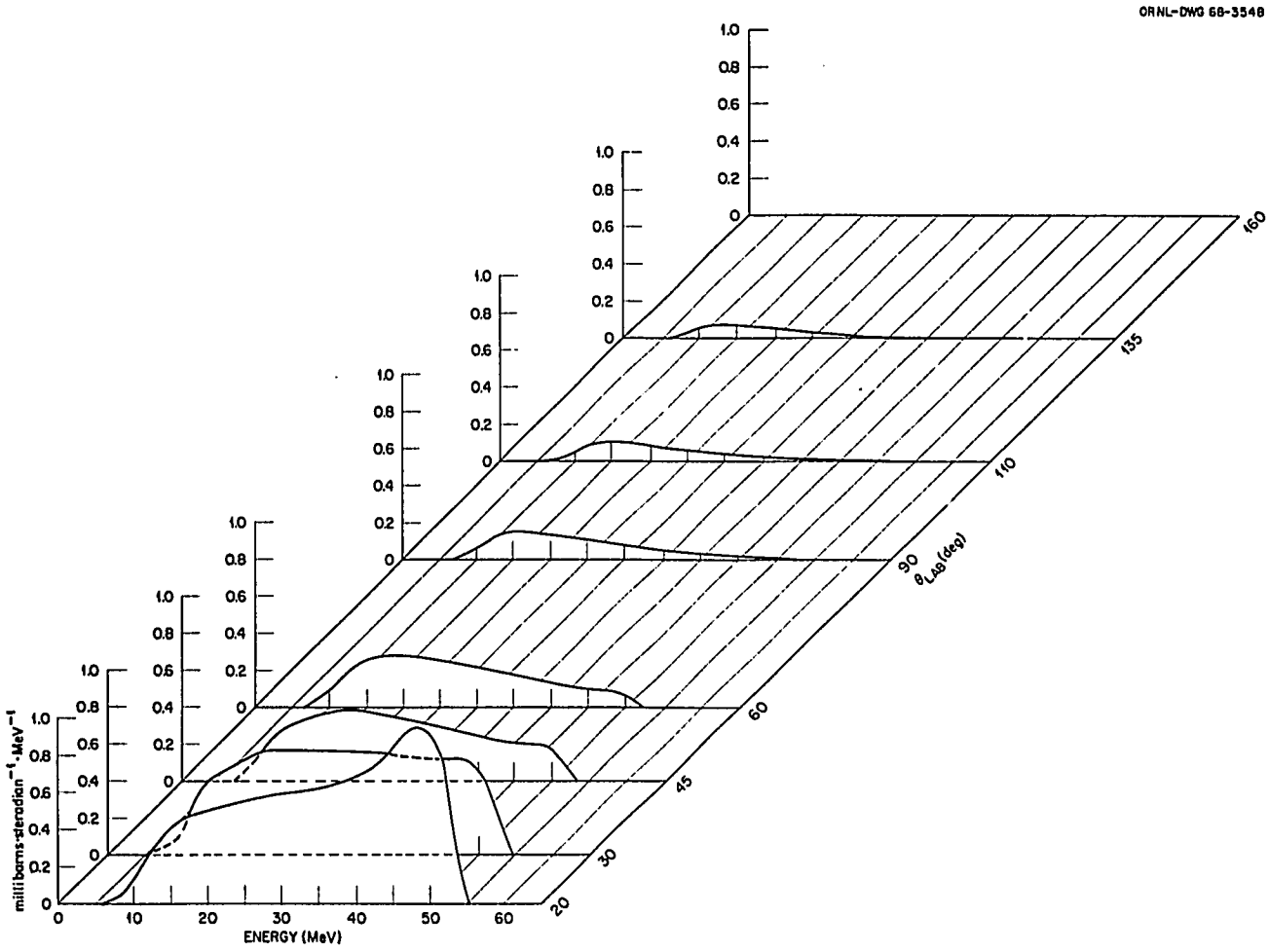

Fig. 40. Deuteron Continuum Spectra from ^{209}Bi.

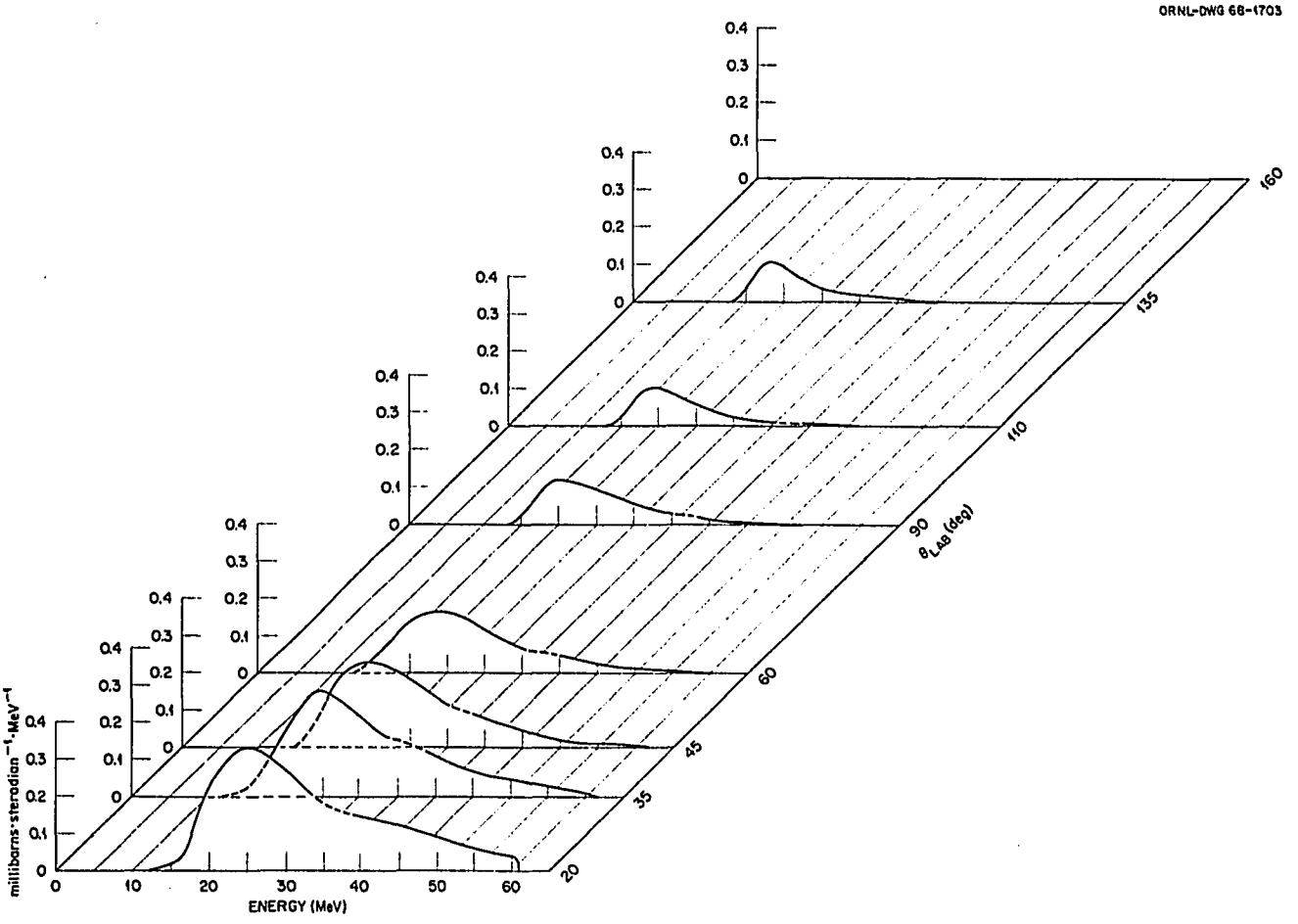

Fig. 41. Alpha Continuum Spectra from ^{209}Bi.

The energy integrated differential cross section for the protons, deuterons, tritons, helium-3, and alpha particles from ^{209}Bi are plotted in Fig. 42 and the cross sections are tabulated in Table XXXIV. The cross sections are seen to be strongly forward peaked and approach a constant value for angles larger than ~100 degrees. The shape of these distributions is the same as those for carbon and iron and again suggests that the mechanism of production is composed of more than one process.

The angle integrated cross sections for the charged particles from bismuth are listed in Table XXXV and the total cross sections integrated over angle and energy are tabulated in Table XVII.

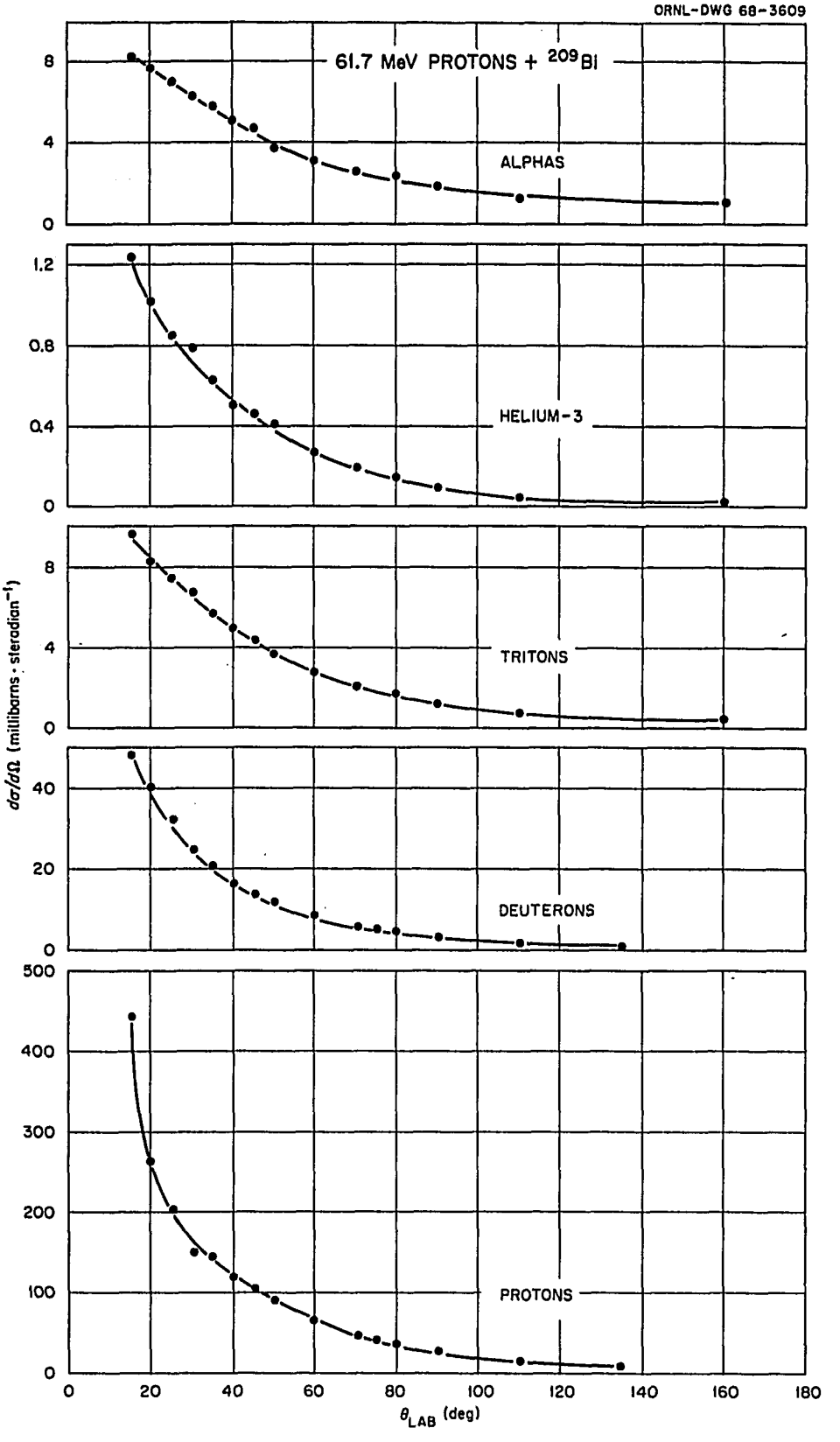

Fig. 42. Energy Integrated Differential Cross Sections for Protons, Deuterons, Tritons, Helium-3's, and Alphas from ^{209}Bi.

TABLE XXXIV. ENERGY INTEGRATED TOTAL DIFFERENTIAL CROSS SECTIONS

^{209}Bi

Lab. Angle (deg)	Total Cross Sections (mb/sr)				
	Proton (nonelastic)	Deuteron	Triton	Helium-3	Alpha
15	446.0	48.4	9.75	1.23	8.23
20	263.8	39.6	8.24	1.03	7.72
25	205.9	32.1	7.44	0.85	6.90
30	161.0	24.5	6.78	0.78	6.29
35	145.6	21.1	5.83	0.63	5.79
40	122.2	16.7	4.95	0.50	5.06
45	107.4	13.7	4.42	0.46	4.75
50	92.3	12.1	3.67	0.41	3.78
60	66.4	8.43	2.74	0.26	3.08
70	48.4	5.81	2.01	0.20	2.43
80	40.0	4.80	1.69	0.15	2.28
90	28.2	3.49	1.21	0.098	1.76
110	17.1	1.95	0.65	0.056	1.17
135	10.6	1.01	0.40	0.022	0.97

TABLE XXXV

Angle Integraged Cross Section

^{209}Bi

Energy (MeV)	Cross Section (mb/MeV)				
	Proton	Deuteron	Triton	Helium-3	Alpha
1.5	0	0	0	0	0
2.6	0	0	0	0	0
3.6	1.50	0	0	0	0
4.6	2.29	0.15	0.01	0	0
5.7	2.72	0.19	0.04	0	0
6.7	3.84	0.20	0.06	0	0
7.8	5.22	0.27	0.08	0	0
8.8	7.13	0.48	0.18	0	0
9.9	9.58	0.90	0.39	0	0
10.9	13.63	1.36	0.67	0	0
12.0	14.02	1.86	0.78	0.01	0
13.0	14.33	2.25	0.87	0	0.04
14.1	15.63	2.26	0.99	0	0.12
15.1	16.55	2.40	1.31	0.01	0.27
16.2	16.77	2.39	1.20	0	0.56
17.2	16.91	2.43	1.12	0	0.98
18.3	17.15	2.53	1.03	0	1.34
19.3	17.23	2.48	1.06	0.01	1.55
20.4	17.46	2.50	1.0	0.01	1.64
21.4	17.18	2.50	0.95	0.02	1.62
22.5	16.77	2.35	0.90	0.03	1.60
23.5	16.77	2.44	0.85	0.03	1.56
24.6	16.64	2.31	0.83	0.04	1.53
25.6	16.19	2.33	0.76	0.05	1.45
26.7	16.02	2.17	0.67	0.05	1.39
27.7	15.87	2.10	0.69	0.06	1.27
28.8	15.83	2.09	0.61	0.08	1.16
29.8	15.18	1.98	0.56	0.07	1.05
30.9	15.11	1.91	0.53	0.10	0.93
31.9	14.85	1.83	0.52	0.10	0.83
32.9	14.46	1.83	0.49	0.15	0.73
34.0	14.47	1.69	0.45	0.08	0.58
35.0	14.32	1.68	0.42	0.07	0.57
36.1	14.28	1.64	0.42	0.08	0.37
37.1	14.54	1.59	0.35	0.06	0.80
38.2	14.17	1.52	0.35	0.07	0.64
39.2	13.88	1.46	0.33	0.06	0.50
40.3	13.59	1.42	0.31	0.06	0.42
41.3	13.28	1.47	0.32	0.05	0.38
42.4	13.11	1.38	0.28	0.06	0.34
43.4	12.91	1.36	0.28	0.06	0.29
44.5	13.02	1.42	0.27	0.05	0.28
45.5	12.71	1.37	0.26	0.05	0.24
46.6	13.16	1.40	0.25	0.04	0.20
47.6	12.70	1.48	0.22	0.04	0.20
48.7	12.78	1.46	0.18	0.05	0.16
49.7	12.57	1.54	0.19	0.06	0.15
50.8	12.44	1.58	0.12	0.09	0.14
51.8	11.33	1.11	0.17	0.09	0.11
52.9	10.55	1.98	0.12	0.05	0.11
53.9	10.43	4.56	0.03	0.01	0.10
55.0	10.28	4.12	0	0.01	0.09
56.0	11.81	3.22	0	0	0.08
57.1	13.70	0	0	0	0.07
58.1	7.18	0	0	0	0.07
59.2	12.42	0	0	0	0.07
60.2	0.31	0	0	0	0.06

CHAPTER V

DISCUSSION

A. Elastic Scattering

Although the data presented in this work was taken from only three targets, there are some clear trends to the elastic scattering differential cross sections, as is seen in Fig. 17. The most obvious trends are (1) the increase in the oscillatory structure with increase in A, (2) the movement of the first minimum in the cross section to smaller angle with increasing A, and (3) the more rapid decrease in the cross section at the most forward angles with increasing A. These trends are not unique to the incident energy of ~60 MeV, but have been observed at other intermediate energies, notably 30-,[54] 40-,[5] and 160 MeV.[1]

In recent years it has been shown that over a wide range of incident energy the observed elastic differential cross sections of nucleon-nucleus scattering can be satisfactorily accounted for by the nuclear optical model.[55] The historical development of the model, which was based largely on agreement with experimental data, has been discussed in several places[48] and the mathematical development has also been well documented.[55,56] Since the basis of the model is so thoroughly discussed elsewhere, and since the application of the model to data taken with 60-MeV incident protons is not unique,[2] only the basic assumption of the nuclear potential used in the model will be described

---

[54] L. N. Blumberg et al., Phys. Rev. 147, 3, 812 (1966).

[55] M. A. Preston, Physics of the Nucleus, Ch. 18, Addison Wesley, 1962.

[56] P. E. Hodgson, The Optical Model of Elastic Scattering. Selected Topics in Nuclear Spectroscopy, compiled by B. J. Verhaar, North-Holland Publishing Company, Amsterdam, 1964.

The distinguishing feature of the optical model is that the potential involved is complex and of the general form (for a spherical core)

$$V(r) = - U_o f(r) - i\, Wg(r) \qquad (5.1)$$

where U_o and W are the depths of the real and imaginary parts of the nuclear optical potential and f(r) and g(r) are their radial form factors. If the incident particle is charged, the Coulomb electrostatic potential $V_c(r)$ must be added to the potential given in Eq. (5.1).

The form factor f(r) most often used with the real central potential is the Saxon-Woods form factor

$$f(r) = \frac{1}{1 + \exp(r - R/a)} \qquad (5.2)$$

In Eq. (5.2) R measures the overall extent of the potential and is expected to be similar to the nuclear size. The parameter a controls the rapidity with which f(r) falls off and the parameter is therefore related to the diffuseness of the nuclear surface.

The imaginary part of the optical potential, Wg(r), accounts for all nonelastic processes through absorption of incident flux, i.e., nucleons are removed from the elastic channel, however, without differentiating between them. The form factor g(r) depends on the incident energy; at low energies the interaction is most likely to be concentrated in the surface region while at higher energies the absorption spreads throughout the nuclear volume. The analytical form often used for surface absorption is $g_s(r) = - 4\, a\, f'(r)$,[56] defined so that $g_s(R) = 1$, where $f'(r)$ denotes differentiation with respect to r. The

form used for volume absorption is usually $g_v(r) = f(r)$. The total imaginary potential may be a combination of both volume and surface absorption and given by

$$Wg(r) = W_v\, f(r) - 4\, a\, W_D\, f'(r) \qquad (5.3)$$

where W_v and W_D denote the volume and surface absorption potential depths, respectively.

It has been found that agreement with experimental data was further improved by including in the potential a spin-orbit term of the form

$$V_{so}(r) = (U_s + i\, W_s)\, h(r)\, \vec{\sigma}\cdot\vec{\ell} \qquad (5.4)$$

where U_s and $i\, W_s$ are the real and imaginary depths of the spin-orbit potential and $\vec{\ell}$ and $\vec{\sigma}$ are the angular momentum and Pauli spin operators, respectively. The spin-orbit radial form factor $h(r)$ is given by

$$h(r) = -\frac{1}{r} f'(r). \qquad (5.5)$$

The addition of V_{so} allowed theoretical calculation of polarization of elastically scattered nucleons for comparison with experiment. Thus, three types of experimental data can be used to determine optical model parameters: differential elastic scattering cross sections, total inelastic reaction cross sections, and polarization of elastically scattered nucleons.

The total optical potential used in this analysis is given by the combination of the terms shown in Eqs. (5.1), (5.2), (5.3), and (5.4). However, since the form factor parameters R and a may not be the same for each of these parts of the potential, the total potential may be written

$$V(r) = V_c(r) - U_o\left(\frac{1}{e^x + 1}\right) - i\left(W_v - 4\,a\,W_D\,\frac{d}{dx_I}\right)\frac{1}{e^{x_I} + 1}$$
$$+ (U_s + i\,W_s)\,\frac{1}{r}\,\frac{d}{dr}\left(\frac{1}{e^{x_s} + 1}\right)\vec{\sigma}\cdot\vec{\ell} \qquad (5.6)$$

where

$$x = (r-R)/a,\ x_I = (r-R_I)/a_I,\ x_s = (r-R_s)/a_s \qquad (5.7)$$

with

$$R = r_o A^{\frac{1}{3}},\ R_I = r_{o_I} A^{\frac{1}{3}},\ R_s = r_{o_s} A^{\frac{1}{3}} \qquad (5.8)$$

In q. (5.8) R is the radius defined for the real potential, imaginary potential and spin-orbit potential, in that order, while a, a_I, and a_s are the Saxon-Woods diffuseness parameters for the same potentials.

The Coulomb interaction term is that for a uniform spherical charge distribution with

$$V_c = Ze^2/r,\ r > Rc$$
$$V_c = \frac{Ze^2}{2Rc}\,(3 - r^2/R_c^2),\ r \le R_c \qquad (5.9)$$

where

$$R_c = r_c\,A^{\frac{1}{3}} \qquad (5.10)$$

The calculation of the elastic differential cross-sections were performed using the computer program JIB III.[57] The program fitted the calculation to the experimental data by varying the various parameters of the potential until the quantity

$$X_T^2 = \frac{\sum_i |\sigma_{th}(\theta_i) - \sigma_{ex}(\theta_i)|^2}{[\Delta\sigma_{ex}(\theta_i)]^2} \qquad (5.11)$$

---

[57] Written by F. G. Perey (unpublished).

is minimized. In Eq. (5.11), $\sigma_{th}(\theta_i)$ and $\sigma_{ex}(\theta_i)$ refer to the calculated and experimental cross section at an angle θ_i, and $\Delta\sigma_{ex}(\theta_i)$ is the experimental error in the cross section measured at angle θ_i. The fitting program starts with an initial set of potential parameters and varies these until X_T^2 is minimized.

Since studies have been previously made of the optical model fits to elastic scattering data at ~60 MeV, it was desired to use the parameters obtained in these works as initial paramaters and only determine whether the present elastic data could be fitted. The parameters obtained for ^{58}Ni and ^{208}Pb by Fulmer et al. at 60 MeV were used as initial parameters for a fit of the present ^{54}Fe and ^{209}Bi data, respectively. Because of a lack of a 60-MeV optical model fit for ^{12}C elastic data, some suggested[58] initial parameters were used. As polarization data at 60 MeV was not available, the spin-orbit parameters, U_s, W_s, r_s, and a_s were not varied for ^{54}Fe and ^{209}Bi. However, some of the spin-orbit parameters were varied for the carbon data. The parameters which were varied in the calculation are shown on Table XXXVI.

The "best fit" optical model parameters for ^{12}C, ^{54}Fe, and ^{209}Bi are listed in Table XXXVI, along with the initial parameters used. The initial and final X_T^2 are also listed in the table. The quality of the fits to the experimental data are shown on Fig. 17, and it is seen that the fit is quite good for all three targets discussed. The fit to the ^{54}Fe data is low in the angle region of 70 to 80 degrees and it is in this region that most of the total X_T^2 is obtained. The fits

---

[58] J. K. Dickens (private communication).

TABLE XXXVI. OPTICAL MODEL PARAMETERS; INITIAL AND "BEST FIT"

Element		Real			Imaginary				Spin Orbit			
		V (MeV)	r (F)	a (F)	W_S (MeV)	W_D (MeV)	r (F)	a (F)	V_{so} (MeV)	r_{so} (F)	a_{so} (F)	χ^2_T
^{12}C	Initial	38.00	1.160	.7000	9.500	.7000	1.400	.6300	6.0	1.060	.7000	678
	Final	26.09	a	.7477	6.618	a	a	.5599	12.0	a	a	166
^{54}Fe	Initial	41.00	1.160	.7300	6.660	2.320	1.330	.5000	6.0	1.060	.7380	416
	Final	38.40	a	.7177	6.751	1.879	a	a	a	a	a	248
^{209}Bi	Initial	41.40	1.220	.5800	2.010	7.810	1.320	.6700	6.0	1.060	.7380	897
	Final	38.60	a	.7422	4.238	3.964	a	a	a	a	a	135

[a]This parameter was not varied.

for all three cases are poorest at the back angles; however, the contribution to X_T^2 from these points is lessened by the large experimental errors assigned to the back angle cross sections.

It is seen on Table XXXVI that the final set of parameters calculated are a considerable improvement over the initial set for each case, as determined by the smaller X_T^2 value. The changes in the real well depth for ^{54}Fe and ^{209}Bi were small between initial and final sets; however, changes in the imaginary potential depths were larger. In the case of carbon, however, the change in the real well depth was considerable, and a large real spin-orbit potential was found to be required for the best fit.

The optical analysis of ^{12}C is confused by the apparent ability to fit the experimental data equally well with any of several sets of potential parameters,[59] whereas good fits to data from medium and heavy nuclei lead to more or less the same parameters. In an effort to determine whether the present 60-MeV carbon data could be fit by any of several sets of parameters, seven initial sets were chosen from the analysis of 45-MeV data reported in reference 59. It was found that the fits to the 60 MeV elastic scattering data were all of nearly equal quality: a quality as good as that obtained with the parameters is shown in Table XXXVI. Elimination of some of the seven final predictions could be based on shapes of the polarization (inferred from 40-MeV data[54]) or on the basis of measured total inelastic reaction cross sections; however, following such an elimination at least three sets were still acceptable. It has been found difficult at other

---

[59]G. R. Satchler, Nuclear Physics A100, 497 (1967).

energies to fit both ^{12}C differential elastic cross sections and elastic polarizations with the same parameters.[54]

It is felt that the optical model predictions shown on Fig. 17 and based on the parameters listed in Table XXXVI provide as good a fit to the present 60-MeV data as fits obtained to other experiments in the intermediate energy region. Although the optical model study under taken here was by no means extensive, it does seem that the ambiguity found in calculations for carbon data at lower energies are present at 60 MeV.

B. Secondary Proton Production

In this section the production of secondary protons in the continuum region will be discussed and the data will be compared to an existing intranuclear cascade model which has been used extensively for incident nucleons with energies above ~150 MeV. The proton continuum is considered to consist of all regions of the proton spectrum except the elastic and inelastic scattering peaks; however, the latter may in some cases rise from the "true" continuum. In order to compare the continuum cross sections with calculations, the cross section provided by the inelastic levels has been included in the energy integrated cross sections and such an inclusion is noted.

The secondary proton spectra from ^{12}C, ^{54}Fe, and ^{209}Bi are shown for comparison on Fig. 43. It should be noted that the cross section scale for the ^{12}C spectrum is twice as large as that for ^{54}Fe and ^{209}Bi. The spectra are dominated at the highest energies by peaks caused by elastic and inelastic scattering of the incident protons. The peak structure is different for the three spectra beacuse of the

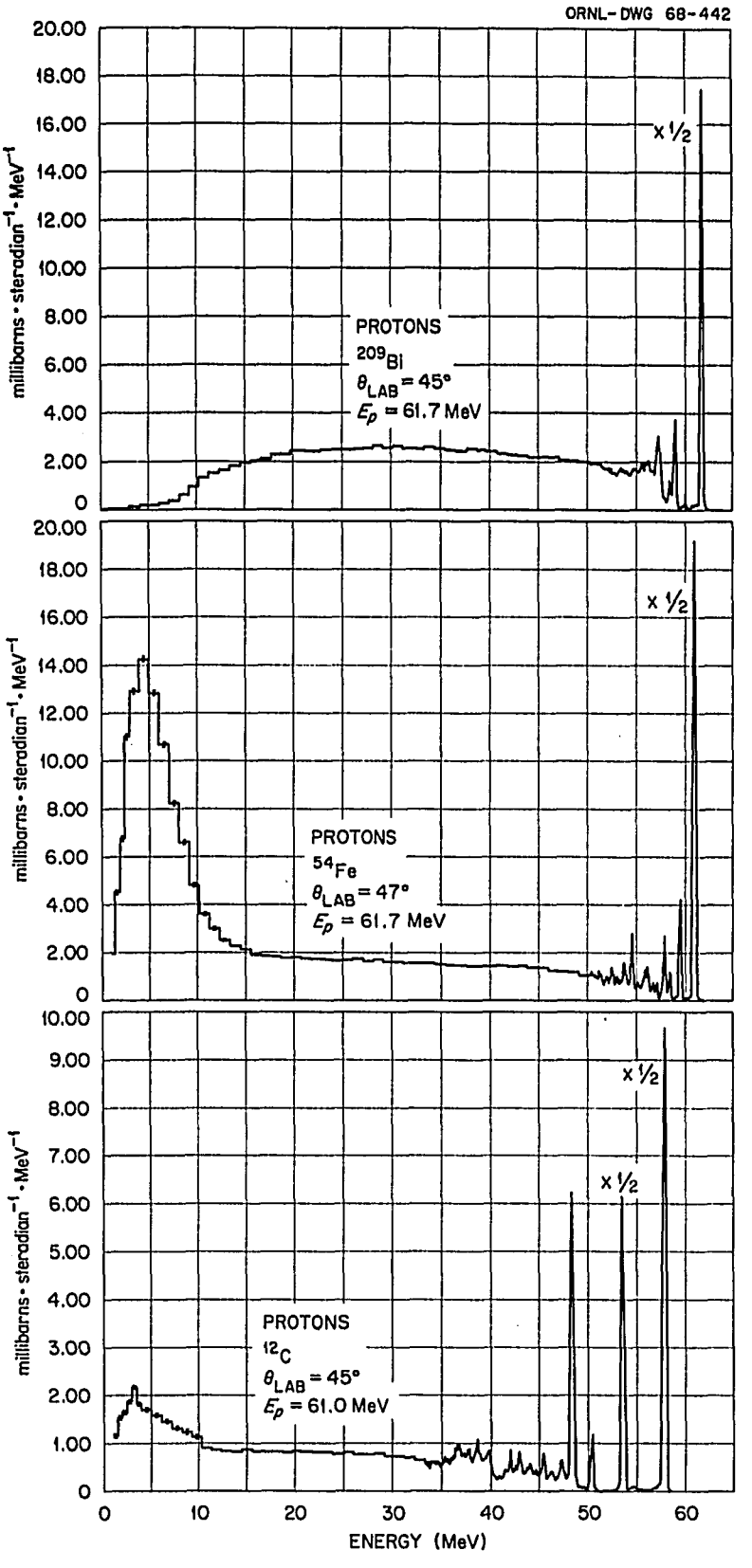

Fig. 43. Secondary Proton Spectra from ^{12}C, ^{54}Fe, and ^{209}Bi at 45 Degrees.

different nuclear level structures of the nuclei.

The proton spectra shown on Fig. 43 are distinctly similar over the energy region between ~20 MeV to just below the inelastic levels and in this region the cross section increases with increasing target mass. In the energy region below ~20 MeV the spectra differ greatly in both shape and magnitude. The comparison between the three spectra is consistent throughout all angles of observation.

The energy-integrated proton (excluding elastic events) differential cross sections for the ^{12}C, ^{54}Fe, and ^{209}Bi targets are compared in Fig. 44, and one observes that the three behave in a similar manner as a function of angle. Each curve is seen to be very strongly peaked at small angles and decrease rapidly with increasing angle until a nearly constant magnitude is reached for angles greater than ~120 degrees. The character of the energy integrated differential cross sections observed in the present work are similar to those found at higher energies.[19]

It has been pointed out in Chapter IV that the shape of these angular distributions supports the contention that more than one process is responsible for the total proton (and other secondary particle) production. Further evidence for this hypothesis is obtained from a comparison, at the same angle, of secondary proton data from the neighboring nuclides, ^{56}Fe and ^{54}Fe. These spectra, at 20 degrees for instance, are fount to have identical cross sections in the energy region above ~20 MeV (excluding differences in peak structure caused by nuclear level differences). However, the magnitude of the cross section in the low energy peak observed in iron (see

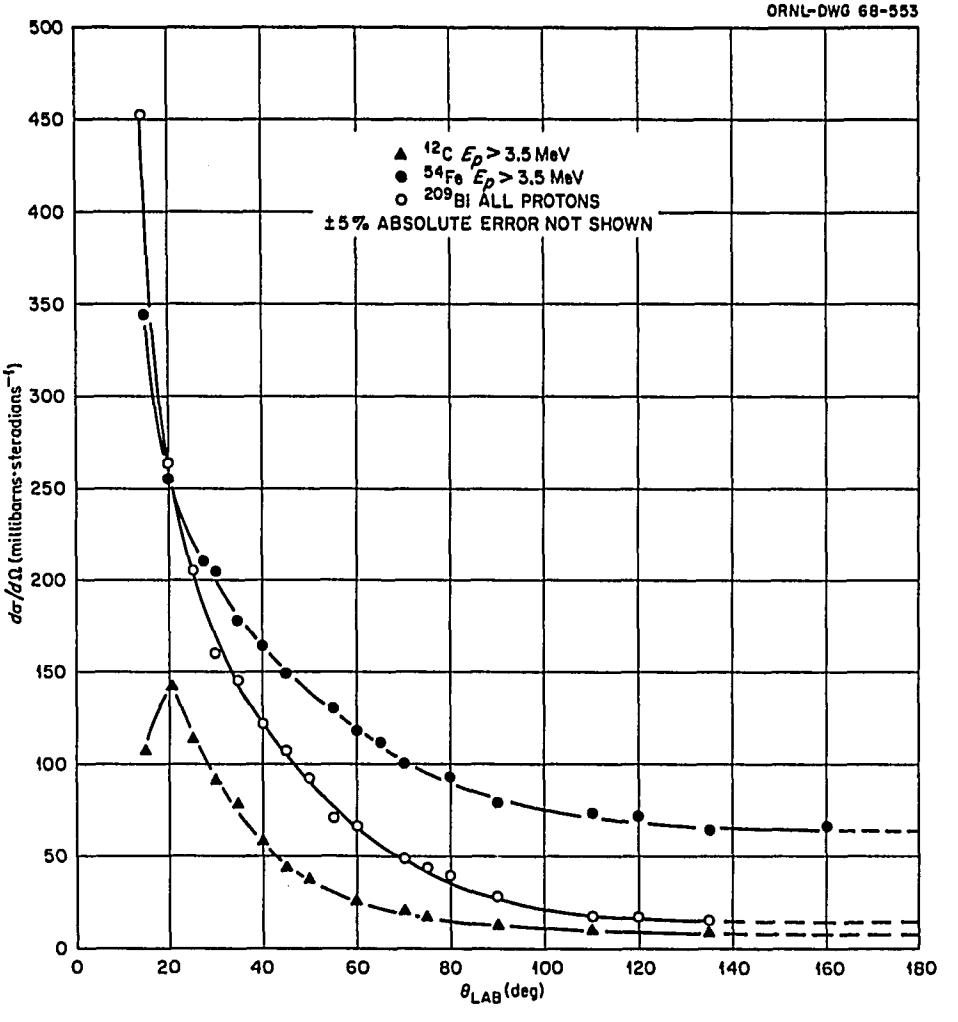

Fig. 44. Energy Integrated Differential Cross Sections for Protons from ^{12}C, ^{54}Fe, and ^{209}Bi.

Fig. 25) is only 70% as large for ^{56}Fe as for ^{54}Fe. Since the process for the low energy (<10 MeV) proton production is apparently isotropic, it may be argued that the mechanism is compound nuclear in nature and further that the process could be nuclear evaporation. Indeed, the difference in magnitude between the low energy data from ^{54}Fe and ^{56}Fe can be can be explained by an evaporation process since neutrons should preferentially be evaporated from ^{56}Fe (therefore reducing proton evaporation) as it is the more neutron-rich isotope. The characteristics which dominate the medium and high energy proton production are the forward peaking and rapid decrease in magnitude with increasing angle of the energy integrated differential cross sections. Such an angular distribution can be explained by a direct interaction process in which the incident nucleon interacts only with a single target nucleon independent of detailed structure. A nucleon-nucleon interaction of this type would account for the equal magnitude in the medium and high energy regions of the proton spectra from ^{54}Fe and ^{56}Fe.

The secondary proton data obtained in this experiment have been compared, in the continuum regions, with calculations based on a nuclear model which employs both direct and evaporation mechanisms of secondary particle production. The model, which is most often called the intranuclear-cascade model, predicts absolute cross sections so that the comparisons with the experimental results are not "fits" to the data as in the case of optical model calculations.

The basic assumption of the calculation is that the interaction of the incident nucleons with the nucleus can be represented by

sequential free nucleon-nucleon collisions inside the nucleus. The usual justification for this assumption[60] is that the wavelength of the incident particle is of the order (or less than) the intranucleon spacing, $\sim 10^{-13}$ cm. The deBroglie wavelength (λ) of a free nucleon at a few energies is:

Energy (MeV)	Nucleon (cm)
10	1.44×10^{-13}
20	1.02×10^{-13}
60	5.88×10^{-14}
100	4.45×10^{-14}
500	1.82×10^{-14}

It is seen that the validity of the assumption of free nucleon-nucleon collisions in the nucleus increases as the energy of the incident nucleon increases, and it is not until ~20 MeV that the nucleon wavelength equals the intranucleon spacing. There must be a region of energy above 20 MeV, perhaps including 60 MeV, in which the assumption begins to break down.

The intranuclear cascade model was introduced by Goldberger;[61] However Metropolis et al.[62] first utilized computer techniques to calculate the resulting particle spectra. Monte Carlo methods are used to follow each incident nucleon and any subsequent reaction products through a model nucleus. The interactions which the nucleons undergo are based on cross sections for free p-p and n-p scattering.

---

[60]H. Bertini, Phys. Rev. 131, 1801 (1963); and Monte Carlo Calculations on Intranuclear Cascades, ORNL-3383 (1963).

[61]M. L. Goldberger, Phys. Rev. 74, 1269 (1948).

[62]M. Metropolis et al., Phys. Rev. 110, 185 (1958)

The nucleons are followed along their "classical" paths in the nucleus until they escape, fall below a cutoff energy, or have a collision with another nucleon (then the reaction products are also followed). In this manner a "cascade" of nucleons may be formed and when no more particles can escape by the cascade process the remaining energy is assumed to become distributed among all the target nucleons and the residual excitation is treated by a nuclear evaporation model.

The calculations shown in this work were based on the intranuclear cascade model of Bertini.[60] In this model the nuclear density distributions found from electron scattering data are approximated by three concentric spherical regions, in each of which the density was set equal to the average value which would be calculated from the electron data for the region. The nucleons were assumed to have a zero temperature Fermi momentum distribution in each region. The potential energy (well depth) in each region was determined by the sum of the zero-temperature Fermi energy of the nucleons in the region plus the binding energy of the most loosely bound nucleon, which was assumed to be 7 MeV for all nuclei. The model nucleus parameters used in the calculations for protons are shown in Table XXXVII. The radii listed are the outer boundaries between the constant density regions of the model nucleus. The potentials listed include the 7-MeV nucleon binding energy.

The output from the Monte Carlo program of Bertini is a magnetic tape which lists kinematic parameters for each escaping neutron or proton. These tapes were analyzed by the program BERDBIND[63] which

---

[63] R. W. Peelle, A Guide to BERDBIND, and Analysis Program for History Tapes from the H. W. Bertini Intranuclear Cascade Calculations, ORNL-CF-67-3-43, (1967).

TABLE XXXVII. INTRANUCLEAR CASCADE PARAMETERS

Nucleus	Outer Radius of Region (F)	Proton Potential (MeV)
^{12}C	1.31	-38
	3.22	-27
	4.96	-12
^{54}Fe	2.85	-43
	4.80	-31
	6.55	-13
^{209}Bi	5.16	-41
	7.11	-30
	8.86	-12

provides calculated differential cross sections for selected energy and angle bins. The evaporation, which carries off the residual nuclear excitation left after each cascade is estimated by the Monte Carlo program EVAP[64] which has been incorporated in the BERDBIND analysis program. The evaporation calculation is based on the compound-nucleus theory of Weisskopf[65] and assumes isotropic emission of particles. The calculation is capable of producing evaporation neutrons, hydrogen isotopes and helium isotopes.

It was mentioned above that one of the means by which a particular cascade process is terminated is for the cascade particle to fall below an arbitrary cutoff energy. Once the nucleon has fallen below this energy it is assumed that the particle can escape only by the evaporation process. The cutoff energy used for the calculations presented here was the Coulomb barrier energy (to nearest 1 MeV) for each nucleus. These cutoffs were: ^{12}C, 2 MeV; ^{54}Fe, 6 MeV; and ^{209}Bi, 16 MeV. The use of a "classical" cutoff is incorrect in the sense that there is a probability of penetration of the protons through the Coulomb barrier. For some calculations the result of ignoring this penetration probability is a discontinuity in the predicted cross sections at the cutoff energy.

In review, the Monte Carlo program of Bertini coupled with the Monte Carlo evaporation program of Dresner provides a prediction of the total nonelastic proton energy spectrum which is based on two distinct reaction mechanisms. The cascade portion of the calculation, which is

---

[64]L. Dresner, A FORTRAN Program for Calculating the Evaporation of Various Particles from Excited Compound Nuclei, ORNL-CF-61-12-30, (1961).

[65]J. M. Blatt and V. E. Weisskopf, Theoretical Nuclear Physics, (John Wiley and Sons, Inc., New York, 1952), pp. 365.

based on a direct interaction assumption, can produce secondary particles over all energies between the cutoff energy and the elastic energy. It would be expected then that the part of the spectrum predicted by this mechanism should correspond to the experimentally observed spectra in the regions attributed earlier to a forward peaked direct interaction process. However, if secondary protons are produced by a direct process with energies less than the cutoff (Coulomb barrier for these calculations) the calculations will be incapable of predicting these. On the other hand, the evaporation portion of the calculation is based on an isotropic, compound-nucleus, mechanism and should predict that portion of the observed spectra which is isotropic in nature, the low energy regions.

Shown in Figs. 22, 30, and 38 are the calculated cascade plus evaporation proton spectra compared to the experimentally observed spectra for ^{12}C, ^{54}Fe, and ^{209}Bi, respectively. The calculated data are shown as histograms and the errors reflect the statistical errors in the Monte Carlo process. The experimental errors in the spectra are quite small, perhaps no larger than the width of the experimental curve. There is no calculation shown on the 21-degree data from ^{12}C or on the 15-degree data from ^{14}Fe. It should be pointed out that the experimental curves shown in the figures listed above do not include the cross section provided by inelastic proton scattering to observably discrete nuclear levels.

The calculation is seen to predict the shape of the observed spectra reasonably well at all angles shown and for all targets. The calculation for ^{54}Fe (and other targets) at 15 degrees shows a definite

quasi-elastic scattering peak; however, the data does not show the presence of this peak and the data shows a higher cross section in the 20- to 45-MeV region than is predicted. It is in general found that the calculation underestimates the number of protons observed at angles of 15 degrees or less.

Above 10 MeV and in the angular range from ~20 to 70 degrees both the shape and the magnitude of the observed spectra are well estimated by the calculation. For the iron and bismuth calculation, it is found that the magnitude of the high energy portion of the spectra falls progressively lower than the observed spectra as the angle of observation is increased beyond 50 degrees. In the case of carbon, the predicted magnitude is higher than the observation between ~30 and 60 degrees while for angles larger than 60 degrees the calculation increasingly underestimates the high energy cross section. However, the underestimate of the high energy cross section is not as large for ^{12}C as for the other targets and there is an apparent trend for this underestimate to increase with increasing target mass.

It is possible to compare the predicted cascade (direct interaction) cross sections to that part of the measured cross section which is attributed to a direct process by subtracting from the measured cross section at all angles the isotropic cross section observed at the back angles. To make the comparison for ^{54}Fe, the measured energy-integrated cross sections (Table XXVI) for 135 and 160 degrees were averaged and this average was subtracted from the energy-integrated cross section at other angles. In the case of ^{209}Bi, the energy-integrated cross section obtained at 135 degrees was subtracted from the cross section at the other angles.

Table XXXVIII lists the measured "direct" and calculated cascade cross sections. The measured cross sections include the contribution from discrete inelastic peaks. The errors shown on the calculated values are based on the Monte Carlo statistics. It should be pointed out that the calculated cascade cross section can extend no lower in energy than the cutoff used which was the approximate Coulomb barrier. However in the case of both iron and bismuth it seems that the non-isotropy (increase) in the low energy cross section at small angles is caused by a contribution from the direct process. Since part of this contribution is below the Coulomb barrier, the calculation cannot account for it.

The results in the table show generally the same agreement as is observed on the comparisons in Figs. 30 and 38. For small angles the calculated cross sections show a decrease in magnitude from a peak at ~20 degrees. The data, at least down to ~12 degrees, shows no such turnover in the cross section magnitude for iron or bismuth. In the angular region between 20 and ~70 degrees, the agreement between the measured and calculated cross sections is quite good, however at angles larger than 70 degrees more protons are observed than are predicted by the cascade calculation.

In summary, it is felt that the intranuclear-cascade model gives surprisingly good estimates of the magnitude and shape of the measured cross sections particularly in view of the low incident proton energy.

The agreement between the calculated and measured spectra in the low energy regions is not as good as that in the cascade portion. The most outstanding disagreement between the data and the evaporation

TABLE XXXVIII. COMPARISON OF EXPERIMENTAL AND CALCULATED "DIRECT" CROSS SECTIONS

^{54}Fe			^{209}Bi		
	Experimental	Cascade		Experimental	Cascade
Lab. Angle (deg)	Cross Section (mb/sr)	Cross Section (mb/sr)	Lab. Angle (deg)	Cross Section (mb/sr)	Cross Section (mb/sr)
15	280	191 ± 11	15	435	230 ± 16
20	190	189 ± 8	20	253	205 ± 11
30	140	161 ± 6	25	195	169 ± 10
35	113	142 ± 6	30	150	169 ± 8
40	99	118 ± 5	45	97	92 ± 6
45	85	92 ± 3.7	60	56	38 ± 2.4
50	73	74 ± 3.9	90	18	4.8 ± 0.78
65	47	35 ± 2	110	6.5	2.5
70	36	26 ± 2			
90	14	8.3 ± 0.72			
110	7.6	3.2 ± 0.26			
135	0	.53 ± 0.16			

calculation is in the magnitude of the cross section in the evaporation peak. Although the shape of the low energy evaporation is well reproduced, the predicted magnitude is considerably higher than that observed. It is also found that the predicted low energy cutoffs for ^{54}Fe and ^{209}Bi are higher than the observed cutoffs. For example, secondary protons from the ^{54}Fe target were identified with energies as low as 1 MeV, and although the cross sections could not be determined due to the time-of-flight foldover, protons were emitted by the iron target with secondary energies less than 1 MeV. However, the evaporation calculation predicted a cutoff at $\sim$ 2.8 MeV.

Perhaps the most interesting discrepancy between the evaporation calculation and the data is that found at the back angles. It has been seen that the secondary proton spectra from all targets for angles greater than ~120 degrees are isotropic. If the process for the production of this isotropic distribution is a compound nucleus evaporation process of the type used in the Bertini calculations, then the calculation would be expected to agree with the observed back angle data. (At back angles no cascade protons are predicted by the Bertini model.) It has already been pointed out above that the calculated evaporation magnitude is too high in the peak and is cut off at too high an energy (feature observed at all angles), and in addition at the back angles (see Figs. 22, 20, and 38) the prediction does not account for the high energy distribution observed. Only in the case of carbon does the evaporation calculation provide an amount of high energy cross section that matches the data. It is also observed that this discrepancy becomes larger with increasing target mass. It appears

then that the isotropic distribution observed cannot be explained by the conventional evaporation process employed in these calculations.

It is perhaps possible that the mechanism responsible for production of this high energy isotropic cross section is not compound-nuclear in nature, but an isotropic direct interaction mechanism. Some evidence for this contention is obtained from the observation that the amount of isotropic cross section not accounted for by the evaporation calculation increases rather steadily as the target mass is increased. However, this argument is based only on observations from three targets and is at best speculative. Hopefully, analysis of data taken from targets in other mass regions will illuminate this problem.

C. Deuteron, Triton, Helium-3, and Alpha Spectra

The most notable trend in the spectra of the secondary charged particles is the similarity between the shapes of the proton, deuteron, triton, helium-3, and alpha spectra, in the high energy regions. This trend is seen in the spectra from carbon, iron, and bismuth and is found at all angles.

It has been pointed out in Chapter IV that, not only are the shapes of the proton and other charged particle spectra similar, but the behavior of the production cross section as a function of angle is also similar between the protons and other particles. By the same argument used for the proton production, it can be argued that the mechanism for production of the other charged particles consists of more than one process; an underlying isotropic process, perhaps

compound nuclear in nature, which is enhanced at angles smaller than ~ 120 degrees by a strongly forward peaked direct interaction mechanism.

Although the intranuclear cascade plus evaporation model described in the previous section cannot predict cascade particles other than neutrons and protons (pions are predicted when incident energy is high enough) the evaporation calculation can produce other charged particles. Figure 45 shows the spectra of protons, deuterons, tritons, helium-3's, and alphas and the cascade plus evaporation for the protons. It is clear, from the comparison of the evaporation calculation with the data for the deuterons, tritons, helium-3's, and alphas, that the calculation predicts the low energy peaks at approximately the right energy; however, the predicted cutoff energy is too high as it was for the protons. Perhaps more striking, however, is the magnitude of high energy cross section for each of the particles. It is clear that the evaporation calculation cannot account for this large high energy cross section. As in the case for protons described in the preceding section, the evaporation calculation does not account for the high energy cross section observed in the spectra of each particle type even at the largest angles.

It would appear, then, that the forward peaked high energy cross section observed in the spectra of deuteron, triton, helium-3, and alpha particles is produced by a mechanism of the direct interaction type. Experiments performed with higher energy incident protons[15,16,20] have observed spectra for the secondary deuteron, triton, helium-3, and alpha particles which are similar in nature to those presented here.

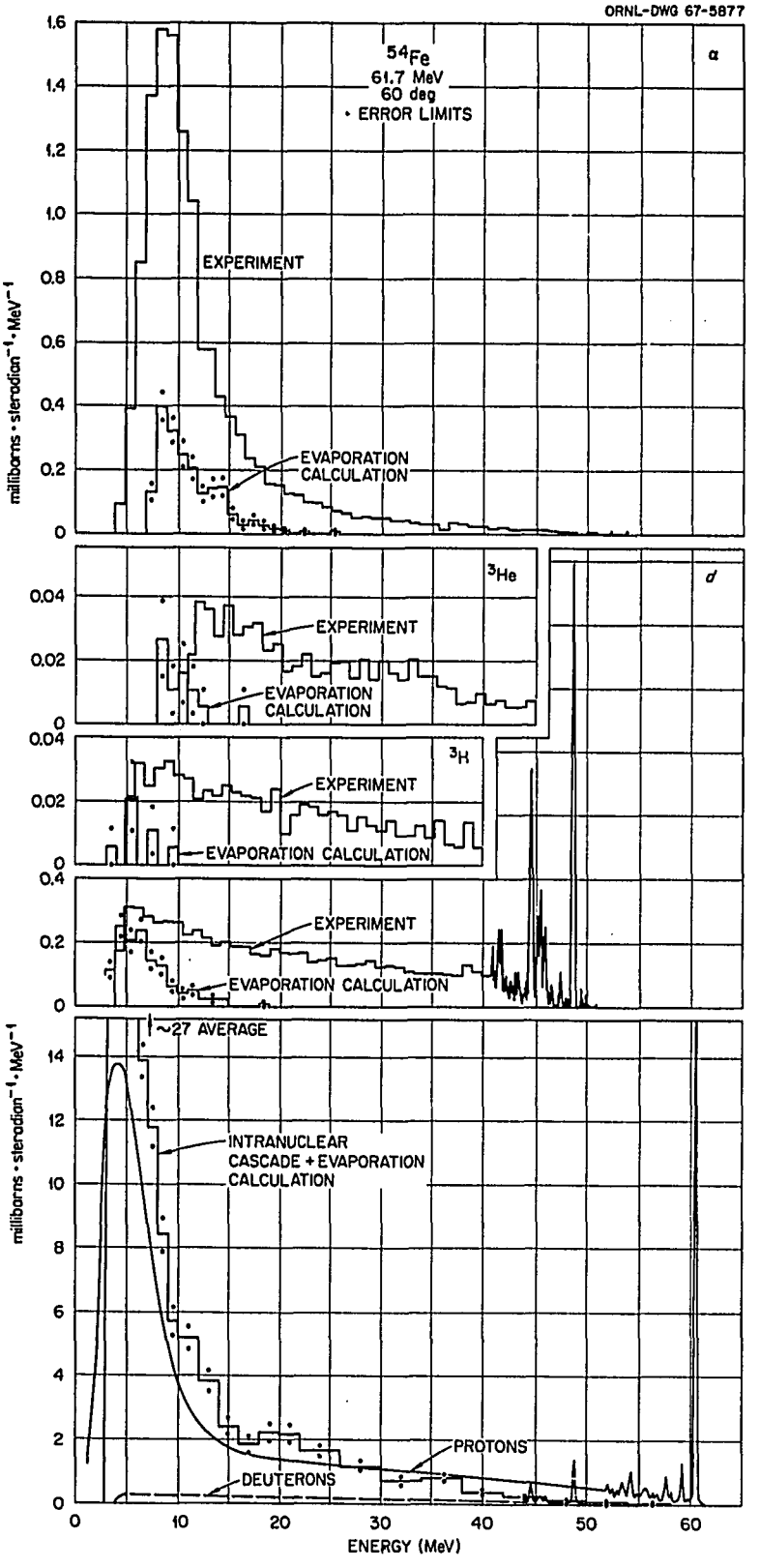

Fig. 45. Charged Particle Spectra from ^{54}Fe at 60 Degrees Compared with Intranuclear Cascade and Evaporation Calculations.

In each study, a considerable high energy cross section was observed at all angles which could not be explained on the basis of an evaporation process. These experiments have also found that the spectra of all charged particles are similar in shape, as was observed in the 60-MeV data.

A second mechanism for composite secondary particle production is that of direct nucleon pick-up. In this process the incident nucleon becomes associated with a target nucleon. In the forward directions it is not difficult to conceive of a momentum match; however, at large angles such as 90 degrees, the target nucleon would be required to have an unreasonably high momentum to become associated with the incident nucleon. Reactions which are credited to the direct pick-up mechanism, such as (p,d) reactions to discrete levels, are found to have very forward peaked differential cross sections (for example, see Fig. 37; ^{209}Bi(p,d)^{202}Bi).

The deuteron spectra obtained in this experiment as well as those at 340[15] and 156[20] MeV show the presence of more high energy deuterons (the same argument holds for tritons) at large angles (>60 degrees) then would be accounted for by the direct pick-up process. The deuteron and triton data obtained in references 15 and 20 have been discussed on the basis of an indirect pick-up mechanism. This process, credited to Bransden,[66] also seems applicable to the data obtained at 60 MeV. In this process it is assumed that cascade nucleons, produced by nucleon-nucleon collisions in a manner such as described in the last section, can pick up target nucleons before leaving the nucleus. In this case the cascade nucleon has been scattered from the forward

[66]B. H. Bransden, Proc. Phys. Soc. A65, 738 (1952).

direction, so the momentum required by the target nucleon to match the cascade nucleon momentum (to form a composite particle) is not unreasonably large. Such a pick-up process would be expected to lead to a similarity in shape between the proton and deuteron (for example) spectra in the high and medium energy regions as is observed.

Since the production of charged particles other than protons appears to be composed of at least two different mechanisms, the total cross section for particle production by each mechanism can be obtained as it was for protons, by subtracting the isotropic contribution found at back angles from all other angles. The contribution to the total cross sections (millibarns) for production of the various types of particles are listed in Table XXXIX for both reaction mechanisms. Also listed on this table for the "direct" cross sections are the ratio of the proton "direct" cross section to the deuteron, triton, etc., direct cross section.

The ratio of the number of observed protons to the number of observed deuterons has been found to be between ~ 10 and 20% over a very large range of incident proton energy.[15,20] It has also been do found that the magnitude of the triton production is ~ 1 to 3% of that for the protons. It should be pointed out, however, that the experiments reported in references 15 and 20 did not cover the entire secondary energy range.

It is found in the present work, as is shown in Table XXXIX, that high energy deuterons contribute a significant portion of the total charged particle flux produced by 60-MeV protons from all targets studied. It is important to note that most of the deuterons observed

TABLE XXXIX. "DIRECT" AND ISOTROPIC CROSS SECTIONS

Target	Proton	Deuteron	Triton	Helium-3	Alpha
"Direct" Cross Section and Ratio to Proton Cross Section (millibarns)					
^{12}C	217	49 (23%)	5.5 (2.5%)	9.8 (4.5%)	119 (55%)
^{54}Fe	455	48 (11%)	3.9 (0.9%)	3.7 (0.8%)	17 (3.7%)
^{209}Bi	566	78 (14%)	20.0 (3.5%)	1.7 (0.3%)	17 (3.0%)
Isotropic Cross Section (millibarns)					
^{12}C	132	1.6	1.5	5.0	54
^{54}Fe	816	22.2	1.7	1.8	119
^{209}Bi	133	13.0	5.0	0.28	12.0

are produced by the "direct" mechanism with energies in the range of 20 to 50 MeV. It is also observed that the "direct" alpha cross section is only appreciable for the carbon target, where direct knockout of alpha clusters may be more important than for the other target. Most of the secondary alphas observed from the other targets are low-energy alphas. The production of mass-3 particles of either high or low energies account for only a very small percentage (1 to 3) of the total flux.

LIST OF REFERENCES

1. P. G. Roos and W. Wall, Phys. Rev. 140, 1237 (1965).
2. C. B. Fulmer et al., Phys. Letters 24B, 505 (1967).
3. H. Kametsobo et al., J. Phys. Soc. Japan 27, 19 (1967).
4. E. S. Burge et al., "Studies of Elastic and Inelastic Proton Scattering", Progress Report of Rutherford Laboratory (1966).
5. F. E. Bertrand et al., Phys. Letters 24B, 653 (1967).
6. D. M. Corley, "Quasi-Free Scattering of 1 GeV Protons from C^{12} and Ca^{40}", Ph.D. Thesis, University of Maryland (1968).
7. L. S. Azhgirey et al.,Nucl. Phys. 13, 258-280 (1958).
8. J. B. Cladis et al., Phys. Rev. 87, 425 (1952).
9. N. S. Wall and P. R. Roos, Phys. Rev. 150, 811 (1966).
10. R. W. Peelle et al., Phys. Rev. 167, 4, 981 (1968); R. W. Peelle et al., "Differential Cross Sections for the Production of Protons in the Reactions of 150-MeV Protons in Complex Nuclei", ORNL-3887, 1966.
11. K. Strauch and F. Titus, Phys. Rev. 104, 1, 191 (1956).
12. I. Nonaka et al., J. Phys. Soc. Japan 17, 12, 1817 (1962).
13. R. Fox and N. F. Ramsey, Phys. Rev. 125, 5, 1609 (1962).
14. L. E. Bailey, UCRL-3334 (1956).
15. W. N. Hess and B. J. Moyer, Phys. Rev. 101, 1, 337 (1956).
16. J. Genin et al., J. Phys. Radium 22, 615 (1961).
17. H. Dubost et al., Phys. Rev. 136, 6B, 1618 (1964).
18. J. Muto et al., Nucl. Phys. 47, 19 (1963).
19. C. Brun et al., Nucl. Phys. A95, 337 (1967).
20. H. Dubost et al., Journal de Physique 28, 257 (1967).
21. K. R. Symon, Ph.D. Thesis, Harvard University (1949).
22. C. Erginson et al., Phys. Rev. Letters 13, 1 (1964).
23. J. W. Wachter, ORNL-4134, Neutron Physics Division Annual Progress Report for Period Ending May 31, 1967, p. 136.

24. F. E. Bertrand et al., "A Total Absorption Detector for 60-MeV Protons Using Lithium-Drifted Germanium", Proceedings of Ninth Scintillation and Semiconductor Symposium, June, 1966, p. 279.

25. L. Eyges, Phys. Rev. 76, 264 (1949).

26. D. F. Measday, Nuclear Instruments and Methods, 34, 353 (1964).

27. The design and construction of the detector mounts and the cryostat for the germanium detector were done in large part by R. W. Ward of the Physics Division, Oak Ridge National Laboratory.

28. The design and implementation of major changes to an existing scattering chamber were done under the direction of R. J. DeBakker of the Plant and Equipment Division, Oak Ridge National Laboratory.

29. N. W. Hill and R. W. Peelle, ORNL-3973, Neutron Physics Division Annual Report for Period Ending May 31, 1966, p. 97.

30. N. W. Hill et al., Vacuum-Hardened, Charge-Sensitive Preamplifier (to be published).

31. The fast amplifiers used were designed by N. W. Hill, Instrumentation and Controls Division, Oak Ridge National Laboratory, and are unpublished.

32. W. R. Burrus et al., "A PDP-8 Interface for a Charged-Particle Nuclear Physics Experiment", ORNL-TM-2013, 1967.

33. E. Madden, "Multi-Analyzer Stored Program Data Acquisition System Interface", ORNL-TM-2153, 1968.

34. The PDP-8 computer programs used in this experiment are found in the following publications by B. W. Rust and W. R. Burrus: "Flexi-Kludge-A Multi-Parameter Nuclear Spectrum Summing System for the PDP-8", ORNL-TM-1879, 1967; and "Super-Flickers-An On-Line Data Acquisition System for the PDP-8", ORNL-TM-1878, 1967.

35. The "Beam Sweeper" System was designed by J. Martin and S. W. Mosko, Electronuclear Division, Oak Ridge National Laboratory.

36. The basic design of the Faraday cup is given in the following reference: R. T. Santoro and R. W. Peelle, "Measurement of the Intensity of the Proton Beam at the Harvard University Synchrocyclotron for Energy-Spectral Measurements of Nuclear Secondaries", ORNL-3505, 1964.

37. F. M. Glass et al., "A New Approach to Direct Current Integration", IEEE Trans. on Nuclear Science, Vol. NS-14, #1, Feb. 1967, p. 143.

38. R. T. Santoro, F. E. Bertrand, et al., "Beam Energy Measurements at the Oak Ridge Isochronous Cyclotron", ORNL-TM-1382, 1966.

39. The analysis program was written initially by P. Aebersold and revised by D. Putzulu.

40. R. W. Peelle, "Rapid Computation of Specific Energy Losses for Energetic Charged Particles", ORNL-TM-977, 1965.

41. Philip G. Roos, "Elastic and Inelastic Scattering of High Energy Proton from Nuclei", Ph.D. Thesis, University of Maryland, 1964.

42. J. H. E. Mattauch et al., Nuclear Phys. 67, 1-31 (1965).

43. J. F. Janni, "Calculations of Energy Loss, Range, Pathlength, Straggling, Multiple Scattering, and the Probability of Inelastic Nuclear Collisions for 0.1- to 1000-MeV Protons", Tech. Report No. AFWL-TR-65-150, Air Force Weapons Lab., Research and Technoloty Div., Air Force System Command, Kirkland AFB, New Mexico.

44. S. Gorodetzky et al., Nuclear Phys. A6702, 133 (1967).

45. A. E. Glassgold et al., Phys. Rev. 106, 6, 1207 (1967).

46. A. E. Glassfold and P. J. Kellog, Phys. Rev. 107, 5, 1372 (1957).

47. H. Bichsel, Passage of Charged Particles Through Matter, American Inst. of Physics Handbook, 2nd ed., McGraw-Hill, 1963.

48. J. K. Dickens et al., Phys. Rev. 129, 2, 743 (1963).

49. M. P. Fricke and G. R. Satchler, Phys. Rev. 139, B567 (1965).

50. H. Taketani et al., "Numerical Differential Cross Sections of Some Reactions on ^{12}C Induced by 54.9 MeV Protons", Inst. for Nuclear Study, University of Tokyo, Report No. INS J-88 (1965).

51. J. K. P. Lee et al., Nuclear Phys. A106, 357 (1967).

52. D. J. Baugh et al., Nuclear Phys. A99, 203 (1967).

53. Y. Ishizaki et al., J. Phys. Soc. Japan 20, 12, 2118 (1965).

54. L. N. Blumberg et al., Phys. Rev. 147, 3, 812 (1966).

55. M. A. Preston, Physics of the Nucleus, Ch. 18, Addison Wesley, 1962.

56. P. E. Hodgson, The Optical Model of Elastic Scattering. Selected Topics in Nuclear Spectroscopy, compiled by B. J. Verhaar, North-Holland Publishing Company, Amsterdam, 1964.

57. Written by F. G. Perey (unpublished).

58. J. K. Dickens (private communication).

59. G. R. Satchler, Nuclear Physics A100, 497 (1967).

60. H. Bertini, Phys. Rev. 131, 1801 (1963); and Monte Carlo Calculations on Intranuclear Cascades, ORNL-3383 (1963).

61. M. L. Goldberger, Phys. Rev. 74, 1269 (1948).

62. M. Metropolis et al., Phys. Rev. 110, 185 (1958).

63. R. W. Peelle, A Guide to BERDBIND, And Analysis Program for History Tapes from the H. W. Bertini Intranuclear Cascade Calculations, ORNL-CF-67-3-43, (1967).

64. L. Dresner, A FORTRAN Program for Calculating the Evaporation of Various Particles from Excited Compound Nuclei, ORNL-CF-61-12-30, (1961).

65. J. M. Blatt and V. E. Weisskopf, Theoretical Nuclear Physics, John Wiley and Sons, Inc., New York, 1952, p. 365.

66. B. H. Bransden, Proc. Phys. Soc. A65, 738 (1952).

APPENDIX A

AVERAGE CROSS SECTIONS FROM ΔE × E ANALYSIS

The tables which appear in this appendix list the cross sections at each angle of observation for protons, deuterons, tritons, helium-3's and alphas from ^{12}C, ^{54}Fe, and ^{209}Bi. The cross sections are shown averaged over ~1-MeV-wide energy intervals, the listed energy (MeV) corresponding to the interval center. The cross sections listed herein are those measured in the ΔE × E system, excluding only proton elastic scattering. The cross sections and the errors, which are only statistical, are both given in millibarns/(steradian·MeV). These errors should be considered with the systematic errors discussed in Chapter III, Section D, and Chapter IV, Section G.

TABLE A I 1. Protons from ^{12}C Bombarded by 60-MeV Protons

15 deg - Run 7110			20.8 deg - Run 2007			25 deg - Run 2052			30 deg - Run 2000		
Energy (MeV)	σ (mb·ster^{-1}·MeV^{-1})	Error	Energy (MeV)	σ (mb·ster^{-1}·MeV^{-1})	Error	Energy (MeV)	σ (mb·ster^{-1}·MeV^{-1})	Error	Energy (MeV)	σ (mb·ster^{-1}·MeV^{-1})	Error
1.03	2.44	.06									
3.08	2.53	.06	4.62	2.71	.10	4.63	3.07	.10	4.65	2.20	.05
5.13	2.80	.07	5.68	2.74	.10	5.68	3.16	.10	5.71	2.17	.05
7.17	2.60	.07	6.73	2.69	.10	6.72	3.55	.10	6.77	1.92	.05
9.02	2.88	.07	7.79	2.56	.09	7.77	3.33	.10	7.83	2.01	.05
9.36	1.69	.05	8.84	2.24	.09	8.82	2.46	.09	8.89	1.53	.04
10.91	1.57	.05	9.90	1.36	.07	9.86	1.21	.06	9.95	1.53	.04
11.96	1.55	.05	10.95	1.34	.07	10.91	1.08	.06	11.01	1.50	.04
13.00	1.47	.05	12.01	1.36	.07	11.95	1.13	.06	12.07	1.38	.04
14.05	1.45	.05	13.06	1.27	.07	13.00	1.14	.06	13.13	1.44	.04
15.10	1.63	.05	14.12	1.22	.07	14.05	1.03	.06	14.19	1.40	.04
16.14	1.61	.05	15.17	1.49	.07	15.09	1.13	.06	15.25	1.53	.04
17.19	1.69	.05	16.23	1.47	.07	16.14	1.17	.06	16.31	1.44	.04
18.23	1.75	.05	17.28	1.39	.07	17.18	1.22	.06	17.38	1.43	.04
19.28	1.71	.05	18.34	1.56	.07	18.23	1.14	.06	18.44	1.51	.04
20.33	1.80	.05	19.39	1.58	.07	19.28	1.25	.06	19.50	1.52	.04
21.37	1.81	.05	20.45	1.51	.07	20.32	1.33	.06	20.56	1.57	.04
22.42	1.80	.05	21.50	1.62	.08	21.37	1.36	.06	21.62	1.45	.04
23.46	1.78	.05	22.56	1.64	.08	22.41	1.31	.06	22.68	1.46	.04
23.51	1.90	.06	23.61	1.66	.08	23.46	1.36	.06	23.74	1.45	.04
25.56	1.73	.05	24.67	1.66	.08	24.51	1.33	.06	24.80	1.53	.04
26.60	1.72	.05	25.72	1.62	.08	25.55	1.47	.07	25.86	1.43	.04
27.65	1.68	.05	26.78	1.62	.08	26.60	1.57	.07	26.92	1.44	.04
28.70	1.90	.06	27.83	1.79	.08	27.64	1.46	.07	27.98	1.53	.04
29.74	1.91	.06	28.89	1.80	.08	28.69	1.56	.07	29.04	1.59	.04
30.79	1.93	.06	29.94	1.75	.08	29.74	1.61	.07	30.10	1.55	.04
31.83	1.74	.05	31.00	1.96	.08	30.78	1.60	.07	31.16	1.62	.04
32.88	1.82	.06	32.05	2.09	.09	31.83	1.65	.07	32.23	1.69	.04
33.93	2.17	.06	33.11	2.11	.09	32.87	1.70	.07	33.29	1.61	.04
34.97	2.17	.06	34.16	2.40	.09	33.92	1.74	.07	34.35	1.58	.04
36.02	2.25	.06	35.22	2.45	.09	34.97	1.80	.07	35.41	1.47	.04
37.07	2.29	.06	36.27	2.64	.10	36.01	1.81	.07	36.47	1.57	.04
38.11	2.74	.07	37.33	2.68	.10	37.06	1.93	.08	37.53	1.56	.04
39.16	2.21	.06	38.38	3.22	.11	38.10	2.18	.08	38.59	1.96	.05
40.20	1.97	.06	39.44	3.13	.10	39.15	2.36	.08	39.65	1.54	.04
41.25	2.16	.06	40.49	2.99	.10	40.20	2.03	.08	40.71	1.67	.04
42.30	1.90	.06	41.55	3.27	.11	41.24	2.22	.08	41.77	1.60	.04
43.34	1.15	.04	42.60	3.44	.11	42.29	2.24	.08	42.83	.93	.03
44.39	1.60	.05	43.66	2.54	.09	43.33	1.55	.07	43.89	1.40	.04
45.44	2.24	.06	44.71	3.23	.11	44.38	2.07	.08	44.95	2.13	.05
46.48	1.03	.04	45.77	3.93	.12	45.43	2.62	.09	46.01	1.32	.04
47.53	1.59	.05	46.82	3.15	.10	46.47	2.02	.08	47.08	.90	.03
48.57	1.15	.04	47.88	3.39	.11	47.52	2.00	.08	48.14	.95	.03
49.62	1.17	.04	48.93	3.34	.11	48.56	2.24	.08	49.20	.76	.03
50.67	2.31	.06	49.99	3.44	.11	49.61	1.92	.08	50.26	1.13	.04
51.71	1.08	.04	51.04	4.26	.12	50.66	3.08	.10	51.32	2.55	.05
52.76	1.13	.04	52.10	3.32	.11	51.70	4.69	.12	52.38	.76	.03
53.80	.79	.04	53.15	3.20	.11	52.75	1.52	.07	53.44	.70	.03
54.85	.71	.03	54.21	2.93	.10	53.79	1.59	.07	54.50	.28	.02
55.90	10.36	.13	55.26	2.66	.10	54.84	1.10	.06	55.56	4.77	.07
56.94	1.01	.04	56.32	10.35	.19	55.89	3.09	.10	56.62	7.64	.09
57.99	.92	.04	57.37	4.73	.13	56.93	9.16	.17	57.68	.21	.02
			58.43	2.47	.09	57.98	.99	.05			

TABLE A I 2. Protons from ^{12}C Bombarded by 60-MeV Protons

35 deg - Run 2001			40 deg - Run 2033			45 deg - Run 7102			60 deg - Run 7115		
Energy (MeV)	σ (mb·ster^{-1}·MeV^{-1})	Error	Energy (MeV)	σ (mb·ster^{-1}·MeV^{-1})	Error	Energy (MeV)	σ (mb·ster^{-1}·MeV^{-1})	Error	Energy (MeV)	σ (mb·ster^{-1}·MeV^{-1})	Error
			4.63	2.11	.06	4.64	1.71	.02	4.65	1.53	.01
4.65	2.12	.03	5.68	1.95	.06	5.68	1.59	.02	5.70	1.35	.01
5.71	2.02	.03	6.72	1.93	.06	6.73	1.46	.02	6.75	1.21	.01
6.77	1.90	.03	7.77	1.79	.06	7.78	1.31	.02	7.80	1.05	.01
7.83	1.78	.03	8.81	1.57	.05	8.82	1.33	.02	8.85	1.08	.01
8.89	1.42	.03	9.86	.92	.04	9.87	1.02	.01	9.90	.80	.01
9.95	1.44	.03	10.90	.85	.04	10.92	.90	.01	10.95	.73	.01
11.01	1.40	.03	11.95	.90	.04	11.97	.86	.01	12.00	.70	.01
12.07	1.37	.03	13.00	.84	.04	13.01	.84	.01	13.05	.74	.01
13.13	1.34	.03	14.04	.93	.04	14.06	.82	.01	14.10	.71	.01
14.19	1.32	.03	15.09	.90	.04	15.11	.88	.01	15.15	.68	.01
15.25	1.32	.03	16.13	.94	.04	16.15	.85	.01	16.20	.64	.01
16.31	1.31	.03	17.18	1.01	.04	17.20	.84	.01	17.25	.60	.01
17.38	1.30	.03	18.22	.97	.04	18.25	.83	.01	18.30	.56	.01
18.44	1.30	.03	19.27	.85	.04	19.29	.82	.01	19.35	.55	.01
19.50	1.32	.03	20.31	1.01	.04	20.34	.83	.01	20.40	.56	.01
20.56	1.35	.03	21.36	.97	.04	21.39	.83	.01	21.45	.54	.01
21.62	1.31	.03	22.41	1.00	.04	22.44	.82	.01	22.49	.51	.01
22.68	1.34	.03	23.45	1.02	.04	23.48	.81	.01	23.54	.50	.01
23.74	1.28	.03	24.50	1.04	.04	24.53	.79	.01	24.59	.48	.01
24.80	1.32	.03	25.54	1.01	.04	25.58	.81	.01	25.64	.44	.01
25.86	1.29	.03	26.59	1.07	.04	26.62	.77	.01	26.69	.47	.01
26.92	1.31	.03	27.63	1.00	.04	27.67	.77	.01	27.74	.45	.01
27.98	1.35	.03	28.68	1.02	.04	28.72	.79	.01	28.79	.41	.01
29.04	1.32	.03	29.72	1.10	.04	29.76	.74	.01	29.84	.40	.01
30.10	1.37	.03	30.77	1.10	.04	30.81	.74	.01	30.89	.39	.01
31.16	1.35	.03	31.82	1.34	.05	31.86	.71	.01	31.94	.33	.01
32.23	1.43	.03	32.86	1.35	.05	32.91	.66	.01	32.99	.32	.01
33.29	1.38	.03	33.91	1.12	.04	33.95	.58	.01	34.04	.37	.01
34.35	1.33	.03	34.95	.97	.04	35.00	.60	.01	35.09	.43	.01
35.41	1.17	.03	36.00	.97	.04	36.05	.73	.01	36.14	.41	.01
36.47	1.16	.03	37.04	.97	.04	37.09	.82	.01	37.19	.45	.01
37.53	1.42	.03	38.09	.97	.04	38.14	.81	.01	38.24	.30	.01
38.59	1.60	.03	39.13	.90	.04	39.19	.70	.01	39.29	.14	.00
39.65	1.57	.03	40.18	1.05	.04	40.23	.48	.01	40.34	.23	.01
40.71	1.88	.03	41.23	.84	.04	41.28	.35	.01	41.39	.23	.01
41.77	.92	.02	42.27	.42	.03	42.33	.54	.01	42.44	.27	.01
42.83	.70	.02	43.32	.72	.04	43.38	.52	.01	43.49	.24	.01
43.89	1.04	.02	44.36	.83	.04	44.42	.43	.01	44.54	.18	.00
44.95	1.25	.03	45.41	.62	.03	45.47	.47	.01	45.59	.20	.01
46.01	.73	.02	46.45	.55	.03	46.52	.34	.01	46.64	.80	.01
47.08	.77	.02	47.50	.57	.03	47.56	.47	.01	47.69	.03	.00
48.14	.53	.02	48.55	.52	.03	48.61	1.98	.02	48.74	.12	.00
49.20	.75	.02	49.59	2.45	.06	49.66	.09	.00	49.79	.01	.00
50.26	3.27	.04	50.64	.33	.02	50.70	.35	.01	50.84	.10	.00
51.32	.24	.01	51.68	.59	.03	51.75	.02	.00	51.89	.94	.01
52.38	1.04	.02	52.73	.07	.01	52.80	.26	.01			
53.44	.12	.01	53.77	.08	.01	53.85	3.53	.03			
54.50	.25	.01	54.82	5.52	.10	54.89	.03	.00			
55.56	10.07	.07	55.86	.08	.01	55.94	.01	.00			
			56.91	.05	.01						

TABLE A I 3. Protons from ^{12}C Bombarded by 60-MeV Protons

70 deg - Run 2032			75 deg - Run 2017			90 deg - Run 2023			110 deg - Run 7113		
Energy (MeV)	σ (mb·ster^{-1}·MeV^{-1})	Error	Energy (MeV)	σ (mb·ster^{-1}·MeV^{-1})	Error	Energy (MeV)	σ (mb·ster^{-1}·MeV^{-1})	Error	Energy (MeV)	σ (mb·ster^{-1}·MeV^{-1})	Error
4.60	1.61	.05	4.63	1.39	.02	4.63	1.36	.02	4.92	.95	.01
5.65	1.41	.04	5.69	1.19	.02	5.67	1.12	.02	5.97	.75	.01
6.70	1.13	.04	6.75	1.06	.02	6.72	.93	.02	6.72	.62	.01
7.75	.90	.03	7.81	.92	.02	7.76	.86	.02	7.78	.53	.01
8.80	.86	.03	8.87	.73	.01	8.80	.70	.02	8.83	.54	.01
9.85	.49	.02	9.92	.49	.01	9.85	.44	.01	9.88	.39	.01
10.90	.52	.03	10.98	.48	.01	10.89	.42	.01	10.94	.33	.01
11.95	.58	.03	12.04	.46	.01	11.94	.43	.01	11.99	.30	.01
13.00	.54	.03	13.10	.43	.01	12.98	.38	.01	13.05	.27	.01
14.05	.47	.02	14.15	.42	.01	14.03	.38	.01	14.10	.25	.01
15.10	.46	.02	15.21	.43	.01	15.07	.35	.01	15.15	.24	.01
16.15	.42	.02	16.27	.40	.01	16.12	.32	.01	16.21	.21	.01
17.20	.46	.02	17.33	.36	.01	17.16	.33	.01	17.26	.19	.00
18.25	.40	.02	18.39	.37	.01	18.21	.31	.01	18.31	.17	.00
19.30	.36	.02	19.44	.34	.01	19.25	.25	.01	19.37	.15	.00
20.36	.40	.02	20.50	.32	.01	20.29	.26	.01	20.42	.14	.00
21.41	.37	.02	21.56	.30	.01	21.34	.23	.01	21.47	.13	.00
22.46	.34	.02	22.62	.31	.01	22.38	.21	.01	22.53	.11	.00
23.51	.34	.02	23.68	.29	.01	23.43	.20	.01	23.58	.10	.00
24.56	.31	.02	24.73	.27	.01	24.47	.18	.01	24.64	.09	.00
25.61	.35	.02	25.79	.26	.01	25.52	.16	.01	25.69	.07	.00
26.66	.29	.02	26.85	.25	.01	26.56	.15	.01	26.74	.07	.00
27.71	.35	.02	27.91	.24	.01	27.61	.15	.01	27.80	.07	.00
28.76	.30	.02	28.96	.22	.01	28.65	.12	.01	28.85	.07	.00
29.81	.25	.02	30.02	.20	.01	29.70	.10	.01	29.90	.07	.00
30.86	.26	.02	31.08	.18	.01	30.74	.10	.01	30.96	.07	.00
31.91	.20	.02	32.14	.16	.01	31.78	.11	.01	32.01	.05	.00
32.96	.22	.02	33.20	.17	.01	32.83	.11	.01	33.07	.02	.00
34.01	.25	.02	34.25	.19	.01	33.87	.10	.01	34.12	.03	.00
35.06	.28	.02	35.31	.18	.01	34.92	.10	.01	35.17	.03	.00
36.11	.28	.02	36.37	.20	.01	35.96	.04	.00	36.23	.03	.00
37.16	.24	.02	37.43	.12	.01	37.01	.06	.00	37.28	.02	.00
38.21	.14	.01	38.48	.07	.00	38.05	.08	.01	38.33	.01	.00
39.26	.11	.01	39.54	.12	.01	39.10	.08	.01	39.39	.02	.00
40.31	.13	.01	40.60	.13	.01	40.14	.07	.01	40.44	.01	.00
41.36	.19	.02	41.66	.13	.01	41.19	.03	.00	41.49	.01	.00
42.41	.17	.01	42.72	.12	.01	42.23	.02	.00	42.55	0	0
43.46	.14	.01	43.77	.08	.00	43.27	.11	.01	43.00	.00	.00
44.51	.14	.01	44.83	.14	.01	44.32	.00	.00			
45.56	.19	.02	45.89	.18	.01	45.36	.01	.00			
46.01	.28	.02	46.95	.02	.00	46.41	.00	.00			
47.06	.04	.01	48.01	.01	.00	47.45	.01	.00			
48.71	.02	.01	49.06	.00	.00	48.50	.05	.00			
49.76	.01	.00	50.12	.27	.01	49.54	.00	.00			
50.81	.40	.02	51.18	.02	.00						
51.86	.03	.01	52.24	.00	.00						
52.91	.01	.00									

TABLE A I 4. Protons from ^{12}C Bombarded by 60-MeV Protons

160 deg - Run 2060

Energy (MeV)	σ (mb·ster^{-1}·MeV^{-1})	Error
4.84	.92	.02
5.89	.75	.02
6.74	.64	.02
7.79	.51	.01
8.84	.39	.01
9.88	.22	.01
10.93	.24	.01
11.98	.23	.01
13.03	.19	.01
14.08	.18	.01
15.13	.19	.01
16.17	.17	.01
17.22	.14	.01
18.27	.13	.01
19.32	.13	.01
20.37	.10	.01
21.42	.09	.01
22.46	.08	.01
23.51	.08	.01
24.56	.07	.01
25.61	.06	.00
26.66	.05	.00
27.71	.04	.00
28.75	.04	.00
29.80	.02	.00
30.85	.01	.00
31.90	.01	.00
32.95	.01	.00
34.00	.02	.00
35.04	.00	.00
36.09	.01	.00
37.14	0	0
38.19	.00	.00
39.24	0	0
40.29	.00	.00
41.33	.02	.00
42.38	0	0

TABLE A II 1. Deuterons from ^{12}C Bombarded by 60-MeV Protons

15 deg - Run 7110			20.8 deg - Run 2007			25 deg - Run 2052			30 deg - Run 2000		
Energy (MeV)	σ (mb·ster^{-1}·MeV^{-1})	Error	Energy (MeV)	σ (mb·ster^{-1}·MeV^{-1})	Error	Energy (MeV)	σ (mb·ster^{-1}·MeV^{-1})	Error	Energy (MeV)	σ (mb·ster^{-1}·MeV^{-1})	Error
5.98	.49	.03									
6.73	.51	.03	5.68	.58	.04	5.68	.43	.04	5.71	.46	.02
7.47	.44	.03	6.73	.52	.04	6.72	.41	.04	6.77	.45	.02
8.22	.38	.03	7.79	.47	.04	7.77	.46	.04	7.83	.42	.02
8.96	.37	.02	8.84	.47	.04	8.82	.46	.04	8.89	.39	.02
9.71	.40	.03	9.90	.35	.04	9.86	.33	.03	9.95	.36	.02
10.46	.41	.03	10.95	.34	.03	10.91	.39	.03	11.01	.37	.02
11.20	.44	.03	12.01	.29	.03	11.95	.36	.03	12.07	.29	.02
11.95	.32	.02	13.06	.22	.03	13.00	.21	.03	13.13	.32	.02
12.70	.29	.02	14.12	.28	.03	14.05	.25	.03	14.19	.32	.02
13.44	.31	.02	15.17	.29	.03	15.09	.23	.03	15.25	.28	.02
14.19	.30	.02	16.23	.23	.03	16.14	.23	.03	16.31	.30	.02
14.93	.36	.02	17.28	.24	.03	17.18	.21	.03	17.38	.32	.02
15.68	.33	.02	18.34	.32	.03	18.23	.29	.03	18.44	.28	.02
16.43	.30	.02	19.39	.28	.03	19.28	.21	.03	19.50	.29	.02
17.17	.35	.02	20.45	.34	.03	20.32	.27	.03	20.56	.29	.02
17.92	.35	.02	21.50	.38	.04	21.37	.28	.03	21.62	.31	.02
18.66	.34	.02	22.56	.25	.03	22.41	.27	.03	22.68	.28	.02
19.41	.35	.02	23.61	.27	.03	23.46	.23	.03	23.74	.28	.02
20.16	.34	.02	24.67	.25	.03	24.51	.23	.03	24.80	.31	.02
20.90	.32	.02	25.72	.37	.04	25.55	.27	.03	25.86	.23	.02
21.65	.31	.02	26.78	.29	.03	26.60	.23	.03	26.92	.23	.02
22.40	.35	.02	27.83	.23	.03	27.64	.23	.03	27.98	.25	.02
23.14	.32	.02	28.89	.26	.03	28.69	.19	.02	29.04	.24	.02
23.89	.31	.02	29.94	.23	.03	29.74	.23	.03	30.10	.20	.02
24.63	.34	.02	31.00	.21	.03	30.78	.17	.02	31.16	.25	.02
25.38	.27	.02	32.05	.24	.03	31.83	.23	.03	32.23	.24	.02
26.13	.22	.02	33.11	.29	.03	32.87	.20	.02	33.29	.21	.02
26.87	.22	.02	34.16	.16	.02	33.92	.13	.02	34.35	.10	.01
27.62	.11	.01	35.22	.13	.02	34.97	.11	.02	35.41	.14	.01
28.37	.72	.03	36.27	.15	.02	36.01	.18	.02	36.47	.42	.02
29.11	.20	.02	37.33	.62	.05	37.06	.48	.04	37.53	.10	.01
29.86	1.81	.05	38.38	.11	.02	38.10	.08	.02	38.59	1.08	.04
30.60	.02	.01	39.44	1.33	.07	39.15	1.13	.06	39.65	.08	.01
31.35	2.90	.07	40.49	.07	.02	40.20	.06	.01	40.71	.34	.02
32.10	.09	.01	41.55	1.02	.06	41.24	.33	.03	41.77	.71	.03
32.84	15.51	.16	42.60	.70	.05	42.29	.79	.05	42.83	4.81	.07
			43.66	7.22	.16	43.33	4.24	.11			

TABLE A II 2. Deuterons from ^{12}C Bombarded by 60-MeV Protons

35 deg - Run 2001			40 deg - Run 2033			45 deg - Run 7102			60 deg - Run 7115		
Energy (MeV)	σ (mb·ster^{-1}·MeV^{-1})	Error	Energy (MeV)	σ (mb·ster^{-1}·MeV^{-1})	Error	Energy (MeV)	σ (mb·ster^{-1}·MeV^{-1})	Error	Energy (MeV)	σ (mb·ster^{-1}·MeV^{-1})	Error
5.71	.44	.02	5.68	.39	.03	5.68	.33	.01	5.70	.26	.01
6.77	.44	.02	6.72	.34	.02	6.73	.31	.01	6.75	.24	.01
7.83	.38	.01	7.77	.31	.02	7.78	.30	.01	7.80	.21	.01
8.89	.35	.01	8.81	.30	.02	8.82	.27	.01	8.85	.18	.00
9.95	.35	.01	9.86	.26	.02	9.87	.25	.01	9.90	.19	.00
11.01	.40	.01	10.90	.28	.02	10.92	.24	.01	10.95	.17	.00
12.07	.26	.01	11.95	.25	.02	11.97	.27	.01	12.00	.19	.00
13.13	.29	.01	13.00	.23	.02	13.01	.23	.01	13.05	.16	.00
14.19	.29	.01	14.04	.20	.02	14.06	.20	.01	14.10	.14	.00
15.25	.29	.01	15.09	.17	.02	15.11	.20	.01	15.15	.13	.00
16.31	.30	.01	16.13	.20	.02	16.15	.19	.01	16.20	.13	.00
17.38	.28	.01	17.18	.20	.02	17.20	.20	.01	17.25	.12	.00
18.44	.30	.01	18.22	.20	.02	18.25	.19	.01	18.30	.11	.00
19.50	.30	.01	19.27	.17	.02	19.29	.17	.01	19.35	.10	.00
20.56	.26	.01	20.31	.19	.02	20.34	.17	.01	20.40	.10	.00
21.62	.25	.01	21.36	.18	.02	21.39	.17	.01	21.45	.10	.00
22.68	.26	.01	22.41	.15	.02	22.44	.15	.01	22.49	.10	.00
23.74	.25	.01	23.45	.16	.02	23.48	.15	.01	23.54	.10	.00
24.80	.22	.01	24.50	.15	.02	24.53	.14	.01	24.59	.10	.00
25.86	.25	.01	25.54	.17	.02	25.58	.16	.01	25.64	.09	.00
26.92	.23	.01	26.59	.14	.02	26.62	.15	.01	26.69	.09	.00
27.98	.24	.01	27.63	.15	.02	27.67	.14	.01	27.74	.09	.00
29.04	.21	.01	28.68	.16	.02	28.72	.16	.01	28.79	.07	.00
30.10	.26	.01	29.72	.17	.02	29.76	.16	.01	29.84	.08	.00
31.16	.22	.01	30.77	.15	.02	30.81	.13	.00	30.89	.04	.00
32.23	.24	.01	31.82	.13	.01	31.86	.08	.00	31.94	.13	.00
33.29	.17	.01	32.86	.11	.01	32.91	.08	.00	32.99	.08	.00
34.35	.18	.01	33.91	.13	.02	33.95	.29	.01	34.04	.12	.00
35.41	.13	.01	34.95	.10	.01	35.00	.01	.00	35.09	.01	.00
36.47	.42	.02	36.00	.29	.02	36.05	.43	.01	36.14	.15	.00
37.53	.48	.02	37.04	.28	.02	37.09	.00	.00	37.19	.26	.01
38.59	.58	.02	38.09	.35	.02	38.14	.24	.01	38.24	.66	.01
39.65	.05	.01	39.13	.01	.00	39.19	.01	.00			
40.71	.71	.02	40.18	.32	.02	40.23	1.98	.02			
41.77	.18	.01	41.23	.23	.02						

TABLE A II 3. Deuterons from ^{12}C Bombarded by 60-MeV Protons

70 deg - Run 2032			75 deg - Run 2017			90 deg - Run 2023			110 deg - Run 7113		
Energy (MeV)	σ (mb·ster^{-1}·MeV^{-1})	Error	Energy (MeV)	σ (mb·ster^{-1}·MeV^{-1})	Error	Energy (MeV)	σ (mb·ster^{-1}·MeV^{-1})	Error	Energy (MeV)	σ (mb·ster^{-1}·MeV^{-1})	Error
5.65	.25	.02	5.69	.22	.01						
6.70	.21	.02	6.75	.18	.01	5.67	.20	.01	5.67	.12	.00
7.75	.19	.02	7.81	.17	.01	6.72	.17	.01	6.72	.11	.00
8.80	.16	.01	8.87	.16	.01	7.76	.16	.01	7.78	.10	.00
9.85	.17	.01	9.92	.15	.01	8.80	.13	.01	8.83	.08	.00
10.90	.15	.01	10.98	.15	.01	9.85	.11	.01	9.88	.07	.00
11.95	.13	.01	12.04	.11	.01	10.89	.13	.01	10.94	.06	.00
13.00	.10	.01	13.10	.08	.00	11.94	.09	.01	11.99	.07	.00
14.05	.09	.01	14.15	.09	.00	12.98	.08	.01	13.05	.05	.00
15.10	.09	.01	15.21	.07	.00	14.03	.06	.00	14.10	.04	.00
16.15	.09	.01	16.27	.08	.00	15.07	.06	.01	15.15	.04	.00
17.20	.07	.01	17.33	.07	.00	16.12	.04	.00	16.21	.03	.00
18.25	.10	.01	18.39	.06	.00	17.16	.05	.00	17.26	.03	.00
19.30	.07	.01	19.44	.06	.00	18.21	.04	.00	18.31	.03	.00
20.36	.07	.01	20.50	.05	.00	19.25	.04	.00	19.37	.02	.00
21.41	.07	.01	21.56	.06	.00	20.29	.03	.00	20.42	.02	.00
22.46	.08	.01	22.62	.05	.00	21.34	.03	.00	21.47	.01	.00
23.51	.07	.01	23.68	.05	.00	22.38	.03	.00	22.53	.02	.00
24.56	.07	.01	24.73	.05	.00	23.43	.03	.00	23.58	.01	.00
25.61	.07	.01	25.79	.05	.00	24.47	.02	.00	24.64	.00	.00
26.66	.06	.01	26.85	.04	.00	25.52	.01	.00	25.69	.02	.00
27.71	.05	.01	27.91	.04	.00	26.56	.01	.00	26.74	.00	.00
28.76	.04	.01	28.96	.03	.00	27.61	.03	.00	27.80	.01	.00
29.81	.03	.01	30.02	.05	.00	28.65	.01	.00	28.85	.03	.00
30.86	.10	.01	31.08	.01	.00	29.70	.04	.00			
31.91	.02	.01	32.14	.06	.00	30.74	.00	.00			
32.96	.09	.01	33.20	.00	.00	31.78	.02	.00			
34.01	.01	.00	34.25	.03	.00	32.83	.06	.01			
35.06	.04	.01	35.31	.08	.00	33.87	.06	.00			
36.11	.06	.01	36.37	.20	.01						
37.16	.41	.02									

TABLE A II 4. Deuterons from ^{12}C Bombarded by 60-MeV Protons

160 deg - Run 2060

Energy (MeV)	σ (mb·ster^{-1}·MeV^{-1})	Error (mb·ster^{-1}·MeV^{-1})
5.69	.11	.01
6.74	.08	.01
7.79	.08	.01
8.84	.06	.00
9.88	.05	.00
10.93	.03	.00
11.98	.03	.00
13.03	.01	.00
14.08	.01	.00
15.13	.01	.00
16.17	.01	.00
17.22	.01	.00
18.27	.00	.00
19.32	.01	.00
20.37	.00	.00
21.42	.00	.00
22.46	.00	.00
23.51	0	0
24.56	0	0
25.61	.01	.00
26.66	0	0
27.71	0	0

TABLE A III 1. Tritons from ^{12}C Bombarded by 60-MeV Protons

15 deg - Run 7110			20.8 deg - Run 2007			25 deg - Run 2052			30 deg - Run 2000		
Energy (MeV)	σ (mb·ster^{-1}·MeV^{-1})	Error	Energy (MeV)	σ (mb·ster^{-1}·MeV^{-1})	Error	Energy (MeV)	σ (mb·ster^{-1}·MeV^{-1})	Error	Energy (MeV)	σ (mb·ster^{-1}·MeV^{-1})	Error
6.73	.16	.02									
7.77	.13	.01	6.73	.08	.02				6.77	.14	.01
8.82	.11	.01	7.79	.08	.02	6.72	.10	.02	7.83	.13	.01
9.86	.12	.01	8.84	.13	.02	7.77	.12	.02	8.89	.09	.01
10.91	.11	.01	9.90	.08	.02	8.82	.09	.02	9.95	.09	.01
11.96	.11	.01	10.95	.07	.02	9.86	.09	.02	11.01	.11	.01
13.00	.12	.01	12.01	.10	.02	10.91	.06	.01	12.07	.10	.01
14.05	.11	.01	13.06	.07	.02	11.95	.07	.01	13.13	.10	.01
15.10	.10	.01	14.12	.05	.01	13.00	.05	.01	14.19	.05	.01
16.14	.08	.01	15.17	.07	.02	14.05	.06	.01	15.25	.07	.01
17.19	.07	.01	16.23	.03	.01	15.09	.05	.01	16.31	.07	.01
18.23	.08	.01	17.28	.05	.01	16.14	.06	.01	17.38	.07	.01
19.28	.06	.01	18.34	.03	.01	17.18	.03	.01	18.44	.07	.01
20.33	.08	.01	19.39	.07	.02	18.23	.07	.01	19.50	.05	.01
21.37	.07	.01	20.45	.08	.02	19.28	.05	.01	20.56	.06	.01
22.42	.07	.01	21.50	.06	.01	20.32	.02	.01	21.62	.07	.01
23.46	.07	.01	22.56	.05	.01	21.37	.05	.01	22.68	.05	.01
24.51	.06	.01	23.61	.02	.01	22.41	.04	.01	23.74	.06	.01
25.56	.06	.01	24.67	.03	.01	23.46	.05	.01	24.80	.06	.01
26.60	.06	.01	25.72	.06	.01	24.51	.04	.01	25.86	.07	.01
27.65	.05	.01	26.78	.07	.02	25.55	.03	.01	26.92	.05	.01
28.70	.04	.01	27.83	.03	.01	26.60	.05	.01	27.98	.04	.01
29.74	.06	.01	28.89	.03	.01	27.64	.05	.01	29.04	.04	.01
30.79	.14	.02	29.94	.03	.01	28.69	.02	.01	30.10	.05	.01
31.83	.01	.00	31.00	.03	.01	29.74	.00	.00	31.16	.02	.01
32.88	.44	.03	32.05	.05	.01	30.78	.02	.01	32.23	.10	.01
33.93	.00	.00	33.11	.35	.03	31.83	.01	.01	33.29	.01	.00
34.97	.01	.00	34.16	.02	.01	32.87	.15	.02	34.35	.02	.00
			35.22	.02	.01	33.92	.00	.00			
			36.27	.26	.03	34.97	.01	.00			
						36.01	.45	.04			

TABLE A III 2. Tritons from ^{12}C Bombarded by 60-MeV Protons

35 deg - Run 2001			40 deg - Run 2033			45 deg - Run 7102			60 deg - Run 7115		
Energy (MeV)	σ (mb·ster^{-1}·MeV^{-1})	Error	Energy (MeV)	σ (mb·ster^{-1}·MeV^{-1})	Error	Energy (MeV)	σ (mb·ster^{-1}·MeV^{-1})	Error	Energy (MeV)	σ (mb·ster^{-1}·MeV^{-1})	Error
			6.72	.11	.01	6.73	.11	.00	6.75	.07	.00
6.77	.13	.01	7.77	.09	.01	7.78	.09	.00	7.80	.06	.00
7.83	.13	.01	8.81	.08	.01	8.82	.08	.00	8.85	.05	.00
8.89	.11	.01	9.86	.06	.01	9.87	.07	.00	9.90	.05	.00
9.95	.10	.01	10.90	.06	.01	10.92	.07	.00	10.95	.04	.00
11.01	.10	.01	11.95	.06	.01	11.97	.06	.00	12.00	.04	.00
12.07	.09	.01	13.00	.06	.01	13.01	.06	.00	13.05	.03	.00
13.13	.10	.01	14.04	.06	.01	14.06	.06	.00	14.10	.03	.00
14.19	.07	.01	15.09	.02	.01	15.11	.05	.00	15.15	.03	.00
15.25	.08	.01	16.13	.04	.01	16.15	.05	.00	16.20	.03	.00
16.31	.08	.01	17.18	.04	.01	17.20	.05	.00	17.25	.02	.00
17.38	.08	.01	18.22	.04	.01	18.25	.04	.00	18.30	.02	.00
18.44	.06	.01	19.27	.04	.01	19.29	.04	.00	19.35	.02	.00
19.50	.06	.01	20.31	.02	.01	20.34	.04	.00	20.40	.02	.00
20.56	.06	.01	21.36	.02	.01	21.39	.04	.00	21.45	.02	.00
21.62	.06	.01	22.41	.03	.01	22.44	.04	.00	22.49	.01	.00
22.68	.05	.01	23.45	.03	.01	23.48	.04	.00	23.54	.01	.00
23.74	.06	.01	24.50	.04	.01	24.53	.04	.00	24.59	.02	.00
24.80	.08	.01	25.54	.05	.01	25.58	.03	.00	25.64	.00	.00
25.86	.06	.01	26.59	.02	.01	26.62	.03	.00	26.69	.02	.00
26.92	.07	.01	27.63	.02	.01	27.67	.05	.00	27.74	.00	.00
27.98	.04	.00	28.68	.05	.01	28.72	.08	.00	28.79	.02	.00
29.04	.06	.01	29.72	.03	.01	29.76	.05	.00			
30.10	.09	.01	30.77	.11	.01	30.81	.00	.00			
31.16	.04	.00	31.82	0	0	31.86	.02	.00			
32.23	.05	.01	32.86	0	0						
33.29	.00	.00	33.91	.04	.01						
34.35	.24	.01									
35.41	.02	.00									

TABLE A III 3. Tritons from ^{12}C Bombarded by 60-MeV Protons

70 deg - Run 2032			75 deg - Run 2017			90 deg - Run 2023			110 deg - Run 7113		
Energy (MeV)	σ (mb·ster^{-1}·MeV^{-1})	Error	Energy (MeV)	σ (mb·ster^{-1}·MeV^{-1})	Error	Energy (MeV)	σ (mb·ster^{-1}·MeV^{-1})	Error	Energy (MeV)	σ (mb·ster^{-1}·MeV^{-1})	Error
									6.72	.02	.00
6.70	.06	.01	6.75	.06	.00	6.72	.04	.00	7.78	.02	.00
7.75	.04	.01	7.81	.04	.00	7.76	.03	.00	8.83	.01	.00
8.80	.04	.01	8.87	.03	.00	8.80	.02	.00	9.88	.01	.00
9.85	.04	.01	9.92	.03	.00	9.85	.02	.00	10.94	.01	.00
10.90	.03	.01	10.98	.03	.00	10.89	.02	.00	11.99	.00	.00
11.95	.03	.01	12.04	.02	.00	11.94	.01	.00	13.05	.00	.00
13.00	.03	.01	13.10	.02	.00	12.98	.01	.00	14.10	.00	.00
14.05	.03	.01	14.15	.01	.00	14.03	.01	.00	15.15	.00	.00
15.10	.02	.00	15.21	.01	.00	15.07	.00	.00	16.21	.00	.00
16.15	.01	.00	16.27	.00	.00	16.12	.00	.00	17.26	.00	.00
17.20	.01	.00	17.33	.01	.00	17.16	.00	.00	18.31	.00	.00
18.25	.02	.00	18.39	.01	.00	18.21	.00	.00	19.37	0	0
19.30	.01	.00	19.44	.01	.00	19.25	.00	.00	20.42	.00	.00
20.36	.01	.00	20.50	.01	.00	20.29	.00	.00			
21.41	.01	.00	21.56	.00	.00	21.34	.00	.00			
22.46	.01	.00	22.62	.00	.00	22.38	.00	.00			
23.51	.02	.00	23.68	.00	.00	23.43	0	0			
24.56	.01	.00	24.73	.01	.00	24.47	.00	.00			
25.61	.02	.00	25.79	0	0						
26.66	0	0	26.85	.00	.00						
27.71	.01	.00									

160 deg - Run 2060		
Energy (MeV)	σ (mb·ster^{-1}·MeV^{-1})	Error
6.74	.01	.00
7.79	.01	.00
8.84	.01	.00
9.88	.00	.00
10.93	.00	.00
11.98	.00	.00
13.03	.00	.00
14.08	.00	.00
15.13	0	0
16.17	0	0
17.22	0	0
18.27	0	0
19.32	0	0

TABLE A IV 1. Helium-3 from ^{12}C Bombarded by 60-MeV Protons

15 deg - Run 7110			20.8 deg - Run 2007			25 deg - Run 2052			30 deg - Run 2000		
Energy (MeV)	σ (mb·ster^{-1}·MeV^{-1})	Error	Energy (MeV)	σ (mb·ster^{-1}·MeV^{-1})	Error	Energy (MeV)	σ (mb·ster^{-1}·MeV^{-1})	Error	Energy (MeV)	σ (mb·ster^{-1}·MeV^{-1})	Error
13.00	.18	.02									
14.05	.19	.02	13.06	.23	.03	13.00	.12	.02			
15.10	.16	.02	14.12	.11	.02	14.05	.15	.02	13.13	.16	.01
16.14	.17	.02	15.17	.14	.02	15.09	.10	.02	14.19	.14	.01
17.19	.13	.01	16.23	.17	.02	16.14	.13	.02	15.25	.14	.01
18.23	.16	.02	17.28	.10	.02	17.18	.12	.02	16.31	.15	.01
19.28	.14	.02	18.34	.11	.02	18.23	.09	.02	17.38	.12	.01
20.33	.13	.01	19.39	.11	.02	19.28	.09	.02	18.44	.10	.01
21.37	.13	.01	20.45	.10	.02	20.32	.08	.02	19.50	.10	.01
22.42	.10	.01	21.50	.08	.02	21.37	.07	.01	20.56	.14	.01
23.46	.09	.01	22.56	.05	.01	22.41	.11	.02	21.62	.09	.01
24.21	.08	.01	23.61	.09	.02	23.46	.05	.01	22.68	.08	.01
25.56	.10	.01	24.67	.07	.02	24.51	.05	.01	23.74	.08	.01
26.60	.07	.01	25.72	.12	.02	25.55	.04	.01	24.80	.08	.01
27.65	.09	.01	26.78	.06	.01	26.60	.06	.01	25.86	.07	.01
28.70	.10	.01	27.83	.06	.01	27.64	.06	.01	26.92	.06	.01
29.74	.06	.01	28.89	.11	.02	28.69	.05	.01	27.98	.06	.01
30.79	.10	.01	29.94	.05	.01	29.74	.06	.01	29.04	.06	.01
31.83	.09	.01	31.00	.07	.02	30.78	.05	.01	30.10	.05	.01
32.88	.13	.01	32.05	.05	.01	31.83	.05	.01	31.16	.06	.01
33.93	.25	.02	33.11	.06	.01	32.87	.05	.01	32.23	.05	.01
34.97	.05	.01	34.16	.17	.02	33.92	.06	.01	33.29	.07	.01
36.02	.04	.01	35.22	.06	.01	34.97	.08	.02	34.35	.06	.01
37.07	.27	.02	36.27	.01	.01	36.01	.00	.00	35.41	.01	.00
38.11	.70	.03	37.33	.16	.02	37.06	.10	.02	36.47	.03	.01
			38.38	.32	.03	38.10	.23	.03	37.53	.20	.02
			39.44	.64	.05	39.15	.45	.04			

TABLE A IV 2. Helium-3 from ^{12}C Bombarded by 60-MeV Protons

35 deg - Run 2001			40 deg - Run 2033			45 deg - Run 7102			60 deg - Run 7115		
Energy (MeV)	σ (mb·ster^{-1}·MeV^{-1})	Error	Energy (MeV)	σ (mb·ster^{-1}·MeV^{-1})	Error	Energy (MeV)	σ (mb·ster^{-1}·MeV^{-1})	Error	Energy (MeV)	σ (mb·ster^{-1}·MeV^{-1})	Error
			13.00	.10	.01	13.01	.11	.00	13.05	.08	.00
13.13	.16	.01	14.04	.11	.01	14.06	.10	.00	14.10	.07	.00
14.19	.15	.01	15.09	.10	.01	15.11	.09	.00	15.15	.07	.00
15.25	.14	.01	16.13	.07	.01	16.15	.09	.00	16.20	.06	.00
16.31	.13	.01	17.18	.07	.01	17.20	.08	.00	17.25	.05	.00
17.38	.12	.01	18.22	.06	.01	18.25	.07	.00	18.30	.05	.00
18.44	.11	.01	19.27	.05	.01	19.29	.06	.00	19.35	.04	.00
19.50	.11	.01	20.31	.05	.01	20.34	.06	.00	20.40	.04	.00
20.56	.09	.01	21.36	.05	.01	21.39	.06	.00	21.45	.04	.00
21.62	.11	.01	22.41	.04	.01	22.44	.05	.00	22.49	.03	.00
22.68	.07	.01	23.45	.05	.01	23.48	.05	.00	23.54	.03	.00
23.74	.07	.01	24.50	.03	.01	24.53	.05	.00	24.59	.02	.00
24.80	.08	.01	25.54	.04	.01	25.58	.05	.00	25.64	.02	.00
25.86	.07	.01	26.59	.05	.01	26.62	.03	.00	26.69	.03	.00
26.92	.06	.01	27.63	.02	.01	27.67	.03	.00	27.74	.05	.00
27.98	.08	.01	28.68	.03	.01	28.72	.04	.00	28.79	.02	.00
29.04	.04	.00	29.72	.03	.01	29.76	.05	.00	29.84	.00	.00
30.10	.07	.01	30.77	.05	.01	30.81	.10	.00	30.89	.03	.00
31.16	.09	.01	31.82	.05	.01	31.86	.03	.00	31.94	.03	.00
32.23	.04	.00	32.86	.05	.01	32.91	.02	.00			
33.29	.07	.01	33.91	.01	.00	33.95	.04	.00			
34.35	.01	.00	34.95	.01	.00	35.00	.11	.00			
35.41	.01	.00	36.00	.03	.01						
36.47	.14	.01	37.04	.11	.01						
37.53	.14	.01									

TABLE A IV 3. Helium-3 from ^{12}C Bombarded by 60-MeV Protons

70 deg - Run 2032			75 deg - Run 2017			90 deg - Run 2023			110 deg - Run 7113		
Energy (MeV)	σ (mb·ster^{-1}·MeV^{-1})	Error	Energy (MeV)	σ (mb·ster^{-1}·MeV^{-1})	Error	Energy (MeV)	σ (mb·ster^{-1}·MeV^{-1})	Error	Energy (MeV)	σ (mb·ster^{-1}·MeV^{-1})	Error
									13.05	.03	.00
13.90	.07	.01	13.10	.06	.00	12.98	.04	.00	14.10	.02	.00
14.95	.07	.01	14.15	.05	.00	14.03	.02	.00	15.15	.02	.00
15.10	.05	.01	15.21	.04	.00	15.07	.02	.00	16.21	.01	.00
16.15	.06	.01	16.27	.03	.00	16.12	.02	.00	17.26	.01	.00
17.20	.04	.01	17.33	.03	.00	17.16	.02	.00	18.31	.01	.00
18.25	.04	.01	18.39	.03	.00	18.21	.01	.00	19.37	.01	.00
19.30	.03	.01	19.44	.02	.00	19.25	.01	.00	20.42	.00	.00
20.36	.04	.01	20.50	.02	.00	20.29	.01	.00	21.47	.00	.00
21.41	.03	.01	21.56	.02	.00	21.34	.01	.00	22.53	.00	.00
22.46	.02	.01	22.62	.01	.00	22.38	.02	.00	23.58	.01	.00
23.51	.02	.00	23.68	.01	.00	23.43	.00	.00			
24.56	.02	.00	24.73	.02	.00	24.47	.00	.00			
25.61	.02	.01	25.79	.02	.00	25.52	.00	.00			
26.66	.04	.01	26.85	.00	.00	26.56	.00	.00			
27.71	.01	.00	27.91	.01	.00						
28.76	.00	.00	28.96	.01	.00						
29.81	.02	.01	30.02	.03	.00						
30.86	.02	.00									
31.91	.05	.01									

160 deg - Run 2060		
Energy (MeV)	σ (mb·ster^{-1}·MeV^{-1})	Error
13.03	.01	.00
14.08	.01	.00
15.13	.01	.00
16.17	.00	.00
17.22	.00	.00
18.27	.01	.00
19.32	0	0
20.37	0	0

TABLE A V 1. Alphas from ^{12}C Bombarded by 60-MeV Protons

15 deg - Run 7110			20.8 deg - Run 2007			25 deg - Run 2052			30 deg - Run 2000		
Energy (MeV)	σ	Error	Energy (MeV)	σ	Error	Energy (MeV)	σ	Error	Energy (MeV)	σ	Error
	(mb·ster^{-1}·MeV^{-1})			(mb·ster^{-1}·MeV^{-1})			(mb·ster^{-1}·MeV^{-1})			(mb·ster^{-1}·MeV^{-1})	
14.05	1.00	.04									
15.10	.98	.04	14.12	1.14	.06	14.05	.87	.05	14.19	.90	.03
16.14	.86	.04	15.17	.85	.05	15.09	.73	.05	15.25	.79	.03
17.19	.71	.03	16.23	.79	.05	16.14	.73	.05	16.31	.75	.03
18.23	.72	.03	17.28	.75	.05	17.18	.58	.04	17.38	.58	.03
19.28	.56	.03	18.34	.56	.04	18.23	.55	.04	18.44	.52	.02
20.33	.51	.03	19.39	.51	.04	19.28	.49	.04	19.50	.45	.02
21.37	.46	.03	20.45	.54	.04	20.32	.41	.04	20.56	.37	.02
22.42	.39	.03	21.50	.42	.04	21.37	.38	.03	21.62	.36	.02
23.46	.43	.03	22.56	.34	.03	22.41	.30	.03	22.68	.34	.02
24.51	.30	.02	23.61	.34	.03	23.46	.26	.03	23.74	.27	.02
25.56	.29	.02	24.67	.28	.03	24.51	.22	.03	24.80	.24	.02
26.60	.30	.02	25.72	.24	.03	25.55	.25	.03	25.86	.20	.02
27.65	.22	.02	26.78	.20	.03	26.60	.17	.02	26.92	.18	.01
28.70	.22	.02	27.83	.20	.03	27.64	.12	.02	27.98	.14	.01
29.74	.16	.02	28.89	.13	.02	28.69	.08	.02	29.04	.15	.01
30.79	.13	.01	29.94	.14	.02	29.74	.14	.02	30.10	.12	.01
31.83	.16	.02	31.00	.08	.02	30.78	.11	.02	31.16	.08	.01
32.88	.10	.01	32.05	.07	.02	31.83	.05	.01	32.23	.08	.01
33.93	.10	.01	33.11	.09	.02	32.87	.06	.01	33.29	.06	.01
34.97	.12	.01	34.16	.08	.02	33.92	.05	.01	34.35	.07	.01
36.02	.10	.01	35.22	.11	.02	34.97	.05	.01	35.41	.09	.01
37.07	.12	.01	36.27	.02	.01	36.01	.01	.01	36.47	.01	.00
38.11	.16	.02	37.33	.09	.02	37.06	.04	.01	37.53	.08	.01
39.16	.13	.01	38.38	.09	.02	38.10	.13	.02	38.59	.09	.01
40.20	.14	.02	39.44	.05	.01	39.15	.05	.01	39.65	.10	.01
41.25	.22	.02	40.49	.12	.02	40.20	.07	.01	40.71	.16	.01
42.30	.14	.02	41.55	.17	.02	41.24	.12	.02	41.77	.14	.01
43.34	.04	.01	42.60	.15	.02	42.29	.12	.02	42.83	.03	.01
44.39	.05	.01	43.66	.03	.01	43.33	.04	.01	43.89	.02	.00
45.44	.11	.01	44.71	.02	.01	44.38	.02	.01	44.95	.10	.01
46.48	.15	.02	45.77	.04	.01	45.43	.04	.01	46.01	.01	.00
47.53	.39	.03	46.82	.02	.01	46.47	.02	.01			
			47.88	.29	.03						

TABLE A V 2. Alphas from ^{12}C Bombarded by 60-MeV Protons

35 deg - Run 2001			40 deg - Run 2033			45 deg - Run 7102			60 deg - Run 7115		
Energy (MeV)	σ (mb·ster^{-1}·MeV^{-1})	Error	Energy (MeV)	σ (mb·ster^{-1}·MeV^{-1})	Error	Energy (MeV)	σ (mb·ster^{-1}·MeV^{-1})	Error	Energy (MeV)	σ (mb·ster^{-1}·MeV^{-1})	Error
14.19	.85	.02									
15.25	.73	.02	14.04	.68	.03	14.06	.53	.01	14.10	.34	.01
16.31	.64	.02	15.09	.61	.03	15.11	.47	.01	15.15	.28	.01
17.38	.54	.02	16.13	.47	.03	16.15	.42	.01	16.20	.24	.01
18.44	.46	.02	17.18	.44	.03	17.20	.36	.01	17.25	.20	.01
19.50	.42	.02	18.22	.43	.03	18.25	.32	.01	18.30	.16	.00
20.56	.37	.01	19.27	.33	.02	19.29	.26	.01	19.35	.15	.00
21.62	.34	.01	20.31	.26	.02	20.34	.24	.01	20.40	.12	.00
22.68	.28	.01	21.36	.27	.02	21.39	.19	.01	21.45	.10	.00
23.74	.23	.01	22.41	.20	.02	22.44	.17	.01	22.49	.08	.00
24.80	.23	.01	23.45	.16	.02	23.48	.14	.01	23.54	.07	.00
25.86	.20	.01	24.50	.11	.01	24.53	.12	.00	24.59	.06	.00
26.92	.16	.01	25.54	.12	.01	25.58	.12	.00	25.64	.05	.00
27.98	.15	.01	26.59	.11	.01	26.62	.09	.00	26.69	.04	.00
29.04	.14	.01	27.63	.12	.01	27.67	.09	.00	27.74	.03	.00
30.10	.10	.01	28.68	.06	.01	28.72	.07	.00	28.79	.04	.00
31.16	.10	.01	29.72	.06	.01	29.76	.06	.00	29.84	.03	.00
32.23	.08	.01	30.77	.05	.01	30.81	.05	.00	30.89	.03	.00
33.29	.07	.01	31.82	.02	.01	31.86	.05	.00	31.94	.02	.00
34.35	.09	.01	32.86	.03	.01	32.91	.03	.00	32.99	.02	.00
35.41	.06	.01	33.91	.02	.01	33.95	.07	.00	34.04	.03	.00
36.47	.02	.00	34.95	.02	.01	35.00	.04	.00	35.09	.02	.00
37.53	.06	.01	36.00	.02	.01	36.05	.04	.00	36.14	.01	.00
38.59	.08	.01	37.04	.01	.00	37.09	.05	.00	37.19	.02	.00
39.65	.09	.01	38.09	.03	.01	38.14	.05	.00	38.24	.01	.00
40.71	.10	.01	39.13	.02	.01	39.19	.02	.00	39.29	.02	.00
41.77	.04	.00	40.18	.02	.01	40.23	.03	.00			
42.83	.03	.00	41.23	.00	.00	41.28	.03	.00			
43.89	.08	.01	42.27	.01	.00	42.33	.02	.00			
44.95	.02	.00	43.32	.03	.01	43.38	.00	.00			
46.01	.09	.01	44.36	.00	.00						

TABLE A V 3. Alphas from ^{12}C Bombarded by 60-MeV Protons

70 deg - Run 2032			75 deg - Run 2017			90 deg - Run 2023			110 deg - Run 7113		
Energy (MeV)	σ (mb·ster^{-1}·MeV^{-1})	Error	Energy (MeV)	σ (mb·ster^{-1}·MeV^{-1})	Error	Energy (MeV)	σ (mb·ster^{-1}·MeV^{-1})	Error	Energy (MeV)	σ (mb·ster^{-1}·MeV^{-1})	Error
14.05	.25	.02	14.15	.20	.01	14.03	.12	.01			
15.10	.19	.02	15.21	.17	.01	15.07	.11	.01	13.10	.06	.00
16.15	.18	.01	16.27	.14	.01	16.12	.09	.01	12.15	.05	.00
17.20	.14	.01	17.33	.11	.01	17.16	.07	.01	16.21	.04	.00
18.25	.14	.01	18.39	.09	.00	18.21	.05	.00	17.26	.03	.00
19.30	.10	.01	19.44	.07	.00	19.25	.03	.00	18.31	.02	.00
20.36	.10	.01	20.50	.06	.00	20.29	.03	.00	19.37	.02	.00
21.41	.08	.01	21.56	.05	.00	21.34	.02	.00	20.42	.01	.00
22.46	.07	.01	22.62	.04	.00	22.38	.02	.00	21.47	.01	.00
23.51	.05	.01	23.68	.03	.00	23.43	.01	.00	22.53	.01	.00
24.56	.05	.01	24.73	.03	.00	24.47	.01	.00	23.58	.01	.00
25.01	.05	.01	25.79	.02	.00	25.52	.00	.00	24.64	.00	.00
26.06	.03	.01	26.85	.02	.00	26.56	.00	.00	25.69	.00	.00
27.71	.04	.01	27.91	.02	.00	27.61	.00	.00	26.74	.00	.00
28.76	.03	.01	28.96	.01	.00	28.65	.00	.00	27.80	.00	.00
29.81	.02	.00	30.02	.01	.00	29.70	.00	.00			
30.86	.02	.01	31.08	.01	.00	30.74	.00	.00			
31.91	.01	.00	32.14	.00	.00	31.78	0	0			
32.96	.01	.00	33.20	.00	.00	32.83	.00	.00			
34.01	.01	.00	34.25	.01	.00	33.87	0	0			
35.06	.00	.00	35.31	0	0						
36.11	.00	.00	36.37	.00	.00						
37.16	.01	.00									
38.21	.00	.00									

160 deg - Run 2060

Energy (MeV)	σ (mb·ster^{-1}·MeV^{-1})	Error
14.08	.03	.00
15.13	.03	.00
16.17	.02	.00
17.22	.01	.00
18.27	.00	.00
19.32	.00	.00
20.37	.00	.00
21.42	.00	.00
22.46	0	0

TABLE AVI 1. Protons From ^{54}Fe Bombarded by 60-MeV Protons

15 deg - Run 5016			20 deg - Run 4020			27 deg - Run 5020			30 deg - Run 5007		
Energy (MeV)	σ (mb·ster^{-1}·MeV^{-1})	Error	Energy (MeV)	σ (mb·ster^{-1}·MeV^{-1})	Error	Energy (MeV)	σ (mb·ster^{-1}·MeV^{-1})	Error	Energy (MeV)	σ (mb·ster^{-1}·MeV^{-1})	Error
4.641	16.369	.220	4.687	15.802	.132						
5.689	15.737	.216	5.757	14.686	.127	4.638	14.680	.067	4.644	15.539	.071
6.737	13.970	.204	6.826	12.493	.117	5.685	13.746	.065	5.692	14.415	.068
7.785	12.262	.191	7.896	9.859	.104	6.733	11.559	.060	6.741	12.318	.063
8.833	11.330	.183	8.966	7.195	.089	7.780	9.308	.053	7.789	10.175	.057
9.881	6.780	.142	10.036	4.127	.068	8.827	7.565	.048	8.838	8.253	.051
10.929	5.625	.129	11.106	3.232	.060	9.874	5.424	.041	9.887	5.151	.041
11.976	4.939	.121	12.175	2.731	.055	10.922	4.145	.036	10.935	3.957	.036
13.024	4.562	.116	13.245	2.569	.053	11.969	3.448	.033	11.984	3.331	.033
14.072	4.229	.112	14.315	2.560	.053	13.016	3.041	.031	13.032	2.940	.031
15.120	4.339	.114	15.385	2.411	.052	14.063	2.806	.029	14.081	2.662	.029
16.168	4.220	.112	16.455	2.465	.052	15.111	2.608	.028	15.130	2.490	.028
17.216	4.229	.112	17.524	2.249	.050	16.158	2.488	.028	16.178	2.432	.028
18.264	4.086	.110	18.594	2.373	.051	17.205	2.441	.027	17.227	2.291	.027
19.312	4.146	.111	19.664	2.326	.051	18.253	2.430	.027	18.275	2.272	.027
20.360	4.371	.114	20.734	2.386	.051	19.300	2.391	.027	19.324	2.286	.027
21.408	4.523	.116	21.804	2.390	.051	20.347	2.371	.027	20.372	2.328	.027
22.456	4.407	.114	22.873	2.392	.051	21.394	2.372	.027	21.421	2.296	.027
23.504	4.158	.111	23.943	2.476	.052	22.442	2.398	.027	22.470	2.252	.027
24.552	4.633	.117	25.013	2.507	.053	23.489	2.403	.027	23.518	2.309	.027
25.600	4.413	.114	26.083	2.472	.052	24.536	2.427	.027	24.567	2.323	.027
26.648	4.395	.114	27.153	2.527	.053	25.584	2.413	.027	25.615	2.330	.027
27.696	4.992	.110	28.222	2.582	.053	26.631	2.468	.028	26.664	2.333	.027
28.743	4.728	.118	29.292	2.714	.055	27.678	2.484	.028	27.713	2.367	.028
29.791	4.577	.110	30.362	2.600	.054	28.725	2.525	.028	28.761	2.426	.028
30.839	4.850	.120	31.432	2.704	.055	29.773	2.510	.028	29.810	2.322	.027
31.887	4.437	.115	32.502	2.613	.054	30.820	2.529	.028	30.858	2.365	.028
32.935	4.383	.114	33.571	2.642	.054	31.867	2.517	.028	31.907	2.392	.028
33.983	4.146	.111	34.641	2.659	.054	32.914	2.503	.028	32.955	2.367	.028
35.031	4.757	.118	35.711	2.786	.055	33.962	2.565	.028	34.004	2.423	.028
36.079	4.930	.121	36.781	2.927	.057	35.009	2.513	.028	35.053	2.416	.028
37.127	5.536	.128	37.851	2.981	.057	36.056	2.540	.028	36.101	2.367	.028
38.175	5.343	.126	38.921	3.343	.061	37.104	2.548	.028	37.150	2.413	.028
39.223	5.622	.129	39.990	3.493	.062	38.151	2.632	.028	38.198	2.473	.028
40.271	5.583	.129	41.060	3.974	.066	39.198	2.694	.029	39.247	2.447	.028
41.319	5.868	.132	42.130	4.052	.067	40.245	2.808	.029	40.296	2.604	.029
42.367	5.770	.131	43.200	4.476	.070	41.293	2.889	.030	41.344	2.662	.029
43.415	6.290	.137	44.270	4.312	.069	42.340	2.982	.030	42.393	2.772	.030
44.463	6.394	.138	45.339	4.726	.072	43.387	3.002	.030	43.441	2.732	.030
45.511	5.862	.132	46.409	4.756	.072	44.435	2.984	.030	44.490	2.591	.029
46.558	6.358	.134	47.479	4.547	.071	45.482	2.867	.030	45.538	2.634	.029
47.606	5.435	.127	48.549	4.294	.069	46.529	2.866	.030	46.587	2.575	.029
48.654	5.334	.126	49.619	4.049	.067	47.576	2.606	.028	47.636	2.383	.028
49.702	5.304	.126	50.688	4.326	.069	48.624	2.807	.029	48.684	2.403	.028
50.750	5.949	.122	51.758	4.000	.066	49.671	2.319	.027	49.733	2.112	.026
51.798	4.784	.119	52.828	4.128	.068	50.718	2.426	.027	50.781	2.294	.027
52.846	5.542	.128	53.898	4.596	.071	51.765	2.246	.026	51.830	2.078	.026
53.894	4.731	.118	54.968	5.290	.076	52.813	2.372	.027	52.879	2.168	.026
54.942	6.753	.142	56.037	4.847	.067	53.860	3.097	.031	53.927	2.817	.030
55.990	2.744	.090	57.107	3.549	.063	54.907	4.950	.039	54.976	3.921	.035
57.038	4.297	.113	58.177	6.385	.083	55.955	1.182	.019	56.024	1.533	.022
58.086	4.671	.118	59.247	10.004	.105	57.002	3.119	.031	57.073	2.882	.030
59.134	4.136	.135				58.049	2.664	.029	58.121	1.759	.024
						59.096	1.136	.019	59.170	.848	.016

TABLE AVI 2. Protons From ^{54}Fe Bombarded by 60-MeV Protons

35 deg - Run 4021			40 deg - Run 5002			45 deg - Run 4031			47 deg - Run 5042		
Energy (MeV)	σ (mb·ster^{-1}·MeV^{-1})	Error (mb·ster^{-1}·MeV^{-1})	Energy (MeV)	σ (mb·ster^{-1}·MeV^{-1})	Error (mb·ster^{-1}·MeV^{-1})	Energy (MeV)	σ (mb·ster^{-1}·MeV^{-1})	Error (mb·ster^{-1}·MeV^{-1})	Energy (MeV)	σ (mb·ster^{-1}·MeV^{-1})	Error (mb·ster^{-1}·MeV^{-1})
4.690	15.001	.146	4.616	14.594	.112	4.639	14.962	.070	4.602	14.233	.086
5.761	13.899	.141	5.669	13.430	.107	5.698	13.773	.067	5.653	12.822	.082
6.831	11.630	.129	6.723	11.633	.100	6.758	11.487	.061	6.703	10.671	.075
7.902	9.547	.117	7.776	10.257	.094	7.817	9.202	.055	7.754	8.230	.065
8.972	6.850	.099	8.830	5.933	.071	8.876	6.707	.047	8.804	6.574	.059
10.043	3.798	.074	9.883	2.658	.048	9.935	3.598	.034	9.854	4.792	.050
11.113	3.039	.066	10.937	2.799	.049	10.994	2.774	.030	10.905	3.571	.043
12.184	2.498	.060	11.990	2.541	.047	12.053	2.410	.028	11.955	2.975	.039
13.255	2.257	.057	13.044	2.370	.045	13.112	2.122	.026	13.006	2.567	.036
14.325	2.232	.056	14.098	2.235	.044	14.171	1.981	.025	14.056	2.276	.034
15.396	2.067	.054	15.151	2.133	.043	15.230	1.872	.025	15.107	2.135	.033
16.466	1.985	.053	16.205	2.020	.042	16.289	1.806	.024	16.157	1.895	.031
17.537	1.918	.052	17.258	1.986	.041	17.348	1.659	.023	17.208	1.839	.031
18.607	1.910	.052	18.312	1.931	.041	18.407	1.675	.023	18.258	1.805	.031
19.678	1.944	.053	19.365	1.969	.041	19.466	1.688	.023	19.309	1.748	.030
20.749	1.860	.052	20.419	1.924	.041	20.525	1.659	.023	20.359	1.764	.030
21.819	1.928	.052	21.472	1.932	.041	21.584	1.597	.023	21.410	1.736	.030
22.890	1.970	.053	22.526	1.881	.040	22.643	1.650	.023	22.460	1.713	.030
23.960	1.981	.053	23.580	1.913	.041	23.702	1.626	.023	23.511	1.716	.030
25.031	1.991	.053	24.633	1.915	.041	24.761	1.677	.023	24.561	1.671	.030
26.101	2.042	.054	25.687	2.025	.042	25.820	1.600	.023	25.612	1.698	.030
27.172	2.021	.054	26.740	1.957	.041	26.879	1.634	.023	26.662	1.717	.030
28.242	1.983	.053	27.794	1.931	.041	27.938	1.585	.023	27.713	1.641	.029
29.313	2.074	.054	28.847	2.043	.042	28.997	1.684	.023	28.763	1.703	.030
30.384	1.954	.053	29.901	2.015	.042	30.056	1.689	.023	29.814	1.600	.029
31.454	2.044	.054	30.954	1.936	.041	31.115	1.655	.023	30.864	1.603	.029
32.525	1.997	.053	32.008	1.856	.040	32.174	1.604	.023	31.914	1.556	.028
33.595	2.067	.054	33.062	1.860	.040	33.233	1.599	.023	32.965	1.563	.029
34.666	2.077	.054	34.115	1.862	.040	34.292	1.557	.022	34.015	1.551	.028
35.736	2.058	.054	35.169	1.846	.040	35.351	1.550	.022	35.066	1.495	.028
36.807	2.091	.055	36.222	1.890	.040	36.410	1.587	.023	36.116	1.471	.028
37.878	2.169	.056	37.276	1.810	.039	37.469	1.565	.022	37.167	1.478	.028
38.948	2.168	.056	38.329	1.868	.040	38.528	1.589	.023	38.217	1.422	.027
40.019	2.251	.057	39.383	1.888	.040	39.587	1.531	.022	39.268	1.420	.027
41.089	2.366	.058	40.436	1.950	.041	40.646	1.571	.023	40.318	1.420	.027
42.160	2.334	.058	41.490	2.012	.042	41.705	1.569	.023	41.369	1.440	.027
43.230	2.232	.056	42.544	1.955	.041	42.764	1.546	.022	42.419	1.419	.027
44.301	2.215	.056	43.597	1.901	.040	43.823	1.535	.022	43.470	1.419	.027
45.371	2.279	.057	44.651	1.878	.040	44.882	1.497	.022	44.520	1.329	.026
46.442	2.140	.055	45.704	1.878	.040	45.941	1.389	.021	45.571	1.336	.026
47.513	2.097	.055	46.758	1.664	.038	47.000	1.329	.021	46.621	1.217	.025
48.583	1.964	.053	47.811	1.667	.038	48.059	1.303	.021	47.672	1.202	.025
49.654	1.984	.053	48.865	1.521	.036	49.118	1.139	.019	48.722	1.175	.025
50.724	1.860	.052	49.918	1.463	.035	50.177	1.148	.019	49.773	1.014	.023
51.795	1.784	.050	50.972	1.387	.035	51.236	.969	.018	50.823	1.047	.023
52.865	1.713	.049	52.026	1.172	.030	52.295	.933	.017	51.874	.848	.021
53.936	2.451	.059	53.079	1.155	.031	53.354	1.018	.018	52.924	.869	.021
55.007	1.704	.049	54.133	1.582	.037	54.413	1.072	.019	53.974	.951	.022
56.077	2.026	.054	55.186	1.426	.035	55.472	.893	.017	55.025	1.025	.023
57.148	1.486	.046	56.240	1.293	.033	56.531	.619	.014	56.075	.854	.021
58.218	1.319	.043	57.293	1.030	.030	57.590	1.069	.019	57.126	.375	.014
			58.347	1.602	.037	58.649	.819	.016	58.176	1.038	.023
			59.401	.412	.035				59.227	.965	.022

TABLE AVI 3. Protons From ^{54}Fe Bombarded by 60-MeV Protons

50 deg - Run 5010			55 deg - Run 4025			60 deg - Run 5043			65 deg - Run 5011		
Energy (MeV)	σ (mb·ster^{-1}·MeV^{-1})	Error	Energy (MeV)	σ (mb·ster^{-1}·MeV^{-1})	Error	Energy (MeV)	σ (mb·ster^{-1}·MeV^{-1})	Error	Energy (MeV)	σ (mb·ster^{-1}·MeV^{-1})	Error
4.644	12.579	.074							4.646	13.641	.046
5.692	11.378	.070	4.69	14.93	.07	4.607	13.599	.081	5.695	12.075	.044
6.741	9.427	.064	5.77	13.57	.07	5.659	12.157	.077	6.743	9.731	.039
7.789	7.251	.056	6.84	11.08	.06	6.711	9.809	.069	7.792	7.595	.035
8.838	6.818	.051	7.91	8.83	.05	7.763	7.660	.061	8.841	6.172	.031
9.886	3.992	.042	8.98	6.64	.05	8.814	6.261	.055	9.890	4.093	.025
10.935	3.074	.036	10.05	3.45	.03	9.866	4.070	.045	10.939	3.054	.022
11.983	2.517	.033	11.13	2.66	.03	10.918	3.103	.039	11.988	2.430	.020
13.032	2.168	.031	12.20	2.21	.03	11.969	2.545	.035	13.037	2.076	.018
14.080	1.994	.029	13.27	2.02	.03	13.021	2.239	.033	14.086	1.836	.017
15.129	1.804	.028	14.34	1.80	.02	14.073	1.888	.030	15.135	1.620	.016
16.177	1.720	.027	15.41	1.72	.02	15.125	1.779	.029	16.184	1.503	.015
17.226	1.664	.027	16.48	1.64	.02	16.176	1.564	.028	17.233	1.394	.015
18.274	1.519	.026	17.56	1.51	.02	17.228	1.491	.027	18.282	1.326	.014
19.323	1.584	.025	18.63	1.45	.02	18.280	1.448	.027	19.331	1.244	.014
20.372	1.449	.025	19.70	1.46	.02	19.331	1.377	.026	20.380	1.230	.014
21.420	1.452	.025	20.77	1.44	.02	20.383	1.337	.026	21.429	1.187	.014
22.469	1.441	.025	21.84	1.41	.02	21.435	1.299	.025	22.478	1.159	.013
23.517	1.444	.025	22.91	1.33	.02	22.487	1.265	.025	23.527	1.136	.013
24.566	1.420	.025	23.99	1.38	.02	23.538	1.310	.025	24.576	1.089	.013
25.614	1.427	.025	25.06	1.34	.02	24.590	1.212	.024	25.625	1.058	.013
26.663	1.428	.025	26.13	1.32	.02	25.642	1.184	.024	26.674	1.015	.013
27.711	1.387	.024	27.20	1.32	.02	26.693	1.154	.024	27.723	.991	.012
28.760	1.369	.024	28.27	1.27	.02	27.745	1.131	.023	28.772	.965	.012
29.808	1.338	.024	29.34	1.28	.02	28.797	1.120	.023	29.821	.936	.012
30.857	1.318	.024	30.42	1.25	.02	29.848	1.088	.023	30.870	.886	.012
31.905	1.276	.023	31.49	1.21	.02	30.900	1.033	.022	31.919	.880	.012
32.954	1.277	.023	32.56	1.18	.02	31.952	.995	.022	32.968	.840	.011
34.003	1.222	.023	33.63	1.17	.02	33.004	1.007	.022	34.017	.811	.011
35.051	1.209	.023	34.70	1.16	.02	34.055	.961	.022	35.066	.789	.011
36.100	1.203	.023	35.77	1.10	.02	35.107	.927	.021	36.115	.736	.011
37.148	1.152	.022	36.85	1.03	.02	36.159	.914	.021	37.164	.736	.011
38.197	1.116	.022	37.92	1.07	.02	37.210	.886	.021	38.213	.671	.010
39.245	1.172	.022	38.99	1.10	.02	38.262	.834	.020	39.262	.683	.010
40.294	1.122	.022	40.06	1.04	.02	39.314	.822	.020	40.311	.670	.010
41.342	1.105	.022	41.13	1.06	.02	40.366	.807	.020	41.360	.630	.010
42.391	1.074	.022	42.20	.97	.02	41.417	.771	.019	42.409	.612	.010
43.439	1.089	.022	43.28	.96	.02	42.469	.764	.019	43.458	.593	.010
44.488	1.049	.021	44.35	.90	.02	43.521	.728	.019	44.507	.559	.009
45.536	1.006	.021	45.42	.87	.02	44.572	.691	.018	45.556	.531	.009
46.585	.954	.020	46.49	.80	.02	45.624	.647	.018	46.605	.488	.009
47.633	.954	.020	47.56	.80	.02	46.676	.603	.017	47.654	.483	.009
48.682	.834	.019	48.63	.71	.02	47.728	.601	.017	48.703	.415	.008
49.731	.798	.019	49.71	.74	.02	48.779	.539	.016	49.752	.429	.008
50.779	.845	.019	50.78	.61	.01	49.831	.499	.016	50.801	.389	.008
51.828	.633	.017	51.85	.61	.01	50.883	.472	.015	51.850	.360	.008
52.876	.674	.017	52.92	.67	.02	51.934	.428	.014	52.899	.353	.007
53.925	.735	.018	53.99	.68	.02	52.986	.425	.014	53.948	.404	.008
54.973	.816	.019	55.06	.51	.01	54.038	.523	.016	54.997	.280	.007
56.022	.654	.017	56.14	.34	.01	55.089	.333	.013	56.046	.194	.006
57.070	.281	.011	57.21	.35	.01	56.141	.280	.012	57.095	.244	.006
58.119	.649	.017	58.28	.23	.01	57.193	.284	.012	58.144	.054	.003
59.167	.619	.016				58.245	.126	.008			

TABLE AVI 4. Protons From ^{54}Fe Bombarded by 60-MeV Protons

70 deg - Run 5044			80 deg - Run 5012			90 deg - Run 4010			110 deg - Run 5015		
Energy (MeV)	σ (mb·ster^{-1}·MeV^{-1})	Error	Energy (MeV)	σ (mb·ster^{-1}·MeV^{-1})	Error	Energy (MeV)	σ (mb·ster^{-1}·MeV^{-1})	Error	Energy (MeV)	σ (mb·ster^{-1}·MeV^{-1})	Error
4.611	13.021	.092							4.603	12.517	.037
5.663	11.723	.087	4.648	13.342	.040				5.653	10.587	.034
6.716	9.229	.078	5.697	11.636	.038	4.602	13.094	.037	6.704	7.906	.029
7.768	7.289	.069	6.747	9.159	.034	5.652	11.343	.035	7.755	5.964	.025
8.821	5.933	.062	7.796	7.006	.029	6.702	8.879	.031	8.805	4.489	.022
9.874	3.678	.049	8.846	5.624	.026	7.753	6.787	.027	9.856	3.042	.018
10.926	2.728	.042	9.895	3.682	.021	8.803	4.822	.023	10.906	2.097	.015
11.979	2.248	.038	10.944	2.674	.018	9.853	2.341	.016	11.957	1.661	.013
13.031	1.926	.035	11.994	2.153	.016	10.904	1.806	.014	13.008	1.350	.012
14.084	1.627	.033	13.043	1.764	.015	11.954	1.464	.013	14.058	1.079	.011
15.136	1.516	.031	14.093	1.525	.014	13.004	1.231	.011	15.109	.911	.010
16.189	1.324	.029	15.142	1.352	.013	14.055	1.079	.011	16.159	.793	.009
17.241	1.266	.029	16.192	1.225	.012	15.105	.965	.010	17.210	.688	.009
18.294	1.165	.028	17.241	1.088	.012	16.155	.866	.010	18.261	.619	.008
19.346	1.139	.027	18.291	1.019	.011	17.206	.763	.009	19.311	.550	.008
20.399	1.047	.026	19.340	.958	.011	18.256	.713	.009	20.362	.492	.007
21.451	1.033	.026	20.390	.877	.010	19.306	.652	.008	21.412	.427	.007
22.504	.984	.025	21.439	.855	.010	20.357	.623	.008	22.463	.392	.007
23.556	.960	.025	22.489	.796	.010	21.407	.572	.008	23.514	.371	.006
24.609	.916	.024	23.538	.768	.010	22.457	.526	.007	24.564	.328	.006
25.661	.908	.024	24.588	.722	.009	23.508	.503	.007	25.615	.293	.006
26.714	.857	.024	25.637	.680	.009	24.558	.463	.007	26.665	.267	.005
27.766	.813	.023	26.687	.652	.009	25.608	.430	.007	27.716	.247	.005
28.819	.788	.023	27.736	.620	.009	26.659	.402	.007	28.767	.227	.005
29.871	.742	.022	28.786	.574	.008	27.709	.389	.006	29.817	.200	.005
30.924	.684	.021	29.835	.551	.008	28.759	.352	.006	30.868	.179	.004
31.976	.681	.021	30.884	.514	.008	29.810	.333	.006	31.919	.155	.004
33.029	.647	.020	31.934	.494	.008	30.860	.310	.006	32.969	.141	.004
34.081	.600	.020	32.983	.456	.007	31.911	.285	.006	34.020	.132	.004
35.134	.582	.019	34.033	.461	.008	32.961	.265	.005	35.070	.117	.004
36.186	.605	.020	35.082	.398	.007	34.011	.253	.005	36.121	.109	.003
37.239	.539	.019	36.132	.382	.007	35.062	.236	.005	37.172	.094	.003
38.291	.533	.019	37.181	.368	.007	36.112	.215	.005	38.222	.085	.003
39.344	.523	.018	38.231	.343	.006	37.162	.200	.005	39.273	.067	.003
40.396	.457	.017	39.280	.324	.006	38.213	.187	.004	40.323	.063	.003
41.449	.493	.018	40.330	.315	.006	39.263	.175	.004	41.374	.055	.002
42.501	.440	.017	41.379	.294	.006	40.313	.163	.004	42.425	.054	.002
43.554	.422	.017	42.429	.281	.006	41.364	.152	.004	43.475	.047	.002
44.606	.367	.015	43.478	.254	.006	42.414	.141	.004	44.526	.036	.002
45.659	.378	.016	44.528	.239	.005	43.464	.120	.004	45.576	.033	.002
46.711	.356	.015	45.577	.214	.005	44.515	.105	.003	46.627	.024	.002
47.764	.310	.014	46.627	.200	.005	45.565	.106	.003	47.678	.024	.002
48.816	.315	.014	47.676	.167	.005	46.615	.082	.003	48.728	.021	.001
49.869	.265	.013	48.725	.165	.004	47.666	.067	.003	49.779	.017	.001
50.921	.247	.013	49.775	.156	.004	48.716	.065	.003	50.830	.016	.001
51.974	.207	.012	50.824	.123	.004	49.766	.050	.002	51.880	.016	.001
53.026	.232	.012	51.874	.116	.004	50.817	.047	.002	52.931	.010	.001
54.079	.275	.013	52.923	.111	.004	51.867	.040	.002	53.981	.009	.001
55.131	.181	.011	53.973	.119	.004	52.917	.037	.002	55.032	.006	.001
56.184	.076	.007	55.022	.103	.004	53.968	.027	.002	56.083	.009	.001
57.236	.157	.010	56.072	.067	.003	55.018	.022	.002	57.133	.008	.001
58.289	.063	.006	57.121	.078	.003	56.068	.043	.002			
			58.171	.069	.003	57.119	.033	.002			

TABLE AVI 5. Protons From ^{54}Fe Bombarded by 60-MeV Protons

120 deg - Run 7002			135 deg - Run 4011			160 deg - Run 2067		
Energy (MeV)	σ (mb·ster^{-1}·MeV^{-1})	Error	Energy (MeV)	σ (mb·ster^{-1}·MeV^{-1})	Error	Energy (MeV)	σ (mb·ster^{-1}·MeV^{-1})	Error
						4.60	13.22	.12
4.604	13.424	.069				5.65	10.29	.10
5.654	11.278	.063	4.605	12.449	.029	6.70	7.87	.09
6.705	8.667	.055	5.656	10.193	.027	7.75	5.83	.08
7.756	6.338	.047	6.707	7.641	.023	8.80	3.92	.06
8.807	5.212	.043	7.758	5.625	.020	9.85	2.00	.05
9.858	3.082	.033	8.809	3.844	.016	10.90	1.58	.04
10.908	2.164	.027	9.860	1.841	.011	11.95	1.27	.04
11.959	1.636	.024	10.911	1.358	.010	13.00	1.04	.03
13.010	1.277	.021	11.962	1.075	.009	14.05	.88	.03
14.061	1.070	.019	13.013	.896	.008	15.10	.75	.03
15.112	.879	.018	14.064	.748	.007	16.15	.60	.03
16.162	.772	.016	15.115	.631	.007	17.20	.53	.02
17.213	.662	.015	16.166	.550	.006	18.25	.43	.02
18.264	.545	.014	17.217	.462	.006	19.30	.45	.02
19.315	.524	.014	18.268	.417	.005	20.35	.36	.02
20.366	.448	.013	19.319	.359	.005	21.40	.33	.02
21.416	.397	.012	20.370	.311	.005	22.45	.26	.02
22.467	.383	.012	21.421	.284	.004	23.50	.25	.02
23.518	.326	.011	22.472	.246	.004	24.55	.21	.01
24.569	.289	.010	23.523	.227	.004	25.60	.16	.01
25.620	.260	.010	24.574	.195	.004	26.65	.16	.01
26.670	.229	.009	25.625	.182	.004	27.70	.16	.01
27.721	.202	.008	26.676	.160	.003	28.75	.13	.01
28.772	.179	.008	27.727	.136	.003	29.80	.12	.01
29.823	.154	.007	28.778	.121	.003	30.85	.08	.01
30.874	.133	.007	29.829	.108	.003	31.90	.08	.01
31.925	.115	.006	30.880	.099	.003	32.95	.07	.01
32.975	.097	.006	31.931	.082	.002	34.00	.07	.01
34.026	.082	.005	32.982	.075	.002	35.05	.06	.01
35.077	.064	.005	34.033	.067	.002	36.10	.04	.01
36.128	.072	.005	35.084	.058	.002	37.15	.04	.01
37.179	.067	.005	36.135	.049	.002	38.20	.03	.01
38.229	.054	.004	37.186	.046	.002	39.25	.02	.00
39.280	.044	.004	38.237	.036	.002	40.30	.01	.00
40.331	.038	.004	39.289	.034	.002	41.35	.01	.00
41.382	.034	.003	40.340	.029	.001	42.40	.03	.01
42.433	.032	.003	41.391	.023	.001	43.45	.01	.00
43.483	.031	.003	42.442	.019	.001	44.50	.01	.00
44.534	.018	.003	43.493	.017	.001	45.55	.01	.00
45.585	.014	.002	44.544	.013	.001	46.60	.01	.00
46.636	.015	.002	45.595	.011	.001	47.65	.00	.00
47.687	.011	.002	46.646	.009	.001	48.70	.01	.00
48.737	.006	.001	47.697	.007	.001	49.75	.00	.00
49.788	.005	.001	48.748	.005	.001	50.80	.00	.00
50.839	.009	.002	49.799	.005	.001	51.85	.00	.00
51.890	.002	.001	50.850	.005	.001	52.90	0	0
52.941	.004	.001	51.901	.002	.000	53.95	0	0
53.991	.008	.002	52.952	.003	.000	55.00	.00	.00
55.042	.000	.000	54.003	.002	.000	56.05	0	0
56.093	.011	.002	55.054	.001	.000	57.10	0	0
			56.105	.002	.000	58.15	0	0
						59.20	0	0

TABLE AVII 1. Deuterons From ^{54}Fe Bombarded by 60-MeV Protons

15 deg - Run 5016			20 deg - Run 4020			27 deg - Run 5020			30 deg - Run 5007		
Energy (MeV)	σ (mb·ster^{-1}·MeV^{-1})	Error	Energy (MeV)	σ (mb·ster^{-1}·MeV^{-1})	Error	Energy (MeV)	σ (mb·ster^{-1}·MeV^{-1})	Error	Energy (MeV)	σ (mb·ster^{-1}·MeV^{-1})	Error
5.689	.359	.033	5.757	.330	.019	5.685	.347	.010	5.692	.339	.010
6.737	.350	.032	6.826	.341	.019	6.733	.382	.011	6.741	.376	.011
7.785	.327	.031	7.896	.433	.022	7.780	.390	.011	7.789	.395	.011
8.833	.365	.033	8.966	.390	.021	8.827	.394	.011	8.838	.353	.011
9.881	.330	.030	10.036	.396	.021	9.874	.365	.011	9.887	.340	.010
10.929	.273	.028	11.106	.352	.020	10.922	.306	.010	10.935	.337	.010
11.976	.362	.033	12.175	.305	.018	11.969	.335	.010	11.984	.356	.011
13.024	.383	.034	13.245	.277	.017	13.016	.369	.011	13.032	.325	.010
14.072	.380	.034	14.315	.261	.017	14.063	.306	.010	14.081	.324	.010
15.120	.321	.031	15.385	.265	.017	15.111	.316	.010	15.130	.300	.010
16.168	.285	.029	16.455	.286	.018	16.158	.311	.010	16.178	.285	.010
17.216	.339	.032	17.524	.298	.018	17.205	.317	.010	17.227	.287	.010
18.264	.282	.029	18.594	.304	.018	18.253	.335	.010	18.275	.314	.010
19.312	.333	.030	19.664	.326	.019	19.300	.320	.010	19.324	.312	.010
20.360	.419	.035	20.734	.325	.019	20.347	.316	.010	20.372	.306	.010
21.408	.365	.033	21.804	.322	.019	21.394	.312	.010	21.421	.316	.010
22.456	.321	.031	22.873	.353	.020	22.442	.344	.010	22.470	.306	.010
23.504	.416	.035	23.943	.350	.020	23.489	.328	.010	23.518	.335	.010
24.552	.369	.033	25.013	.353	.020	24.536	.330	.010	24.567	.307	.010
25.600	.377	.033	26.083	.382	.021	25.584	.346	.010	25.615	.324	.010
26.648	.359	.033	27.153	.361	.020	26.631	.317	.010	26.664	.307	.010
27.696	.457	.037	28.222	.377	.020	27.678	.350	.010	27.713	.312	.010
28.743	.445	.036	29.292	.425	.022	28.725	.359	.011	28.761	.310	.010
29.791	.451	.037	30.362	.349	.020	29.773	.322	.010	29.810	.318	.010
30.839	.481	.038	31.432	.451	.022	30.820	.331	.010	30.858	.303	.010
31.887	.535	.040	32.502	.432	.022	31.867	.309	.010	31.907	.311	.010
32.935	.529	.040	33.571	.446	.022	32.914	.311	.010	32.955	.299	.010
33.983	.585	.042	34.641	.473	.023	33.962	.321	.010	34.004	.293	.010
35.031	.559	.041	35.711	.579	.025	35.009	.323	.010	35.053	.295	.010
36.079	.612	.043	36.781	.579	.025	36.056	.342	.010	36.101	.322	.010
37.127	.647	.044	37.851	.637	.027	37.104	.334	.010	37.150	.311	.010
38.175	.763	.048	38.921	.723	.028	38.151	.349	.010	38.198	.323	.010
39.223	.748	.047	39.990	.762	.029	39.198	.379	.011	39.247	.348	.011
40.271	.932	.053	41.060	.759	.029	40.245	.406	.011	40.296	.368	.011
41.319	.588	.042	42.130	1.309	.038	41.293	.345	.010	41.344	.341	.010
42.367	.950	.053	43.200	.945	.032	42.340	.492	.012	42.393	.515	.013
43.415	2.025	.078	44.270	.649	.027	43.387	.488	.012	43.441	.295	.010
44.463	.472	.037	45.339	2.000	.047	44.435	.249	.009	44.490	.197	.008
45.511	1.595	.069	46.409	2.346	.051	45.482	1.023	.018	45.538	.877	.017
46.558	2.658	.089	47.479	.419	.022	46.529	.894	.017	46.587	.806	.016
47.606	1.437	.065	48.549	.548	.025	47.576	.333	.010	47.636	.136	.007
48.654	.116	.019	49.619	2.862	.056	48.624	.076	.005	48.684	.085	.005
49.702	1.782	.073				49.671	1.755	.023	49.733	1.593	.023

TABLE AVII 2. Deuterons From ^{54}Fe Bombarded by 60-MeV Protons

35 deg - Run 4021			40 deg - Run 5002			45 deg - Run 4031			47 deg - Run 5042		
Energy (MeV)	σ	Error	Energy (MeV)	σ	Error	Energy (MeV)	σ	Error	Energy (MeV)	σ	Error
	(mb·ster^{-1}·MeV^{-1})			(mb·ster^{-1}·MeV^{-1})			(mb·ster^{-1}·MeV^{-1})			(mb·ster^{-1}·MeV^{-1})	
5.761	.360	.023	5.669	.322	.017	5.698	.310	.010	5.653	.298	.012
6.831	.350	.022	6.723	.338	.017	6.758	.343	.011	6.703	.326	.013
7.902	.361	.023	7.776	.346	.017	7.817	.370	.011	7.754	.310	.013
8.972	.357	.023	8.838	.345	.017	8.876	.335	.010	8.804	.332	.013
10.043	.364	.023	9.883	.323	.017	9.935	.305	.010	9.854	.303	.013
11.113	.290	.020	10.937	.340	.017	10.994	.279	.009	10.905	.255	.012
12.184	.315	.021	11.990	.179	.012	12.053	.248	.009	11.955	.252	.011
13.255	.284	.017	13.044	.833	.005	13.112	.266	.008	13.006	.264	.012
14.325	.223	.018	14.098	.095	.009	14.171	.205	.008	14.056	.225	.011
15.396	.267	.020	15.151	.197	.013	15.230	.204	.008	15.107	.242	.011
16.466	.237	.018	16.205	.215	.014	16.289	.207	.008	16.157	.232	.011
17.537	.228	.018	17.258	.198	.013	17.348	.199	.008	17.208	.236	.011
18.607	.258	.019	18.312	.241	.014	18.407	.218	.008	18.258	.233	.011
19.678	.238	.018	19.365	.245	.014	19.466	.204	.008	19.309	.201	.010
20.749	.251	.019	20.419	.228	.014	20.525	.213	.008	20.359	.218	.011
21.819	.234	.018	21.472	.214	.014	21.584	.208	.008	21.410	.212	.011
22.890	.251	.019	22.526	.217	.014	22.643	.217	.008	22.460	.181	.010
23.960	.283	.020	23.580	.246	.015	23.702	.209	.008	23.511	.204	.010
25.031	.255	.019	24.633	.245	.014	24.761	.189	.008	24.561	.220	.011
26.101	.254	.019	25.687	.221	.014	25.820	.211	.008	25.612	.216	.011
27.172	.261	.019	26.740	.225	.014	26.879	.186	.008	26.662	.198	.010
28.242	.260	.019	27.794	.240	.014	27.938	.183	.008	27.713	.196	.010
29.313	.258	.019	28.847	.246	.015	28.997	.199	.008	28.763	.193	.010
30.384	.244	.019	29.901	.223	.014	30.056	.193	.008	29.814	.179	.010
31.454	.253	.019	30.954	.216	.014	31.115	.180	.008	30.864	.172	.009
32.525	.245	.019	32.008	.223	.014	32.174	.178	.008	31.914	.177	.010
33.595	.253	.019	33.062	.202	.013	33.233	.173	.007	32.965	.176	.010
34.666	.308	.021	34.115	.217	.014	34.292	.182	.008	34.015	.164	.009
35.736	.297	.021	35.169	.200	.013	35.351	.163	.007	35.066	.174	.010
36.807	.285	.020	36.222	.200	.013	36.410	.180	.008	36.116	.161	.009
37.878	.280	.020	37.276	.217	.014	37.469	.191	.008	37.167	.148	.009
38.948	.308	.021	38.329	.196	.013	38.528	.196	.008	38.217	.155	.009
40.019	.321	.021	39.383	.229	.014	39.587	.169	.007	39.268	.169	.009
41.089	.347	.022	40.436	.184	.013	40.646	.166	.007	40.318	.139	.009
42.160	.472	.026	41.490	.198	.013	41.705	.228	.009	41.369	.159	.009
43.230	.245	.019	42.544	.369	.018	42.764	.131	.007	42.419	.197	.010
44.301	.317	.021	43.597	.137	.011	43.823	.157	.007	43.470	.082	.007
45.371	.812	.034	44.651	.268	.015	44.882	.353	.011	44.520	.092	.007
46.442	.545	.028	45.704	.691	.024	45.941	.300	.010	45.571	.432	.015
47.513	.138	.014	46.758	.356	.017	47.000	.061	.004	46.621	.170	.009
48.583	.274	.020	47.811	.059	.007	48.059	.123	.006	47.672	.043	.005
			48.865	.311	.016	49.118	.497	.013	48.722	.050	.005

TABLE AVII 3. Deutérons From ^{64}Fe Bombarded by 60-MeV Protons

50 deg - Run 5010			55 deg - Run 4025			60 deg - Run 5043			65 deg - Run 5011		
Energy (MeV)	σ (mb·ster^{-1}·MeV^{-1})	Error	Energy (MeV)	σ (mb·ster^{-1}·MeV^{-1})	Error	Energy (MeV)	σ (mb·ster^{-1}·MeV^{-1})	Error	Energy (MeV)	σ (mb·ster^{-1}·MeV^{-1})	Error
5.692	.288	.011							5.695	.303	.007
6.741	.298	.011	5.77	.32	.01	5.659	.297	.012	6.743	.321	.007
7.789	.284	.011	6.84	.34	.01	6.711	.285	.012	7.792	.300	.007
8.838	.290	.011	7.91	.35	.01	7.763	.274	.012	8.841	.259	.006
9.886	.257	.011	8.98	.31	.01	8.814	.253	.011	9.890	.241	.006
10.935	.235	.010	10.05	.28	.01	9.866	.256	.011	10.939	.219	.006
11.983	.243	.010	11.13	.25	.01	10.918	.220	.010	11.988	.224	.006
13.032	.230	.010	12.20	.25	.01	11.969	.228	.011	13.037	.219	.006
14.080	.207	.009	13.27	.17	.01	13.021	.196	.010	14.086	.171	.005
15.129	.196	.009	14.34	.17	.01	14.073	.190	.010	15.135	.166	.005
16.177	.179	.009	15.41	.17	.01	15.125	.187	.010	16.184	.157	.005
17.226	.193	.009	16.48	.17	.01	16.176	.168	.009	17.233	.158	.005
18.274	.163	.008	17.56	.16	.01	17.228	.168	.009	18.282	.155	.005
19.323	.179	.009	18.63	.17	.01	18.280	.155	.009	19.331	.136	.005
20.372	.174	.009	19.70	.16	.01	19.331	.161	.009	20.380	.140	.005
21.420	.168	.009	20.77	.16	.01	20.383	.166	.009	21.429	.143	.005
22.469	.166	.008	21.84	.17	.01	21.435	.154	.009	22.478	.133	.005
23.517	.167	.008	22.91	.17	.01	22.487	.155	.009	23.527	.130	.005
24.566	.172	.009	23.99	.15	.01	23.538	.123	.008	24.576	.122	.004
25.614	.168	.009	25.06	.16	.01	24.590	.141	.008	25.625	.122	.004
26.663	.152	.008	26.13	.16	.01	25.642	.132	.008	26.674	.116	.004
27.711	.167	.008	27.20	.15	.01	26.693	.123	.008	27.723	.108	.004
28.760	.156	.008	28.27	.16	.01	27.745	.113	.007	28.772	.109	.004
29.808	.155	.008	29.34	.13	.01	28.797	.134	.008	29.821	.108	.004
30.857	.143	.008	30.42	.15	.01	29.848	.122	.008	30.870	.098	.004
31.905	.153	.008	31.49	.14	.01	30.900	.118	.008	31.919	.100	.004
32.954	.140	.008	32.56	.14	.01	31.952	.111	.007	32.968	.091	.004
34.003	.139	.008	33.63	.14	.01	33.004	.101	.007	34.017	.087	.004
35.051	.145	.008	34.70	.13	.01	34.055	.098	.007	35.066	.084	.004
36.100	.141	.008	35.77	.14	.01	35.107	.086	.006	36.115	.088	.004
37.148	.129	.007	36.85	.15	.01	36.159	.095	.007	37.164	.089	.004
38.197	.146	.008	37.92	.16	.01	37.210	.096	.007	38.213	.091	.004
39.245	.136	.008	38.99	.15	.01	38.262	.100	.007	39.262	.076	.003
40.294	.119	.007	40.06	.12	.01	39.314	.108	.007	40.311	.067	.003
41.342	.120	.007	41.13	.16	.01	40.366	.090	.007	41.360	.102	.004
42.391	.155	.008	42.20	.12	.01	41.417	.134	.008	42.409	.053	.003
43.439	.079	.006	43.28	.11	.01	42.469	.060	.005	43.458	.042	.003
44.488	.102	.007	44.35	.29	.01	43.521	.042	.005	44.507	.149	.005
45.536	.363	.013	45.42	.22	.01	44.572	.197	.010	45.556	.131	.005
46.585	.121	.007	46.49	.04	.00	45.624	.169	.009	46.605	.019	.001
47.633	.037	.004	47.56	.09	.01	46.676	.018	.003	47.654	.024	.002
48.682	.081	.006	48.63	.35	.01	47.728	.032	.004			

TABLE AVII 4. Deuterons From ^{54}Fe Bombarded by 60-MeV Protons

70 deg - Run 5044			80 deg - Run 5012			90 deg - Run 4010			110 deg - Run 5015		
Energy (MeV)	σ	Error	Energy (MeV)	σ	Error	Energy (MeV)	σ	Error	Energy (MeV)	σ	Error
	(mb·ster^{-1}·MeV^{-1})			(mb·ster^{-1}·MeV^{-1})			(mb·ster^{-1}·MeV^{-1})			(mb·ster^{-1}·MeV^{-1})	
5.663	.282	.014				5.652	.250	.005	5.653	.249	.005
6.716	.291	.014	5.697	.309	.006	6.702	.260	.005	6.704	.224	.005
7.768	.263	.013	6.747	.284	.006	7.753	.226	.005	7.755	.197	.005
8.821	.240	.013	7.796	.269	.006	8.803	.196	.005	8.805	.165	.004
9.874	.225	.012	8.846	.229	.005	9.853	.166	.004	9.856	.143	.004
10.926	.175	.011	9.895	.201	.005	10.904	.154	.004	10.906	.126	.004
11.979	.190	.011	10.944	.193	.005	11.954	.126	.004	11.957	.104	.003
13.031	.160	.010	11.994	.179	.005	13.004	.086	.003	13.008	.098	.003
14.084	.152	.010	13.043	.158	.004	14.055	.075	.003	14.058	.075	.003
15.136	.139	.010	14.093	.137	.004	15.105	.078	.003	15.109	.073	.003
16.189	.125	.009	15.142	.126	.004	16.155	.070	.003	16.159	.057	.002
17.241	.128	.009	16.192	.113	.004	17.206	.068	.003	17.210	.051	.002
18.294	.123	.009	17.241	.108	.004	18.256	.072	.003	18.261	.053	.002
19.346	.109	.008	18.291	.113	.004	19.306	.064	.003	19.311	.041	.002
20.399	.105	.008	19.340	.100	.003	20.357	.061	.003	20.362	.038	.002
21.451	.111	.009	20.390	.096	.003	21.407	.055	.002	21.412	.036	.002
22.504	.095	.008	21.439	.090	.003	22.457	.054	.002	22.463	.032	.002
23.556	.106	.008	22.489	.090	.003	23.508	.048	.002	23.514	.033	.002
24.609	.089	.008	23.538	.089	.003	24.558	.050	.002	24.564	.029	.002
25.661	.083	.007	24.588	.083	.003	25.608	.047	.002	25.615	.026	.002
26.714	.094	.008	25.637	.078	.003	26.659	.046	.002	26.665	.024	.002
27.766	.073	.007	26.687	.069	.003	27.709	.038	.002	27.716	.017	.001
28.819	.073	.007	27.736	.063	.003	28.759	.037	.002	28.767	.019	.001
29.871	.064	.006	28.786	.063	.003	29.810	.036	.002	29.817	.016	.001
30.924	.078	.007	29.835	.059	.003	30.860	.034	.002	30.868	.015	.001
31.976	.074	.007	30.884	.059	.003	31.911	.031	.002	31.919	.011	.001
33.029	.063	.006	31.934	.053	.003	32.961	.027	.002	32.969	.012	.001
34.081	.047	.006	32.983	.050	.002	34.011	.029	.002	34.020	.011	.001
35.134	.070	.007	34.033	.048	.002	35.062	.026	.002	35.070	.009	.001
36.186	.057	.006	35.082	.049	.002	36.112	.025	.002	36.121	.010	.001
37.239	.052	.006	36.132	.043	.002	37.162	.023	.002	37.172	.008	.001
38.291	.066	.007	37.181	.047	.002	38.213	.021	.002	38.222	.007	.001
39.344	.035	.005	38.231	.042	.002	39.263	.018	.001	39.273	.006	.001
40.396	.050	.006	39.280	.034	.002	40.313	.023	.002	40.323	.003	.001
41.449	.067	.007	40.330	.037	.002	41.364	.019	.001	41.374	.002	.000
42.501	.036	.005	41.379	.035	.002	42.414	.033	.002	42.425	.012	.001
43.554	.032	.005	42.429	.021	.002	43.464	.025	.002	43.475	.007	.001
44.606	.151	.010	43.478	.074	.003	44.515	.012	.001	44.526	.001	.000
45.659	.057	.006	44.528	.057	.003	45.565	.008	.001	45.576	.002	.000
46.711	.010	.003	45.577	.020	.002	46.615	.037	.002	46.627	.011	.001
47.764	.037	.005	46.627	.012	.001	47.666	.003	.001	47.678	.000	.000
48.816	.117	.009	47.676	.092	.003	48.716	.000	.000	48.728	0	0
									49.779	0	0
									50.830	0	0
									51.880	0	0
									52.931	0	0
									53.981	0	0
									55.032	0	0
									56.083	0	0
									57.133	0	0
									58.184	0	0

TABLE AVII 5. Deuterons From ^{54}Fe Bombarded by 60-MeV Protons

120 deg - Run 7002			135 deg - Run 4011			160 deg - Run 2067		
Energy (MeV)	σ (mb·ster^{-1}·MeV^{-1})	Error	Energy (MeV)	σ (mb·ster^{-1}·MeV^{-1})	Error	Energy (MeV)	σ (mb·ster^{-1}·MeV^{-1})	Error
						5.65	.24	.02
5.654	.264	.010	5.656	.233	.004	6.70	.21	.01
6.705	.228	.009	6.707	.205	.004	7.75	.17	.01
7.756	.196	.008	7.758	.172	.003	8.80	.16	.01
8.807	.165	.008	8.809	.148	.003	9.85	.12	.01
9.858	.145	.007	9.860	.121	.003	10.90	.11	.01
10.908	.122	.007	10.911	.085	.002	11.95	.08	.01
11.959	.117	.006	11.962	.070	.002	13.00	.05	.01
13.010	.088	.006	13.013	.048	.002	14.05	.04	.01
14.061	.063	.005	14.064	.045	.002	15.10	.06	.01
15.112	.056	.004	15.115	.040	.002	16.15	.04	.01
16.162	.053	.004	16.166	.036	.002	17.20	.03	.01
17.213	.045	.004	17.217	.030	.001	18.25	.03	.01
18.264	.041	.004	18.268	.027	.001	19.30	.03	.01
19.315	.036	.004	19.319	.024	.001	20.35	.02	.00
20.366	.020	.003	20.370	.022	.001	21.40	.02	.00
21.416	.030	.003	21.421	.017	.001	22.45	.02	.00
22.467	.021	.003	22.472	.019	.001	23.50	.01	.00
23.518	.019	.003	23.523	.016	.001	24.55	.01	.00
24.569	.015	.002	24.574	.015	.001	25.60	.01	.00
25.620	.015	.002	25.625	.012	.001	26.65	.01	.00
26.670	.009	.002	26.676	.010	.001	27.70	.00	.00
27.721	.012	.002	27.727	.009	.001	28.75	.00	.00
28.772	.007	.002	28.778	.008	.001	29.80	.01	.00
29.823	.005	.001	29.829	.006	.001	30.85	.00	.00
30.874	.006	.001	30.880	.006	.001	31.90	.00	.00
31.925	.007	.002	31.931	.005	.001	32.95	.00	.00
32.975	.005	.001	32.982	.004	.001	34.00	.00	.00
34.026	.008	.002	34.033	.005	.001	35.05	.00	.00
35.077	.002	.001	35.084	.003	.000	36.10	.00	.00
36.128	.003	.001	36.135	.003	.000	37.15	.00	.00
37.179	.001	.001	37.186	.003	.000	38.20	0	0
38.229	.000	.000	38.237	.002	.000	39.25	0	0
39.280	.001	.001	39.289	.003	.000	40.30	.00	.00
40.331	.001	.000	40.340	.001	.000	41.35	.00	.00
41.382	.008	.002	41.391	.004	.001	42.40	0	0
42.433	.001	.000	42.442	.001	.000	43.45	.00	.00
43.483	.001	.001	43.493	.001	.000	44.50	0	0
44.534	.003	.001	44.544	.002	.000	45.55	0	0
			45.595	.001	.000	46.60	0	0
			46.646	0	0	47.65	0	0
			47.697	0	0	48.70	0	0
			48.748	0	0	49.75	0	0
						50.80	0	0
						51.85	0	0
						52.90	0	0
						53.95	0	0
						55.00	0	0
						56.05	0	0
						57.10	0	0
						58.15	0	0
						59.20	0	0

TABLE AVIII 1. Tritons From ^{54}Fe Bombarded by 60-MeV Protons

15 deg - Run 5016			20 deg - Run 4020			27 deg - Run 5020			30 deg - Run 5007		
Energy (MeV)	σ (mb·ster^{-1}·MeV^{-1})	Error	Energy (MeV)	σ (mb·ster^{-1}·MeV^{-1})	Error	Energy (MeV)	σ (mb·ster^{-1}·MeV^{-1})	Error	Energy (MeV)	σ (mb·ster^{-1}·MeV^{-1})	Error
1.497	0	0	1.477	0	0	1.496	0	0	1.498	0	0
2.545	0	0	2.547	0	0	2.543	0	0	2.547	0	0
3.593	0	0	3.617	0	0	3.591	0	0	3.595	0	0
4.641	.003	.003	4.687	.009	.003	4.638	.006	.001	4.644	.006	.001
5.689	.006	.004	5.757	.033	.006	5.685	.031	.003	5.692	.029	.003
6.737	0	0	6.826	.038	.006	6.733	.034	.003	6.741	.033	.003
7.785	.009	.005	7.896	.043	.007	7.780	.038	.003	7.789	.038	.003
8.833	.015	.007	8.966	.035	.006	8.827	.035	.003	8.838	.036	.003
9.881	.033	.010	10.036	.040	.007	9.874	.035	.003	9.887	.039	.004
10.929	.015	.007	11.106	.041	.007	10.922	.041	.004	10.935	.038	.003
11.976	.003	.003	12.175	.043	.007	11.969	.033	.003	11.984	.030	.003
13.024	.024	.008	13.245	.035	.006	13.016	.031	.003	13.032	.034	.003
14.072	.033	.010	14.315	.042	.007	14.063	.036	.003	14.081	.043	.004
15.120	.027	.009	15.385	.036	.006	15.111	.045	.004	15.130	.038	.003
16.168	.036	.010	16.455	.040	.007	16.158	.045	.004	16.178	.043	.004
17.216	.018	.007	17.524	.050	.007	17.205	.042	.004	17.227	.034	.003
18.264	.012	.006	18.594	.057	.008	18.253	.037	.003	18.275	.043	.004
19.312	.018	.007	19.664	.042	.007	19.300	.047	.004	19.324	.045	.004
20.360	.024	.008	20.734	.039	.007	20.347	.049	.004	20.372	.045	.004
21.408	.018	.007	21.804	.041	.007	21.394	.041	.004	21.421	.037	.003
22.456	.027	.009	22.873	.046	.007	22.442	.044	.004	22.470	.038	.003
23.504	.021	.008	23.943	.064	.008	23.489	.040	.003	23.518	.036	.003
24.552	.033	.003	25.013	.067	.009	24.536	.041	.004	24.567	.038	.003
25.600	.339	.011	26.083	.057	.008	25.584	.038	.003	25.615	.039	.004
26.648	.030	.009	27.153	.053	.008	26.631	.038	.003	26.664	.041	.004
27.696	.030	.009	28.222	.066	.009	27.678	.045	.004	27.713	.039	.004
28.743	.015	.007	29.292	.068	.009	28.725	.043	.004	28.761	.033	.003
29.791	.024	.008	30.362	.062	.008	29.773	.044	.004	29.810	.038	.003
30.839	.027	.009	31.432	.052	.008	30.820	.041	.004	30.858	.039	.004
31.887	.027	.009	32.502	.061	.008	31.867	.046	.004	31.907	.038	.003
32.935	.027	.009	33.571	.055	.008	32.914	.034	.003	32.955	.027	.003
33.983	.024	.008	34.641	.063	.008	33.962	.041	.004	34.004	.045	.004
35.031	.033	.010	35.711	.070	.009	35.009	.030	.003	35.053	.033	.003
36.079	.024	.008	36.781	.116	.011	36.056	.057	.004	36.101	.056	.004
37.127	.080	.015	37.851	.036	.006	37.104	.060	.004	37.150	.037	.003
38.175	.012	.006	38.921	.078	.009	38.151	.020	.002	38.198	.018	.002
39.223	.036	.010	39.990	.028	.006	39.198	.062	.004	39.247	.052	.004
40.271	.021	.008	41.060	.035	.006	40.245	.034	.003	40.296	.030	.003
41.319	.050	.012	42.130	.014	.004	41.293	.022	.003	41.344	.011	.002
42.367	.033	.003	43.200	.009	.003	42.340	.004	.001	42.393	.004	.001
43.415	.003	.003	44.270	.040	.007	43.387	.004	.001	43.441	.003	.001
44.463	.342	.011	45.339	.061	.008	44.435	.016	.002	44.490	.013	.002
45.511	.048	.012	46.409	.004	.002	45.482	.033	.003	45.538	.009	.002
46.558	.036	.004				46.529	.001	.000	46.587	.000	.000
47.606	0	0				47.576	0	0			
48.654	.006	.004				48.624	.001	.000			
						49.671	0	0			

TABLE AVIII 2. Tritons From ^{54}Fe Bombarded by 60-MeV Protons

35 deg - Run 4021			40 deg - Run 5002			45 deg - Run 4031			47 deg - Run 5042		
Energy (MeV)	σ (mb·ster^{-1}·MeV^{-1})	Error	Energy (MeV)	σ (mb·ster^{-1}·MeV^{-1})	Error	Energy (MeV)	σ (mb·ster^{-1}·MeV^{-1})	Error	Energy (MeV)	σ (mb·ster^{-1}·MeV^{-1})	Error
1.478	0	0									
2.549	0	0									
3.620	0	0	1.455	0	0	1.462	0	0	1.451	0	0
4.690	.010	.004	2.508	0	0	2.521	0	0	2.501	0	0
5.761	.030	.007	3.562	0	0	3.580	0	0	3.552	0	0
6.831	.043	.008	4.616	0	0	4.639	.004	.001	4.602	.002	.001
7.902	.023	.006	5.669	.021	.004	5.698	.024	.003	5.653	.017	.003
8.972	.047	.008	6.723	.016	.004	6.758	.032	.003	6.703	.024	.004
10.043	.040	.008	7.776	.023	.004	7.817	.034	.003	7.754	.028	.004
11.113	.040	.008	8.830	.027	.005	8.876	.035	.003	8.804	.021	.003
12.184	.043	.008	9.883	.011	.003	9.935	.038	.003	9.854	.029	.004
13.255	.043	.008	10.937	.032	.005	10.994	.035	.003	10.905	.023	.003
14.325	.033	.007	11.990	.025	.005	12.053	.036	.003	11.955	.019	.003
15.396	.024	.006	13.044	.021	.004	13.112	.028	.003	13.006	.020	.003
16.466	.024	.006	14.098	.020	.004	14.171	.025	.003	14.056	.011	.002
17.537	.019	.005	15.151	0	0	15.230	.027	.003	15.107	.021	.003
18.607	.029	.006	16.205	.001	.001	16.289	.026	.003	16.157	.026	.004
19.678	.039	.007	17.258	.003	.001	17.348	.024	.003	17.208	.024	.004
20.749	.040	.008	18.312	.011	.003	18.407	.024	.003	18.258	.015	.003
21.819	.023	.006	19.365	.007	.002	19.466	.028	.003	19.309	.016	.003
22.890	.033	.007	20.419	.015	.004	20.525	.024	.003	20.359	.019	.003
23.960	.034	.007	21.472	.012	.003	21.584	.021	.003	21.410	.020	.003
25.031	.040	.008	22.526	.019	.004	22.643	.026	.003	22.460	.017	.003
26.101	.033	.007	23.580	.009	.003	23.702	.027	.003	23.511	.018	.003
27.172	.036	.007	24.633	.015	.004	24.761	.025	.003	24.561	.018	.003
28.242	.031	.007	25.687	.009	.003	25.820	.025	.003	25.612	.013	.003
29.313	.031	.007	26.740	.015	.004	26.879	.026	.003	26.662	.012	.002
30.384	.034	.009	27.794	.010	.003	27.938	.024	.003	27.713	.010	.002
31.454	.046	.008	28.847	.018	.004	28.997	.029	.003	28.763	.013	.003
32.525	.029	.006	29.901	.013	.003	30.056	.026	.003	29.814	.012	.002
33.595	.044	.008	30.954	.014	.003	31.115	.025	.003	30.864	.006	.002
34.666	.027	.006	32.008	.008	.003	32.174	.024	.003	31.914	.011	.002
35.736	.076	.010	33.062	.014	.003	33.233	.023	.003	32.965	.011	.002
36.807	.021	.006	34.115	.014	.003	34.292	.021	.003	34.015	.006	.002
37.878	.044	.008	35.169	.019	.004	35.351	.031	.003	35.066	.014	.003
38.948	.026	.006	36.222	.029	.005	36.410	.017	.002	36.116	.028	.004
40.019	.026	.006	37.276	.010	.003	37.469	.021	.003	37.167	.004	.001
41.089	.006	.003	38.329	.027	.005	38.528	.021	.003	38.217	.008	.002
42.160	.003	.002	39.383	.007	.002	39.587	.007	.002	39.268	.010	.002
43.230	.004	.002	40.436	.005	.002	40.646	.004	.001	40.318	.003	.001
44.301	.007	.003	41.490	.001	.001	41.705	.003	.001	41.369	.001	.001
45.371	.003	.002	42.544	0	0	42.764	.006	.001	42.419	.001	.001
46.442	.001	.001	43.597	0	0	43.823	.008	.002	43.470	.002	.001
47.513	.001	.001	44.651	.009	.003	44.882	.001	.001	44.520	.002	.001
48.583	0	0	45.704	0	0	45.941	.002	.001	45.571	0	0
49.654	0	0	46.758	0	0	47.000	.001	.000	46.621	0	0
50.724	.001	.001	47.811	0	0	48.059	.001	.001	47.672	0	0
51.795	0	0	48.865	0	0	49.118	.001	.001	48.722	0	0
52.865	0	0									
53.936	.001	.001									

TABLE AVIII 3. Tritons From ^{54}Fe Bombarded by 60-MeV Protons

50 deg - Run 5010			55 deg - Run 4025			60 deg - Run 5043			65 deg - Run 5011		
Energy (MeV)	σ (mb·ster^{-1}·MeV^{-1})	Error	Energy (MeV)	σ (mb·ster^{-1}·MeV^{-1})	Error	Energy (MeV)	σ (mb·ster^{-1}·MeV^{-1})	Error	Energy (MeV)	σ (mb·ster^{-1}·MeV^{-1})	Error
			1.48	0	0	1.452	0	0	1.499	0	0
1.498	0	0	2.55	0	0	2.504	0	0	2.548	0	0
2.546	0	0	3.62	0	0	3.556	0	0	3.597	0	0
3.595	0	0	4.69	.06	.00	4.607	.002	.001	4.646	.006	.001
4.644	.006	.002	5.77	.02	.00	5.659	.017	.003	5.695	.025	.002
5.692	.021	.003	6.84	.03	.00	6.711	.020	.003	6.743	.029	.002
6.741	.022	.003	7.91	.04	.00	7.763	.021	.003	7.792	.023	.002
7.789	.022	.003	8.98	.04	.00	8.814	.021	.003	8.841	.027	.002
8.838	.025	.003	10.05	.04	.00	9.866	.021	.003	9.890	.024	.002
9.886	.024	.003	11.13	.03	.00	10.918	.019	.003	10.939	.024	.002
10.935	.025	.003	12.20	.03	.00	11.969	.013	.002	11.988	.021	.002
11.983	.018	.003	13.27	.02	.00	13.021	.014	.003	13.037	.019	.002
13.032	.021	.003	14.34	.02	.00	14.073	.015	.003	14.086	.021	.002
14.080	.020	.003	15.41	.02	.00	15.125	.014	.003	15.135	.017	.002
15.129	.023	.003	16.48	.02	.00	16.176	.013	.003	16.184	.016	.002
16.177	.018	.003	17.56	.01	.00	17.228	.015	.003	17.233	.017	.002
17.226	.021	.003	18.63	.02	.00	18.280	.007	.002	18.282	.016	.002
18.274	.019	.003	19.70	.02	.00	19.331	.014	.003	19.331	.015	.002
19.323	.014	.002	20.77	.02	.00	20.383	.004	.001	20.380	.011	.001
20.372	.016	.003	21.84	.02	.00	21.435	.008	.002	21.429	.014	.001
21.420	.015	.003	22.91	.02	.00	22.487	.010	.002	22.478	.010	.001
22.469	.012	.002	23.99	.02	.00	23.538	.011	.002	23.527	.011	.001
23.517	.012	.002	25.06	.02	.00	24.590	.009	.002	24.576	.011	.001
24.566	.011	.002	26.13	.02	.00	25.642	.006	.002	25.625	.011	.001
25.614	.015	.003	27.20	.02	.00	26.693	.005	.002	26.674	.007	.001
26.663	.009	.002	28.27	.02	.00	27.745	.008	.002	27.723	.008	.001
27.711	.008	.002	29.34	.02	.00	28.797	.004	.001	28.772	.007	.001
28.760	.012	.002	30.42	.02	.00	29.848	.004	.001	29.821	.006	.001
29.808	.013	.002	31.49	.01	.00	30.900	.005	.002	30.870	.006	.001
30.857	.009	.002	32.56	.01	.00	31.952	.003	.001	31.919	.006	.001
31.905	.010	.002	33.63	.02	.00	33.004	.002	.001	32.968	.004	.001
32.954	.008	.002	34.70	.02	.00	34.055	.004	.001	34.017	.004	.001
34.003	.007	.002	35.77	.01	.00	35.107	.008	.002	35.066	.008	.001
35.051	.010	.002	36.85	.01	.00	36.159	.001	.001	36.115	.002	.001
36.100	.015	.003	37.92	.01	.00	37.210	0	0	37.164	.005	.001
37.148	.004	.001	38.99	.01	.00	38.262	.005	.002	38.213	.007	.001
38.197	.004	.001	40.06	.01	.00	39.314	.002	.001	39.262	.000	.000
39.245	.010	.002	41.13	.00	.00	40.366	0	0	40.311	.000	.000
40.294	.003	.001	42.20	.00	.00	41.417	0	0	41.360	0	0
41.342	.000	.000	43.28	.00	.00	42.469	0	0	42.409	0	0
42.391	0	0	44.35	.00	.00	43.521	0	0	43.458	.001	.000
43.439	.002	.001	45.42	.00	.00	44.572	0	0	44.507	0	0
44.488	0	0	46.49	.00	.00	45.624	0	0	45.556	0	0
45.536	0	0	47.56	.00	.00	46.676	0	0	46.605	0	0
46.585	0	0	48.63	.00	.00	47.728	0	0	47.654	0	0
47.633	0	0				48.779	0	0	48.703	0	0
48.682	0	0									
49.731	0	0									
50.779	0	0									
51.828	0	0									
52.876	0	0									
53.925	0	0									
54.973	0	0									
56.022	0	0									
57.070	0	0									
58.119	0	0									
59.167	0	0									

TABLE AVIII 4. Tritons From ^{54}Fe Bombarded by 60-MeV Protons

70 deg - Run 5044			80 deg - Run 5012			90 deg - Run 4010			110 deg - Run 5015		
Energy (MeV)	σ (mb·ster^{-1}·MeV^{-1})	Error	Energy (MeV)	σ (mb·ster^{-1}·MeV^{-1})	Error	Energy (MeV)	σ (mb·ster^{-1}·MeV^{-1})	Error	Energy (MeV)	σ (mb·ster^{-1}·MeV^{-1})	Error
			1.499	0	0						
1.453	0	0	2.549	0	0	1.450	0	0	1.451	0	0
2.506	0	0	3.598	0	0	2.501	0	0	2.501	0	0
3.558	0	0	4.648	.005	.001	3.551	0	0	3.552	0	0
4.611	.002	.001	5.697	.022	.002	4.602	.004	.001	4.603	.004	.001
5.663	.014	.003	6.747	.024	.002	5.652	.017	.001	5.653	.019	.001
6.716	.018	.003	7.796	.021	.002	6.702	.022	.002	6.704	.018	.001
7.768	.010	.003	8.846	.023	.002	7.753	.021	.002	7.755	.017	.001
8.821	.016	.003	9.895	.020	.002	8.803	.019	.001	8.805	.015	.001
9.874	.010	.003	10.944	.014	.001	9.853	.016	.001	9.856	.013	.001
10.926	.011	.003	11.994	.017	.001	10.904	.016	.001	10.906	.011	.001
11.979	.009	.002	13.043	.011	.001	11.954	.014	.001	11.957	.007	.001
13.031	.008	.002	14.093	.014	.001	13.004	.012	.001	13.008	.006	.001
14.084	.018	.003	15.142	.013	.001	14.055	.009	.001	14.058	.005	.001
15.136	.010	.003	16.192	.011	.001	15.105	.009	.001	15.109	.004	.001
16.189	.009	.002	17.241	.010	.001	16.155	.009	.001	16.159	.004	.001
17.241	.007	.002	18.291	.009	.001	17.206	.006	.001	17.210	.004	.001
18.294	.009	.002	19.340	.007	.001	18.256	.006	.001	18.261	.002	.001
19.346	.005	.002	20.390	.007	.001	19.306	.008	.001	19.311	.002	.000
20.399	.007	.002	21.439	.007	.001	20.357	.004	.001	20.362	.002	.000
21.451	.010	.003	22.489	.006	.001	21.407	.006	.001	21.412	.001	.000
22.504	.006	.002	23.538	.006	.001	22.457	.006	.001	22.463	.001	.000
23.556	.002	.001	24.588	.004	.001	23.508	.004	.001	23.514	.001	.000
24.609	.001	.001	25.637	.004	.001	24.558	.004	.001	24.564	.001	.000
25.661	.006	.002	26.687	.004	.001	25.608	.004	.001	25.615	.000	.000
26.714	.003	.001	27.736	.004	.001	26.659	.004	.001	26.665	.001	.000
27.766	.003	.001	28.786	.003	.001	27.709	.003	.001	27.716	.001	.000
28.819	.001	.001	29.835	.002	.000	28.759	.004	.001	28.767	.000	.000
29.871	.001	.001	30.884	.001	.000	29.810	.002	.000	29.817	.000	.000
30.924	.001	.001	31.934	.002	.000	30.860	.002	.000	30.868	0	0
31.976	.001	.001	32.983	.001	.000	31.911	.002	.001	31.919	.000	.000
33.029	.001	.001	34.033	.003	.001	32.961	.003	.001	32.969	.000	.000
34.081	.001	.001	35.082	.001	.000	34.011	.003	.001	34.020	0	0
35.134	.001	.001	36.132	.002	.001	35.062	.001	.000	35.070	.000	.000
36.186	.001	.001	37.181	.001	.000	36.112	.002	.000	36.121	0	0
37.239	0	0	38.231	.001	.000	37.162	.001	.000	37.172	0	0
38.291	.002	.001	39.280	0	0	38.213	.000	.000	38.222	0	0
39.344	.001	.001	40.330	0	0	39.263	.000	.000	39.273	0	0
40.396	0	0	41.379	0	0	40.313	.000	.000	40.323	0	0
41.449	0	0	42.429	0	0	41.364	.000	.000	41.374	0	0
42.501	0	0	43.478	0	0	42.414	.000	.000	42.425	0	0
43.554	0	0	44.528	0	0	43.464	0	0	43.475	0	0
			45.577	0	0	44.515	.000	.000	44.526	0	0
			46.627	0	0	45.565	.000	.000	45.576	0	0
			47.676	0	0	46.615	0	0	46.627	0	0
			48.725	0	0	47.666	.000	.000	47.678	0	0
						48.716	0	0	48.728	0	0

TABLE AVIII 5. Tritons From ^{54}Fe Bombarded by 60-MeV Protons

120 deg - Run 7002			135 deg - Run 4011			160 deg - Run 2067		
Energy (MeV)	σ	Error	Energy (MeV)	σ	Error	Energy (MeV)	σ	Error
	(mb·ster^{-1}·MeV^{-1})			(mb·ster^{-1}·MeV^{-1})			(mb·ster^{-1}·MeV^{-1})	
						1.45	0	0
1.451	0	0	1.451	0	0	2.50	0	0
2.502	0	0	2.502	0	0	3.55	0	0
3.553	0	0	3.553	0	0	4.60	0	0
4.604	0	0	4.605	.003	.000	5.65	.03	.01
5.654	.011	.002	5.656	.013	.001	6.70	.01	.00
6.705	.016	.002	6.707	.016	.001	7.75	.02	.00
7.756	.012	.002	7.758	.020	.001	8.80	.02	.00
8.807	.010	.002	8.809	.016	.001	9.85	.01	.00
9.858	.008	.002	9.860	.012	.001	10.90	.01	.00
10.908	.010	.002	10.911	.009	.001	11.95	.01	.00
11.959	.004	.001	11.962	.006	.001	13.00	.00	.00
13.010	.001	.001	13.013	.004	.001	14.05	.00	.00
14.061	.002	.001	14.064	.005	.001	15.10	0	0
15.112	.003	.001	15.115	.004	.001	16.15	.00	.00
16.162	.002	.001	16.166	.003	.000	17.20	0	0
17.213	.001	.001	17.217	.002	.000	18.25	.00	.00
18.264	0	0	18.268	.002	.000	19.30	.00	.00
19.315	.001	.001	19.319	.002	.000	20.35	0	0
20.366	.001	.001	20.370	.002	.000	21.40	.00	.00
21.416	.001	.000	21.421	.002	.000	22.45	0	0
22.467	.001	.000	22.472	.001	.000	23.50	0	0
23.518	0	0	23.523	.001	.000	24.55	.00	.00
24.569	0	0	24.574	.001	.000	25.60	.00	.00
25.620	0	0	25.625	.001	.000	26.65	0	0
26.670	0	0	26.676	.001	.000	27.70	0	0
27.721	0	0	27.727	.001	.000	28.75	.00	.00
28.772	0	0	28.778	.000	.000	29.80	0	0
29.823	0	0	29.829	.000	.000	30.85	0	0
30.874	0	0	30.880	.000	.000	31.90	0	0
31.925	0	0	31.931	.000	.000	32.95	0	0
32.975	0	0	32.982	.000	.000	34.00	0	0
34.026	0	0	34.033	.000	.000	35.05	0	0
35.077	0	0	35.084	.000	.000	36.10	0	0
36.128	0	0	36.135	0	0	37.15	0	0
37.179	0	0	37.186	0	0	38.20	0	0
38.229	0	0	38.237	0	0	39.25	0	0
39.280	0	0	39.289	0	0	40.30	0	0
40.331	0	0	40.340	.000	.000	41.35	0	0
41.382	0	0	41.391	0	0	42.40	0	0
42.433	0	0	42.442	.000	.000	43.45	0	0
43.483	0	0	43.493	0	0	44.50	0	0
44.534	0	0	44.544	0	0	45.55	0	0
45.585	0	0	45.595	0	0	46.60	0	0
46.636	0	0	46.646	.000	.000	47.65	0	0
47.687	0	0	47.697	0	0	48.70	0	0
48.737	0	0	48.748	0	0	49.75	0	0
						50.80	0	0
						51.85	0	0
						52.90	0	0
						53.95	0	0
						55.00	0	0
						56.05	0	0
						57.10	0	0
						58.15	0	0
						59.20	0	0

TABLE AIX 1. Helium-3 From ^{54}Fe Bombarded by 60-MeV Protons

15 deg - Run 5016			20 deg - Run 4020			27 deg - Run 5020			30 deg - Run 5007		
Energy (MeV)	σ (mb·ster^{-1}·MeV^{-1})	Error	Energy (MeV)	σ (mb·ster^{-1}·MeV^{-1})	Error	Energy (MeV)	σ (mb·ster^{-1}·MeV^{-1})	Error	Energy (MeV)	σ (mb·ster^{-1}·MeV^{-1})	Error
1.497	0	0	1.477	0	0	1.496	0	0	1.498	0	0
2.545	0	0	2.547	0	0	2.543	0	0	2.547	0	0
3.593	0	0	3.617	0	0	3.591	0	0	3.595	0	0
4.641	0	0	4.687	0	0	4.638	0	0	4.644	0	0
5.689	0	0	5.757	0	0	5.685	0	0	5.692	0	0
6.737	0	0	6.826	0	0	6.733	0	0	6.741	0	0
7.785	0	0	7.896	0	0	7.780	0	0	7.789	0	0
8.833	0	0	8.966	0	0	8.827	0	0	8.838	0	0
9.881	0	0	10.036	0	0	9.874	0	0	9.887	0	0
10.929	0	0	11.106	.021	.005	10.922	.008	.002	10.935	.010	.002
11.976	.027	.009	12.175	.085	.010	11.969	.043	.004	11.984	.046	.004
13.024	.030	.009	13.245	.107	.011	13.016	.045	.004	13.032	.038	.003
14.072	.012	.006	14.315	.098	.010	14.063	.045	.004	14.081	.050	.004
15.120	.021	.008	15.385	.094	.010	15.111	.040	.004	15.130	.044	.004
16.168	.006	.004	16.455	.081	.009	16.158	.038	.003	16.178	.030	.003
17.216	.023	.003	17.524	.073	.009	17.205	.040	.004	17.227	.036	.003
18.264	.033	.009	18.594	.071	.009	18.253	.034	.003	18.275	.030	.003
19.312	.018	.007	19.664	.051	.007	19.300	.041	.004	19.324	.038	.003
20.360	.036	.010	20.734	.080	.009	20.347	.040	.004	20.372	.037	.003
21.408	.012	.006	21.804	.056	.008	21.394	.036	.003	21.421	.032	.003
22.456	.029	.005	22.873	.063	.008	22.442	.034	.003	22.470	.040	.004
23.504	.030	.009	23.943	.063	.008	23.489	.050	.004	23.518	.040	.004
24.552	.018	.007	25.013	.074	.009	24.536	.032	.003	24.567	.037	.003
25.600	.026	.004	26.083	.077	.009	25.584	.037	.003	25.615	.035	.003
26.648	.033	.010	27.153	.075	.009	26.631	.029	.003	26.664	.032	.003
27.696	.012	.006	28.222	.073	.009	27.678	.034	.003	27.713	.030	.003
28.743	.021	.008	29.292	.083	.010	28.725	.046	.004	28.761	.029	.003
29.791	.018	.007	30.362	.086	.010	29.773	.032	.003	29.810	.032	.003
30.839	.021	.008	31.432	.080	.009	30.820	.032	.003	30.858	.040	.004
31.887	.018	.007	32.502	.081	.009	31.867	.033	.003	31.907	.031	.003
32.935	.062	.014	33.571	.138	.012	32.914	.071	.005	32.955	.057	.004
33.983	.050	.012	34.641	.061	.008	33.962	.049	.004	34.004	.047	.004
35.031	.033	.010	35.711	.057	.008	35.009	.039	.003	35.053	.033	.003
36.079	.045	.012	36.781	.056	.008	36.056	.049	.004	36.101	.046	.004
37.127	.053	.013	37.851	.059	.008	37.104	.042	.004	37.150	.037	.003
38.175	.050	.012	38.921	.057	.008	38.151	.049	.004	38.198	.041	.004
39.223	.033	.010	39.990	.046	.007	39.198	.049	.004	39.247	.038	.003
40.271	.033	.010	41.060	.057	.008	40.245	.044	.004	40.296	.034	.003
41.319	.045	.012	42.130	.059	.008	41.293	.054	.004	41.344	.040	.004
42.367	.062	.014	43.200	.102	.011	42.340	.054	.004	42.393	.044	.004
43.415	.107	.018	44.270	.145	.013	43.387	.090	.005	43.441	.069	.005
44.463	.086	.016	45.339	.039	.007	44.435	.062	.004	44.490	.038	.003
45.511	.003	.003	46.409	.062	.008	45.482	.037	.003	45.538	.046	.004
46.558	.018	.007				46.529	.033	.003	46.587	.029	.003
47.606	0	0				47.576	.001	.000	47.636	.001	.001
48.654	0	0				48.624	0	0	48.684	0	0

TABLE AIX 2. Helium-3 From ^{54}Fe Bombarded by 60-MeV Protons

35 deg - Run 4021			40 deg - Run 5002			45 deg - Run 4031			47 deg - Run 5042		
Energy (MeV)	σ	Error	Energy (MeV)	σ	Error	Energy (MeV)	σ	Error	Energy (MeV)	σ	Error
	(mb·ster^{-1}·MeV^{-1})			(mb·ster^{-1}·MeV^{-1})			(mb·ster^{-1}·MeV^{-1})			(mb·ster^{-1}·MeV^{-1})	
1.478	0	0									
2.549	0	0	1.455	0	0	1.462	0	0	1.451	0	0
3.620	0	0	2.508	0	0	2.521	0	0	2.501	0	0
4.690	0	0	3.562	0	0	3.580	0	0	3.552	0	0
5.761	0	0	4.616	0	0	4.639	0	0	4.602	0	0
6.831	0	0	5.669	0	0	5.698	0	0	5.653	0	0
7.902	0	0	6.723	0	0	6.758	0	0	6.703	0	0
8.972	0	0	7.776	0	0	7.817	0	0	7.754	0	0
10.043	0	0	8.830	0	0	8.876	0	0	8.804	0	0
11.113	.013	.004	9.883	0	0	9.935	0	0	9.854	0	0
12.184	.059	.009	10.937	.005	.002	10.994	.009	.002	10.905	.003	.001
13.255	.107	.012	11.990	.032	.005	12.053	.070	.005	11.955	.034	.004
14.325	.103	.012	13.044	.032	.005	13.112	.071	.005	13.006	.037	.004
15.396	.071	.010	14.098	.031	.005	14.171	.071	.005	14.056	.029	.004
16.466	.064	.010	15.151	.021	.004	15.230	.058	.004	15.107	.029	.004
17.537	.049	.008	16.205	.022	.004	16.289	.049	.004	16.157	.017	.003
18.607	.053	.009	17.258	.017	.004	17.348	.044	.004	17.208	.016	.003
19.678	.053	.009	18.312	.022	.004	18.407	.042	.004	18.258	.018	.003
20.749	.034	.007	19.365	.021	.004	19.466	.041	.004	19.309	.019	.003
21.819	.039	.007	20.419	.020	.004	20.525	.039	.004	20.359	.022	.003
22.890	.044	.008	21.472	.017	.004	21.584	.037	.003	21.410	.020	.003
23.960	.044	.008	22.526	.015	.004	22.643	.037	.003	22.460	.024	.004
25.031	.036	.007	23.580	.013	.003	23.702	.038	.004	23.511	.018	.003
26.101	.043	.008	24.633	.015	.004	24.761	.030	.003	24.561	.014	.003
27.172	.036	.007	25.687	.009	.003	25.820	.036	.003	25.612	.017	.003
28.242	.047	.008	26.740	.021	.004	26.879	.027	.003	26.662	.014	.003
29.313	.059	.009	27.794	.017	.004	27.938	.032	.003	27.713	.012	.002
30.384	.057	.009	28.847	.035	.005	28.997	.030	.003	28.763	.015	.003
31.454	.063	.009	29.901	.022	.004	30.056	.037	.003	29.814	.012	.002
32.525	.080	.011	30.954	.032	.005	31.115	.031	.003	30.864	.015	.003
33.595	.044	.008	32.008	.021	.004	32.174	.038	.004	31.914	.013	.003
34.666	.039	.007	33.062	.014	.003	33.233	.046	.004	32.965	.026	.004
35.736	.030	.007	34.115	.013	.003	34.292	.022	.003	34.015	.015	.003
36.807	.027	.006	35.169	.013	.003	35.351	.020	.003	35.066	.020	.003
37.878	.036	.007	36.222	.003	.002	36.410	.017	.002	36.116	.014	.003
38.948	.031	.007	37.276	.003	.002	37.469	.021	.003	37.167	.008	.002
40.019	.024	.006	38.329	.001	.001	38.528	.017	.002	38.217	.007	.002
41.089	.027	.006	39.383	0	0	39.587	.016	.002	39.268	.004	.001
42.160	.020	.005	40.436	.003	.001	40.646	.015	.002	40.318	.008	.002
43.230	.033	.009	41.490	.002	.001	41.705	.021	.003	41.369	.008	.002
44.301	.027	.006	42.544	.003	.002	42.764	.028	.003	42.419	.010	.002
45.371	.040	.008	43.597	.005	.002	43.823	.010	.002	43.470	.015	.003
46.442	.009	.003	44.651	0	0	44.882	.022	.003	44.520	.006	.002
47.513	0	0	45.704	0	0	45.941	.005	.001	45.571	.013	.003
48.583	0	0	46.758	0	0	47.000	0	0	46.621	0	0
49.654	0	0	47.811	0	0	48.059	0	0	47.672	0	0
50.724	0	0	48.865	0	0	49.118	0	0	48.722	0	0
51.795	0	0									
52.865	0	0									
53.936	0	0									

TABLE AIX 3. Helium-3 From ^{54}Fe Bombarded by 60-MeV Protons

50 deg - Run 5010			55 deg - Run 4025			60 deg - Run 5043			65 deg - Run 5011		
Energy (MeV)	σ (mb·ster^{-1}·MeV^{-1})	Error	Energy (MeV)	σ (mb·ster^{-1}·MeV^{-1})	Error	Energy (MeV)	σ (mb·ster^{-1}·MeV^{-1})	Error	Energy (MeV)	σ (mb·ster^{-1}·MeV^{-1})	Error
									1.499	0	0
			1.48	0	0	1.452	0	0	2.548	0	0
1.498	0	0	2.55	0	0	2.504	0	0	3.597	0	0
2.546	0	0	3.62	0	0	3.556	0	0	4.646	0	0
3.595	0	0	4.69	0	0	4.607	0	0	5.695	0	0
4.644	0	0	5.77	0	0	5.659	0	0	6.743	0	0
5.692	0	0	6.84	0	0	6.711	0	0	7.792	0	0
6.741	0	0	7.91	0	0	7.763	0	0	8.841	0	0
7.789	0	0	8.98	0	0	8.814	0	0	9.890	0	0
8.838	0	0	10.05	0	0	9.866	0	0	10.939	.004	.001
9.886	0	0	11.13	.05	.00	10.918	.004	.001	11.988	.033	.002
10.935	.003	.001	12.20	.05	.00	11.969	.027	.004	13.037	.027	.002
11.983	.029	.004	13.27	.05	.00	13.021	.026	.004	14.086	.033	.002
13.032	.034	.004	14.34	.06	.00	14.073	.019	.003	15.135	.027	.002
14.080	.025	.003	15.41	.05	.00	15.125	.021	.003	16.184	.024	.002
15.129	.025	.003	16.48	.04	.00	16.176	.016	.003	17.233	.029	.002
16.177	.025	.003	17.56	.03	.00	17.228	.013	.002	18.282	.023	.002
17.226	.019	.003	18.63	.03	.00	18.280	.015	.003	19.331	.028	.002
18.274	.020	.003	19.70	.03	.00	19.331	.016	.003	20.380	.021	.002
19.323	.021	.003	20.77	.03	.00	20.383	.007	.002	21.429	.018	.002
20.372	.020	.003	21.84	.02	.00	21.435	.010	.002	22.478	.018	.002
21.420	.022	.003	22.91	.02	.00	22.487	.010	.002	23.527	.016	.002
22.469	.010	.002	23.99	.03	.00	23.538	.008	.002	24.576	.019	.002
23.517	.018	.003	25.06	.02	.00	24.590	.008	.002	25.625	.015	.002
24.566	.014	.002	26.13	.02	.00	25.642	.006	.002	26.674	.014	.001
25.614	.011	.002	27.20	.03	.00	26.693	.007	.002	27.723	.011	.001
26.663	.014	.002	28.27	.02	.00	27.745	.007	.002	28.772	.008	.001
27.711	.012	.002	29.34	.03	.00	28.797	.007	.002	29.821	.007	.001
28.760	.013	.002	30.42	.03	.00	29.848	.006	.002	30.870	.011	.001
29.808	.008	.002	31.49	.03	.00	30.900	.008	.002	31.919	.009	.001
30.857	.011	.002	32.56	.03	.00	31.952	.008	.002	32.968	.014	.001
31.905	.009	.002	33.63	.03	.00	33.004	.013	.002	34.017	.011	.001
32.954	.018	.003	34.70	.02	.00	34.055	.006	.002	35.066	.008	.001
34.003	.014	.002	35.77	.01	.00	35.107	.005	.002	36.115	.006	.001
35.051	.014	.002	36.85	.01	.00	36.159	.004	.001	37.164	.006	.001
36.100	.012	.002	37.92	.01	.00	37.210	.003	.001	38.213	.004	.001
37.148	.008	.002	38.99	.01	.00	38.262	.002	.001	39.262	.003	.001
38.197	.007	.002	40.06	.01	.00	39.314	.003	.001	40.311	.003	.001
39.245	.009	.002	41.13	.01	.00	40.366	.000	.000	41.360	.004	.001
40.294	.004	.001	42.20	.01	.00	41.417	.000	.000	42.409	.005	.001
41.342	.005	.001	43.28	.01	.00	42.469	.000	.000	43.458	.001	.000
42.391	.010	.002	44.35	.01	.00	43.521	.000	.000	44.507	.004	.001
43.439	.004	.001	45.42	.01	.00	44.572	.001	.001	45.556	.000	.000
44.488	.004	.001	46.49	.00	.00	45.624	0	0	46.605	0	0
45.536	.006	.002	47.56	0	0	46.676	0	0	47.654	0	0
46.585	.000	.000	48.63	0	0	47.728	0	0	48.703	0	0
47.633	0	0				48.779	0	0			
48.682	0	0									
49.731	0	0									
50.779	0	0									
51.828	0	0									
52.876	0	0									
53.925	0	0									
54.973	0	0									
56.022	0	0									
57.070	0	0									
58.119	0	0									
59.167	0	0									

TABLE AIX 4. Helium-3 From ^{54}Fe Bombarded by 60-MeV Protons

70 deg - Run 5044			80 deg - Run 5012			90 deg - Run 4010			110 deg - Run 5015		
Energy (MeV)	σ (mb·ster^{-1}·MeV^{-1})	Error	Energy (MeV)	σ (mb·ster^{-1}·MeV^{-1})	Error	Energy (MeV)	σ (mb·ster^{-1}·MeV^{-1})	Error	Energy (MeV)	σ (mb·ster^{-1}·MeV^{-1})	Error
			1.499	0	0						
1.453	0	0	2.549	0	0	1.450	0	0	1.451	0	0
2.506	0	0	3.598	0	0	2.501	0	0	2.501	0	0
3.558	0	0	4.648	0	0	3.551	0	0	3.552	0	0
4.611	0	0	5.697	0	0	4.602	0	0	4.603	0	0
5.663	0	0	6.747	0	0	5.652	0	0	5.653	0	0
6.716	0	0	7.796	0	0	6.702	0	0	6.704	0	0
7.768	0	0	8.846	0	0	7.753	0	0	7.755	0	0
8.821	0	0	9.895	0	0	8.803	0	0	8.805	0	0
9.874	0	0	10.944	.005	.001	9.853	0	0	9.856	0	0
10.926	.003	.001	11.994	.026	.002	10.904	.006	.001	10.906	.002	.000
11.979	.020	.004	13.043	.031	.002	11.954	.047	.002	11.957	.019	.001
13.031	.021	.004	14.093	.024	.002	13.004	.046	.002	13.008	.015	.001
14.084	.018	.003	15.142	.020	.002	14.055	.040	.002	14.058	.015	.001
15.136	.007	.002	16.192	.015	.001	15.105	.032	.002	15.109	.009	.001
16.189	.008	.002	17.241	.015	.001	16.155	.024	.002	16.159	.007	.001
17.241	.010	.003	18.291	.013	.001	17.206	.018	.001	17.210	.005	.001
18.294	.004	.002	19.340	.016	.001	18.256	.016	.001	18.261	.004	.001
19.346	.009	.002	20.390	.011	.001	19.306	.015	.001	19.311	.006	.001
20.399	.012	.003	21.439	.011	.001	20.357	.013	.001	20.362	.004	.001
21.451	.007	.002	22.489	.013	.001	21.407	.009	.001	21.412	.002	.001
22.504	.004	.002	23.538	.007	.001	22.457	.009	.001	22.463	.003	.001
23.556	.005	.002	24.588	.009	.001	23.508	.009	.001	23.514	.002	.000
24.609	.004	.002	25.637	.006	.001	24.558	.008	.001	24.564	.002	.000
25.661	.008	.002	26.687	.007	.001	25.608	.009	.001	25.615	.002	.000
26.714	.003	.001	27.736	.005	.001	26.659	.007	.001	26.665	.001	.000
27.766	.003	.001	28.786	.005	.001	27.709	.006	.001	27.716	.001	.000
28.819	.002	.001	29.835	.005	.001	28.759	.007	.001	28.767	.001	.000
29.871	.005	.002	30.884	.004	.001	29.810	.006	.001	29.817	.000	.000
30.924	.002	.001	31.934	.003	.001	30.860	.006	.001	30.868	.001	.000
31.976	.003	.001	32.983	.005	.001	31.911	.007	.001	31.919	.000	.000
33.029	.006	.002	34.033	.004	.001	32.961	.006	.001	32.969	.001	.000
34.081	.001	.001	35.082	.004	.001	34.011	.002	.001	34.020	.001	.000
35.134	0	0	36.132	.001	.000	35.062	.003	.001	35.070	.000	.000
36.186	.001	.001	37.181	.002	.000	36.112	.002	.000	36.121	.000	.000
37.239	0	0	38.231	.001	.000	37.162	.001	.000	37.172	.000	.000
38.291	.001	.001	39.280	.001	.000	38.213	.001	.000	38.222	.000	.000
39.344	.001	.001	40.330	.001	.000	39.263	.001	.000	39.273	.000	.000
40.396	.001	.001	41.379	.001	.000	40.313	.002	.000	40.323	0	0
41.449	.001	.001	42.429	.000	.000	41.364	.001	.000	41.374	0	0
42.501	.001	.001	43.478	.001	.000	42.414	.001	.000	42.425	.000	.000
43.554	0	0	44.528	0	0	43.464	0	0	43.475	0	0
44.606	0	0	45.577	0	0	44.515	0	0	44.526	0	0
45.659	0	0	46.627	0	0	45.565	0	0	45.576	0	0
46.711	0	0	47.676	0	0	46.615	0	0	46.627	0	0
47.764	0	0	48.725	0	0	47.666	0	0	47.678	0	0
48.816	0	0				48.716	0	0	48.728	0	0

TABLE AIX 5. Helium-3 From ^{64}Fe Bombarded by 60-MeV Protons

120 deg - Run 7002			135 deg - Run 4011			160 deg - Run 2067		
Energy (MeV)	σ (mb·ster^{-1}·MeV^{-1})	Error	Energy (MeV)	σ (mb·ster^{-1}·MeV^{-1})	Error	Energy (MeV)	σ (mb·ster^{-1}·MeV^{-1})	Error
						1.45	0	0
1.451	0	0				2.50	0	0
2.502	0	0				3.55	0	0
3.553	0	0	1.451	0	0	4.60	0	0
4.604	0	0	2.502	0	0	5.65	0	0
5.654	0	0	3.553	0	0	6.70	0	0
6.705	0	0	4.605	0	0	7.75	0	0
7.756	0	0	5.656	0	0	8.80	0	0
8.807	0	0	6.707	0	0	9.85	0	0
9.858	0	0	7.758	0	0	10.90	0	0
10.908	0	0	8.809	0	0	11.95	.01	.00
11.959	.003	.001	9.860	0	0	13.00	.01	.00
13.010	.014	.002	10.911	.004	.001	14.05	.02	.00
14.061	.011	.002	11.962	.031	.001	15.10	.00	.00
15.112	.007	.002	13.013	.030	.001	16.15	.01	.00
16.162	.005	.001	14.064	.027	.001	17.20	.01	.00
17.213	.004	.001	15.115	.017	.001	18.25	.00	.00
18.264	.004	.001	16.166	.013	.001	19.30	.00	.00
19.315	.002	.001	17.217	.010	.001	20.35	.00	.00
20.366	.004	.001	18.268	.008	.001	21.40	.00	.00
21.416	.001	.001	19.319	.006	.001	22.45	.00	.00
22.467	.001	.001	20.370	.005	.001	23.50	.00	.00
23.518	.001	.000	21.421	.004	.001	24.55	.00	.00
24.569	.000	.000	22.472	.004	.001	25.60	.00	.00
25.620	.000	.000	23.523	.003	.000	26.65	.00	.00
26.670	0	0	24.574	.003	.000	27.70	.00	.00
27.721	0	0	25.625	.003	.000	28.75	0	0
28.772	0	0	26.676	.002	.000	29.80	0	0
29.823	0	0	27.727	.002	.000	30.85	.00	.00
30.874	.000	.000	28.778	.002	.000	31.90	0	0
31.925	0	0	29.829	.001	.000	32.95	.00	.00
32.975	0	0	30.880	.002	.000	34.00	0	0
34.026	0	0	31.931	.001	.000	35.05	0	0
35.077	0	0	32.982	.002	.000	36.10	0	0
36.128	0	0	34.033	.000	.000	37.15	0	0
37.179	0	0	35.084	.000	.000	38.20	0	0
38.229	0	0	36.135	.000	.000	39.25	0	0
39.280	0	0	37.186	.000	.000	40.30	0	0
40.331	0	0	38.237	.000	.000	41.35	0	0
41.382	0	0	39.289	.000	.000	42.40	0	0
42.433	0	0	40.340	.000	.000	43.45	0	0
43.483	0	0	41.391	0	0	44.50	0	0
44.534	0	0	42.442	0	0	45.55	0	0
45.585	0	0	43.493	0	0	46.60	0	0
46.636	0	0	44.544	0	0	47.65	0	0
47.687	0	0	45.595	0	0	48.70	0	0
48.737	0	0	46.646	0	0	49.75	0	0
			47.697	0	0	50.80	0	0
			48.748	0	0	51.85	0	0
						52.90	0	0
						53.95	0	0
						55.00	0	0
						56.05	0	0
						57.10	0	0
						58.15	0	0
						59.20	0	0

TABLE AX 1. Alphas From ^{54}Fe Bombarded by 60-MeV Protons

15 deg - Run 5016			20 deg - Run 4020			27 deg - Run 5020			30 deg - Run 5007		
Energy (MeV)	σ (mb·ster^{-1}·MeV^{-1})	Error	Energy (MeV)	σ (mb·ster^{-1}·MeV^{-1})	Error	Energy (MeV)	σ (mb·ster^{-1}·MeV^{-1})	Error	Energy (MeV)	σ (mb·ster^{-1}·MeV^{-1})	Error
14.072	.817	.049	14.315	.754	.029	14.063	.806	.016	14.081	.756	.016
15.120	.627	.043	15.385	.609	.026	15.111	.638	.014	15.130	.576	.014
16.168	.511	.039	16.455	.441	.022	16.158	.513	.013	16.178	.477	.012
17.216	.451	.036	17.524	.371	.020	17.205	.424	.011	17.227	.384	.011
18.264	.353	.032	18.594	.345	.020	18.253	.371	.011	18.275	.340	.010
19.312	.261	.028	19.664	.254	.017	19.300	.312	.010	19.324	.293	.010
20.360	.267	.028	20.734	.239	.016	20.347	.272	.009	20.372	.239	.009
21.408	.196	.024	21.804	.237	.016	21.394	.216	.008	21.421	.222	.008
22.456	.175	.023	22.873	.199	.015	22.442	.211	.008	22.470	.210	.008
23.504	.163	.022	23.943	.203	.015	23.489	.199	.008	23.518	.171	.007
24.552	.157	.022	25.013	.186	.014	24.536	.174	.007	24.567	.173	.007
25.600	.119	.019	26.083	.141	.012	25.584	.158	.007	25.615	.140	.007
26.648	.104	.018	27.153	.114	.011	26.631	.152	.007	26.664	.134	.007
27.696	.074	.015	28.222	.119	.011	27.678	.145	.007	27.713	.125	.006
28.743	.104	.018	29.292	.095	.010	28.725	.116	.006	28.761	.118	.006
29.791	.077	.015	30.362	.085	.010	29.773	.104	.006	29.810	.101	.006
30.839	.068	.014	31.432	.084	.010	30.820	.091	.005	30.858	.081	.005
31.887	.068	.014	32.502	.084	.010	31.867	.088	.005	31.907	.084	.005
32.935	.050	.012	33.571	.065	.008	32.914	.067	.005	32.955	.074	.005
33.983	.027	.009	34.641	.047	.007	33.962	.053	.004	34.004	.059	.004
35.031	.036	.010	35.711	.044	.007	35.009	.058	.004	35.053	.063	.005
36.079	.021	.008	36.781	.024	.005	36.056	.042	.004	36.101	.039	.004
37.127	.038	.017	37.851	.099	.010	37.104	.102	.006	37.150	.105	.006
38.175	.083	.016	38.921	.072	.009	38.151	.084	.005	38.198	.070	.005
39.223	.062	.014	39.990	.057	.008	39.198	.079	.005	39.247	.058	.004
40.271	.056	.013	41.060	.057	.008	40.245	.071	.005	40.296	.071	.005
41.319	.045	.012	42.130	.055	.008	41.293	.068	.005	41.344	.052	.004
42.367	.059	.013	43.200	.059	.008	42.340	.063	.004	42.393	.054	.004
43.415	.036	.010	44.270	.066	.009	43.387	.067	.005	43.441	.051	.004
44.463	.086	.016	45.339	.050	.007	44.435	.068	.005	44.490	.054	.004
45.511	.045	.012	46.409	.063	.008	45.482	.062	.004	45.538	.054	.004
46.558	.053	.013	47.479	.049	.007	46.529	.061	.004	46.587	.050	.004
47.606	.039	.011	48.549	.051	.007	47.576	.053	.004	47.636	.038	.003
48.654	.059	.013	49.619	.038	.006	48.624	.044	.004	48.684	.036	.003
49.702	.039	.011	50.688	.035	.006	49.671	.034	.003	49.733	.022	.003
50.750	.048	.012	51.758	.043	.007	50.718	.027	.003	50.781	.021	.003
51.798	.053	.013	52.828	.017	.004	51.765	.030	.003	51.830	.013	.002
52.846	0	0	53.898	.009	.003	52.813	.008	.002	52.879	.004	.001
53.894	.006	.004	54.968	.009	.003	53.860	.001	.000	53.927	.000	.000
54.942	0	0				54.907	.002	.001	54.976	.001	.000
55.990	.003	.003				55.955	.004	.001	56.024	.001	.001
57.038	.003	.003							57.073	0	0
58.086	0	0							58.121	.000	.000
59.134	0	0							59.170	0	0

TABLE AX 2. Alphas From ^{54}Fe Bombarded by 60-MeV Protons

35 deg - Run 4021			40 deg - Run 5002			45 deg - Run 4031			47 deg - Run 5042		
Energy (MeV)	σ (mb·ster^{-1}·MeV^{-1})	Error	Energy (MeV)	σ (mb·ster^{-1}·MeV^{-1})	Error	Energy (MeV)	σ (mb·ster^{-1}·MeV^{-1})	Error	Energy (MeV)	σ (mb·ster^{-1}·MeV^{-1})	Error
14.325	.669	.031									
15.398	.532	.028									
16.466	.414	.024	14.098	.696	.024	14.171	.594	.014	14.056	.603	.018
17.537	.293	.020	15.151	.547	.022	15.230	.458	.012	15.107	.467	.016
18.607	.258	.019	16.205	.454	.020	16.289	.374	.011	16.157	.384	.014
19.678	.204	.017	17.258	.330	.017	17.348	.290	.010	17.208	.305	.013
20.749	.198	.017	18.312	.307	.016	18.407	.245	.009	18.258	.270	.012
21.819	.149	.014	19.365	.240	.014	19.466	.200	.008	19.309	.207	.010
22.890	.157	.015	20.419	.215	.014	20.525	.168	.007	20.359	.168	.009
23.960	.143	.014	21.472	.198	.013	21.584	.144	.007	21.410	.157	.009
25.031	.123	.013	22.526	.158	.012	22.643	.141	.007	22.460	.130	.008
26.101	.127	.013	23.580	.156	.012	23.702	.107	.006	23.511	.119	.008
27.172	.108	.012	24.633	.135	.011	24.761	.095	.006	24.561	.096	.007
28.242	.088	.011	25.687	.100	.009	25.820	.105	.006	25.612	.082	.007
29.313	.079	.011	26.740	.097	.009	26.879	.080	.005	26.662	.090	.007
30.384	.057	.009	27.794	.094	.009	27.938	.068	.005	27.713	.066	.006
31.454	.071	.010	28.847	.070	.008	28.997	.062	.004	28.763	.057	.005
32.525	.051	.009	29.901	.064	.007	30.056	.060	.004	29.814	.057	.005
33.595	.039	.007	30.954	.064	.007	31.115	.046	.004	30.864	.051	.005
34.666	.039	.007	32.008	.055	.007	32.174	.047	.004	31.914	.029	.004
35.736	.040	.008	33.062	.044	.006	33.233	.037	.003	32.965	.026	.004
36.807	.019	.005	34.115	.035	.005	34.292	.032	.003	34.015	.021	.003
37.878	.056	.009	35.169	.040	.006	35.351	.029	.003	35.066	.021	.003
38.948	.051	.009	36.222	.013	.003	36.410	.018	.002	36.116	.006	.002
40.019	.038	.007	37.276	0	0	37.469	.039	.004	37.167	.045	.005
41.089	.039	.007	38.329	0	0	38.528	.033	.003	38.217	.031	.004
42.160	.040	.008	39.383	0	0	39.587	.017	.002	39.268	.021	.003
43.230	.016	.005	40.436	0	0	40.646	.029	.003	40.318	.024	.004
44.301	.030	.007	41.490	0	0	41.705	.021	.003	41.369	.031	.004
45.371	.043	.008	42.544	0	0	42.764	.024	.003	42.419	.021	.003
46.442	.020	.005	43.597	0	0	43.823	.022	.003	43.470	.019	.003
47.513	.027	.006	44.651	0	0	44.882	.024	.003	44.520	.013	.003
48.583	.029	.006	45.704	0	0	45.941	.016	.002	45.571	.020	.003
49.654	.021	.006	46.758	0	0	47.000	.015	.002	46.621	.013	.003
50.724	.011	.004	47.811	0	0	48.059	.015	.002	47.672	.010	.002
51.795	.014	.005	48.865	.001	.001	49.118	.016	.002	48.722	.005	.002
52.865	.007	.003	49.918	0	0	50.177	.008	.002	49.773	.003	.001
53.936	0	0	50.972	0	0	51.236	.009	.002	50.823	.006	.002
						52.295	.001	.001	51.874	.002	.001
						53.354	0	0	52.924	0	0
						54.413	.001	.000			

TABLE AX 3. Alphas From ^{54}Fe Bombarded by 60-MeV Protons

50 deg - Run 5010			55 deg - Run 4025			60 deg - Run 5043			65 deg - Run 5011		
Energy (MeV)	σ (mb·ster^{-1}·MeV^{-1})	Error	Energy (MeV)	σ (mb·ster^{-1}·MeV^{-1})	Error	Energy (MeV)	σ (mb·ster^{-1}·MeV^{-1})	Error	Energy (MeV)	σ (mb·ster^{-1}·MeV^{-1})	Error
14.080	.538	.015	14.34	.54	.01	14.073	.471	.015	14.086	.453	.008
15.129	.438	.014	15.41	.40	.01	15.125	.367	.013	15.135	.350	.007
16.177	.326	.012	16.48	.31	.01	16.176	.301	.012	16.184	.268	.006
17.226	.248	.010	17.56	.24	.01	17.228	.230	.011	17.233	.213	.006
18.274	.197	.009	18.63	.21	.01	18.280	.187	.010	18.282	.174	.005
19.323	.181	.009	19.70	.15	.01	19.331	.142	.008	19.331	.137	.005
20.372	.149	.008	20.77	.14	.01	20.383	.129	.008	20.380	.119	.004
21.420	.146	.008	21.84	.12	.01	21.435	.120	.008	21.429	.099	.004
22.469	.104	.007	22.91	.11	.01	22.487	.098	.007	22.478	.092	.004
23.517	.103	.007	23.99	.11	.01	23.538	.080	.006	23.527	.075	.003
24.566	.090	.006	25.06	.08	.01	24.590	.075	.006	24.576	.067	.003
25.614	.075	.006	26.13	.08	.01	25.642	.062	.005	25.625	.056	.003
26.663	.063	.005	27.20	.07	.00	26.693	.050	.005	26.674	.058	.003
27.711	.060	.005	28.27	.05	.00	27.745	.040	.004	27.723	.043	.003
28.760	.063	.005	29.34	.05	.00	28.797	.035	.004	28.772	.044	.003
29.808	.048	.005	30.42	.04	.00	29.848	.035	.004	29.821	.033	.002
30.857	.040	.004	31.49	.03	.00	30.900	.031	.004	30.870	.038	.002
31.905	.046	.004	32.56	.04	.00	31.952	.024	.003	31.919	.032	.002
32.954	.037	.004	33.63	.03	.00	33.004	.017	.003	32.968	.023	.002
34.003	.032	.004	34.70	.02	.00	34.055	.017	.003	34.017	.021	.002
35.051	.025	.003	35.77	.01	.00	35.107	.011	.002	35.066	.018	.002
36.100	.013	.002	36.85	.01	.00	36.159	.002	.001	36.115	.012	.001
37.148	.044	.004	37.92	.03	.00	37.210	.023	.003	37.164	.030	.002
38.197	.027	.003	38.99	.02	.00	38.262	.016	.003	38.213	.018	.002
39.245	.029	.004	40.06	.02	.00	39.314	.018	.003	39.262	.013	.001
40.294	.026	.003	41.13	.01	.00	40.366	.011	.002	40.311	.012	.001
41.342	.011	.002	42.20	.01	.00	41.417	.008	.002	41.360	.008	.001
42.391	.013	.002	43.28	.01	.00	42.469	.010	.002	42.409	.009	.001
43.439	.009	.002	44.35	.01	.00	43.521	.002	.001	43.458	.008	.001
44.488	.016	.003	45.42	.01	.00	44.572	.007	.002	44.507	.007	.001
45.536	.014	.002	46.49	.01	.00	45.624	.005	.002	45.556	.005	.001
46.585	.006	.002	47.56	.01	.00	46.676	.002	.001	46.605	.006	.001
47.633	.007	.002	48.63	.01	.00	47.728	.001	.001	47.654	.002	.001
48.682	.003	.001	49.71	.00	.00	48.779	.001	.001	48.703	.002	.001
49.731	.001	.001	50.78	.01	.00				49.752	.003	.001
50.779	.003	.001	51.85	.00	.00				50.801	.000	.000
51.828	.000	.000	52.92	0	0						
52.876	0	0	53.99	.00	.00						
53.925	0	0									
54.973	0	0									
56.022	0	0									
57.070	0	0									
58.119	0	0									
59.167	0	0									

TABLE AX 4. Alphas From ^{54}Fe Bombarded by 60-MeV Protons

70 deg - Run 5044			80 deg - Run 5012			90 deg - Run 4010			110 deg - Run 5015		
Energy (MeV)	σ (mb·ster^{-1}·MeV^{-1})	Error	Energy (MeV)	σ (mb·ster^{-1}·MeV^{-1})	Error	Energy (MeV)	σ (mb·ster^{-1}·MeV^{-1})	Error	Energy (MeV)	σ (mb·ster^{-1}·MeV^{-1})	Error
			14.093	.349	.007	14.055	.237	.005			
			15.142	.266	.006	15.105	.176	.004			
14.884	.389	.016	16.192	.194	.005	16.155	.128	.004	14.958	.217	.005
15.136	.282	.014	17.241	.157	.004	17.206	.103	.003	15.109	.158	.004
16.189	.239	.012	18.291	.139	.004	18.256	.084	.003	16.159	.118	.003
17.241	.179	.011	19.340	.099	.003	19.306	.060	.003	17.210	.082	.003
18.294	.136	.009	20.390	.083	.003	20.357	.049	.002	18.261	.068	.003
19.346	.104	.008	21.439	.070	.003	21.407	.040	.002	19.311	.050	.002
20.399	.085	.007	22.489	.059	.003	22.457	.033	.002	20.362	.040	.002
21.451	.075	.007	23.538	.049	.002	23.508	.027	.002	21.412	.031	.002
22.504	.063	.006	24.588	.043	.002	24.558	.024	.002	22.463	.024	.002
23.556	.055	.006	25.637	.038	.002	25.608	.021	.001	23.514	.018	.001
24.609	.046	.005	26.687	.028	.002	26.659	.018	.001	24.564	.016	.001
25.661	.033	.005	27.736	.030	.002	27.709	.016	.001	25.615	.014	.001
26.714	.033	.005	28.786	.020	.002	28.759	.012	.001	26.665	.011	.001
27.766	.021	.004	29.835	.022	.002	29.810	.008	.001	27.716	.009	.001
28.819	.022	.004	30.884	.018	.002	30.860	.007	.001	28.767	.006	.001
29.871	.016	.003	31.934	.017	.001	31.911	.006	.001	29.817	.006	.001
30.924	.012	.003	32.983	.016	.001	32.961	.006	.001	30.868	.003	.001
31.976	.013	.003	34.033	.009	.001	34.011	.003	.001	31.919	.004	.001
33.029	.011	.003	35.082	.008	.001	35.062	.003	.001	32.969	.002	.000
34.081	.007	.002	36.132	.006	.001	36.112	.002	.000	34.020	.001	.000
35.134	.002	.001	37.181	.014	.001	37.162	.005	.001	35.070	.001	.000
36.186	.004	.002	38.231	.009	.001	38.213	.004	.001	36.121	.001	.000
37.239	.016	.003	39.280	.008	.001	39.263	.004	.001	37.172	.002	.000
38.291	.007	.002	40.330	.004	.001	40.313	.002	.000	38.222	.001	.000
39.344	.006	.002	41.379	.004	.001	41.364	.002	.001	39.273	.000	.000
40.396	.003	.001	42.429	.004	.001	42.414	.003	.001	40.323	.001	.000
41.449	.003	.001	43.478	.004	.001	43.464	.002	.000	41.374	.000	.000
42.501	.003	.001	44.528	.002	.001	44.515	.002	.000	42.425	.000	.000
43.554	.002	.001	45.577	.002	.000	45.565	.001	.000	43.475	.000	.000
44.606	.001	.001	46.627	.001	.000	46.615	.000	.000	44.526	0	0
45.659	.003	.001	47.676	.001	.000	47.666	.002	.000	45.576	.000	.000
46.711	0	0	48.725	.000	.000	48.716	0	0	46.627	0	0
47.764	0	0							47.678	.000	.000
48.816	.001	.001							48.728	0	0
49.869	0	0									
50.921	0	0									
51.974	0	0									
53.026	0	0									
54.079	0	0									

TABLE AX 5. Alphas From ^{54}Fe Bombarded by 60-MeV Protons

120 deg - Run 7002			135 deg - Run 4011			160 deg - Run 2067		
Energy (MeV)	σ	Error	Energy (MeV)	σ	Error	Energy (MeV)	σ	Error
	(mb·ster^{-1}·MeV^{-1})			(mb·ster^{-1}·MeV^{-1})			(mb·ster^{-1}·MeV^{-1})	
						14.05	.18	.01
14.061	.193	.008	14.064	.135	.003	15.10	.12	.01
15.112	.152	.007	15.115	.096	.003	16.15	.09	.01
16.162	.103	.006	16.166	.068	.002	17.20	.06	.01
17.213	.076	.005	17.217	.046	.002	18.25	.06	.01
18.264	.062	.005	18.268	.036	.002	19.30	.04	.01
19.315	.042	.004	19.319	.027	.001	20.35	.02	.00
20.366	.037	.004	20.370	.021	.001	21.40	.02	.00
21.416	.025	.003	21.421	.017	.001	22.45	.02	.00
22.467	.017	.002	22.472	.014	.001	23.50	.01	.00
23.518	.011	.002	23.523	.012	.001	24.55	.01	.00
24.569	.013	.002	24.574	.008	.001	25.60	.01	.00
25.620	.008	.002	25.625	.006	.001	26.65	.01	.00
26.670	.007	.002	26.676	.005	.001	27.70	.00	.00
27.721	.002	.001	27.727	.003	.000	28.75	.01	.00
28.772	.003	.001	28.778	.003	.000	29.80	.00	.00
29.823	.002	.001	29.829	.003	.000	30.85	.00	.00
30.874	.000	.000	30.880	.002	.000	31.90	.00	.00
31.925	.001	.001	31.931	.001	.000	32.95	.00	.00
32.975	0	0	32.982	.001	.000	34.00	0	0
34.026	.001	.000	34.033	.001	.000	35.05	.00	.00
35.077	.000	.000	35.084	.001	.000	36.10	0	0
36.128	.001	.000	36.135	.000	.000	37.15	0	0
37.179	0	0	37.186	.001	.000	38.20	0	0
38.229	.000	.000	38.237	.000	.000	39.25	0	0
39.280	0	0	39.289	.000	.000	40.30	0	0
40.331	0	0	40.340	.000	.000	41.35	0	0
41.382	.000	.000	41.391	.000	.000	42.40	0	0
42.433	0	0	42.442	.000	.000	43.45	0	0
43.483	0	0	43.493	0	0	44.50	0	0
44.534	0	0	44.544	0	0	45.55	0	0
45.585	0	0	45.595	.000	.000	46.60	0	0
46.636	0	0	46.646	0	0	47.65	0	0
47.687	0	0	47.697	0	0	48.70	0	0
48.737	0	0	48.748	0	0	49.75	0	0
						50.80	0	0
						51.85	0	0
						52.90	0	0
						53.95	0	0
						55.00	0	0
						56.05	0	0
						57.10	0	0
						58.15	0	0
						59.20	0	0

TABLE A XI 1. Protons from ^{209}Bi Bombarded by 60-MeV Protons

15 deg - Run 5030			20 deg - Run 5027			25 deg - Run 5026			30 deg - Run 5021		
Energy (MeV)	σ (mb·ster^{-1}·MeV^{-1})	Error	Energy (MeV)	σ (mb·ster^{-1}·MeV^{-1})	Error	Energy (MeV)	σ (mb·ster^{-1}·MeV^{-1})	Error	Energy (MeV)	σ (mb·ster^{-1}·MeV^{-1})	Error
1.50	0	0	1.50	0	0	1.50	0	0	1.50	0	0
2.55	0	0	2.54	0	0	2.54	0	0	2.55	0	0
3.59	1.30	.06	3.59	.76	.03	3.59	.50	.03	3.60	.18	.01
4.64	2.36	.08	4.64	1.02	.04	4.64	.69	.03	4.65	.22	.01
5.69	2.97	.09	5.69	1.32	.04	5.69	.77	.04	5.70	.25	.01
6.74	3.63	.10	6.74	1.55	.04	6.74	1.08	.04	6.75	.35	.01
7.79	4.42	.11	7.78	1.89	.05	7.78	1.50	.05	7.79	.51	.02
8.83	5.05	.12	8.83	2.11	.05	8.83	1.49	.05	8.84	.73	.02
9.88	3.03	.09	9.88	1.67	.05	9.88	1.32	.05	9.89	1.02	.02
10.93	4.06	.11	10.93	2.33	.05	10.93	1.76	.05	10.94	1.40	.03
11.98	4.22	.11	11.98	2.32	.05	11.97	1.91	.06	11.99	1.60	.03
13.03	4.37	.11	13.02	2.52	.06	13.02	2.04	.06	13.04	1.75	.03
14.08	4.94	.12	14.07	2.90	.06	14.07	2.26	.06	14.09	2.01	.03
15.12	5.32	.12	15.12	3.12	.06	15.12	2.52	.06	15.14	2.15	.04
16.17	5.27	.12	16.17	3.10	.06	16.16	2.55	.06	16.19	2.35	.04
17.22	5.49	.12	17.21	3.19	.06	17.21	2.68	.07	17.24	2.44	.04
18.27	5.83	.13	18.26	3.42	.07	18.26	2.77	.07	18.29	2.58	.04
19.32	5.99	.13	19.31	3.56	.07	19.31	3.02	.07	19.34	2.76	.04
20.36	6.33	.13	20.36	3.69	.07	20.36	3.22	.07	20.39	2.81	.04
21.41	6.80	.14	21.41	3.94	.07	21.40	3.31	.07	21.43	2.79	.04
22.46	6.69	.14	22.45	3.92	.07	22.45	3.19	.07	22.48	2.98	.04
23.51	6.80	.14	23.50	4.00	.07	23.50	3.60	.08	23.53	3.00	.04
24.56	7.12	.14	24.55	4.30	.07	24.55	3.65	.08	24.58	2.98	.04
25.60	6.98	.14	25.60	4.14	.07	25.59	3.50	.07	25.63	3.13	.04
26.65	7.01	.14	26.65	4.27	.07	26.64	3.70	.08	26.68	3.16	.04
27.70	7.17	.14	27.69	4.32	.07	27.69	3.72	.08	27.73	3.27	.04
28.75	7.45	.14	28.74	4.44	.07	28.74	3.93	.08	28.78	3.38	.04
29.80	6.96	.14	29.79	4.55	.08	29.79	3.55	.08	29.83	3.43	.04
30.85	7.56	.15	30.84	4.63	.08	30.83	3.73	.08	30.88	3.34	.04
31.89	7.58	.15	31.88	4.75	.08	31.88	3.84	.08	31.93	3.33	.04
32.94	7.38	.14	32.93	4.64	.08	32.93	3.78	.08	32.98	3.26	.04
33.99	7.51	.15	33.98	4.59	.08	33.98	3.84	.08	34.03	3.41	.04
35.04	7.99	.15	35.03	4.69	.08	35.02	4.15	.08	35.07	3.42	.04
36.09	8.17	.15	36.08	5.10	.08	36.07	4.22	.08	36.12	3.49	.04
37.13	9.20	.16	37.12	5.63	.08	37.12	4.47	.08	37.17	3.60	.05
38.18	9.03	.16	38.17	5.31	.08	38.17	4.40	.08	38.22	3.58	.05
39.23	9.16	.16	39.22	5.44	.08	39.21	4.66	.09	39.27	3.53	.04
40.28	9.04	.16	40.27	5.48	.08	40.26	4.52	.09	40.32	3.57	.05
41.33	9.14	.16	41.32	5.35	.08	41.31	4.46	.08	41.37	3.60	.05
42.38	9.44	.16	42.36	5.63	.08	42.36	4.61	.09	42.42	3.54	.05
43.42	9.68	.17	43.41	5.91	.09	43.41	4.61	.09	43.47	3.65	.05
44.47	10.83	.17	44.46	5.95	.09	44.45	4.62	.09	44.52	3.59	.05
45.52	10.39	.17	45.51	5.84	.09	45.50	4.71	.09	45.57	3.62	.05
46.57	11.41	.18	46.55	6.63	.09	46.55	4.98	.09	46.62	3.83	.05
47.62	11.85	.18	47.60	6.33	.09	47.60	4.73	.09	47.67	3.84	.05
48.66	11.79	.18	48.65	6.53	.09	48.64	5.06	.09	48.71	3.78	.05
49.71	11.91	.18	49.70	6.81	.09	49.69	5.11	.09	49.76	3.94	.05
50.76	12.33	.19	50.75	6.88	.09	50.74	5.53	.09	50.81	3.91	.05
51.81	11.89	.18	51.79	6.44	.09	51.79	4.97	.09	51.86	3.35	.04
52.86	11.38	.18	52.84	6.09	.09	52.84	4.68	.09	52.91	3.12	.04
53.91	10.63	.17	53.89	5.87	.09	53.88	4.53	.09	53.96	3.21	.04
54.95	9.65	.16	54.94	5.79	.09	54.93	4.59	.09	55.01	3.31	.04
56.00	11.24	.18	55.98	7.39	.10	55.98	5.52	.09	56.06	3.83	.05
57.05	12.47	.19	57.03	8.88	.11	57.03	7.00	.11	57.11	5.40	.06
58.10	10.07	.17	58.08	9.05	.08	58.07	3.45	.07	58.16	2.06	.03
59.15	17.09	.22	59.13	11.34	.12	59.12	5.04	.08	59.21	3.24	.04
									60.26	.53	.02

TABLE A XI 2. Protons from ^{209}Bi Bombarded by 60-MeV Protons

35 deg - Run 5025			40 deg - Run 5031			45 deg - Run 5024			50 deg - Run 5032		
Energy (MeV)	σ (mb·ster^{-1}·MeV^{-1})	Error	Energy (MeV)	σ (mb·ster^{-1}·MeV^{-1})	Error	Energy (MeV)	σ (mb·ster^{-1}·MeV^{-1})	Error	Energy (MeV)	σ (mb·ster^{-1}·MeV^{-1})	Error
1.50	0	0				1.50	0	0			
2.54	0	0	1.50	0	0	2.55	0	0	1.50	0	0
3.59	.19	.01	2.54	0	0	3.59	.10	.01	2.55	0	0
4.64	.27	.01	3.59	.15	.01	4.64	.13	.01	3.59	.10	.01
5.69	.32	.01	4.64	.21	.01	5.69	.15	.01	4.64	.15	.01
6.73	.40	.01	5.69	.24	.01	6.74	.24	.01	5.69	.16	.01
7.78	.54	.02	6.74	.31	.01	7.79	.35	.01	6.74	.22	.01
8.83	.75	.02	7.78	.44	.01	8.83	.58	.02	7.79	.34	.01
9.88	1.01	.02	8.83	.63	.02	9.88	.92	.02	8.83	.54	.01
10.92	1.41	.03	9.88	.94	.02	10.93	1.30	.02	9.88	.87	.02
11.97	1.59	.03	10.93	1.34	.03	11.98	1.47	.02	10.93	1.30	.02
13.02	1.74	.03	11.97	1.50	.03	13.03	1.59	.03	11.98	1.39	.02
14.07	2.02	.03	13.02	1.63	.03	14.07	1.79	.03	13.03	1.46	.02
15.11	2.06	.03	14.07	1.83	.03	15.12	1.93	.03	14.07	1.66	.02
16.16	2.28	.03	15.12	1.91	.03	16.17	2.00	.03	15.12	1.84	.02
17.21	2.33	.03	16.16	2.11	.03	17.22	2.08	.03	16.17	1.94	.03
18.26	2.47	.04	17.21	2.16	.03	18.27	2.25	.03	17.22	1.94	.03
19.30	2.60	.04	18.26	2.28	.03	19.31	2.26	.03	18.27	2.09	.03
20.35	2.69	.04	19.31	2.36	.03	20.36	2.38	.03	19.31	2.11	.03
21.40	2.76	.04	20.36	2.51	.04	21.41	2.38	.03	20.36	2.16	.03
22.45	2.76	.04	21.40	2.52	.04	22.46	2.40	.03	21.41	2.18	.03
23.49	2.85	.04	22.45	2.58	.04	23.51	2.45	.03	22.46	2.17	.03
24.54	2.87	.04	23.50	2.61	.04	24.55	2.46	.03	23.51	2.25	.03
25.59	2.91	.04	24.55	2.61	.04	25.60	2.47	.03	24.55	2.27	.03
26.63	2.93	.04	25.59	2.70	.04	26.65	2.50	.03	25.60	2.28	.03
27.68	3.04	.04	26.64	2.76	.04	27.70	2.53	.03	26.65	2.25	.03
28.73	3.06	.04	27.69	2.71	.04	28.75	2.63	.03	27.70	2.25	.03
29.78	3.13	.04	28.74	2.77	.04	29.80	2.55	.03	28.75	2.28	.03
30.82	3.10	.04	29.78	2.80	.04	30.84	2.61	.03	29.80	2.22	.03
31.87	3.16	.04	30.83	2.72	.04	31.89	2.51	.03	30.84	2.21	.03
32.92	3.19	.04	31.88	2.85	.04	32.94	2.50	.03	31.89	2.21	.03
33.97	3.23	.04	32.93	2.78	.04	33.99	2.56	.03	32.94	2.18	.03
35.01	3.20	.04	33.98	2.83	.04	35.04	2.54	.03	33.99	2.14	.03
36.06	3.22	.04	35.02	2.84	.04	36.08	2.47	.03	35.04	2.13	.03
37.11	3.36	.04	36.07	2.88	.04	37.13	2.44	.03	36.08	2.10	.03
38.16	3.33	.04	37.12	2.94	.04	38.18	2.55	.03	37.13	2.08	.03
39.20	3.28	.04	38.17	2.88	.04	39.23	2.48	.03	38.18	2.05	.03
40.25	3.32	.04	39.21	2.82	.04	40.28	2.41	.03	39.23	2.03	.03
41.30	3.37	.04	40.26	2.80	.04	41.32	2.32	.03	40.28	1.99	.03
42.35	3.30	.04	41.31	2.72	.04	42.37	2.29	.03	41.32	1.94	.03
43.39	3.20	.04	42.36	2.78	.04	43.42	2.23	.03	42.37	1.89	.02
44.44	3.26	.04	43.40	2.62	.04	44.47	2.17	.03	43.42	1.85	.02
45.49	3.17	.04	44.45	2.65	.04	45.52	2.16	.03	44.47	1.73	.02
46.54	3.35	.04	45.50	2.54	.04	46.56	2.16	.03	45.52	1.71	.02
47.58	3.26	.04	46.55	2.61	.04	47.61	2.06	.03	46.56	1.71	.02
48.63	3.34	.04	47.60	2.60	.04	48.66	2.02	.03	47.61	1.67	.02
49.68	3.18	.04	48.64	2.58	.04	49.71	1.97	.03	48.66	1.60	.02
50.73	3.02	.04	49.69	2.44	.03	50.76	1.92	.03	49.71	1.45	.02
51.77	2.66	.04	50.74	2.32	.03	51.80	1.69	.03	50.76	1.39	.02
52.82	2.48	.04	51.79	2.14	.03	52.85	1.53	.02	51.81	1.24	.02
53.87	2.58	.04	52.83	1.92	.03	53.90	1.53	.02	52.85	1.09	.02
54.92	2.63	.04	53.88	2.10	.03	54.95	1.61	.03	53.90	1.20	.02
55.96	3.11	.04	54.93	2.04	.03	56.00	1.82	.03	54.95	1.23	.02
57.01	4.02	.05	55.98	2.37	.03	57.04	2.09	.03	56.00	1.38	.02
58.06	1.24	.03	57.02	2.79	.04	58.09	.72	.02	57.05	1.39	.02
59.11	3.76	.04	58.07	.82	.02	59.14	1.11	.02	58.09	.45	.01
			59.12	1.42	.03	60.19	.10	.01	59.14	1.25	.02
									60.19	.14	.01

TABLE A XI 3. Protons from ^{209}Bi Bombarded by 60-MeV Protons

60 deg - Run 5033			70 deg - Run 5037			75 deg - Run 7006			80 deg - Run 5035		
Energy (MeV)	σ (mb·ster^{-1}·MeV^{-1})	Error	Energy (MeV)	σ (mb·ster^{-1}·MeV^{-1})	Error	Energy (MeV)	σ (mb·ster^{-1}·MeV^{-1})	Error	Energy (MeV)	σ (mb·ster^{-1}·MeV^{-1})	Error
1.498	0	0	1.500	0	0	1.475	0	0	1.499	0	0
2.547	0	0	2.550	0	0	2.543	0	0	2.549	0	0
3.595	.088	.004	3.600	.057	.004	3.611	.112	.008	3.598	.063	.004
4.644	.099	.005	4.650	.077	.005	4.679	.215	.011	4.648	.080	.005
5.692	.126	.006	5.700	.097	.005	5.748	.206	.010	5.697	.087	.005
6.741	.179	.007	6.750	.157	.007	6.816	.282	.012	6.746	.150	.007
7.790	.270	.008	7.800	.251	.009	7.884	.322	.013	7.796	.247	.009
8.838	.452	.010	8.850	.390	.011	8.952	.484	.016	8.845	.428	.012
9.887	.791	.014	9.900	.728	.015	10.020	.810	.021	9.895	.827	.016
10.936	1.128	.017	10.950	1.097	.018	11.088	1.086	.024	10.944	1.154	.019
11.984	1.234	.017	12.000	1.104	.018	12.156	1.103	.024	11.994	1.139	.019
13.033	1.309	.018	13.050	1.186	.019	13.225	1.179	.025	13.043	1.158	.019
14.081	1.445	.019	14.100	1.295	.020	14.293	1.232	.025	14.093	1.267	.020
15.130	1.581	.020	15.150	1.418	.021	15.361	1.351	.027	15.142	1.381	.021
16.179	1.650	.020	16.200	1.422	.021	16.429	1.430	.027	16.191	1.372	.021
17.227	1.700	.020	17.249	1.488	.021	17.497	1.391	.027	17.241	1.367	.021
18.276	1.690	.020	18.299	1.505	.021	18.565	1.439	.028	18.290	1.378	.021
19.324	1.794	.021	19.349	1.462	.021	19.633	1.443	.028	19.340	1.392	.021
20.373	1.846	.021	20.399	1.534	.021	20.701	1.443	.028	20.389	1.368	.021
21.422	1.784	.021	21.449	1.470	.021	21.770	1.374	.027	21.439	1.323	.020
22.470	1.787	.021	22.499	1.408	.021	22.838	1.321	.026	22.488	1.260	.020
23.519	1.804	.021	23.549	1.450	.021	23.906	1.330	.026	23.538	1.224	.020
24.568	1.748	.021	24.599	1.384	.020	24.974	1.294	.026	24.587	1.200	.019
25.616	1.774	.021	25.649	1.389	.020	26.042	1.262	.026	25.637	1.159	.019
26.665	1.758	.021	26.699	1.359	.020	27.110	1.234	.025	26.686	1.094	.019
27.713	1.761	.021	27.749	1.316	.020	28.178	1.192	.025	27.735	1.102	.019
28.762	1.711	.020	28.799	1.298	.020	29.247	1.142	.025	28.785	1.037	.018
29.811	1.655	.020	29.849	1.235	.019	30.315	1.070	.024	29.834	.984	.018
30.859	1.644	.020	30.899	1.198	.019	31.383	1.045	.023	30.884	.929	.017
31.908	1.597	.020	31.949	1.117	.018	32.451	1.026	.023	31.933	.885	.017
32.956	1.558	.019	32.999	1.122	.018	33.519	.929	.022	32.983	.850	.016
34.005	1.545	.019	34.049	1.065	.018	34.587	.899	.022	34.032	.813	.016
35.054	1.474	.019	35.099	1.045	.018	35.655	.814	.021	35.082	.781	.016
36.102	1.471	.019	36.149	.965	.017	36.724	.808	.021	36.131	.749	.015
37.151	1.431	.019	37.199	.985	.017	37.792	.777	.020	37.180	.690	.015
38.200	1.384	.018	38.249	.902	.016	38.860	.758	.020	38.230	.659	.014
39.248	1.328	.018	39.299	.857	.016	39.928	.663	.019	39.279	.638	.014
40.297	1.299	.018	40.349	.812	.016	40.996	.657	.019	40.329	.582	.014
41.345	1.268	.018	41.399	.775	.015	42.064	.615	.018	41.378	.525	.013
42.394	1.190	.017	42.449	.746	.015	43.132	.570	.017	42.428	.475	.012
43.443	1.142	.017	43.499	.676	.014	44.200	.535	.017	43.477	.467	.012
44.491	1.070	.016	44.549	.648	.014	45.269	.533	.017	44.527	.407	.011
45.540	1.077	.016	45.599	.623	.014	46.337	.482	.016	45.576	.427	.012
46.588	1.030	.016	46.649	.593	.013	47.405	.446	.015	46.625	.381	.011
47.637	1.005	.016	47.699	.552	.013	48.473	.408	.015	47.675	.353	.011
48.686	.931	.015	48.749	.515	.012	49.541	.368	.014	48.724	.318	.010
49.734	.893	.015	49.798	.466	.012	50.609	.377	.014	49.774	.299	.010
50.783	.824	.014	50.848	.440	.011	51.677	.308	.013	50.823	.260	.009
51.832	.738	.013	51.898	.371	.011	52.746	.261	.012	51.873	.224	.008
52.880	.649	.013	52.948	.351	.010	53.814	.237	.011	52.922	.209	.008
53.929	.667	.013	53.998	.334	.010	54.882	.284	.012	53.972	.194	.008
54.977	.719	.013	55.048	.368	.010	55.950	.259	.012	55.021	.202	.008
56.026	.748	.013	56.098	.339	.010	57.018	.270	.012	56.071	.200	.008
57.075	.781	.014	57.148	.296	.009	58.086	.136	.008	57.120	.165	.007
58.123	.269	.008	58.198	.165	.007	59.154	.084	.007	58.169	.183	.008
59.172	.364	.009	59.248	.122	.006	60.222	.011	.002	59.219	.061	.004
60.220	.041	.003									

TABLE A XI 4. Protons from ^{209}Bi Bombarded by 60-MeV Protons

90 deg - Run 5023			110 deg - Run 5036			135 deg - Run 2064			deg - Run		
Energy (MeV)	σ	Error	Energy (MeV)	σ	Error	Energy (MeV)	σ	Error	Energy (MeV)	σ	Error
	(mb·ster^{-1}·MeV^{-1})			(mb·ster^{-1}·MeV^{-1})			(mb·ster^{-1}·MeV^{-1})			(mb·ster^{-1}·MeV^{-1})	
1.497	0	0	1.450	0	0	1.48	0	0			
2.545	0	0	2.500	0	0	2.52	.00	.00			
3.593	.052	.003	3.550	.041	.003	3.56	.04	.00			
4.641	.064	.003	4.600	.056	.003	4.60	.06	.00			
5.690	.079	.004	5.650	.059	.003	5.64	.08	.00			
6.738	.124	.004	6.700	.100	.004	6.68	.20	.01			
7.786	.209	.006	7.750	.167	.005	7.72	.26	.01			
8.834	.363	.008	8.800	.305	.007	8.75	.29	.01			
9.882	.724	.011	9.850	.629	.010	9.79	.32	.01			
10.930	.987	.013	10.900	.849	.012	10.83	.60	.01			
11.978	.987	.013	11.950	.804	.011	11.87	.55	.01			
13.026	.974	.013	13.000	.784	.011	12.91	.53	.01			
14.074	1.053	.013	14.050	.796	.011	13.95	.58	.01			
15.122	1.083	.013	15.100	.797	.011	14.99	.61	.01			
16.170	1.102	.013	16.150	.785	.011	16.03	.57	.01			
17.218	1.112	.013	17.200	.755	.011	17.06	.54	.01			
18.266	1.056	.013	18.250	.727	.011	18.10	.53	.01			
19.314	1.036	.013	19.300	.696	.010	19.14	.48	.01			
20.363	1.029	.013	20.350	.647	.010	20.18	.43	.01			
21.411	.984	.013	21.400	.597	.010	21.22	.40	.01			
22.459	.934	.012	22.450	.564	.009	22.26	.37	.01			
23.507	.875	.012	23.500	.524	.009	23.30	.32	.01			
24.555	.856	.012	24.550	.497	.009	24.33	.31	.01			
25.603	.803	.011	25.600	.453	.008	25.37	.24	.01			
26.651	.782	.011	26.650	.427	.008	26.41	.20	.01			
27.699	.764	.011	27.700	.390	.008	27.45	.17	.01			
28.747	.726	.011	28.750	.385	.008	28.49	.14	.01			
29.795	.664	.010	29.800	.336	.007	29.53	.13	.01			
30.843	.642	.010	30.850	.305	.007	30.57	.10	.00			
31.891	.585	.010	31.900	.287	.007	31.60	.10	.00			
32.939	.535	.009	32.950	.264	.006	32.64	.11	.01			
33.987	.536	.009	34.000	.251	.006	33.68	.11	.01			
35.035	.481	.009	35.050	.221	.006	34.72	.10	.00			
36.084	.449	.009	36.100	.213	.006	35.76	.10	.00			
37.132	.408	.008	37.150	.186	.005	36.80	.10	.00			
38.180	.390	.008	38.200	.163	.005	37.84	.08	.00			
39.228	.356	.008	39.250	.147	.005	38.88	.07	.00			
40.276	.332	.007	40.300	.126	.004	39.91	.07	.00			
41.324	.304	.007	41.350	.117	.004	40.95	.05	.00			
42.372	.278	.007	42.400	.106	.004	41.99	.04	.00			
43.420	.248	.006	43.450	.103	.004	43.03	.03	.00			
44.468	.236	.006	44.500	.082	.004	44.07	.04	.00			
45.516	.217	.006	45.550	.080	.004	45.11	.03	.00			
46.564	.199	.006	46.600	.069	.003	46.15	.02	.00			
47.612	.187	.006	47.650	.066	.003	47.18	.02	.00			
48.660	.170	.005	48.700	.052	.003	46.22	.02	.00			
49.708	.151	.005	49.750	.050	.003	49.26	.01	.00			
50.757	.132	.005	50.800	.042	.003	50.30	.01	.00			
51.805	.113	.004	51.850	.039	.002	51.34	.01	.00			
52.853	.093	.004	52.900	.035	.002	52.38	.01	.00			
53.901	.093	.004	53.950	.034	.002	53.42	.01	.00			
54.949	.089	.004	55.000	.031	.002	54.46	.01	.00			
55.997	.084	.004	56.050	.027	.002	55.49	.01	.00			
57.045	.095	.004	57.100	.025	.002	56.53	.01	.00			
58.093	.069	.003	58.150	.027	.002	57.57	.00	.00			
59.141	.016	.002	59.200	.002	.001	58.61	.00	.00			
60.189	.004	.001									

TABLE A XII 1. Deuterons from ^{209}Bi Bombarded by 60-MeV Protons

15 deg - Run 5030			20 deg - Run 5027			25 deg - Run 5026			30 deg - Run 5021		
Energy (MeV)	σ (mb·ster^{-1}·MeV^{-1})	Error	Energy (MeV)	σ (mb·ster^{-1}·MeV^{-1})	Error	Energy (MeV)	σ (mb·ster^{-1}·MeV^{-1})	Error	Energy (MeV)	σ (mb·ster^{-1}·MeV^{-1})	Error
			1.50	0	0						
1.50	0	0	2.54	0	0	1.50	0	0			
2.55	0	0	3.59	0	0	2.54	0	0	1.50	0	0
3.59	0	0	4.64	.03	.01	3.59	0	0	2.55	0	0
4.64	.01	.01	5.69	.01	.00	4.64	.01	.00	3.60	.00	.00
5.69	.03	.01	6.74	.02	.00	5.69	.01	.00	4.65	.01	.00
6.74	.01	.01	7.78	.03	.01	6.74	.01	.00	5.70	.01	.00
7.79	.02	.01	8.83	.07	.01	7.78	.01	.00	6.75	.02	.00
8.83	.06	.01	9.88	.13	.01	8.83	.04	.01	7.79	.03	.00
9.88	.11	.02	10.93	.19	.02	9.88	.10	.01	8.84	.06	.01
10.93	.18	.02	11.98	.29	.02	10.93	.16	.02	9.89	.10	.01
11.98	.26	.03	13.02	.36	.02	11.97	.26	.02	10.94	.19	.01
13.03	.32	.03	14.07	.40	.02	13.02	.32	.02	11.99	.27	.01
14.08	.35	.03	15.12	.37	.02	14.07	.35	.02	13.04	.34	.01
15.12	.42	.03	16.17	.42	.02	15.12	.34	.02	14.09	.37	.01
16.17	.37	.03	17.21	.50	.03	16.16	.39	.03	15.14	.40	.02
17.22	.44	.04	18.26	.51	.03	17.21	.40	.03	16.19	.42	.02
18.27	.50	.04	19.31	.46	.02	18.26	.49	.03	17.24	.40	.02
19.32	.48	.04	20.36	.50	.02	19.31	.46	.03	18.29	.44	.02
20.36	.47	.04	21.41	.51	.03	20.36	.46	.03	19.34	.48	.02
21.41	.56	.04	22.45	.53	.03	21.40	.55	.03	20.39	.52	.02
22.46	.50	.04	23.50	.56	.03	22.45	.51	.03	21.43	.52	.02
23.51	.61	.04	24.55	.54	.03	23.50	.56	.03	22.48	.52	.02
24.56	.54	.04	25.60	.59	.03	24.55	.53	.03	23.53	.50	.02
25.60	.57	.04	26.65	.53	.03	25.59	.53	.03	24.58	.47	.02
26.65	.68	.04	27.69	.59	.03	26.64	.50	.03	25.63	.53	.02
27.70	.55	.04	28.74	.63	.03	27.69	.53	.03	26.68	.53	.02
28.75	.59	.04	29.79	.60	.03	28.74	.55	.03	27.73	.48	.02
29.80	.61	.04	30.84	.66	.03	29.79	.54	.03	28.78	.52	.02
30.85	.57	.04	31.88	.61	.03	30.83	.55	.03	29.83	.52	.02
31.89	.58	.04	32.93	.60	.03	31.88	.58	.03	30.88	.51	.02
32.94	.64	.04	33.98	.57	.03	32.93	.54	.03	31.93	.51	.02
33.99	.57	.04	35.03	.63	.03	33.98	.50	.03	32.98	.51	.02
35.04	.63	.04	36.08	.66	.03	35.02	.52	.03	34.03	.48	.02
36.09	.67	.04	37.12	.64	.03	36.07	.53	.03	35.07	.50	.02
37.13	.76	.05	38.17	.69	.03	37.12	.54	.03	36.12	.51	.02
38.18	.68	.04	39.22	.67	.03	38.17	.58	.03	37.17	.51	.02
39.23	.71	.04	40.27	.66	.03	39.21	.54	.03	38.22	.47	.02
40.28	.76	.05	41.32	.69	.03	40.26	.52	.03	39.27	.46	.02
41.33	.93	.05	42.36	.72	.03	41.31	.58	.03	40.32	.47	.02
42.38	.81	.05	43.41	.77	.03	42.36	.58	.03	41.37	.47	.02
43.42	.98	.05	44.46	.81	.03	43.41	.57	.03	42.42	.45	.02
44.47	1.09	.06	45.51	.87	.03	44.45	.60	.03	43.47	.45	.02
45.52	1.04	.05	46.55	.92	.03	45.50	.64	.03	44.52	.48	.02
46.57	1.03	.05	47.60	.97	.03	46.55	.65	.03	45.57	.48	.02
47.62	1.21	.06	48.65	.96	.03	47.60	.72	.03	46.62	.46	.02
48.66	1.23	.06	49.70	.99	.04	48.64	.73	.03	47.67	.48	.02
49.71	1.34	.06	50.75	1.14	.04	49.69	.84	.04	48.71	.53	.02
50.76	1.62	.07	51.79	.79	.03	50.74	.81	.04	49.76	.52	.02
51.81	1.07	.05	52.84	1.40	.04	51.79	.53	.03	50.81	.51	.02
52.86	2.25	.08	53.89	3.36	.06	52.84	.90	.04	51.86	.34	.01
53.91	5.30	.12	54.94	3.68	.07	58.88	2.74	.07	52.91	.62	.02
54.95	5.10	.12	55.98	2.77	.06	54.93	2.36	.06	53.96	1.58	.03
56.00	5.00	.12				55.98	1.89	.06	55.01	1.43	.03
57.05	.01	.01							56.06	1.01	.02
58.10	0	0							57.11	.00	.00
59.15	.00	.00							58.16	.00	.00
									59.21	.00	.00

TABLE A XII 2. Deuterons from ^{209}Bi Bombarded by 60-MeV Protons

35 deg - Run 5025			40 deg - Run 5031			45 deg - Run 5024			50 deg - Run 5032		
Energy (MeV)	σ (mb·ster^{-1}·MeV^{-1})	Error	Energy (MeV)	σ (mb·ster^{-1}·MeV^{-1})	Error	Energy (MeV)	σ (mb·ster^{-1}·MeV^{-1})	Error	Energy (MeV)	σ (mb·ster^{-1}·MeV^{-1})	Error
1.50	0	0				1.50	0	0			
2.54	0	0	1.50	0	0	2.55	0	0	1.50	0	0
3.59	0	0	2.54	0	0	3.59	0	0	2.55	0	0
4.64	.02	.00	3.59	.00	.00	4.64	.01	.00	3.59	0	0
5.69	.02	.00	4.64	.02	.00	5.69	.01	.00	4.64	.01	.00
6.73	.01	.00	5.69	.02	.00	6.74	.01	.00	5.69	.01	.00
7.78	.02	.00	6.74	.02	.00	7.79	.02	.00	6.74	.02	.00
8.83	.05	.01	7.78	.03	.00	8.83	.06	.00	7.79	.03	.00
9.88	.12	.01	8.83	.06	.01	9.88	.10	.01	8.83	.05	.00
10.92	.18	.01	9.88	.10	.01	10.93	.16	.01	9.88	.10	.01
11.97	.25	.01	10.93	.17	.01	11.98	.22	.01	10.93	.15	.01
13.02	.33	.01	11.97	.26	.01	13.03	.28	.01	11.98	.21	.01
14.07	.34	.01	13.02	.30	.01	14.07	.29	.01	13.03	.28	.01
15.11	.38	.01	14.07	.32	.01	15.12	.32	.01	14.07	.26	.01
16.16	.40	.01	15.12	.34	.01	16.17	.33	.01	15.12	.32	.01
17.21	.38	.01	16.16	.37	.01	17.22	.35	.01	16.17	.31	.01
18.26	.41	.01	17.21	.37	.01	18.27	.36	.01	17.22	.32	.01
19.30	.45	.02	18.26	.40	.01	19.31	.37	.01	18.27	.34	.01
20.35	.43	.01	19.31	.41	.01	20.36	.37	.01	19.31	.34	.01
21.40	.49	.02	20.36	.44	.01	21.41	.39	.01	20.36	.36	.01
22.45	.46	.02	21.40	.42	.01	22.46	.40	.01	21.41	.35	.01
23.49	.48	.02	22.45	.43	.01	23.51	.39	.01	22.46	.34	.01
24.54	.47	.02	23.50	.44	.01	24.55	.38	.01	23.51	.35	.01
25.59	.48	.02	24.55	.40	.01	25.60	.38	.01	24.55	.33	.01
26.63	.44	.02	25.59	.44	.01	26.65	.34	.01	25.60	.35	.01
27.68	.45	.02	26.64	.38	.01	27.70	.34	.01	26.65	.33	.01
28.73	.45	.02	27.69	.43	.01	28.75	.37	.01	27.70	.31	.01
29.78	.45	.02	28.74	.43	.01	29.80	.34	.01	28.75	.32	.01
30.82	.43	.01	29.78	.42	.01	30.84	.34	.01	29.80	.30	.01
31.87	.44	.02	30.83	.41	.01	31.89	.33	.01	30.84	.29	.01
32.92	.42	.01	31.88	.39	.01	32.94	.31	.01	31.89	.27	.01
33.97	.41	.01	32.93	.39	.01	33.99	.32	.01	32.94	.26	.01
35.01	.42	.01	33.98	.36	.01	35.04	.30	.01	33.99	.24	.01
36.06	.41	.01	35.02	.36	.01	36.08	.29	.01	35.04	.26	.01
37.11	.40	.01	36.07	.37	.01	37.13	.29	.01	36.08	.25	.01
38.16	.38	.01	37.12	.33	.01	38.18	.27	.01	37.13	.24	.01
39.20	.40	.01	38.17	.33	.01	39.23	.25	.01	38.18	.22	.01
40.25	.41	.01	39.21	.32	.01	40.28	.25	.01	39.23	.21	.01
41.30	.37	.01	40.26	.32	.01	41.32	.24	.01	40.28	.20	.01
42.35	.38	.01	41.31	.30	.01	42.37	.22	.01	41.32	.21	.01
43.39	.38	.01	42.36	.30	.01	43.42	.22	.01	42.37	.20	.01
44.44	.38	.01	43.40	.26	.01	44.47	.21	.01	43.42	.17	.01
45.49	.38	.01	44.45	.28	.01	45.52	.20	.01	44.47	.18	.01
46.54	.39	.01	45.50	.27	.01	46.56	.21	.01	45.52	.16	.01
47.58	.40	.01	46.55	.26	.01	47.61	.21	.01	46.56	.15	.01
48.63	.41	.01	47.60	.28	.01	48.66	.19	.01	47.61	.17	.01
49.68	.43	.01	48.64	.25	.01	49.71	.21	.01	48.66	.16	.01
50.73	.40	.01	49.69	.26	.01	50.76	.21	.01	49.71	.15	.01
51.77	.38	.01	50.74	.27	.01	51.80	.11	.01	50.76	.15	.01
52.82	.52	.02	51.79	.16	.01	52.85	.21	.01	51.81	.10	.01
53.87	1.08	.02	52.83	.27	.01	53.90	.45	.01	52.85	.17	.01
54.92	1.00	.02	53.88	.73	.02	54.95	.38	.01	53.90	.41	.01
55.96	.74	.02	54.93	.65	.02	56.00	.22	.01	54.95	.25	.01
			55.98	.36	.01				56.00	.10	.01

TABLE A XII 3. Deuterons from ^{209}Bi Bombarded by 60-MeV Protons

60 deg - Run 5033			70 deg - Run 5037			75 deg - Run 7006			80 deg - Run 5035		
Energy (MeV)	σ (mb·ster^{-1}·MeV^{-1})	Error	Energy (MeV)	σ (mb·ster^{-1}·MeV^{-1})	Error	Energy (MeV)	σ (mb·ster^{-1}·MeV^{-1})	Error	Energy (MeV)	σ (mb·ster^{-1}·MeV^{-1})	Error
1.498	0	0	1.500	0	0	1.475	0	0	1.499	0	0
2.547	0	0	2.550	0	0	2.543	0	0	2.549	0	0
3.595	.000	.000	3.600	0	0	3.611	0	0	3.598	0	0
4.644	.014	.002	4.650	.007	.001	4.679	.006	.002	4.648	.006	.001
5.692	.014	.002	5.700	.007	.001	5.748	.021	.003	5.697	.008	.002
6.741	.019	.002	6.750	.007	.001	6.816	.013	.003	6.746	.009	.002
7.790	.021	.002	7.800	.015	.002	7.884	.016	.003	7.796	.018	.002
8.838	.046	.003	8.850	.037	.003	8.952	.032	.004	8.845	.034	.003
9.887	.087	.005	9.900	.066	.004	10.020	.069	.006	9.895	.070	.005
10.936	.124	.005	10.950	.108	.006	11.088	.108	.008	10.944	.112	.006
11.984	.174	.006	12.000	.143	.007	12.156	.166	.009	11.994	.157	.007
13.033	.230	.007	13.050	.204	.008	13.225	.172	.010	13.043	.182	.008
14.081	.235	.008	14.100	.191	.008	14.293	.189	.010	14.093	.192	.008
15.130	.249	.008	15.150	.209	.008	15.361	.191	.010	15.142	.202	.008
16.179	.268	.008	16.200	.194	.008	16.429	.175	.010	16.191	.191	.008
17.227	.271	.008	17.249	.214	.008	17.497	.190	.010	17.241	.201	.008
18.276	.279	.008	18.299	.228	.008	18.565	.194	.010	18.290	.203	.008
19.324	.285	.008	19.349	.198	.008	19.633	.189	.010	19.340	.190	.008
20.373	.282	.008	20.399	.228	.008	20.701	.186	.010	20.389	.197	.008
21.422	.270	.008	21.449	.219	.008	21.770	.202	.010	21.439	.192	.008
22.470	.263	.008	22.499	.213	.008	22.838	.180	.010	22.488	.169	.007
23.519	.248	.008	23.549	.208	.008	23.906	.155	.009	23.538	.169	.007
24.568	.256	.008	24.599	.182	.007	24.974	.157	.009	24.587	.157	.007
25.616	.252	.008	25.649	.188	.008	26.042	.154	.009	25.637	.149	.007
26.665	.256	.008	26.699	.171	.007	27.110	.150	.009	26.686	.145	.007
27.713	.237	.008	27.749	.168	.007	28.178	.143	.009	27.735	.140	.007
28.762	.232	.007	28.799	.166	.007	29.247	.137	.009	28.785	.136	.007
29.811	.215	.007	29.849	.149	.007	30.315	.112	.008	29.834	.121	.006
30.859	.217	.007	30.899	.141	.006	31.383	.128	.008	30.884	.100	.006
31.908	.208	.007	31.949	.143	.007	32.451	.113	.008	31.933	.102	.006
32.956	.196	.007	32.999	.127	.006	33.519	.098	.007	32.983	.097	.006
34.005	.179	.007	34.049	.124	.006	34.587	.091	.007	34.032	.083	.005
35.054	.186	.007	35.099	.115	.006	35.655	.090	.007	35.082	.085	.005
36.102	.183	.007	36.149	.116	.006	36.724	.075	.006	36.131	.079	.005
37.151	.169	.006	37.199	.093	.005	37.792	.064	.006	37.180	.060	.004
38.200	.143	.006	38.249	.094	.005	38.860	.069	.006	38.230	.056	.004
39.248	.140	.006	39.299	.086	.005	39.928	.051	.005	39.279	.056	.004
40.297	.137	.006	40.349	.074	.005	40.996	.059	.006	40.329	.050	.004
41.345	.132	.006	41.399	.072	.005	42.064	.051	.005	41.378	.044	.004
42.394	.114	.005	42.449	.062	.004	43.132	.043	.005	42.428	.044	.004
43.443	.116	.005	43.499	.059	.004	44.200	.047	.005	43.477	.044	.004
44.491	.101	.005	44.549	.057	.004	45.269	.042	.005	44.527	.034	.003
45.540	.101	.005	45.599	.042	.004	46.337	.033	.004	45.576	.031	.003
46.588	.097	.005	46.649	.049	.004	47.405	.037	.004	46.625	.034	.003
47.637	.102	.005	47.699	.042	.004	48.473	.029	.004	47.675	.026	.003
48.686	.095	.005	48.749	.042	.004	49.541	.024	.004	48.724	.022	.003
49.734	.095	.005	49.798	.038	.003	50.609	.027	.004	49.774	.025	.003
50.783	.079	.004	50.848	.032	.003	51.677	.034	.004	50.823	.017	.002
51.832	.057	.004	51.898	.037	.003	52.746	.049	.005	51.873	.026	.003
52.880	.079	.004	52.948	.050	.004	53.814	.057	.005	52.922	.032	.003
53.929	.162	.006	53.998	.067	.004	54.882	.026	.004	53.972	.040	.004
54.977	.095	.005	55.048	.046	.004	55.950	.007	.002	55.021	.024	.003
56.026	.030	.003	56.098	.007	.001				56.071	.004	.001

TABLE A XII 4. Deuterons from ^{209}Bi Bombarded by 60-MeV Protons

90 deg - Run 5023			110 deg - Run 5036			135 deg - Run 2064			deg - Run		
Energy (MeV)	σ (mb·ster^{-1}·MeV^{-1})	Error	Energy (MeV)	σ (mb·ster^{-1}·MeV^{-1})	Error	Energy (MeV)	σ (mb·ster^{-1}·MeV^{-1})	Error	Energy (MeV)	σ (mb·ster^{-1}·MeV^{-1})	Error
1.497	0	0	1.450	0	0	1.48	0	0			
2.545	0	0	2.500	0	0	2.52	0	0			
3.593	.000	.000	3.550	0	0	3.56	0	0			
4.641	.010	.001	4.600	.007	.001	4.60	.01	.00			
5.690	.008	.001	5.650	.010	.001	5.64	.01	.00			
6.738	.012	.001	6.700	.006	.001	6.68	.01	.00			
7.786	.015	.002	7.750	.013	.001	7.72	.02	.00			
8.834	.035	.002	8.800	.029	.002	8.75	.03	.00			
9.882	.063	.003	9.850	.045	.003	9.79	.05	.00			
10.930	.096	.004	10.900	.071	.003	10.83	.08	.00			
11.978	.118	.004	11.950	.085	.004	11.87	.06	.00			
13.026	.158	.005	13.000	.106	.004	12.91	.05	.00			
14.074	.144	.005	14.050	.097	.004	13.95	.05	.00			
15.122	.153	.005	15.100	.105	.004	14.99	.06	.00			
16.170	.159	.005	16.150	.094	.004	16.03	.06	.00			
17.218	.144	.005	17.200	.096	.004	17.06	.06	.00			
18.266	.147	.005	18.250	.098	.004	18.10	.05	.00			
19.314	.142	.005	19.300	.084	.004	19.14	.05	.00			
20.363	.142	.005	20.350	.087	.004	20.18	.04	.00			
21.411	.130	.005	21.400	.079	.003	21.22	.04	.00			
22.459	.130	.005	22.450	.066	.003	22.26	.03	.00			
23.507	.121	.004	23.500	.068	.003	23.30	.03	.00			
24.555	.111	.004	24.550	.068	.003	24.33	.02	.00			
25.603	.121	.004	25.600	.064	.003	25.37	.02	.00			
26.651	.100	.004	26.650	.051	.003	26.41	.02	.00			
27.699	.096	.004	27.700	.048	.003	27.45	.01	.00			
28.747	.090	.004	28.750	.044	.003	28.49	.01	.00			
29.795	.085	.004	29.800	.039	.002	29.53	.01	.00			
30.843	.072	.003	30.850	.034	.002	30.57	.01	.00			
31.891	.072	.003	31.900	.028	.002	31.60	.01	.00			
32.939	.067	.003	32.950	.030	.002	32.64	.01	.00			
33.987	.059	.003	34.000	.027	.002	33.68	.01	.00			
35.035	.053	.003	35.050	.021	.002	34.72	.01	.00			
36.084	.047	.003	36.100	.017	.002	35.76	.01	.00			
37.132	.044	.003	37.150	.016	.002	36.80	.01	.00			
38.180	.043	.003	38.200	.017	.002	37.84	.01	.00			
39.228	.039	.003	39.250	.016	.002	38.88	.01	.00			
40.276	.032	.002	40.300	.012	.001	39.91	.01	.00			
41.324	.031	.002	41.350	.011	.001	40.95	.00	.00			
42.372	.027	.002	42.400	.010	.001	41.99	.00	.00			
43.420	.023	.002	43.450	.009	.001	43.03	.00	.00			
44.468	.022	.002	44.500	.008	.001	44.07	.00	.00			
45.516	.022	.002	45.550	.006	.001	45.11	.00	.00			
46.564	.021	.002	46.600	.006	.001	46.15	.00	.00			
47.612	.018	.002	47.650	.006	.001	47.18	.00	.00			
48.660	.018	.002	48.700	.005	.001	48.22	.00	.00			
49.708	.017	.002	49.750	.006	.001	49.26	.00	.00			
50.757	.011	.001	50.800	.004	.001	50.30	.00	.00			
51.805	.017	.002	51.850	.003	.001	51.34	.00	.00			
52.853	.016	.002	52.900	.003	.001	52.38	.00	.00			
53.901	.025	.002	53.950	.004	.001	53.42	.00	.00			
54.949	.008	.001	55.000	.001	.000	54.46	.00	.00			
55.997	.001	.000									

TABLE A XIII 1. Tritons from ^{209}Bi Bombarded by 60-MeV Protons

15 deg - Run 5030			20 deg - Run 5027			25 deg - Run 5026			30 deg - Run 5021		
Energy (MeV)	σ (mb·ster^{-1}·MeV^{-1})	Error	Energy (MeV)	σ (mb·ster^{-1}·MeV^{-1})	Error	Energy (MeV)	σ (mb·ster^{-1}·MeV^{-1})	Error	Energy (MeV)	σ (mb·ster^{-1}·MeV^{-1})	Error
1.50	0	0				1.50	0	0			
2.55	0	0	1.50	0	0	2.54	0	0	1.50	0	0
3.59	0	0	2.54	0	0	3.59	0	0	2.55	0	0
4.64	0	0	3.59	0	0	4.64	0	0	3.60	0	0
5.69	.00	.00	4.64	0	0	5.69	.00	.00	4.65	0	0
6.74	.01	.00	5.69	0	0	6.74	0	0	5.70	.00	.00
7.79	.01	.00	6.74	0	0	7.78	0	0	6.75	.00	.00
8.83	.01	.00	7.78	.00	.00	8.83	.01	.00	7.79	.00	.00
9.88	.02	.01	8.83	.01	.00	9.88	.04	.01	8.84	.02	.00
10.93	.08	.02	9.88	.04	.01	10.93	.08	.01	9.89	.05	.01
11.98	.10	.02	10.93	.10	.01	11.97	.07	.01	10.94	.08	.01
13.03	.12	.02	11.98	.11	.01	13.02	.12	.01	11.99	.11	.01
14.08	.15	.02	13.02	.14	.01	14.07	.14	.01	13.04	.13	.01
15.12	.21	.02	14.07	.17	.01	15.12	.22	.02	14.09	.18	.01
16.17	.25	.03	15.12	.24	.02	16.16	.20	.02	15.14	.26	.01
17.22	.19	.02	16.17	.21	.02	17.21	.20	.02	16.19	.22	.01
18.27	.17	.02	17.21	.22	.02	18.26	.16	.02	17.24	.21	.01
19.32	.18	.02	18.26	.21	.02	19.31	.20	.02	18.29	.21	.01
20.36	.21	.02	19.31	.25	.02	20.36	.24	.02	19.34	.24	.01
21.41	.22	.03	20.36	.21	.02	21.40	.19	.02	20.39	.19	.01
22.46	.23	.03	21.41	.20	.02	22.45	.18	.02	21.43	.22	.01
23.51	.20	.02	22.45	.21	.02	23.50	.18	.02	22.48	.21	.01
24.56	.21	.02	23.50	.20	.02	24.55	.22	.02	23.53	.21	.01
25.60	.16	.02	24.55	.20	.02	25.59	.17	.02	24.58	.18	.01
26.65	.16	.02	25.60	.20	.02	26.64	.18	.02	25.63	.20	.01
27.70	.19	.02	26.65	.16	.01	27.69	.17	.02	26.68	.17	.01
28.75	.17	.02	27.69	.21	.02	28.74	.19	.02	27.73	.17	.01
29.80	.16	.02	28.74	.17	.01	29.79	.17	.02	28.78	.16	.01
30.85	.15	.02	29.79	.18	.02	30.83	.15	.02	29.83	.16	.01
31.89	.17	.02	30.84	.19	.02	31.88	.17	.02	30.88	.16	.01
32.94	.16	.02	31.88	.17	.01	32.93	.14	.02	31.93	.14	.01
33.99	.17	.02	32.93	.15	.01	33.98	.16	.02	32.98	.15	.01
35.04	.16	.02	33.98	.17	.01	35.02	.12	.01	34.03	.14	.01
36.09	.17	.02	35.03	.14	.01	36.07	.12	.01	35.07	.13	.01
37.13	.15	.02	36.08	.16	.01	37.12	.09	.01	36.12	.13	.01
38.18	.15	.02	37.12	.16	.01	38.17	.10	.01	37.17	.14	.01
39.23	.14	.02	38.17	.14	.01	39.21	.13	.01	38.22	.12	.01
40.28	.15	.02	39.22	.13	.01	40.26	.12	.01	39.27	.11	.01
41.33	.21	.02	40.27	.12	.01	41.31	.13	.01	40.32	.11	.01
42.38	.15	.02	41.32	.13	.01	42.36	.08	.01	41.37	.09	.01
43.42	.15	.02	42.36	.14	.01	43.41	.10	.01	42.42	.10	.01
44.47	.15	.02	43.41	.13	.01	44.45	.10	.01	43.47	.10	.01
45.52	.16	.02	44.46	.18	.02	45.50	.10	.01	44.52	.11	.01
46.57	.17	.02	45.51	.14	.01	46.55	.10	.01	45.57	.10	.01
47.62	.16	.02	46.55	.13	.01	47.60	.09	.01	46.62	.10	.01
48.66	.12	.02	47.60	.14	.01	48.64	.06	.01	47.67	.08	.01
49.71	.14	.02	48.65	.11	.01	49.69	.07	.01	48.71	.06	.01
50.76	.09	.02	49.70	.14	.01	50.74	.04	.01	49.76	.09	.01
51.81	.17	.02	50.75	.08	.01	51.79	.09	.01	50.81	.04	.01
52.86	.10	.02	51.79	.09	.01	52.84	.04	.01	51.86	.07	.01
53.91	.02	.01	52.84	.09	.01	53.88	.01	.00	52.91	.05	.01
54.95	0	0	53.89	.02	.01	54.93	0	0	53.96	.01	.00
56.00	0	0	54.94	.00	.00	55.98	0	0	55.01	.00	.00
57.05	0	0							56.06	0	0
58.10	0	0									
59.15	0	0									

TABLE A XIII 2. Tritons from ^{209}Bi Bombarded by 60-MeV Protons

35 deg - Run 5025			40 deg - Run 5031			45 deg - Run 5024			50 deg - Run 5032		
Energy (MeV)	σ (mb·ster^{-1}·MeV^{-1})	Error (mb·ster^{-1}·MeV^{-1})	Energy (MeV)	σ (mb·ster^{-1}·MeV^{-1})	Error (mb·ster^{-1}·MeV^{-1})	Energy (MeV)	σ (mb·ster^{-1}·MeV^{-1})	Error (mb·ster^{-1}·MeV^{-1})	Energy (MeV)	σ (mb·ster^{-1}·MeV^{-1})	Error (mb·ster^{-1}·MeV^{-1})
1.50	0	0				1.50	0	0			
2.54	0	0	1.50	0	0	2.55	0	0	1.50	0	0
3.59	0	0	2.54	0	0	3.59	0	0	2.55	0	0
4.64	.00	.00	3.59	0	0	4.64	.00	.00	3.59	0	0
5.69	0	0	4.64	.00	.00	5.69	.00	.00	4.64	0	0
6.73	.00	.00	5.69	.00	.00	6.74	.00	.00	5.69	.00	.00
7.78	.00	.00	6.74	.00	.00	7.79	.01	.00	6.74	.00	.00
8.83	.01	.00	7.78	.01	.00	8.83	.01	.00	7.79	.00	.00
9.88	.05	.00	8.83	.02	.00	9.88	.04	.00	8.83	.01	.00
10.92	.09	.01	9.88	.05	.01	10.93	.08	.01	9.88	.04	.00
11.97	.11	.01	10.93	.08	.01	11.98	.10	.01	10.93	.07	.00
13.02	.14	.01	11.97	.11	.01	13.03	.12	.01	11.98	.08	.01
14.07	.15	.01	13.02	.13	.01	14.07	.15	.01	13.03	.09	.01
15.11	.21	.01	14.07	.16	.01	15.12	.19	.01	14.07	.12	.01
16.16	.19	.01	15.12	.21	.01	16.17	.17	.01	15.12	.16	.01
17.21	.21	.01	16.16	.20	.01	17.22	.17	.01	16.17	.15	.01
18.26	.19	.01	17.21	.20	.01	18.27	.16	.01	17.22	.16	.01
19.30	.20	.01	18.26	.19	.01	19.31	.18	.01	18.27	.15	.01
20.35	.21	.01	19.31	.19	.01	20.36	.16	.01	19.31	.15	.01
21.40	.20	.01	20.36	.19	.01	21.41	.15	.01	20.36	.15	.01
22.45	.20	.01	21.40	.19	.01	22.46	.14	.01	21.41	.12	.01
23.49	.18	.01	22.45	.19	.01	23.51	.14	.01	22.46	.13	.01
24.54	.20	.01	23.50	.17	.01	24.55	.15	.01	23.51	.12	.01
25.59	.17	.01	24.55	.15	.01	25.60	.15	.01	24.55	.13	.01
26.63	.15	.01	25.59	.16	.01	26.65	.12	.01	25.60	.12	.01
27.68	.16	.01	26.64	.13	.01	27.70	.12	.01	26.65	.11	.01
28.73	.15	.01	27.69	.14	.01	28.75	.11	.01	27.70	.10	.01
29.78	.13	.01	28.74	.13	.01	29.80	.10	.01	28.75	.08	.01
30.82	.13	.01	29.78	.12	.01	30.84	.09	.01	29.80	.09	.01
31.87	.13	.01	30.83	.12	.01	31.89	.09	.01	30.84	.09	.01
32.92	.12	.01	31.88	.10	.01	32.94	.09	.01	31.89	.07	.00
33.97	.14	.01	32.93	.12	.01	33.99	.07	.01	32.94	.08	.00
35.01	.11	.01	33.98	.11	.01	35.04	.07	.01	33.99	.06	.00
36.06	.10	.01	35.02	.09	.01	36.08	.07	.01	35.04	.06	.00
37.11	.08	.01	36.07	.09	.01	37.13	.06	.00	36.08	.06	.00
38.16	.09	.01	37.12	.09	.01	38.18	.06	.00	37.13	.05	.00
39.20	.09	.01	38.17	.09	.01	39.23	.05	.00	38.18	.05	.00
40.25	.09	.01	39.21	.08	.01	40.28	.05	.00	39.23	.05	.00
41.30	.08	.01	40.26	.08	.01	41.32	.06	.00	40.28	.04	.00
42.35	.08	.01	41.31	.08	.01	42.37	.05	.00	41.32	.04	.00
43.39	.07	.01	42.36	.06	.01	43.42	.05	.00	42.37	.03	.00
44.44	.08	.01	43.40	.07	.01	44.47	.05	.00	43.42	.03	.00
45.49	.07	.01	44.45	.05	.01	45.52	.05	.00	44.47	.03	.00
46.54	.08	.01	45.50	.06	.01	46.56	.04	.00	45.52	.03	.00
47.58	.06	.01	46.55	.06	.01	47.61	.03	.00	46.56	.02	.00
48.63	.05	.00	47.60	.05	.01	48.66	.03	.00	47.61	.02	.00
49.68	.04	.00	48.64	.05	.01	49.71	.02	.00	48.66	.01	.00
50.73	.02	.00	49.69	.05	.00	50.76	.01	.00	49.71	.01	.00
51.77	.04	.00	50.74	.03	.00	51.80	.02	.00	50.76	.01	.00
52.82	.03	.00	51.79	.03	.00	52.85	.01	.00	51.81	.01	.00
53.87	.01	.00	52.83	.03	.00	53.90	.00	.00	52.85	.01	.00
54.92	.00	.00	53.88	.01	.00	54.95	.00	.00	53.90	0	0
55.96	0	0				56.00	0	0	54.95	0	0
57.01	0	0				57.04	0	0	56.00	0	0
						58.09	0	0	57.05	0	0
						59.14	0	0	58.09	0	0
									59.14	0	0

TABLE A XIII 3. Tritons from ^{209}Bi Bombarded by 60-MeV Protons

60 deg - Run 5033			70 deg - Run 5037			75 deg - Run 7006			80 deg - Run 5035		
Energy (MeV)	σ (mb·ster^{-1}·MeV^{-1})	Error	Energy (MeV)	σ (mb·ster^{-1}·MeV^{-1})	Error	Energy (MeV)	σ (mb·ster^{-1}·MeV^{-1})	Error	Energy (MeV)	σ (mb·ster^{-1}·MeV^{-1})	Error
1.498	0	0	1.500	0	0	1.475	0	0	1.499	0	0
2.547	0	0	2.550	0	0	2.543	0	0	2.549	0	0
3.595	0	0	3.600	0	0	3.611	0	0	3.598	0	0
4.644	.000	.000	4.650	0	0	4.679	0	0	4.648	0	0
5.692	.004	.001	5.700	.000	.000	5.748	0	0	5.697	.001	.001
6.741	.004	.001	6.750	.001	.001	6.816	.004	.001	6.746	.000	.000
7.790	.004	.001	7.800	.002	.001	7.884	.001	.001	7.796	.003	.001
8.838	.010	.002	8.850	.005	.001	8.952	.009	.002	8.845	.014	.002
9.887	.042	.003	9.900	.035	.003	10.020	.021	.003	9.895	.025	.003
10.936	.068	.004	10.950	.053	.004	11.088	.053	.005	10.944	.047	.004
11.984	.084	.005	12.000	.065	.004	12.156	.061	.006	11.994	.064	.004
13.033	.087	.005	13.050	.069	.005	13.225	.075	.006	13.043	.066	.005
14.081	.110	.005	14.100	.074	.005	14.293	.085	.007	14.093	.074	.005
15.130	.142	.006	15.150	.110	.006	15.361	.103	.007	15.142	.099	.006
16.179	.131	.006	16.200	.104	.006	16.429	.097	.007	16.191	.085	.005
17.227	.137	.006	17.249	.089	.005	17.497	.093	.007	17.241	.082	.005
18.276	.126	.006	18.299	.091	.005	18.565	.072	.006	18.290	.078	.005
19.324	.114	.005	19.349	.086	.005	19.633	.076	.006	19.340	.075	.005
20.373	.115	.005	20.399	.089	.005	20.701	.062	.006	20.389	.072	.005
21.422	.105	.005	21.449	.064	.004	21.770	.059	.006	21.439	.065	.005
22.470	.110	.005	22.499	.070	.005	22.838	.044	.005	22.488	.052	.004
23.519	.104	.005	23.549	.065	.004	23.906	.054	.005	23.538	.060	.004
24.568	.100	.005	24.599	.068	.005	24.974	.053	.005	24.587	.059	.004
25.616	.097	.005	25.649	.049	.004	26.042	.041	.005	25.637	.047	.004
26.665	.077	.004	26.699	.048	.004	27.110	.038	.004	26.686	.044	.004
27.713	.072	.004	27.749	.051	.004	28.178	.035	.004	27.735	.033	.003
28.762	.067	.004	28.799	.042	.004	29.247	.036	.004	28.785	.032	.003
29.811	.070	.004	29.849	.037	.003	30.315	.024	.004	29.834	.026	.003
30.859	.060	.004	30.899	.033	.003	31.383	.026	.004	30.884	.021	.003
31.908	.060	.004	31.949	.039	.003	32.451	.022	.003	31.933	.026	.003
32.956	.058	.004	32.999	.031	.003	33.519	.018	.003	32.983	.015	.002
34.005	.050	.003	34.049	.024	.003	34.587	.014	.003	34.032	.014	.002
35.054	.049	.003	35.099	.021	.003	35.655	.011	.002	35.082	.016	.002
36.102	.042	.003	36.149	.024	.003	36.724	.013	.003	36.131	.014	.002
37.151	.037	.003	37.199	.018	.002	37.792	.011	.002	37.180	.010	.002
38.200	.033	.003	38.249	.016	.002	38.860	.013	.003	38.230	.010	.002
39.248	.029	.003	39.299	.016	.002	39.928	.005	.002	39.279	.011	.002
40.297	.024	.002	40.349	.011	.002	40.996	.004	.001	40.329	.007	.001
41.345	.020	.003	41.399	.011	.002	42.064	.008	.002	41.378	.008	.002
42.394	.021	.002	42.449	.011	.002	43.132	.007	.002	42.428	.004	.001
43.443	.022	.002	43.499	.009	.002	44.200	.007	.002	43.477	.002	.001
44.491	.021	.002	44.549	.006	.001	45.269	.004	.001	44.527	.002	.001
45.540	.019	.002	45.599	.007	.001	46.337	.005	.002	45.576	.001	.001
46.588	.015	.002	46.649	.006	.001	47.405	.002	.001	46.625	.001	.001
47.637	.013	.002	47.699	.004	.001	48.473	.003	.001	47.675	.001	.000
48.686	.012	.002	48.749	.004	.001	49.541	.001	.001	48.724	.001	.000
49.734	.011	.002	49.798	.001	.001	50.609	0	0	49.774	.000	.000
50.783	.007	.001	50.848	.001	.000	51.677	.001	.001	50.823	.000	.000
51.832	.008	.001	51.898	.001	.000	52.746	0	0	51.873	.000	.000
52.880	.004	.001	52.948	.000	.000	53.814	0	0	52.922	0	0
53.929	.002	.001	53.998	0	0	54.882	0	0	53.972	0	0
54.977	0	0	55.048	0	0	55.950	0	0	55.021	0	0
56.026	0	0	56.098	0	0	57.018	0	0	56.071	0	0
57.075	0	0	57.148	0	0	58.086	0	0	57.120	0	0
58.123	0	0	58.198	0	0	59.154	0	0	58.169	0	0
59.172	0	0	59.248	0	0				59.219	0	0

TABLE A XIII 4. Tritons from ^{209}Bi Bombarded by 60-MeV Protons

90 deg - Run 5023			110 deg - Run 5036			135 deg - Run 2064			deg - Run		
Energy (MeV)	σ (mb·ster^{-1}·MeV^{-1})	Error	Energy (MeV)	σ (mb·ster^{-1}·MeV^{-1})	Error	Energy (MeV)	σ (mb·ster^{-1}·MeV^{-1})	Error	Energy (MeV)	σ (mb·ster^{-1}·MeV^{-1})	Error
1.497	0	0	1.450	0	0	1.48	0	0			
2.545	0	0	2.500	0	0	2.52	0	0			
3.593	0	0	3.550	0	0	3.56	0	0			
4.641	.001	.000	4.600	.000	.000	4.60	0	0			
5.690	.003	.001	5.650	.004	.001	5.64	.00	.00			
6.738	.003	.001	6.700	.003	.001	6.68	.00	.00			
7.786	.008	.001	7.750	.003	.001	7.72	.01	.00			
8.834	.013	.001	8.800	.011	.001	8.75	.01	.00			
9.882	.027	.002	9.850	.019	.002	9.79	.02	.00			
10.930	.046	.003	10.900	.029	.002	10.83	.03	.00			
11.978	.056	.003	11.950	.039	.002	11.87	.03	.00			
13.026	.062	.003	13.000	.036	.002	12.91	.04	.00			
14.074	.066	.003	14.050	.032	.002	13.95	.03	.00			
15.122	.084	.004	15.100	.034	.003	14.99	.02	.00			
16.170	.078	.004	16.150	.042	.003	16.03	.02	.00			
17.218	.066	.003	17.200	.040	.003	17.06	.02	.00			
18.266	.056	.003	18.250	.036	.002	18.10	.02	.00			
19.314	.059	.003	19.300	.034	.002	19.14	.01	.00			
20.363	.050	.003	20.350	.027	.002	20.18	.01	.00			
21.411	.052	.003	21.400	.029	.002	21.22	.01	.00			
22.459	.047	.003	22.450	.023	.002	22.26	.01	.00			
23.507	.040	.003	23.500	.021	.002	23.30	.01	.00			
24.555	.035	.002	24.550	.018	.002	24.33	.01	.00			
25.603	.036	.002	25.600	.015	.002	25.37	.01	.00			
26.651	.029	.002	26.650	.014	.001	26.41	.01	.00			
27.699	.030	.002	27.700	.014	.001	27.45	.00	.00			
28.747	.024	.002	28.750	.012	.001	28.49	.00	.00			
29.795	.022	.002	29.800	.009	.001	29.53	.00	.00			
30.843	.020	.002	30.850	.008	.001	30.57	.00	.00			
31.891	.018	.002	31.900	.008	.001	31.60	.00	.00			
32.939	.018	.002	32.950	.007	.001	32.64	.00	.00			
33.987	.014	.002	34.000	.005	.001	33.68	.00	.00			
35.035	.014	.002	35.050	.005	.001	34.72	.00	.00			
36.084	.014	.002	36.100	.004	.001	35.76	.00	.00			
37.132	.008	.001	37.150	.003	.001	36.80	.00	.00			
38.180	.008	.001	38.200	.003	.001	37.84	.00	.00			
39.228	.006	.001	39.250	.003	.001	38.88	.00	.00			
40.276	.007	.001	40.300	.001	.000	39.91	.00	.00			
41.324	.005	.001	41.350	.003	.001	40.95	.00	.00			
42.372	.005	.001	42.400	.002	.001	41.99	.00	.00			
43.420	.005	.001	43.450	.002	.001	43.03	.00	.00			
44.468	.003	.001	44.500	.002	.001	44.07	.00	.00			
45.516	.003	.001	45.550	.001	.000	45.11	.00	.00			
46.564	.004	.001	46.600	.001	.000	46.15	.00	.00			
47.612	.001	.000	47.650	.001	.000	47.18	.00	.00			
48.660	.002	.001	48.700	.001	.000	48.22	0	0			
49.708	.002	.001	49.750	.000	.000	49.26	.00	.00			
50.757	.002	.001	50.800	.001	.000	50.30	.00	.00			
51.805	.001	.000	51.850	0	0	51.34	.00	.00			
52.853	.000	.000	52.900	.000	.000						
53.901	.000	.000	53.950	.000	.000						
54.949	.000	.000	55.000	0	0						
55.997	0	0	56.050	0	0						
57.045	0	0	57.100	0	0						
58.093	0	0	58.150	0	0						
59.141	0	0	59.200	0	0						

TABLE A XIV 1. Helium-3's from ^{209}Bi Bombarded by 60-MeV Protons

15 deg - Run 5030			20 deg - Run 5027			25 deg - Run 5026			30 deg - Run 5021		
Energy (MeV)	σ (mb·ster^{-1}·MeV^{-1})	Error	Energy (MeV)	σ (mb·ster^{-1}·MeV^{-1})	Error	Energy (MeV)	σ (mb·ster^{-1}·MeV^{-1})	Error	Energy (MeV)	σ (mb·ster^{-1}·MeV^{-1})	Error
1.50	0	0	1.50	0	0	1.50	0	0	1.50	0	0
2.55	0	0	2.54	0	0	2.54	0	0	2.55	0	0
3.59	0	0	3.59	0	0	3.59	0	0	3.60	0	0
4.64	0	0	4.64	0	0	4.64	0	0	4.65	0	0
5.69	0	0	5.69	0	0	5.69	0	0	5.70	0	0
6.74	0	0	6.74	0	0	6.74	0	0	6.75	0	0
7.79	0	0	7.78	0	0	7.78	0	0	7.79	0	0
8.83	0	0	8.83	0	0	8.83	0	0	8.84	0	0
9.88	0	0	9.88	0	0	9.88	0	0	9.89	0	0
10.93	0	0	10.93	0	0	10.93	0	0	10.94	0	0
11.98	0	0	11.98	.00	.00	11.97	0	0	11.99	0	0
13.03	0	0	13.02	0	0	13.02	0	0	13.04	0	0
14.08	0	0	14.07	.00	.00	14.07	0	0	14.09	0	0
15.12	0	0	15.12	0	0	15.12	0	0	15.14	0	0
16.17	0	0	16.17	0	0	16.16	0	0	16.19	0	0
17.22	0	0	17.21	0	0	17.21	0	0	17.24	0	0
18.27	0	0	18.26	0	0	18.26	0	0	18.29	0	0
19.32	0	0	19.31	0	0	19.31	0	0	19.34	.00	.00
20.36	0	0	20.36	.00	.00	20.36	0	0	20.39	.00	.00
21.41	0	0	21.41	0	0	21.40	0	0	21.43	.00	.00
22.46	.01	.00	22.45	.00	.00	22.45	0	0	22.48	.00	.00
23.51	.00	.00	23.50	0	0	23.50	.00	.00	23.53	.00	.00
24.56	0	0	24.55	0	0	24.55	0	0	24.58	.00	.00
25.60	0	0	25.60	.00	.00	25.59	.00	.00	25.63	.01	.00
26.65	0	0	26.65	.00	.00	26.64	.00	.00	26.68	.00	.00
27.70	0	0	27.69	.01	.00	27.69	.00	.00	27.73	.01	.00
28.75	.02	.01	28.74	.01	.00	28.74	.00	.00	28.78	.01	.00
29.80	.00	.00	29.79	.00	.00	29.79	.00	.00	29.83	.01	.00
30.85	.02	.01	30.84	.01	.00	30.83	.01	.00	30.88	.02	.00
31.89	.01	.01	31.88	.01	.00	31.88	.01	.00	31.93	.02	.00
32.94	.03	.01	32.93	.04	.01	32.93	.01	.00	32.98	.03	.00
33.99	.01	.00	33.98	.02	.00	33.98	.01	.00	34.03	.01	.00
35.04	.00	.00	35.03	.01	.00	35.02	.00	.00	35.07	.01	.00
36.09	.01	.01	36.08	.01	.00	36.07	.01	.00	36.12	.02	.00
37.13	0	0	37.12	.01	.00	37.12	.01	.00	37.17	.01	.00
38.18	0	0	38.17	.01	.00	38.17	.02	.01	38.22	.01	.00
39.23	.00	.00	39.22	.01	.00	39.21	.01	.00	39.27	.01	.00
40.28	.01	.00	40.27	.01	.00	40.26	.01	.00	40.32	.01	.00
41.33	.00	.00	41.32	.02	.01	41.31	.00	.00	41.37	.02	.00
42.38	.02	.01	42.36	.01	.00	42.36	.01	.00	42.42	.01	.00
43.42	.01	.00	43.41	.02	.00	43.41	.01	.00	43.47	.02	.00
44.47	.01	.00	44.46	.01	.00	44.45	.01	.00	44.52	.02	.00
45.52	.01	.00	45.51	.01	.00	45.50	.01	.00	45.57	.01	.00
46.57	.01	.00	46.55	.01	.00	46.55	.00	.00	46.62	.01	.00
47.62	.02	.01	47.60	.01	.00	47.60	.00	.00	47.67	.01	.00
48.66	.01	.00	48.65	.02	.01	48.64	.01	.00	48.71	.01	.00
49.71	.02	.01	49.70	.02	.00	49.69	.01	.00	49.76	.02	.00
50.76	.04	.01	50.75	.05	.01	50.74	.04	.01	50.81	.04	.00
51.81	.05	.01	51.79	.06	.01	51.79	.02	.01	51.86	.03	.00
52.86	.03	.01	52.84	.03	.01	52.84	.01	.00	52.91	.01	.00
53.91	.01	.00	53.89	.00	.00	53.88	0	0	53.96	.00	.00
54.95	0	0	54.94	0	0	54.93	.00	.00	55.01	0	0
56.00	.00	.00	55.98	0	0	55.98	0	0	56.06	0	0
57.05	.00	.00	57.03	0	0	57.03	0	0	57.11	.00	.00
58.10	0	0				58.07	0	0	58.16	0	0
59.15	0	0				59.12	0	0	59.21	0	0
60.19	0	0							60.26	0	0

TABLE A XIV 2. Helium-3's from ^{209}Bi Bombarded by 60-MeV Protons

35 deg - Run 5025			40 deg - Run 5031			45 deg - Run 5024			50 deg - Run 5032		
Energy (MeV)	σ (mb·ster^{-1}·MeV^{-1})	Error	Energy (MeV)	σ (mb·ster^{-1}·MeV^{-1})	Error	Energy (MeV)	σ (mb·ster^{-1}·MeV^{-1})	Error	Energy (MeV)	σ (mb·ster^{-1}·MeV^{-1})	Error
1.50	0	0				1.50	0	0			
2.54	0	0	1.50	0	0	2.55	0	0	1.50	0	0
3.59	0	0	2.54	0	0	3.59	0	0	2.55	0	0
4.64	0	0	3.59	0	0	4.64	0	0	3.59	0	0
5.69	0	0	4.64	0	0	5.69	0	0	4.64	0	0
6.73	0	0	5.69	0	0	6.74	0	0	5.69	0	0
7.78	0	0	6.74	0	0	7.79	0	0	6.74	0	0
8.83	0	0	7.78	0	0	8.83	0	0	7.79	0	0
9.88	0	0	8.83	0	0	9.88	0	0	8.83	0	0
10.92	0	0	9.88	0	0	10.93	0	0	9.88	0	0
11.97	0	0	10.93	.00	.00	11.98	0	0	10.93	0	0
13.02	0	0	11.97	.00	.00	13.03	0	0	11.98	0	0
14.07	0	0	13.02	.00	.00	14.07	0	0	13.03	0	0
15.11	0	0	14.07	.00	.00	15.12	0	0	14.07	0	0
16.16	0	0	15.12	.00	.00	16.17	0	0	15.12	0	0
17.21	0	0	16.16	.00	.00	17.22	0	0	16.17	0	0
18.26	0	0	17.21	.00	.00	18.27	.00	.00	17.22	0	0
19.30	0	0	18.26	.00	.00	19.31	.00	.00	18.27	0	0
20.35	0	0	19.31	.00	.00	20.36	.00	.00	19.31	0	0
21.40	.00	.00	20.36	.00	.00	21.41	0	0	20.36	.00	.00
22.45	.00	.00	21.40	.00	.00	22.46	.00	.00	21.41	0	0
23.49	.00	.00	22.45	.01	.00	23.51	.00	.00	22.46	0	0
24.54	.00	.00	23.50	.01	.00	24.55	.00	.00	23.51	.00	.00
25.59	.00	.00	24.55	.01	.00	25.60	.01	.00	24.55	.00	.00
26.63	.00	.00	25.59	.01	.00	26.65	.00	.00	25.60	.01	.00
27.68	.01	.00	26.64	.01	.00	27.70	.00	.00	26.65	.00	.00
28.73	.01	.00	27.69	.01	.00	28.75	.01	.00	27.70	.01	.00
29.78	.01	.00	28.74	.01	.00	29.80	.01	.00	28.75	.01	.00
30.82	.01	.00	29.78	.01	.00	30.84	.01	.00	29.80	.01	.00
31.87	.01	.00	30.83	.02	.00	31.89	.01	.00	30.84	.01	.00
32.92	.03	.00	31.88	.03	.00	32.94	.02	.00	31.89	.02	.00
33.97	.01	.00	32.93	.03	.00	33.99	.01	.00	32.94	.03	.00
35.01	.02	.00	33.98	.02	.00	35.04	.01	.00	33.99	.01	.00
36.06	.01	.00	35.02	.02	.00	36.08	.01	.00	35.04	.01	.00
37.11	.02	.00	36.07	.02	.00	37.13	.01	.00	36.08	.01	.00
38.16	.01	.00	37.12	.02	.00	38.18	.01	.00	37.13	.00	.00
39.20	.01	.00	38.17	.01	.00	39.23	.01	.00	38.18	.00	.00
40.25	.01	.00	39.21	.01	.00	40.28	.01	.00	39.23	.01	.00
41.30	.01	.00	40.26	.02	.00	41.32	.01	.00	40.28	.01	.00
42.35	.01	.00	41.31	.02	.00	42.37	.01	.00	41.32	.00	.00
43.39	.01	.00	42.36	.02	.00	43.42	.01	.00	42.37	.00	.00
44.44	.01	.00	43.40	.02	.00	44.47	.01	.00	43.42	.01	.00
45.49	.01	.00	44.45	.01	.00	45.52	.00	.00	44.47	.00	.00
46.54	.01	.00	45.50	.01	.00	46.56	.01	.00	45.52	.00	.00
47.58	.01	.00	46.55	.01	.00	47.61	.01	.00	46.56	.00	.00
48.63	.01	.00	47.60	.01	.00	48.66	.01	.00	47.61	.00	.00
49.68	.01	.00	48.64	.01	.00	49.71	.01	.00	48.66	.01	.00
50.73	.02	.00	49.69	.02	.00	50.76	.01	.00	49.71	.01	.00
51.77	.02	.00	50.74	.02	.00	51.80	.01	.00	50.76	.01	.00
52.82	.02	.00	51.79	.03	.00	52.85	.00	.00	51.81	.01	.00
53.87	.00	.00	52.83	.01	.00	53.90	0	0	52.85	.00	.00
54.92	.00	.00	53.88	.00	.00	54.95	0	0	53.90	0	0
55.96	.00	.00	54.93	.00	.00	56.00	0	0	54.95	0	0
57.01	0	0				57.04	0	0	56.00	0	0
						58.09	0	0	57.05	0	0
						59.14	0	0	58.09	0	0
									59.14	0	0

TABLE A XIV 3. Helium-3's from ^{209}Bi Bombarded by 60-MeV Protons

60 deg - Run 5033			70 deg - Run 5037			75 deg - Run 7006			80 deg - Run 5035		
Energy (MeV)	σ (mb·ster^{-1}·MeV^{-1})	Error	Energy (MeV)	σ (mb·ster^{-1}·MeV^{-1})	Error	Energy (MeV)	σ (mb·ster^{-1}·MeV^{-1})	Error	Energy (MeV)	σ (mb·ster^{-1}·MeV^{-1})	Error
1.498	0	0	1.500	0	0	1.475	0	0	1.499	0	0
2.547	0	0	2.550	0	0	2.543	0	0	2.549	0	0
3.595	0	0	3.600	0	0	3.611	0	0	3.598	0	0
4.644	0	0	4.650	0	0	4.679	0	0	4.648	0	0
5.692	0	0	5.700	0	0	5.748	0	0	5.697	0	0
6.741	0	0	6.750	0	0	6.816	0	0	6.746	0	0
7.790	0	0	7.800	0	0	7.884	0	0	7.796	0	0
8.838	0	0	8.850	0	0	8.952	0	0	8.845	0	0
9.887	0	0	9.900	0	0	10.020	0	0	9.895	0	0
10.936	0	0	10.950	0	0	11.088	0	0	10.944	0	0
11.984	.001	.001	12.000	0	0	12.156	.001	.001	11.994	0	0
13.033	.001	.001	13.050	0	0	13.225	0	0	13.043	0	0
14.081	.000	.000	14.100	0	0	14.293	0	0	14.093	.000	.000
15.130	.000	.000	15.150	0	0	15.361	0	0	15.142	0	0
16.179	0	0	16.200	0	0	16.429	0	0	16.191	0	0
17.227	.001	.000	17.249	0	0	17.497	0	0	17.241	0	0
18.276	.000	.000	18.299	0	0	18.565	0	0	18.290	0	0
19.324	.002	.001	19.349	0	0	19.633	0	0	19.340	0	0
20.373	.000	.000	20.399	0	0	20.701	0	0	20.389	.000	.000
21.422	.002	.001	21.449	.001	.000	21.770	.001	.001	21.439	.000	.000
22.470	.003	.001	22.499	.001	.001	22.838	0	0	22.488	.000	.000
23.519	.004	.001	23.549	.001	.001	23.906	0	0	23.538	.001	.000
24.568	.005	.001	24.599	0	0	24.974	0	0	24.587	0	0
25.616	.007	.001	25.649	.001	.001	26.042	.001	.001	25.637	.002	.001
26.665	.006	.001	26.699	.003	.001	27.110	.001	.001	26.686	.001	.001
27.713	.008	.001	27.749	.002	.001	28.178	.005	.002	27.735	.003	.001
28.762	.011	.002	28.799	.004	.001	29.247	.001	.001	28.785	.002	.001
29.811	.011	.002	29.849	.004	.001	30.315	.001	.001	29.834	.004	.001
30.859	.013	.002	30.899	.008	.002	31.383	.002	.001	30.884	.003	.001
31.908	.014	.002	31.949	.008	.002	32.451	.001	.001	31.933	.003	.001
32.956	.020	.002	32.999	.015	.002	33.519	.001	.001	32.983	.008	.002
34.005	.018	.002	34.049	.005	.001	34.587	.001	.001	34.032	.003	.001
35.054	.011	.002	35.099	.003	.001	35.655	.002	.001	35.082	.002	.001
36.102	.011	.002	36.149	.003	.001	36.724	.001	.001	36.131	.003	.001
37.151	.008	.001	37.199	.001	.001	37.792	.001	.001	37.180	.003	.001
38.200	.009	.001	38.249	.002	.001	38.860	.002	.001	38.230	.002	.001
39.248	.008	.001	39.299	.002	.001	39.928	.001	.001	39.279	.000	.000
40.297	.008	.001	40.349	.002	.001	40.996	.001	.001	40.329	.001	.001
41.345	.006	.001	41.399	.003	.001	42.064	.001	.001	41.378	.000	.000
42.394	.009	.001	42.449	.002	.001	43.132	.001	.001	42.428	.000	.000
43.443	.007	.001	43.499	.001	.001	44.200	.001	.001	43.477	.001	.001
44.491	.007	.001	44.549	.002	.001	45.269	.001	.001	44.527	.002	.001
45.540	.006	.001	45.599	0	0	46.337	.001	.001	45.576	.001	.001
46.588	.005	.001	46.649	.001	.001	47.405	0	0	46.625	.000	.000
47.637	.002	.001	47.699	.000	.000	48.473	.001	.001	47.675	0	0
48.686	.006	.001	48.749	0	0	49.541	.001	.001	48.724	.001	.000
49.734	.004	.001	49.798	.001	.000	50.609	.001	.001	49.774	.000	.000
50.783	.007	.001	50.848	.000	.000	51.677	0	0	50.823	0	0
51.832	.004	.001	51.898	.000	.000	52.746	0	0	51.873	0	0
52.880	.003	.001	52.948	0	0	53.814	0	0	52.922	.000	.000
53.929	.000	.000	53.998	0	0	54.882	0	0	53.972	0	0
54.977	.001	.000	55.048	0	0	55.950	0	0	55.021	0	0
56.026	.000	.000	56.098	0	0	57.018	0	0	56.071	0	0
57.075	.000	.000	57.148	0	0	58.086	0	0	57.120	0	0
58.123	0	0	58.198	0	0	59.154	0	0	58.169	0	0
59.172	0	0	59.248	0	0				59.219	0	0

TABLE A XIV 4. Helium-3's from ^{209}Bi Bombarded by 60-MeV Protons

90 deg - Run 5023			110 deg - Run 5036			135 deg - Run 2064			deg - Run		
Energy (MeV)	σ	Error	Energy (MeV)	σ	Error	Energy (MeV)	σ	Error	Energy (MeV)	σ	Error
	(mb·ster^{-1}·MeV^{-1})			(mb·ster^{-1}·MeV^{-1})			(mb·ster^{-1}·MeV^{-1})			(mb·ster^{-1}·MeV^{-1})	
1.497	0	0	1.450	0	0	1.48	0	0			
2.545	0	0	2.500	0	0	2.52	0	0			
3.593	0	0	3.550	0	0	3.56	0	0			
4.641	0	0	4.600	0	0	4.60	0	0			
5.690	0	0	5.650	0	0	5.64	0	0			
6.738	0	0	6.700	0	0	6.68	0	0			
7.786	0	0	7.750	0	0	7.72	0	0			
8.834	0	0	8.800	0	0	8.75	0	0			
9.882	0	0	9.850	0	0	9.79	0	0			
10.930	0	0	10.900	0	0	10.83	0	0			
11.978	.001	.000	11.950	.000	.000	11.87	0	0			
13.026	0	0	13.000	.000	.000	12.91	.00	.00			
14.074	.000	.000	14.050	0	0	13.95	.00	.00			
15.122	.001	.000	15.100	.001	.000	14.99	0	0			
16.170	.000	.000	16.150	.000	.000	16.03	0	0			
17.218	.000	.000	17.200	.000	.000	17.06	0	0			
18.266	0	0	18.250	0	0	18.10	.00	.00			
19.314	.001	.000	19.300	.001	.000	19.14	.00	.00			
20.363	.001	.000	20.350	.001	.000	20.18	.00	.00			
21.411	.001	.000	21.400	.002	.001	21.22	.00	.00			
22.459	.002	.001	22.450	.002	.001	22.26	.00	.00			
23.507	.003	.001	23.500	.001	.000	23.30	.00	.00			
24.555	.004	.001	24.550	.002	.001	24.33	.00	.00			
25.603	.004	.001	25.600	.002	.001	25.37	.00	.00			
26.651	.004	.001	26.650	.002	.001	26.41	.00	.00			
27.699	.004	.001	27.700	.002	.001	27.45	.00	.00			
28.747	.004	.001	28.750	.003	.001	28.49	.00	.00			
29.795	.005	.001	29.800	.003	.001	29.53	.00	.00			
30.843	.003	.001	30.850	.004	.001	30.57	.00	.00			
31.891	.004	.001	31.900	.004	.001	31.60	.00	.00			
32.939	.007	.001	32.950	.003	.001	32.64	0	0			
33.987	.005	.001	34.000	.003	.001	33.68	.00	.00			
35.035	.004	.001	35.050	.001	.000	34.72	.00	.00			
36.084	.005	.001	36.100	.002	.001	35.76	.00	.00			
37.132	.003	.001	37.150	.002	.001	36.80	.00	.00			
38.180	.003	.001	38.200	.002	.001	37.84	.00	.00			
39.228	.003	.001	39.250	.001	.000	38.88	.00	.00			
40.276	.003	.001	40.300	.001	.000	39.91	.00	.00			
41.324	.003	.001	41.350	.001	.000						
42.372	.002	.001	42.400	.001	.000						
43.420	.003	.001	43.450	.001	.000						
44.468	.001	.000	44.500	.000	.000						
45.516	.002	.001	45.550	.000	.000						
46.564	.002	.001	46.600	.000	.000						
47.612	.002	.001	47.650	.000	.000						
48.660	.001	.000	48.700	.000	.000						
49.708	.001	.000	49.750	0	0						
50.757	.001	.000	50.800	.000	.000						
51.805	.001	.000	51.850	.000	.000						
52.853	0	0	52.900	0	0						
53.901	0	0	53.950	0	0						
54.949	.000	.000	55.000	0	0						
55.997	0	0	56.050	0	0						
57.045	0	0	57.100	0	0						
58.093	0	0	58.150	0	0						
59.141	0	0	59.200	0	0						

TABLE A XV 1. Alphas from ^{209}Bi Bombarded by 60-MeV Protons

15 deg - Run 5030			20 deg - Run 5027			25 deg - Run 5026			30 deg - Run 5021		
Energy (MeV)	σ (mb·ster^{-1}·MeV^{-1})	Error	Energy (MeV)	σ (mb·ster^{-1}·MeV^{-1})	Error	Energy (MeV)	σ (mb·ster^{-1}·MeV^{-1})	Error	Energy (MeV)	σ (mb·ster^{-1}·MeV^{-1})	Error
			1,50	0	0	1,50	0	0			
1,50	0	0	2,54	0	0	2,54	0	0	1,50	0	0
2,55	0	0	3,59	0	0	3,59	0	0	2,55	0	0
						4,64	0	0	3,60	0	0
3,59	0	0	4,64	0	0	5,69	0	0	4,65	0	0
4,64	0	0	5,69	0	0	6,74	0	0	5,70	0	0
5,69	0	0	6,74	0	0	7,78	0	0	6,75	0	0
6,74	0	0	7,78	0	0	8,83	0	0	7,79	0	0
7,79	0	0	8,83	0	0	9,88	0	0	8,84	0	0
8,83	0	0	9,88	0	0	10,93	0	0	9,89	0	0
9,88	0	0	10,93	0	0	11,97	0	0	10,94	0	0
10,93	0	0	11,98	0	0	13,02	0	0	11,99	,00	,00
11,98	0	0	13,02	0	0	14,07	,01	,00	13,04	,00	,00
13,03	,00	,00	14,07	,00	,00	15,12	,01	,00	14,09	,01	,00
14,08	,00	,00	15,12	,01	,00	16,16	,02	,01	15,14	,01	,00
15,12	0	0	16,17	,02	,00	17,21	,04	,01	16,19	,04	,00
16,17	,02	,01	17,21	,04	,01	18,26	,09	,01	17,24	,08	,01
17,22	,04	,01	18,26	,12	,01	19,31	,15	,02	18,29	,11	,01
18,27	,07	,01	19,31	,16	,01	20,36	,16	,02	19,34	,14	,01
19,32	,14	,02	20,36	,22	,02	21,40	,19	,02	20,39	,20	,01
20,36	,20	,02	21,41	,23	,02	22,45	,26	,02	21,43	,24	,01
21,41	,23	,03	22,45	,26	,02	23,50	,24	,02	22,48	,26	,01
22,46	,23	,03	23,50	,29	,02	24,55	,27	,02	23,53	,29	,01
23,51	,28	,03	24,55	,30	,02	25,59	,30	,02	24,58	,27	,01
24,56	,30	,03	25,60	,32	,02	26,64	,25	,02	25,63	,27	,01
25,60	,27	,03	26,65	,30	,02	27,69	,27	,02	26,68	,29	,01
26,65	,26	,03	27,69	,29	,02	28,74	,25	,02	27,73	,26	,01
27,70	,24	,03	28,74	,27	,02	29,79	,21	,02	28,78	,24	,01
28,75	,29	,03	29,79	,22	,02	30,83	,20	,02	29,83	,22	,01
29,80	,24	,03	30,84	,24	,02	31,88	,15	,02	30,88	,20	,01
30,85	,20	,02	31,88	,24	,02	32,93	,17	,02	31,93	,18	,01
31,89	,22	,02	32,93	,21	,02	33,98	,13	,01	32,98	,16	,01
32,94	,17	,02	33,98	,19	,01	35,02	,13	,01	34,03	,13	,01
33,99	,10	,02	35,03	,15	,01	36,07	,10	,01	35,07	,12	,01
35,04	,15	,02	36,08	,11	,01	37,12	,25	,02	36,12	,08	,01
36,09	,07	,01	37,12	,27	,02	38,17	,15	,02	37,17	,22	,01
37,13	,24	,03	38,17	,19	,02	39,21	,15	,02	38,22	,17	,01
38,18	,23	,03	39,22	,14	,01	40,26	,09	,01	39,27	,15	,01
39,23	,13	,02	40,27	,11	,01	41,31	,12	,01	40,32	,12	,01
40,28	,16	,02	41,32	,15	,01	42,36	,10	,01	41,37	,11	,01
41,33	,13	,02	42,36	,13	,01	43,41	,09	,01	42,42	,10	,01
42,38	,13	,02	43,41	,11	,01	44,45	,08	,01	43,47	,09	,01
43,42	,10	,02	44,46	,12	,01	45,50	,07	,01	44,52	,08	,01
44,47	,10	,02	45,51	,10	,01	46,55	,07	,01	45,57	,07	,01
45,52	,07	,01	46,55	,09	,01	47,60	,06	,01	46,62	,07	,01
46,57	,06	,01	47,60	,09	,01	48,64	,04	,01	47,67	,06	,01
47,62	,06	,01	48,65	,07	,01	49,69	,04	,01	48,71	,05	,01
48,66	,05	,01	49,70	,08	,01	50,74	,05	,01	49,76	,06	,01
49,71	,04	,01	50,75	,05	,01	51,79	,04	,01	50,81	,05	,01
50,76	,05	,01	51,79	,05	,01	52,84	,04	,01	51,86	,04	,00
51,81	,05	,01	52,84	,06	,01	53,88	,03	,01	52,91	,04	,00
52,86	,05	,01	53,89	,06	,01	54,93	,03	,01	53,96	,03	,00
53,91	,05	,01	54,94	,04	,01	55,98	,02	,01	55,01	,03	,00
54,95	,02	,01	55,98	,03	,01	57,03	,03	,01	56,06	,03	,00
56,00	,04	,01	57,03	,04	,01	58,07	,03	,01	57,11	,03	,00
57,05	,02	,01	58,08	,06	,01	59,12	,04	,01	58,16	,03	,00
58,10	,06	,01	59,13	,05	,01	60,17	,04	,01	59,21	,02	,00
59,15	,04	,01	60,18	,04	,01				60,26	,02	,00
60,19	,04	,01									

TABLE A XV 2. Alphas from ^{209}Bi Bombarded by 60-MeV Protons

35 deg - Run 5025			40 deg - Run 5031			45 deg - Run 5024			50 deg - Run 5032		
Energy (MeV)	σ	Error	Energy (MeV)	σ	Error	Energy (MeV)	σ	Error	Energy (MeV)	σ	Error
	(mb·ster^{-1}·MeV^{-1})			(mb·ster^{-1}·MeV^{-1})			(mb·ster^{-1}·MeV^{-1})			(mb·ster^{-1}·MeV^{-1})	
1.50	0	0				1.50	0	0			
2.54	0	0	1.50	0	0	2.55	0	0	1.50	0	0
3.59	0	0	2.54	0	0	3.59	0	0	2.55	0	0
4.64	0	0	3.59	0	0	4.64	0	0	3.59	0	0
5.69	0	0	4.64	0	0	5.69	0	0	4.64	0	0
6.73	0	0	5.69	0	0	6.74	0	0	5.69	0	0
7.78	0	0	6.74	0	0	7.79	0	0	6.74	0	0
8.83	0	0	7.78	0	0	8.83	0	0	7.79	0	0
9.88	0	0	8.83	0	0	9.88	0	0	8.83	0	0
10.92	0	0	9.88	0	0	10.93	0	0	9.88	0	0
11.97	0	0	10.93	0	0	11.98	0	0	10.93	0	0
13.02	.00	.00	11.97	.00	.00	13.03	.00	.00	11.98	.00	.00
14.07	.01	.00	13.02	.01	.00	14.07	.00	.00	13.03	.00	.00
15.11	.01	.00	14.07	.01	.00	15.12	.01	.00	14.07	.01	.00
16.16	.03	.00	15.12	.02	.00	16.17	.03	.00	15.12	.02	.00
17.21	.05	.01	16.16	.04	.00	17.22	.07	.01	16.17	.03	.00
18.26	.11	.01	17.21	.07	.01	18.27	.11	.01	17.22	.07	.00
19.30	.16	.01	18.26	.12	.01	19.31	.14	.01	18.27	.10	.01
20.35	.17	.01	19.31	.16	.01	20.36	.18	.01	19.31	.13	.01
21.40	.21	.01	20.36	.18	.01	21.41	.21	.01	20.36	.16	.01
22.45	.24	.01	21.40	.21	.01	22.46	.23	.01	21.41	.17	.01
23.49	.27	.01	22.45	.23	.01	23.51	.21	.01	22.46	.18	.01
24.54	.28	.01	23.50	.23	.01	24.55	.23	.01	23.51	.20	.01
25.59	.27	.01	24.55	.26	.01	25.60	.23	.01	24.55	.20	.01
26.63	.24	.01	25.59	.24	.01	26.65	.24	.01	25.60	.18	.01
27.68	.25	.01	26.64	.26	.01	27.70	.22	.01	26.65	.18	.01
28.73	.23	.01	27.69	.24	.01	28.75	.19	.01	27.70	.17	.01
29.78	.22	.01	28.74	.20	.01	29.80	.18	.01	28.75	.14	.01
30.82	.19	.01	29.78	.21	.01	30.84	.17	.01	29.80	.13	.01
31.87	.17	.01	30.83	.17	.01	31.89	.14	.01	30.84	.11	.01
32.92	.16	.01	31.88	.17	.01	32.94	.13	.01	31.89	.09	.01
33.97	.13	.01	32.93	.15	.01	33.99	.13	.01	32.94	.08	.01
35.01	.13	.01	33.98	.13	.01	35.04	.11	.01	33.99	.06	.00
36.06	.09	.01	35.02	.12	.01	36.08	.08	.01	35.04	.06	.00
37.11	.21	.01	36.07	.08	.01	37.13	.13	.01	36.08	.04	.00
38.16	.16	.01	37.12	.17	.01	38.18	.10	.01	37.13	.13	.01
39.20	.13	.01	38.17	.14	.01	39.23	.10	.01	38.18	.10	.01
40.25	.11	.01	39.21	.11	.01	40.28	.08	.01	39.23	.07	.00
41.30	.10	.01	40.26	.09	.01	41.32	.07	.01	40.28	.06	.00
42.35	.07	.01	41.31	.08	.01	42.37	.06	.00	41.32	.05	.00
43.39	.08	.01	42.36	.09	.01	43.42	.05	.00	42.37	.05	.00
44.44	.07	.01	43.40	.06	.01	44.47	.05	.00	43.42	.04	.00
45.49	.07	.01	44.45	.08	.01	45.52	.05	.00	44.47	.04	.00
46.54	.05	.00	45.50	.06	.01	46.56	.04	.00	45.52	.04	.00
47.58	.06	.01	46.55	.05	.01	47.61	.03	.00	46.56	.03	.00
48.63	.06	.01	47.60	.06	.01	48.66	.04	.00	47.61	.03	.00
49.68	.04	.00	48.64	.03	.00	49.71	.02	.00	48.66	.02	.00
50.73	.04	.00	49.69	.04	.00	50.76	.02	.00	49.71	.02	.00
51.77	.02	.00	50.74	.04	.00	51.80	.02	.00	50.76	.01	.00
52.82	.03	.00	51.79	.03	.00	52.85	.01	.00	51.81	.01	.00
53.87	.03	.00	52.83	.03	.00	53.90	.01	.00	52.85	.01	.00
54.92	.03	.00	53.88	.03	.00	54.95	.01	.00	53.90	.01	.00
55.96	.02	.00	54.93	.02	.00	56.00	.01	.00	54.95	.01	.00
57.01	.02	.00	55.98	.02	.00	57.04	.01	.00	56.00	.01	.00
58.06	.02	.00	57.02	.02	.00	58.09	.01	.00	57.05	.01	.00
59.11	.02	.00	58.07	.01	.00	59.14	.01	.00	58.09	.01	.00
60.15	.02	.00	59.12	.01	.00	60.19	.01	.00	59.14	.01	.00
			60.17	.01	.00				60.19	.00	.00

TABLE A XV 3. Alphas from ^{209}Bi Bombarded by 60-MeV Protons

60 deg - Run 5033			70 deg - Run 5037			75 deg - Run 7006			80 deg - Run 5035		
Energy (MeV)	σ (mb·ster^{-1}·MeV^{-1})	Error	Energy (MeV)	σ (mb·ster^{-1}·MeV^{-1})	Error	Energy (MeV)	σ (mb·ster^{-1}·MeV^{-1})	Error	Energy (MeV)	σ (mb·ster^{-1}·MeV^{-1})	Error
1.498	0	0	1.500	0	0	1.475	0	0	1.499	0	0
2.547	0	0	2.550	0	0	2.543	0	0	2.549	0	0
3.595	0	0	3.600	0	0	3.611	0	0	3.598	0	0
4.644	0	0	4.650	0	0	4.679	0	0	4.648	0	0
5.692	0	0	5.700	0	0	5.748	0	0	5.697	0	0
6.741	0	0	6.750	0	0	6.816	0	0	6.746	0	0
7.790	0	0	7.800	0	0	7.884	0	0	7.796	0	0
8.838	0	0	8.850	0	0	8.952	0	0	8.845	0	0
9.887	0	0	9.900	0	0	10.020	0	0	9.895	0	0
10.936	0	0	10.950	0	0	11.088	0	0	10.944	0	0
11.984	.000	.000	12.000	.000	.000	12.156	0	0	11.994	0	0
13.033	.004	.001	13.050	.002	.001	13.225	.001	.001	13.043	.003	.001
14.081	.010	.002	14.100	.004	.001	14.293	.003	.001	14.093	.004	.001
15.130	.021	.002	15.150	.013	.002	15.361	.011	.002	15.142	.014	.002
16.179	.037	.003	16.200	.042	.004	16.429	.029	.004	16.191	.040	.004
17.227	.070	.004	17.249	.074	.005	17.497	.054	.005	17.241	.072	.005
18.276	.096	.005	18.299	.092	.005	18.565	.076	.006	18.290	.108	.006
19.324	.134	.006	19.349	.117	.006	19.633	.120	.008	19.340	.131	.006
20.373	.145	.006	20.399	.132	.006	20.701	.132	.008	20.389	.141	.007
21.422	.158	.006	21.449	.133	.006	21.770	.124	.008	21.439	.137	.007
22.470	.162	.006	22.499	.136	.006	22.838	.120	.008	22.488	.116	.006
23.519	.155	.006	23.549	.133	.006	23.906	.128	.008	23.538	.126	.006
24.568	.166	.006	24.599	.128	.006	24.974	.119	.008	24.587	.121	.006
25.616	.166	.006	25.649	.129	.006	26.042	.123	.008	25.637	.129	.006
26.665	.146	.006	26.699	.114	.006	27.110	.106	.007	26.686	.110	.006
27.713	.147	.006	27.749	.098	.005	28.178	.101	.007	27.735	.094	.005
28.762	.129	.006	28.799	.092	.005	29.247	.102	.007	28.785	.081	.005
29.811	.120	.005	29.849	.076	.005	30.315	.084	.007	29.834	.075	.005
30.859	.108	.005	30.899	.063	.004	31.383	.074	.006	30.884	.065	.005
31.908	.095	.005	31.949	.062	.004	32.451	.075	.006	31.933	.057	.004
32.956	.088	.005	32.999	.049	.004	33.519	.059	.006	32.983	.045	.004
34.005	.067	.004	34.049	.038	.003	34.587	.049	.005	34.032	.031	.003
35.054	.067	.004	35.099	.025	.003	35.655	.054	.005	35.082	.032	.003
36.102	.049	.003	36.149	.021	.002	36.724	.043	.005	36.131	.016	.002
37.151	.100	.005	37.199	.062	.004	37.792	.035	.004	37.180	.045	.004
38.200	.066	.004	38.249	.049	.004	38.860	.045	.005	38.230	.032	.003
39.248	.064	.004	39.299	.037	.003	39.928	.025	.004	39.279	.023	.003
40.297	.048	.003	40.349	.028	.003	40.996	.018	.003	40.329	.019	.002
41.345	.044	.003	41.399	.022	.003	42.064	.014	.003	41.378	.014	.002
42.394	.041	.003	42.449	.016	.002	43.132	.011	.002	42.428	.014	.002
43.443	.033	.003	43.499	.013	.002	44.200	.006	.002	43.477	.011	.002
44.491	.032	.003	44.549	.016	.002	45.269	.008	.002	44.527	.004	.001
45.540	.024	.003	45.599	.012	.002	46.337	.005	.002	45.576	.009	.002
46.588	.023	.002	46.649	.008	.002	47.405	.005	.002	46.625	.005	.001
47.637	.023	.002	47.699	.008	.002	48.473	.003	.001	47.675	.005	.001
48.686	.013	.002	48.749	.006	.001	49.541	.003	.001	48.724	.002	.001
49.734	.014	.002	49.798	.003	.001	50.609	.002	.001	49.774	.003	.001
50.783	.015	.002	50.848	.003	.001	51.677	0	0	50.823	.002	.001
51.832	.011	.002	51.898	.002	.001	52.746	0	0	51.873	.001	.001
52.880	.006	.001	52.948	.004	.001	53.814	0	0	52.922	.001	.000
53.929	.009	.001	53.998	.002	.001	54.882	.002	.001	53.972	.001	.001
54.977	.006	.001	55.048	.001	.001	55.950	.001	.001	55.021	.000	.000
56.026	.007	.001	56.098	.001	.000	57.018	.001	.001	56.071	0	0
57.075	.007	.001	57.148	.002	.001	58.086	.001	.001	57.120	.000	.000
58.123	.004	.001	58.198	.002	.001	59.154	.003	.001	58.169	.002	.001
59.172	.005	.001	59.248	.002	.001	60.222	.001	.001	59.219	.001	.001
60.220	.003	.001	60.298	.002	.001				60.268	.001	.000

TABLE A XV 4. Alphas from ^{209}Bi Bombarded by 60-MeV Protons

90 deg - Run 5023			110 deg - Run 5036			135 deg - Run 2064			deg - Run		
Energy (MeV)	σ (mb·ster^{-1}·MeV^{-1})	Error	Energy (MeV)	σ (mb·ster^{-1}·MeV^{-1})	Error	Energy (MeV)	σ (mb·ster^{-1}·MeV^{-1})	Error	Energy (MeV)	σ (mb·ster^{-1}·MeV^{-1})	Error
						1.48	0	0			
1.497	0	0	1.450	0	0	2.52	0	0			
2.545	0	0	2.500	0	0	3.56	0	0			
3.593	0	0	3.550	0	0	4.60	0	0			
4.641	0	0	4.600	0	0	5.64	0	0			
5.690	0	0	5.650	0	0	6.68	0	0			
6.738	0	0	6.700	0	0	7.72	0	0			
7.786	0	0	7.750	0	0	8.75	0	0			
8.834	0	0	8.800	0	0	9.79	0	0			
9.882	0	0	9.850	0	0	10.83	0	0			
10.930	0	0	10.900	0	0	11.87	0	0			
11.978	0	0	11.950	0	0	12.91	.00	.00			
13.026	.004	.001	13.000	.005	.001	13.95	.01	.00			
14.074	.010	.001	14.050	.011	.001	14.99	.03	.00			
15.122	.023	.002	15.100	.022	.002	16.03	.06	.00			
16.170	.047	.003	16.150	.049	.003	17.06	.10	.00			
17.218	.079	.004	17.200	.080	.004	18.10	.11	.01			
18.266	.110	.004	18.250	.102	.004	19.14	.10	.00			
19.314	.123	.004	19.300	.102	.004	20.18	.09	.00			
20.363	.123	.004	20.350	.101	.004	21.22	.07	.00			
21.411	.112	.004	21.400	.087	.004	22.26	.06	.00			
22.459	.108	.004	22.450	.083	.004	23.30	.05	.00			
23.507	.101	.004	23.500	.067	.003	24.33	.04	.00			
24.555	.095	.004	24.550	.059	.003	25.37	.03	.00			
25.603	.086	.004	25.600	.048	.003	26.41	.04	.00			
26.651	.078	.004	26.650	.049	.003	27.45	.03	.00			
27.699	.074	.003	27.700	.038	.002	28.49	.02	.00			
28.747	.069	.003	28.750	.030	.002	29.53	.02	.00			
29.795	.057	.003	29.800	.024	.002	30.57	.02	.00			
30.843	.049	.003	30.850	.025	.002	31.60	.01	.00			
31.891	.042	.003	31.900	.019	.002	32.64	.01	.00			
32.939	.041	.003	32.950	.015	.002	33.68	.01	.00			
33.987	.031	.002	34.000	.014	.001	34.72	.01	.00			
35.035	.030	.002	35.050	.011	.001	35.76	.00	.00			
36.084	.017	.002	36.100	.005	.001	36.80	.00	.00			
37.132	.032	.002	37.150	.014	.002	37.84	.00	.00			
38.180	.026	.002	38.200	.012	.001	38.88	.00	.00			
39.228	.017	.002	39.250	.008	.001	39.91	.00	.00			
40.276	.014	.001	40.300	.006	.001	40.95	.00	.00			
41.324	.011	.001	41.350	.006	.001	41.99	.00	.00			
42.372	.011	.001	42.400	.005	.001	43.03	.00	.00			
43.420	.012	.001	43.450	.003	.001	44.07	.00	.00			
44.468	.009	.001	44.500	.003	.001	45.11	.00	.00			
45.516	.007	.001	45.550	.002	.001	46.15	.00	.00			
46.564	.005	.001	46.600	.002	.001						
47.612	.005	.001	47.650	.003	.001						
48.660	.004	.001	48.700	.001	.000						
49.708	.005	.001	49.750	.001	.000						
50.757	.003	.001	50.800	.001	.000						
51.805	.002	.001	51.850	.000	.000						
52.853	.002	.001	52.900	.000	.000						
53.901	.001	.000	53.950	.000	.000						
54.949	.001	.000	55.000	.000	.000						
55.997	.000	.000	56.050	.000	.000						
57.045	.000	.000	57.100	.000	.000						
58.093	.001	.000	58.150	.000	.000						
59.141	.000	.000	59.200	.000	.000						
60.189	.000	.000	60.250	.000	.000						

APPENDIX B

AVERAGE CROSS SECTIONS FROM TIME-OF-FLIGHT ANALYSIS

The cross section data obtained from the time-of-flight analysis system are listed in this appendix. The data listed are for protons, deuterons, helium-3's, alphas and "total" mass-3 from ^{12}C and alphas from ^{54}Fe. The cross sections are listed in millibarns/(steradian·MeV) and are averaged over ~1-MeV-wide bins. The energy listed in the center of the bin.

Statistical errors are not listed on these tables; however, the largest errors are ±10% for both the ^{54}Fe and the ^{12}C data. Statistical errors for each run may be obtained by use of the factors listed in Table V. These errors should be considered with the systematic errors discussed in Chapter III, Section D, and Chapter IV, Section G.

TABLE BI. CROSS SECTIONS FROM TIME-OF-FLIGHT SYSTEM

^{12}C

Cross Section

(mb/sr-MeV)

Energy[a] (MeV)	15°	20.8°	30°	35°	40°	45°	50°	60°	70°	90°	110°	135°	160°
						PROTONS							
1.5	1.47	2.28	1.72	1.83	1.86	1.46	1.71	1.49	1.52	1.47	1.28	1.70	1.54
2.5	1.50	2.22	2.00	2.07	2.02	1.92	1.85	1.66	1.66	1.64	1.38	1.59	1.43
3.5	2.40	3.24	2.74	2.93	2.72	2.01	2.59	1.99	2.07	1.90	1.37	1.83	1.20
						DEUTERONS							
1.5	.314	.505	.486	.446	.462	.302	.383	.281	.309	.287	.206	.267	.255
2.5	.418	.562	.530	.462	.654	.369	.488	.326	.314	.263	.193	.207	.195
3.5	.488	.581	.508	.539	.550	.412	.452	.332	.319	.230	.171	.200	.155
4.5	.547	.588	.663	.670	.586	.407	.543	.318	.364	.293	.175	.215	.109
						TOTAL MASS-3							
4.5		.496	.354	.409	.355		.288		.238	.173		.162	.144
3.5		.496	.382	.396	.315		.301		.228	.208		.166	.148
2.5		.474	.348	.338	.311		.294		.289	.201		.187	.172
						HELIUM-3							
6.5		.331	.233	.264	.223		.193		.134	.119		.085	.073
7.5		.335	.256	.238	.227		.181		.140	.098		.069	.051
8.5		.353	.241	.237	.202		.180		.099	.086		.063	.044
9.5		.309	.241	.251	.182		.146		.093	.072		.039	.042
10.5		.232	.238	.219	.191		.141		.081	.075		.042	.010
11.5		.393	.247	.303	.184		.165		.103	.072		.043	0

TABLE BI. (Continued)

					ALPHAS				
2.8	4.51	4.17	3.99	3.96	3.39	2.38	1.50	1.10	1.03
3.5	4.37	3.96	3.75	3.61	3.29	2.10	1.40	.923	.831
4.5	4.03	3.59	3.49	3.35	2.72	1.72	1.13	.697	.659
5.5	3.61	3.08	3.09	2.86	2.31	1.42	.899	.535	.487
6.5	3.43	2.73	2.71	2.43	2.04	1.25	.777	.411	.390
7.5	2.82	2.37	2.31	2.05	1.65	1.00	.587	.321	.320
8.5	2.62	2.01	1.92	1.89	1.40	.866	.499	.244	.249
9.5	2.29	1.82	1.71	1.44	1.19	.665	.384	.190	.188
10.5	2.02	1.54	1.51	1.34	.993	.548	.288	.122	.139
11.5	1.87	1.37	1.29	1.22	.831	.426	.246	.107	.105
12.5	1.53	1.13	1.12	1.00	.705	.351	.184	.079	.080

[a]Center of 1 MeV bin.

TABLE B II. CROSS SECTIONS FROM TIME-OF-FLIGHT SYSTEM

^{54}Fe

Cross Section

(mb/sr-MeV)

Energy (MeV)	12° Run 0123	27° Run 5020	47° Run 5042	60° Run 5043	70° Run 5044	100° Run 2070	160° Run 2067
13.5	0.88	a	a	a	a	0.42	0.28
12.5	1.2	a	a	a	a	0.55	0.38
11.5	1.75 ± .15	1.50	1.18	1.00	1.10	0.67	0.52
10.5	1.70 ± .14	1.73	1.43	1.23	1.33	0.92	0.69
9.5	1.76 ± .15	1.88	1.63	1.47	1.52	1.17	0.95
8.5	0.96	1.72	1.66	1.53	1.55	1.39	1.26
7.5	0.65	1.25	1.29	1.35	1.20	1.52	1.46
6.5	0.14	0.67	0.73	0.83	0.69	1.25	1.47
5.5		0.26	0.30	0.38	0.28	0.68	1.07
4.5		0.12	0.11	0.14	0.12	0.29	0.54
3.5	0	0	0	0	0	0.05	0.21

[a]Due to a flaw in the experimental system this data is unavailable.

VITA

Fred Edmond Bertrand, Jr., was born on September 27, 1938, at New Orleans, Louisiana, where he attended public grade and high schools, graduating from John McDonogh Senior High School in 1956.

From 1956 to 1960 he as a student at Southwestern at Memphis College. In June 1960, he received the Bachelor of Science Degree.

He enrolled in the Graduate School, Department of Physics, Louisiana State University, in September 1960. In August 1962, he received the Master of Science Degree. In November 1964, he was awarded an Oak Ridge Graduate Fellowship and performed his dissertation research with the Neutron Physics Division, Oak Ridge National Laboratory.

In July 1965, he married the former Miss Jeanne A. Merilh, and they have a son, Fred Edmond Bertrand, III, born November 17, 1966.

He is presently a candidate for the degree of Doctor of Philosophy.

EXAMINATION AND THESIS REPORT

Candidate: Fred Edmond Bertrand, Jr.

Major Field: Physics

Title of Thesis: Differential Cross Sections for the Charged Particles Produced by 60-MeV Proton Bombardment of Carbon, Iron and Bismuth.

Approved:

Major Professor and Chairman

Dean of the Graduate School

EXAMINING COMMITTEE:

Date of Examination:

9 May 1968